

**The Formation of Carbocations from Excited States:**

**The meta Methoxy Effect in  
Photofragmentations and Photoadditions**

By

Jeffrey Charles Roberts

Submitted in partial fulfillment of the requirements  
for the degree of Doctor of Philosophy

at

Dalhousie University  
Halifax, Nova Scotia  
March 2005

© Copyright by Jeffrey Charles Roberts, 2005



Library and  
Archives Canada

Bibliothèque et  
Archives Canada

Published Heritage  
Branch

Direction du  
Patrimoine de l'édition

395 Wellington Street  
Ottawa ON K1A 0N4  
Canada

395, rue Wellington  
Ottawa ON K1A 0N4  
Canada

*Your file    Votre référence*

*ISBN: 0-494-00957-8*

*Our file    Notre référence*

*ISBN: 0-494-00957-8*

#### NOTICE:

The author has granted a non-exclusive license allowing Library and Archives Canada to reproduce, publish, archive, preserve, conserve, communicate to the public by telecommunication or on the Internet, loan, distribute and sell theses worldwide, for commercial or non-commercial purposes, in microform, paper, electronic and/or any other formats.

The author retains copyright ownership and moral rights in this thesis. Neither the thesis nor substantial extracts from it may be printed or otherwise reproduced without the author's permission.

#### AVIS:

L'auteur a accordé une licence non exclusive permettant à la Bibliothèque et Archives Canada de reproduire, publier, archiver, sauvegarder, conserver, transmettre au public par télécommunication ou par l'Internet, prêter, distribuer et vendre des thèses partout dans le monde, à des fins commerciales ou autres, sur support microforme, papier, électronique et/ou autres formats.

L'auteur conserve la propriété du droit d'auteur et des droits moraux qui protègent cette thèse. Ni la thèse ni des extraits substantiels de celle-ci ne doivent être imprimés ou autrement reproduits sans son autorisation.

---

In compliance with the Canadian Privacy Act some supporting forms may have been removed from this thesis.

Conformément à la loi canadienne sur la protection de la vie privée, quelques formulaires secondaires ont été enlevés de cette thèse.

While these forms may be included in the document page count, their removal does not represent any loss of content from the thesis.

Bien que ces formulaires aient inclus dans la pagination, il n'y aura aucun contenu manquant.

  
**Canada**

DALHOUSIE UNIVERSITY

To comply with the Canadian Privacy Act the National Library of Canada has requested that the following pages be removed from this copy of the thesis:

Preliminary Pages

Examiners Signature Page (pii)

Dalhousie Library Copyright Agreement (piii)

Appendices

Copyright Releases (if applicable)

# Table of Contents

List of Figures . . . . .	x
List of Schemes . . . . .	xvi
List of Tables . . . . .	xix
Abstract . . . . .	xxiv
Lists of Abbreviations and Symbols Used . . . . .	xxv
Acknowledgments . . . . .	xxxix
 <b>Chapter 1.                    Introduction to Carbocation Intermediates and                                  Their Formation <i>via</i> Excited State Reactions</b>	 1
1.1    Overview of Thesis . . . . .	1
1.2    Carbocations . . . . .	2
1.2.1   Early Studies of Carbocations. . . . .	2
1.2.2   Measurements of Carbocation Stability . . . . .	6
1.2.3   Measurements of Carbocation Reactivity . . . . .	13
1.3    Fundamentals of Photochemistry . . . . .	17
1.3.1   Photophysical Processes . . . . .	17
1.3.2   Photochemical Reactions . . . . .	19
1.3.3   Generation of Carbocations <i>via</i> Photofragmentation . . . . .	21
 <b>Chapter 2.                    Investigations of Rearrangements of                                  Photochemically Generated Carbocations</b>	 30
2.1    Introduction . . . . .	30
2.1.1   Rearrangements of Photochemically Generated Carbocations . . . . .	30



2.1.2	Project Proposal	35
2.2	Experimental Results	37
2.2.1	Synthesis and Photophysical Characterization of Substrate <b>44</b>	37
2.2.2	Photolysis of Ester <b>44</b> in Methanol	40
2.2.3	Photolysis of Ester <b>44</b> in TFE.	44
2.2.4	Photolysis of Methoxy-Substituted <i>trans</i> -Stilbene <b>52</b> in Methanol and TFE	47
2.3	Discussion of Results	50
2.3.1	The Photochemistry of Ester <b>44</b>	50
2.3.2	Future Directions: Carbocation Rearrangements and Stilbene Photochemistry	54
<b>Chapter 3.</b>	<b>The Photochemical Addition of Alcohols to Methoxy-Substituted Stilbene Derivatives</b>	57
3.1	Introduction	57
3.1.1	The Photochemistry of <i>cis</i> - and <i>trans</i> -Stilbene	57
3.1.2	The meta-Amino Effect in Stilbene Photochemistry	61
3.1.3	The Photochemical Addition of Alcohols to Stilbene Derivatives	64
3.1.4	Project Proposal	68
3.2	Experimental Results	70
3.2.1	Synthesis of Methoxy-Substituted Stilbene Derivatives	70
3.2.2	Photophysical Characterization of Methoxy-Substituted Stilbene Derivatives	71
3.2.3	Irradiation of <i>trans</i> - <b>60</b> and <i>trans</i> - <b>71-74</b> in Methanol	78
3.2.4	Irradiation of <i>trans</i> - <b>60</b> and <i>trans</i> - <b>71-74</b> in TFE	83

3.2.5	Irradiation of <i>cis</i> - <b>60</b> and <i>cis</i> - <b>71-74</b> in TFE . . . . .	87
3.2.6	Quenching of <i>trans</i> - <b>73</b> Fluorescence by TFE. . . . .	89
3.3	Discussion of Results . . . . .	93
3.3.1	Reliability of the Photophysical Measurements . . . . .	93
3.3.2	The Photophysics of Methoxy-Substituted Stilbene Derivatives . . . . .	98
3.3.3	Addition of Alcohols to the Excited States of Methoxy-Substituted Stilbene Derivatives . . . . .	99
<b>Chapter 4.</b>	<b>Mechanistic Aspects of the Addition of Alcohols to Methoxy-Substituted Stilbenes, Styrenes, and 1-Arylpropenes . . . . .</b>	<b>105</b>
4.1	Introduction . . . . .	105
4.1.1	Early Examples of the Photochemical Addition of Alcohols to Alkenes . . . . .	105
4.1.2	The Photochemical Addition of Water and Alcohols to Substituted Styrenes . . . . .	108
4.1.3	Direct Observation of Carbocations Formed <i>via</i> Photoprotonation . . . . .	111
4.1.4	Project Proposal . . . . .	113
4.2	Experimental Results . . . . .	117
4.2.1	Synthesis of Methoxy-Substituted Styrenes and <i>trans</i> -1-Arylpropenes . . . . .	117
4.2.2	Photophysical Properties of Methoxy-Substituted Styrenes and <i>trans</i> -1-Arylpropenes . . . . .	118
4.2.3	Photophysical Properties of Methoxy-Substituted Styrenes, Arylpropenes, and Stilbenes in Solvents of Varying Polarity . . . . .	124
4.2.4	Irradiations of <b>91-94</b> and <i>trans</i> - <b>96-99</b> in TFE. . . . .	138
4.2.5	Quenching of Fluorescence and Singlet Lifetimes by TFE . . . . .	143

4.2.6	LFP of Methoxy-Substituted Stilbenes <i>trans</i> -71-74 . . . . .	145
4.2.7	The Photochemical Addition of Deuterated TFE to Methoxy-Substituted Aryl Alkenes and Stilbenes. . . . .	150
4.3	Discussion of Results . . . . .	162
4.3.1	Summary of Chapter 4 Experiments . . . . .	162
4.3.2	Photophysical Properties of Methoxy-Substituted Arylalkenes . . . . .	166
4.3.3	The Mechanism of the TFE Addition Reactions . . . . .	172
<b>Chapter 5.</b>	<b>Intramolecular Charge Transfer States in the Photochemistry of Methoxy-Substituted Stilbene Derivatives . . . . .</b>	<b>181</b>
5.1	Introduction . . . . .	181
5.1.1	Twisted Intramolecular Charge Transfer (TICT) States . . . . .	181
5.1.2	Formation of ICT States <i>via</i> Excitation of Donor- Acceptor Stilbenes . . . . .	183
5.1.3	Project Proposal . . . . .	188
5.2	Experimental Results . . . . .	189
5.2.1	Synthesis of <i>trans</i> -111-120 . . . . .	189
5.2.2	Photophysical Properties of <i>trans</i> -111-120 in Acetonitrile Solution . . . . .	191
5.2.3	Solvent Dependence of the Photophysical Properties of <i>trans</i> -111-120 . . . . .	193
5.2.4	Irradiations of <i>trans</i> -111-120 in TFE . . . . .	211
5.3	Discussion of Results . . . . .	216
5.3.1	Photophysical Properties of the Substituted Derivatives of <i>trans</i> -3,5-dimethoxystilbene . . . . .	216

5.3.2	Photoprotonation of the Substituted Derivatives of <i>trans</i> -3,5-dimethoxystilbene	222
<b>Chapter 6.</b>	<b>Conclusions and Future Work</b>	226
6.1	Summary and Conclusions	226
6.2	Future Work	228
<b>Chapter 7.</b>	<b>Experimental Details</b>	233
7.1	General Methods and Techniques	233
7.1.1	Introduction	233
7.1.2	Experimental Methods	233
7.1.3	Common Laboratory Reagents	234
7.2	Procedures for Chapter 2 Experiments	235
7.2.1	Synthetic Procedures	235
7.2.2	Photolysis Procedures	244
7.3	Procedures for Chapter 3 Experiments	247
7.3.1	Synthetic Procedures	247
7.3.2	Photophysical Characterization Procedures	251
7.3.3	Irradiation Procedures	252
7.3.4	Analysis of Fluorescence Quenching Results	258
7.4	Procedures for Chapter 4 Experiments	259
7.4.1	Synthetic Procedures	259
7.4.2	Irradiation Procedures	262
7.4.3	Calculation of Excited State Dipole Moments	265
7.4.4	LFP Procedures	266

7.4.5	<sup>1</sup> H NMR Calculations . . . . .	267
7.5	Procedures for Chapter 5 Experiments . . . . .	268
7.5.1	Synthetic Procedures . . . . .	268
7.5.2	Irradiation Procedures . . . . .	272
<b>References</b>	. . . . .	<b>278</b>

## List of Figures

Figure 1.1	Electron density and formal charges (in parenthesis) for the ground state and first excited state of anisole, calculated using extended HMO theory . . . . .	22
Figure 2.1	Absorption spectra (all solutions $2.3 \times 10^{-4}$ M). <b>A.</b> Ester <b>44</b> . <b>B.</b> 1-(3,5-dimethoxyphenyl)ethyl ethanoate (solid line) and 4-methylanisole (dashed line). <b>C.</b> Summation of spectra in <b>B</b> . <b>D.</b> Subtraction of experimental spectrum of <b>44</b> in <b>A</b> from summation spectrum in <b>C</b> . . . . .	39
Figure 2.2	Product yields as a function of time for the photolysis of ester <b>44</b> in methanol (compounds <b>55</b> and <b>56</b> have been removed for improved clarity) . . . . .	41
Figure 2.3	Product yields as a function of time for the photolysis of ester <b>44</b> in TFE (compounds <b>55</b> and <b>56</b> have been removed for improved clarity) . . . . .	45
Figure 2.4	<b>A.</b> The change in optical density following 266 nm LFP of ester <b>44</b> in TFE ( $0.8 \mu\text{s} - 13 \mu\text{s}$ ). <b>B.</b> Comparison of the absorption spectra of ester <b>44</b> and methoxy-substituted <i>trans</i> -stilbene <b>52</b> (both $3.45 \times 10^{-5}$ M in methanol) . . . . .	46
Figure 2.5	Product yields as a function of time for the irradiation of the methoxy-substituted <i>trans</i> -stilbene <b>52</b> in methanol ( <b>A</b> ) and TFE ( <b>B</b> ) . . . . .	49
Figure 2.6	Newman projections of ester <b>44</b> ( <b>A</b> ) and carbocation intermediate <b>45</b> ( <b>B</b> ) . . . . .	53
Figure 3.1	The energy-coordinate diagram for stilbene isomerization <i>via</i> ground and excited states (not to scale) . . . . .	58
Figure 3.2	The barriers for singlet state bond torsion for <b>A.</b> <i>trans</i> - <b>60</b> and <i>trans</i> - <b>64</b> ; <b>B.</b> <i>trans</i> - <b>62</b> and <i>trans</i> - <b>63</b> . . . . .	63
Figure 3.3	Absorption spectra of various stilbene derivatives in acetonitrile. <b>A.</b> <i>trans</i> - <b>60</b> and <i>cis</i> - <b>60</b> (both $8.9 \times 10^{-6}$ M), <b>B.</b> <i>trans</i> - <b>71</b> and <i>cis</i> - <b>71</b> (both $1.7 \times 10^{-5}$ M), <b>C.</b> <i>trans</i> - <b>72</b> and <i>cis</i> - <b>72</b> (both $1.8 \times 10^{-5}$ M), <b>D.</b> <i>trans</i> - <b>73</b> and <i>cis</i> - <b>73</b> (both $1.7 \times 10^{-5}$ M), <b>E.</b> <i>trans</i> - <b>74</b> and <i>cis</i> - <b>74</b> (both $1.7 \times 10^{-5}$ M) . . . . .	73

Figure 3.4	Comparison of fluorescence intensity for <i>trans</i> - <b>60</b> and <i>trans</i> - <b>71-74</b> in acetonitrile solution ( $A = 0.25$ at 295 nm for all solutions)	75
Figure 3.5	Yield versus time plots for the irradiation of <i>trans</i> - <b>60</b> and <i>trans</i> - <b>71-74</b> in acetonitrile solution	77
Figure 3.6	Yield versus time plots for 300 nm irradiation of <i>trans</i> - <b>60</b> and <i>trans</i> - <b>71-74</b> in methanol (product <b>78</b> has been omitted for improved clarity)	81
Figure 3.7	GC-MS spectra of compounds present in irradiation mixture of <i>trans</i> - <b>73</b> ( <i>trans</i> - <b>73</b> , <i>cis</i> - <b>73</b> , <b>77-3</b> , <b>78-3</b> , <b>75a-3</b> , and <b>76a-3</b> )	83
Figure 3.8	Yield versus time plots for 300 nm irradiation of <i>trans</i> - <b>60</b> and <i>trans</i> - <b>71-74</b> in TFE (product <b>78</b> has been omitted for improved clarity)	85
Figure 3.9	Yield versus time plots for 300 nm irradiation of <i>cis</i> - <b>60</b> and <i>cis</i> - <b>71-74</b> in TFE (product <b>78</b> has been omitted for improved clarity)	88
Figure 3.10	Fluorescence quantum yield $\phi_f$ of <i>trans</i> - <b>73</b> in mixtures of acetonitrile and either TFE (crosses) or TFE-OD (diamonds)	90
Figure 3.11	Stern-Volmer plot for the quenching of <i>trans</i> - <b>73</b> in mixtures of acetonitrile and either TFE (crosses) or TFE-OD (diamonds)	92
Figure 3.12	The combined yields of <i>cis</i> - and <i>trans</i> - <b>73</b> (diamonds) and the combined yields of TFE-adducts <b>75b-3</b> and <b>76b-3</b> after ten minutes irradiation, plotted as a function of percent TFE in acetonitrile	93
Figure 4.1	Absorption spectra of methoxy-substituted styrenes <b>90-94</b> in acetonitrile. Each plot provides a spectrum taken at $1.2 \times 10^{-4}$ M (dark line) and $1.2 \times 10^{-5}$ M (pale line)	120
Figure 4.2	Absorption spectra of arylpropenes <i>trans</i> - <b>95-99</b> in acetonitrile. Each plot provides a spectrum taken at $1.2 \times 10^{-4}$ M (dark line) and $1.2 \times 10^{-5}$ M (pale line)	121

Figure 4.3	Comparison of fluorescence intensity for methoxy-substituted styrenes <b>90-94</b> in acetonitrile solution ( $A = 0.25$ at 254 nm for all solutions).	122
Figure 4.4	Comparison of fluorescence intensity for arylpropenes <i>trans</i> - <b>95-99</b> in acetonitrile solution ( $A = 0.25$ at 254 nm for all solutions).	122
Figure 4.5	Plot of the solvent induced Stokes' shift ( $\lambda_{\text{max}}(\text{fluor}) - \lambda_{\text{max}}(\text{ex})$ ) versus the solvent parameter $\Delta f$ for five methoxy-substituted <i>trans</i> -stilbenes	130
Figure 4.6	Plot of fluorescence quantum yields versus the solvent parameter $\Delta f$ for five methoxy-substituted <i>trans</i> -stilbenes.	132
Figure 4.7	Plot of monoexponential singlet lifetimes for <i>trans</i> - <b>72</b> and <i>trans</i> - <b>73</b> versus the solvent polarity function $\Delta f$ .	134
Figure 4.8	Analysis of the fluorescence decay of <i>trans</i> - <b>73</b> using a monoexponential kinetic fit. <b>A.</b> Experimental data (points) and fitting curve (line). <b>B.</b> Weighted residuals (experimental - fit)	135
Figure 4.9	Analysis of the fluorescence decay of <i>trans</i> - <b>73</b> using a biexponential kinetic fit. <b>A.</b> Experimental data (points) and fitting curve (line). <b>B.</b> Weighted residuals (experimental - fit)	136
Figure 4.10	The two components of the biexponential lifetime of <i>trans</i> - <b>73</b> versus the solvent parameter $\Delta f$ for a series of six solvents	136
Figure 4.11	Yield versus time plots for the irradiation of methoxy-substituted styrenes in TFE ( <b>91</b> and <b>92</b> for ten minutes, <b>93</b> and <b>94</b> for five minutes)	139
Figure 4.12	Yield versus time plots for the irradiation of methoxy-substituted <i>trans</i> -arylpropenes in TFE (ten minutes for all four compounds)	141
Figure 4.13	Kinetic trace at 315 nm following LFP of <i>trans</i> - <b>73</b> in TFE	146



Figure 4.14	Kinetic trace at 320 nm following LFP of <i>trans</i> - <b>73</b> 1) in pure HFIP, and 2) in HFIP saturated with sodium azide . . . . .	147
Figure 4.15	Kinetic trace at 340 nm following LFP of <i>trans</i> - <b>71</b> 1) in pure HFIP, 2) in HFIP with a small amount of sodium azide added, and 3) in HFIP saturated with sodium azide . . . . .	148
Figure 4.16	Kinetic trace at 380 nm following LFP of <i>trans</i> - <b>73</b> in HFIP . . . . .	149
Figure 4.17	<sup>1</sup> H NMR spectrum of 1-(trifluoroethoxy)-1- (3,5-dimethoxyphenyl)ethane <b>100-3</b> following irradiation of 3,5-dimethoxystyrene <b>93</b> in TFE . . . . .	151
Figure 4.18	<sup>1</sup> H NMR spectrum of 1-(trifluoroethoxy)-1- (3,5-dimethoxyphenyl)-2-deuterioethane <b>100-3d</b> following irradiation of 3,5-dimethoxystyrene <b>93</b> in TFE-OD . . . . .	151
Figure 4.19	Neuman projection for photoproduct <b>75b-0</b> , and analysis of the ABX coupling pattern following irradiation in TFE or TFE-OD . . . . .	158
Figure 4.20	The three possible isomers of <b>75b-0</b> that may be formed by addition of TFE-OD to stilbene ( <i>trans</i> - <b>60</b> ) . . . . .	159
Figure 4.21	Plot of the difference between isomerization quantum yields $\phi_{ic}$ in acetonitrile and cyclohexane <i>versus</i> the excited state dipole moment $\mu_e$ for <i>trans</i> - <b>60</b> , <i>trans</i> - <b>71</b> , <i>trans</i> - <b>72</b> , and <i>trans</i> - <b>74</b> . . . . .	169
Figure 4.22	Cation intermediates detected following 308 nm LFP of <i>trans</i> - <b>71-74</b> in HFIP . . . . .	176
Figure 5.1	Fluorescence spectra of <i>trans</i> - <b>111</b> (4'-methoxy) in a series of four solvents . . . . .	194
Figure 5.2	Fluorescence spectra of <i>trans</i> - <b>112</b> (3'-methoxy) in a series of four solvents . . . . .	194
Figure 5.3	Fluorescence spectra of <i>trans</i> - <b>113</b> (4'-methyl) in a series of four solvents . . . . .	195

Figure 5.4	Fluorescence spectra of <i>trans</i> - <b>114</b> (3'-methyl) in a series of four solvents . . . . .	195
Figure 5.5	Fluorescence spectra of <i>trans</i> - <b>115</b> (4'-fluoro) in a series of four solvents . . . . .	196
Figure 5.6	Fluorescence spectra of <i>trans</i> - <b>116</b> (3'-fluoro) in a series of four solvents . . . . .	196
Figure 5.7	Fluorescence spectra of <i>trans</i> - <b>117</b> (4'-trifluoromethyl) in a series of four solvents . . . . .	197
Figure 5.8	Fluorescence spectra of <i>trans</i> - <b>118</b> (3'-trifluoromethyl) in a series of four solvents . . . . .	197
Figure 5.9	Fluorescence spectra of <i>trans</i> - <b>118</b> (4'-cyano) in a series of four solvents . . . . .	198
Figure 5.10	Fluorescence spectra of <i>trans</i> - <b>118</b> (3'-cyano) in a series of four solvents . . . . .	198
Figure 5.11	Fluorescence spectra of <i>trans</i> - <b>73</b> ( <i>trans</i> -3,5-dimethoxystilbene) in a series of four solvents . . . . .	199
Figure 5.12	Plot of the Stokes' shift (in wavenumbers) versus the solvent parameter $\Delta f$ for the <i>para</i> -substituted derivatives of <i>trans</i> - <b>73</b> in a series of six solvents . . . . .	200
Figure 5.13	Plot of the Stokes' shift (in wavenumbers) versus the solvent parameter $\Delta f$ for the <i>meta</i> -substituted derivatives of <i>trans</i> - <b>73</b> in a series of six solvents . . . . .	201
Figure 5.14	Plot of fluorescence quantum yield $\phi_f$ versus solvent parameter $\Delta f$ for the <i>para</i> -substituted derivatives of <i>trans</i> - <b>73</b> in a series of six solvents . . . . .	203
Figure 5.15	Plot of fluorescence quantum yield $\phi_f$ versus solvent parameter $\Delta f$ for the <i>meta</i> -substituted derivatives of <i>trans</i> - <b>73</b> in a series of six solvents . . . . .	204
Figure 5.16	Plot of the <i>short</i> component of biexponential singlet lifetimes for the <i>para</i> -substituted derivatives of <i>trans</i> - <b>73</b> in a series of six solvents . . . . .	206

Figure 5.17	Plot of the <i>short</i> component of biexponential singlet lifetimes for the <i>meta</i> -substituted derivatives of <i>trans</i> - <b>73</b> in a series of six solvents . . .	207
Figure 5.18	Plot of the <i>long</i> component of biexponential singlet lifetimes for the <i>para</i> -substituted derivatives of <i>trans</i> - <b>73</b> in a series of six solvents . . .	208
Figure 5.19	Plot of the <i>long</i> component of biexponential singlet lifetimes for the <i>meta</i> -substituted derivatives of <i>trans</i> - <b>73</b> in a series of six solvents . . .	209
Figure 5.20	Yield <i>versus</i> time plots for the irradiation of <i>trans</i> - <b>111</b> (4'-methoxy, 30 minutes) and <i>trans</i> - <b>112</b> (3'-methoxy, 10 minutes) in TFE (300 nm) . . .	213
Figure 5.21	Yield <i>versus</i> time plots for the irradiation of <i>trans</i> - <b>113</b> (4'-methyl) and <i>trans</i> - <b>114</b> (3'-methyl) in TFE (300 nm, 10 minutes each) . . .	213
Figure 5.22	Yield <i>versus</i> time plots for the irradiation of <i>trans</i> - <b>115</b> (4'-fluoro) and <i>trans</i> - <b>116</b> (3'-fluoro) in TFE (300 nm, 10 minutes each) . . .	214
Figure 5.23	Yield <i>versus</i> time plots for the irradiation of <i>trans</i> - <b>117</b> (4'-trifluoromethyl) and <i>trans</i> - <b>118</b> (3'-trifluoromethyl) in TFE (300 nm, 10 minutes each) . . .	214
Figure 5.24	Yield <i>versus</i> time plots for the irradiation of <i>trans</i> - <b>119</b> (4'-cyano, 50 minutes) and <i>trans</i> - <b>120</b> (3'-cyano, 30 minutes) in TFE (300 nm) . . .	215
Figure 5.25	Plot of the yield of TFE adduct <b>121</b> (data in Table 5.14) <i>versus</i> $\sigma^+$ (values in Table 1.1) using a modified Hammett treatment (Equation 5.1) . . .	225
Figure 5.26	Plot of the yield of TFE adduct <b>122</b> (data in Table 5.14) <i>versus</i> $\sigma^+$ (values in Table 1.1) using a modified Hammett treatment (Equation 5.2) . . .	225

## List of Schemes

Scheme 1.1	Rearrangement of camphene hydrochloride <b>1</b> to isobornyl chloride <b>2</b> <i>via</i> a carbocation intermediate . . . . .	3
Scheme 1.2	Addition of hydrochloric acid to 3-methyl-1-butene (R = H) and 3,3-dimethyl-1-butene (R = CH <sub>3</sub> ), with rearrangement of the carbocation intermediate . . . . .	5
Scheme 1.3	Rates and activation energies for degenerate carbocation rearrangements . . . . .	12
Scheme 1.4	Ionization of generic substrate R-X and formation of Solvent adduct R-OS and nucleophile adduct R-Nu . . . . .	13
Scheme 1.5	A simplified energy state diagram illustrating basic photophysical processes . . . . .	18
Scheme 1.6	A schematic representation of the relationship between photophysical processes and photochemical reactions . . . . .	20
Scheme 1.7	Comparison of product distributions following the irradiation of a series of methoxy-substituted benzyl acetates . . . . .	23
Scheme 1.8	Irradiations of substituted benzyl esters ( <b>16a</b> ) and 1-naphthylmethyl esters ( <b>16b</b> ) in methanol solution . . . . .	25
Scheme 1.9	Preferred mechanistic pathways for formation of radical-derived and ion-derived products from the photolysis of arylmethyl esters . . . . .	27
Scheme 1.10	Formation and reactivity of triene intermediate <b>22</b> following irradiation of 3,5-dimethoxybenzyl acetate <b>12c</b> in methanol . . . . .	28
Scheme 2.1	Early observation of photochemical bond cleavage followed by carbocation rearrangement . . . . .	31
Scheme 2.2	Competition between elimination and rearrangement of photochemically generated carbocation <b>31</b> , Ar = 4-(CH <sub>3</sub> ) <sub>2</sub> N(C <sub>6</sub> H <sub>4</sub> ) . . . . .	32
Scheme 2.3	The formation of ketone <b>35</b> via the photochemical pinacol rearrangement of carbocation <b>36</b> . . . . .	33

Scheme 2.4	The photochemistry of fluorenol derivative <b>38</b> in methanol . . . . .	34
Scheme 2.5	Proposed reactivity of substrate <b>44</b> : photofragmentation, carbocation rearrangement ( <b>45</b> to <b>46</b> ), and trapping by nucleophiles . . . . .	36
Scheme 2.6	The synthesis of 1-(3,5-dimethoxyphenyl)-2-(4-methoxyphenyl)ethyl ethanoate <b>44</b> . . . . .	38
Scheme 2.7	The synthesis of aldehydes <b>49</b> and <b>58</b> <i>via</i> Darzens' sequence . . . . .	38
Scheme 2.8	Products formed by photolysis of ester <b>44</b> in methanol and TFE . . . . .	41
Scheme 2.9	Independent synthesis of <b>52</b> , <b>53</b> , and <b>54</b> for comparison with products formed <i>via</i> photolysis of ester <b>44</b> . . . . .	43
Scheme 2.10	Products detected following the irradiation of the methoxy-substituted <i>trans</i> -stilbene <b>52</b> in methanol and TFE . . . . .	48
Scheme 3.1	Photochemical addition of methanol to 1,2-diphenylcyclobutene <b>65</b> . . . . .	65
Scheme 3.2	The photochemical addition of methanol to <i>trans</i> - <b>60</b> <i>via</i> competing mechanisms (direct addition and carbene insertion) . . . . .	66
Scheme 3.3	Synthesis of methoxy-substituted stilbene derivatives <b>71-74</b> . . . . .	71
Scheme 3.4	Products detected following 300 nm irradiation of <i>trans</i> - <b>60</b> and <i>trans</i> - <b>71-74</b> in methanol . . . . .	79
Scheme 3.5	Products detected following 300 nm irradiation of <i>trans</i> - <b>60</b> and <i>trans</i> - <b>71-74</b> in TFE . . . . .	84
Scheme 3.6	Products detected following 300 nm irradiation of <i>cis</i> - <b>60</b> and <i>cis</i> - <b>71-74</b> in TFE . . . . .	87
Scheme 3.7	Changing of the product from irradiation of <sup>-</sup> <i>trans</i> -4-methoxystilbene ( <i>trans</i> - <b>71</b> ) with changing concentration of hydrochloric acid in acetonitrile . . . . .	101

Scheme 4.1	Products resulting from the irradiation of 2,3-dimethyl-2-butene <b>79</b> in either octane or methanol . . . . .	106
Scheme 4.2	Photohydration of a substituted styrene derivative, with two possible electronic structures for the reactive excited state species . . . . .	109
Scheme 4.3	Comparison of the mechanism for photohydration of 3-methoxystyrene with the supposed mechanism for photochemical TFE addition to <i>trans</i> - <b>72</b> . . . . .	115
Scheme 4.4	Syntheses of methoxy-substituted <i>trans</i> -1-arylpropenes <i>trans</i> - <b>96-99</b> . . . . .	117
Scheme 4.5	Products detected following irradiation of methoxy-substituted styrenes <b>91-94</b> in TFE . . . . .	138
Scheme 4.6	Products detected following irradiation of methoxy-substituted <i>trans</i> -arylpropenes <i>trans</i> - <b>96-99</b> in TFE . . . . .	141
Scheme 4.7	Mechanism for the addition of TFE-OD to the excited state of <i>trans</i> - <b>73</b> . . . . .	178
Scheme 4.8	Mechanism for the addition of TFE-OD to the excited state of <i>trans</i> - <b>71</b> . . . . .	179
Scheme 5.1	The energy-coordinate diagram for 4- <i>N,N</i> -dimethylaminobenzonitrile <b>106</b> in non-polar solvents (solid line) or polar solvents (dashed line) . . . . .	183
Scheme 5.2	Simplified energy state diagram for the excited state behaviour of donor-acceptor stilbene derivatives . . . . .	186
Scheme 5.3	Syntheses of <b>113-120</b> (cis and trans isomers for each) . . . . .	190
Scheme 5.4	Synthesis of <b>112</b> (both cis and trans isomers). . . . .	190
Scheme 5.5	Products detected following 300 nm irradiation of <i>trans</i> - <b>111-120</b> in TFE . . . . .	212
Scheme 7.1	The method used to process the raw chromatogram data for Chapter 2 photolysis experiments using the irradiation of <b>52</b> in TFE as an example . . . . .	246
Scheme 7.2	The method used to process the raw chromatogram data for Chapter 3 irradiation experiments using the irradiation of <i>trans</i> - <b>52</b> in TFE as an example . . . . .	253

## List of Tables

Table 1.1	Comparison of $\sigma^+$ values for the solvolysis rates of substituted cumyl chlorides in 90% aqueous acetone .	8
Table 1.2	Compilation of measurements for the comparison of carbocation stabilities in the gas phase and in solution .	10
Table 1.3	Rate constants for the decay of selected arylmethyl carbocations in TFE and HFIP (from Reference 47) .	16
Table 2.1	Product yields after photolysis of ester <b>44</b> for 1 hour in methanol and TFE . . . . .	40
Table 2.2	Product yields after irradiation of methoxy-substituted <i>trans</i> -stilbene <b>52</b> in methanol and TFE . . . . .	48
Table 3.1	Photophysical data in non-polar and polar solvents (hexanes and acetonitrile) for <i>trans</i> -stilbene ( <i>trans</i> - <b>60</b> ) and the three isomeric mono-amino stilbenes <i>trans</i> - <b>62</b> , <i>trans</i> - <b>63</b> , and <i>trans</i> - <b>64</b> . . . . .	62
Table 3.2	Summary of photophysical data for methoxy-substituted stilbene derivatives in acetonitrile . . . . .	72
Table 3.3	Percent conversions and product yields following one-hour irradiation of <i>trans</i> - <b>60</b> and <i>trans</i> - <b>71-74</b> in methanol (300 nm) . . . . .	79
Table 3.4	Percent conversions and product yields following ten-minute irradiation of <i>trans</i> - <b>60</b> and <i>trans</i> - <b>71-74</b> in TFE (300 nm) . . . . .	84
Table 3.5	Percent conversions and product yields following one-hour irradiation of <i>cis</i> - <b>60</b> and <i>cis</i> - <b>71-74</b> in TFE (300 nm) . . . . .	87
Table 3.6	Quantum yields of fluorescence $\phi_f$ for <i>trans</i> - <b>73</b> in various mixtures of acetonitrile and TFE or TFE, and Stern-Volmer ratios $\phi_f^0/\phi_f$ . . . . .	90
Table 3.7	Summary of photophysical data for methoxy-substituted stilbene derivatives in acetonitrile, taken from Reference 110 . . . . .	95

Table 4.1	Rate constants for the quenching of excited state styrene derivatives by hydronium ion ( $k_{H^+}$ ) and substituent constants for the $\sigma^{hv}$ scale.	111
Table 4.2	Summary of photophysical data for methoxy-substituted styrenes <b>90-94</b> in acetonitrile	119
Table 4.3	Summary of photophysical data for arylpropenes <i>trans</i> - <b>94-99</b> in acetonitrile	119
Table 4.4	Comparison of photophysical properties for methoxy-substituted styrenes <b>91-94</b> in cyclohexane and acetonitrile	125
Table 4.5	Comparison of photophysical properties for methoxy-substituted arylpropenes <i>trans</i> - <b>96-99</b> in hexanes and acetonitrile	125
Table 4.6	Quantum yields of isomerization $\phi_{ic}$ for the methoxy-substituted <i>trans</i> -1-arylpropenes <i>trans</i> - <b>96-99</b> in hexanes and acetonitrile	127
Table 4.7	The fluorescence maxima (in nanometers) for the methoxy-substituted <i>trans</i> -stilbenes in a series of six solvents	128
Table 4.8	Literature values for the dielectric constant $\epsilon$ and the refractive index $n$ , as well as values for the solvent parameter $\Delta f$ (calculated using Equation 4.8).	129
Table 4.9	Stokes' shifts (in nanometers) for the fluorescence of <i>trans</i> - <b>60</b> and <i>trans</i> - <b>71-74</b> in a series of six solvents	130
Table 4.10	Analysis of the solvatochromic behaviour of <i>trans</i> - <b>60</b> and <i>trans</i> - <b>71-74</b> using the Lippert-Mataga treatment (Equation 4.7).	131
Table 4.11	Fluorescence quantum yields for <i>trans</i> - <b>60</b> and <i>trans</i> - <b>71-74</b> in a series of six solvents.	132
Table 4.12	Monoexponential singlet lifetimes for <i>trans</i> - <b>72</b> and <i>trans</i> - <b>73</b> in a series of six solvents, as well as the fast and slow components for the biexponential decay of <i>trans</i> - <b>73</b>	134



Table 4.13	Quantum yields of isomerization for the methoxy-substituted stilbenes <i>trans</i> - <b>60</b> and <i>trans</i> - <b>71-74</b> in cyclohexane and acetonitrile . . . . .	138
Table 4.14	Percent conversions of the methoxy-substituted styrenes <b>91-94</b> after two minutes of 300 nm irradiation in TFE . . . . .	140
Table 4.15	Percent conversions of the arylpropenes <i>trans</i> - <b>96-99</b> after two minutes of 300 nm irradiation in TFE . . . . .	142
Table 4.16	Quenching of fluorescence quantum yields $\phi_f$ and singlet lifetimes $\tau_s$ by TFE for stilbenes <i>trans</i> - <b>60</b> and <i>trans</i> - <b>71-74</b> . . . . .	143
Table 4.17	Quenching of fluorescence quantum yields $\phi_f$ and singlet lifetimes $\tau_s$ by TFE for styrenes <b>91-94</b> . . . . .	143
Table 4.18	Quenching of fluorescence quantum yields $\phi_f$ and singlet lifetimes $\tau_s$ by TFE for arylpropenes <i>trans</i> - <b>96-99</b> . . . . .	144
Table 4.19	$^1\text{H}$ NMR results for the $\text{A}_3\text{X}$ coupling pattern of the solvent adducts following irradiation of styrenes <b>91-94</b> in TFE or TFE-OD . . . . .	153
Table 4.20	GC-MS data for the solvent adducts produced following irradiation of styrenes <b>91-94</b> in TFE . . . . .	154
Table 4.21	GC-MS data for the solvent adducts produced following irradiation of styrenes <b>91-94</b> in TFE-OD . . . . .	154
Table 4.22	GC-MS data for the solvent adducts produced following irradiation of arylpropenes <i>trans</i> - <b>96-99</b> in TFE . . . . .	156
Table 4.23	GC-MS data for the solvent adducts produced following irradiation of arylpropenes <i>trans</i> - <b>96-99</b> in TFE-OD . . . . .	156
Table 4.24	Summary of the $^1\text{H}$ NMR spectra of the products derived from irradiation of the stilbenes <i>trans</i> - <b>60</b> and <i>trans</i> - <b>71-74</b> in TFE and TFE-OD. . . . .	157
Table 4.25	Estimates of the solvent isotope effect $k_{\text{H}}/k_{\text{D}}$ for irradiations of the stilbenes, styrenes, and <i>trans</i> -1-arylpropenes in TFE and TFE-OD . . . . .	162

Table 4.26	Excited state dipole moments $\mu_e$ and the quantum yields of isomerization $\phi_{tc}$ for the methoxy-substituted <i>trans</i> -stilbene derivatives in cyclohexane (Cyc) or acetonitrile (AcN) . . . . .	169
Table 5.1	Photophysical data for donor-acceptor stilbenes <b>109</b> and <b>110</b> (data from Reference 101) . . . . .	187
Table 5.2	Summary of photophysical data for the substituted derivatives of <i>trans</i> -3,5-dimethoxystilbene in acetonitrile . . . . .	191
Table 5.3	Stokes' shifts (in wavenumbers, $\text{cm}^{-1}$ ) for the fluorescence of the <i>para</i> -substituted derivatives of <i>trans</i> - <b>73</b> in a series of six solvents . . . . .	200
Table 5.4	Stokes' shifts (in wavenumbers, $\text{cm}^{-1}$ ) for the fluorescence of the <i>meta</i> -substituted derivatives of <i>trans</i> - <b>73</b> in a series of six solvents . . . . .	200
Table 5.5	Data for the solvatochromic plots (Figure 5.12) of the <i>para</i> -substituted derivatives of <i>trans</i> -3,5-dimethoxystilbene . . . . .	202
Table 5.6	Data for the solvatochromic plots (Figure 5.13) of the <i>meta</i> -substituted derivatives of <i>trans</i> -3,5-dimethoxystilbene . . . . .	202
Table 5.7	Fluorescence quantum yields for the <i>para</i> -substituted derivatives of <i>trans</i> -3,5-dimethoxystilbene in a series of six solvents . . . . .	203
Table 5.8	Fluorescence quantum yields for the <i>meta</i> -substituted derivatives of <i>trans</i> -3,5-dimethoxystilbene in a series of six solvents . . . . .	204
Table 5.9	<i>Short</i> component of biexponential singlet lifetimes for the <i>para</i> -substituted derivatives of <i>trans</i> - <b>73</b> in a series of six solvents (all values in nanoseconds) . . . . .	206
Table 5.10	<i>Short</i> component of biexponential singlet lifetimes for the <i>meta</i> -substituted derivatives of <i>trans</i> - <b>73</b> in a series of six solvents (all values in nanoseconds) . . . . .	207

Table 5.11	<i>Long</i> component of biexponential singlet lifetimes for the <i>para</i> -substituted derivatives of <i>trans</i> - <b>73</b> in a series of six solvents (all values in nanoseconds)	208
Table 5.12	<i>Long</i> component of biexponential singlet lifetimes for the <i>meta</i> -substituted derivatives of <i>trans</i> - <b>73</b> in a series of six solvents (all values in nanoseconds)	209
Table 5.13	Quantum yields of isomerization for <i>trans</i> - <b>73</b> and the substituted derivatives <i>trans</i> - <b>111-120</b> in cyclohexane and acetonitrile	211
Table 5.14	Percent conversions and product yields following ten minute irradiation of <i>trans</i> - <b>73</b> and <i>trans</i> - <b>111-120</b> in TFE (300 nm)	215
Table 7.1	Ratios of cis:trans FID response for stilbene substrates	252
Table 7.2	Stokes' shifts (in wavenumbers) for the fluorescence of <i>trans</i> - <b>60</b> and <i>trans</i> - <b>71-74</b> in a series of six solvents	265

## Abstract

The photochemistry of 1-(3,5-dimethoxyphenyl)-2-(4-methoxyphenyl)ethyl ethanoate was investigated in methanol and 2,2,2-trifluoroethanol (TFE). Following photolysis of this ester in either solvent, two ether products were obtained: one resulting from trapping of the cation formed directly by photofragmentation, and one that was expected to form *via* a carbocation rearrangement mechanism. Closer inspection of the data revealed that the second product was actually formed by photoaddition of the solvent to *trans*-3,4',5-trimethoxystilbene, a byproduct of the initial ester photofragmentation.

A set of five methoxy-substituted stilbene derivatives demonstrated the same TFE photoaddition chemistry. An important difference in reactivity was observed for *trans*-3,5-dimethoxystilbene (which reacted after 10 minutes of irradiation in TFE), and *trans*-4-methoxystilbene (which required one hour to react under the same conditions). The fluorescence of all five *trans* isomers was quenched by addition of TFE. Nuclear magnetic resonance spectroscopy of the products formed by irradiation in TFE-OD indicated that the proton and nucleophile are attached to two adjacent atoms of the original alkene double bond. Irradiation of the corresponding methoxy-substituted styrenes and *trans*-1-arylpropenes in TFE produced the analogous solvent adducts. Transient carbocation intermediates were observed following laser flash photolysis of the stilbenes in 1,1,1,3,3,3-hexafluoroisopropanol. The results are consistent with a mechanism that involves photoprotonation of the methoxy-substituted *trans*-stilbenes by TFE, followed by nucleophilic trapping of short-lived carbocation intermediates.

Compared to the other stilbenes, *trans*-3,5-dimethoxystilbene displayed a large quantum yield of fluorescence ( $\phi_f = 0.32$ ) and a low quantum yield of *trans*-*cis* isomerization ( $\phi_{tc} = 0.29$ ). The singlet state of this substrate was unusually long-lived, and decayed according to biexponential kinetics (fast decay  $\tau_s = 3.9$  ns; slow decay  $\tau_s = 18.5$  ns). Analysis of the solvent-induced Stokes' shifts of the fluorescence maxima allowed calculation of the excited state dipole moment,  $\mu_e = 13.2$  D. Several substituted derivatives of *trans*-3,5-dimethoxystilbene displayed similar photophysical properties and the same high reactivity towards TFE. The results indicate that the excited state of the *trans*-3,5-dimethoxystilbene chromophore has substantial charge transfer character.

## List of Symbols and Abbreviations Used

### *Physical Organic Chemistry*

$S_N1$	unimolecular nucleophilic substitution
$S_N2$	bimolecular nucleophilic substitution
$E1$	unimolecular elimination
$\rho$	reaction constant
$\sigma$	substituent constant
$pK_{R^+}$	scale of carbocation stability (defined in Eq. 1.2)
$H_R$	acidity function (defined in Eq. 1.3)
$a_{H^+}$	activity coefficient for $H^+$
$a_w$	activity coefficient for water
$a_{R^+}$	activity coefficient for carbocation
$a_{ROH}$	activity coefficient for alcohol
$IE$	ionization energy
$E_{1/2}(ox)$	oxidation potential
$\Delta H_{hydride}$	hydride ion affinity
$\ddagger$	transition state
$\Delta G^\ddagger$	free energy of activation
$\delta\nu$	difference between broadened and natural line width
$\nu_{AB}$	difference between averaged NMR signals

### *Kinetics*

$k_C$	rate constant for cation formation
$k_{CO_2}$	rate constant for decarboxylation
$k_{ET}$	rate constant for electron transfer
$k_{HFIP}$	rate constant for cation reaction with HFIP
$k_{H^+}$	rate constant for protonation
$k_N$	rate constant for cation reaction with nucleophile
$k_{N_3}$	rate constant for cation reaction with azide ion
$k_S$	rate constant for cation reaction with solvent
$k_{TFE}$	rate constant for cation reaction with TFE
$k_X$	rate constant for cation reaction with leaving group
$N_+$	Ritchie selectivity constant (defined in Eq. 1.7)

### *General Photochemistry*

$h\nu$	irradiation
$S_0$	singlet ground state
$S_1$	first singlet excited state
$S_2$	second singlet excited state
$T_1$	first triplet excited state
$R_s^*$	reactive intermediate (singlet pathway)
$R_t^*$	reactive intermediate (triplet pathway)

$P_s$	product (singlet pathway)
$P_t$	product (triplet pathway)
$k_f$	rate constant for fluorescence
$k_{ic}$	rate constant for internal conversion
$k_{isc}$	rate constant for intersystem crossing
$k_q$	rate constant for bimolecular quenching
$Q$	quencher
$k_t$	total rate of excited state decay
$\tau_s$	excited state lifetime (defined in Eq. 1.8)
$\phi_f$	quantum yield of fluorescence
$\phi_{isc}$	quantum yield of intersystem crossing
$\phi_{tc}$	quantum yield of trans-cis isomerization

### *Stilbene Photochemistry*

$t_{S0}$	singlet ground state, trans geometry
$t_{S1}$	first singlet excited state, trans geometry
$t_{T1}$	first triplet excited state, trans geometry
$p_{S0}$	singlet ground state, perpendicular geometry
$p_{S1}$	first singlet excited state, perpendicular geometry
$p_{T1}$	first triplet excited state, perpendicular geometry
$c_{S0}$	singlet ground state, cis geometry
$c_{S1}$	first singlet excited state, cis geometry

FC	Frank-Condon excited state
CT	charge transfer excited state
ICT	internal charge transfer
TICT	twisted internal charge transfer
$B_{S_0}$	singlet ground state, planar geometry
$B_{S_1}$	first singlet excited state, planar geometry
$A_{S_0}$	singlet ground state, twisted geometry
$A_{S_1}$	first singlet excited state, twisted geometry

### *Solvatochromic Analysis*

$\nu_{\text{ex}}$	excitation maximum (in wavenumbers)
$\nu_{\text{fluor}}$	fluorescence maximum (in wavenumbers)
$\mu_{\text{e}}$	excited state dipole moment
$\mu_{\text{g}}$	ground state dipole moment
$\Delta f$	solvent parameter (defined in Eq. 4.8)
$\epsilon$	solvent dielectric constant
$\eta$	solvent refractive index
$\epsilon_0$	permittivity of a vacuum
$h$	Plank's constant
$c$	speed of light
$a$	solvent cavity radius



### *Solvents and Chemicals*

AcN	acetonitrile
Cyc	cyclohexane
HFIP	1,1,1,3,3,3-hexafluoroisopropanol
DCC	dicyclohexylcarbodiimide
DMAP	4-N,N-dimethylaminopyridine
DMSO	dimethylsulphoxide
TFE	2,2,2-trifluoroethanol
TFE-OD	deuterated TFE ( $\text{CF}_3\text{CH}_2\text{OD}$ )
THF	tetrahydrofuran

### *Experimental Techniques*

UV	ultraviolet
Vis	visible
$\lambda_{\text{max}}$ (abs)	wavelength of maximum absorption
A	absorbance
$\lambda_{\text{max}}$ (ex)	wavelength of highest intensity in excitation spectrum
$\lambda_{0,0}$	wavelength of 0,0 transition
$\epsilon_{\text{max}}$	extinction coefficient for absorption maximum
$\lambda_{\text{max}}$ (fluor)	wavelength of maximum fluorescence
F	integral of fluorescence intensity

LFP	laser flash photolysis
$\Delta OD$	change in optical density
GC-MS	gas chromatography, mass selective detector
$m/z$	mass to charge ratio
GC-FID	gas chromatography, flame ionization detector
NMR	nuclear magnetic resonance
$\delta$	chemical shift
C	relative yield of cis isomer formation

## Acknowledgments

I must begin this section by sincerely thanking my supervisor, Dr. James Pincock. I believe that my experience in his research group has been what every student has in mind when they begin graduate studies. His sound advice and constant support have been of enormous assistance in my progress over the past five years. I am extremely fortunate to have benefited from Dr. Pincock's great skill as a research supervisor and teacher.

Through the course of my graduate work, I have had the pleasure of working with many wonderful people. Alex Pincock and Carlos González have both made life in the Pincock lab an enjoyable experience. Too many times I have called on Alex to help me finish a late experiment, and she has never turned me down. Carlos has been the perfect colleague during our time together – I am grateful for his willingness to share laboratory equipment and to accommodate my research needs, particularly during the important last year of experiments. Over the course of my program many talented undergraduate students have completed honours projects in Dr. Pincock's laboratory, and they have all helped to make the lab a fun place to work. The members of the research groups of Dr. Fran Cozens and Dr. Norm Schepp deserve special mention for their assistance in the lab, and also for their engaging discussions during group meetings. In addition, Amy Keirstead took on the task of proofreading many of the chapters in this report, and I very much appreciate her attention to detail.

The research described in this thesis has been made possible through the kind help of many collaborators. Jim Hilborn and Sepracor Canada have been unfaltering in their support for Dr. Pincock's research program – their generous donation of chemicals has allowed my research to progress much faster than it would have otherwise. I am very

grateful for the assistance of Dr. Dayal DeCosta, who prepared several of the stilbene substrates described in Chapter 5. The laser experiments described in Chapter 4 were performed with much assistance from Dr. Norm Schepp, and I appreciate his patience in helping me obtain those important results. Much of my research has relied on the use of GC-MS, and so I am indebted to Marc Diotte and Miles Snow of Perkin Elmer for their technical support. In addition, Brian Millier, Dr. Stuart Grossert, and Dr. Louis Ramaley were always quick to lend a hand whenever my knowledge of instrumental maintenance was at its limits. The calculations reported in Chapters 4 and 5 were performed with assistance from Heidi Muchall and the members of the Centre for Research in Molecular Modeling at Concordia University. I must thank Mike Lumsden and Bob Berno for helping me obtain all of my NMR data using the excellent resources at ARMRC. I would also like to acknowledge a former member of the Pincock group, Roumiana Stefanova, who instructed me on the use of the GC-FID instrument that I used to obtain many of the results described in this report.

I am grateful for the financial support provided to me by the Dalhousie University Faculty of Graduate Studies, the Department of Chemistry, and the Natural Sciences and Engineering Research Council of Canada. I also acknowledge travel grants from the Dalhousie Student Union and the Dalhousie Chemistry Graduate Student Society.

There are many other people that need to be thanked for their help over the past five years. My time as a graduate student has been fantastic, due in large part to my friends and family. I must thank my parents Dave and Carol, and my sister Janet for all of their kind understanding and encouragement. Finally, my deepest thanks go to my wife Julie for all her love and support – I simply could not have done this without you.

# Chapter 1. Introduction to Carbocation Intermediates and Their Formation *via* Excited State Reactions

## 1.1 Overview of Thesis

The study of a reaction mechanism requires the identification of the presence or absence of any reactive intermediates that may be formed during the conversion of product to reactant.<sup>1</sup> One of the classic examples of an intermediate involved in reactions of organic compounds is a trivalent carbon species bearing a positive charge ( $R_3C^+$ ). Although the precise term for these intermediates is *carbenium ion*,<sup>2</sup> this report will employ the more general term *carbocation*. While the vast majority of reactions that involve carbocationic intermediates are ground state reactions, this thesis deals with the generation of these species *via* photochemical processes.

The first chapter of this report will provide an introduction to the selected field of research, beginning with the general aspects of carbocation chemistry in Section 1.2. The important aspects of carbocation generation, stability, and reactivity will be addressed, although a complete discussion of such a vast subject is beyond the scope of the current work. Section 1.3 will provide an introduction to the photophysical processes that a molecule may undergo upon absorption of a photon, and the relationship between these processes and photochemical reactions. Section 1.4 will focus on the generation of benzylic carbocations ( $ArC^+R_2$ ) *via* photochemical bond cleavage reactions, with particular attention to the photofragmentation of arylmethyl esters.

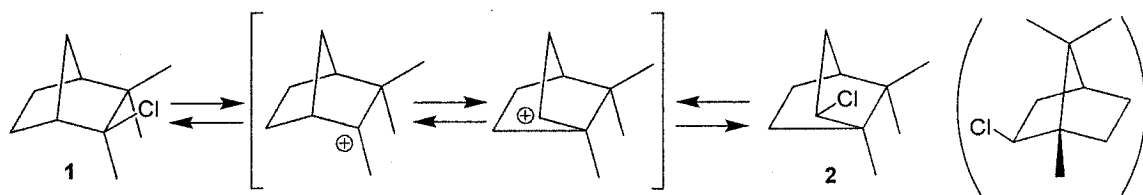
The discussion of the current research program begins in Chapter 2, with a report on the photochemistry of a substrate designed to allow the direct observation of benzylic carbocation rearrangements. Chapter 3 will detail the preliminary investigations of the photochemical addition of alcohols to several methoxy-substituted derivatives of *E*-1,2-diphenylethenes (*trans*-stilbenes). Chapter 4 will compare the photochemical addition of alcohols to stilbenes with the corresponding reactions of methoxy-substituted arylethenes (styrenes) and *trans*-1-arylpropenes ( $\beta$ -methyl styrenes), and provide evidence for the presence of carbocation intermediates in all three cases. Chapter 5 reports on the excited state charge transfer properties observed for various derivatives of *trans*-3,5-dimethoxystilbene, in order to further the understanding of the photoaddition reactions described in Chapters 3 and 4. Finally, Chapter 6 provides the experimental details for the various research projects.

## 1.2 Carbocations

### 1.2.1 Early Studies of Carbocations

The first proposals of carbocations as viable entities in chemical reactions appeared at the beginning of the 20<sup>th</sup> century.<sup>3</sup> Baeyer and Villiger<sup>4</sup> discovered that the treatment of triphenylmethanol with sulphuric acid, and of triphenylmethyl chloride with aluminium trichloride (both colourless), produced brightly coloured reaction mixtures. Shortly thereafter, electrical conductivity measurements of triarylmethyl halides in liquid sulphur dioxide led Gomberg<sup>5</sup> to propose a cationic carbon species, designated  $(\text{C}_6\text{H}_5)_3\text{C}^+$  as a formula representation and “carbyl salt” as a general term. Several years later, isolation of the perchlorate salts of several triarylmethyl carbocations<sup>6</sup> led to the general acceptance of these species throughout the chemical community.

The involvement of carbocations as intermediates in chemical reactions was first proposed in a 1922 study by Meerwein and van Emster,<sup>7</sup> which examined the conversion of camphene hydrochloride **1** to isobornyl chloride **2** (Scheme 1.1). The yield of the rearrangement product **2** was increased by using solvents with high dielectric constants (e.g., nitromethane and sulphur dioxide) or by the addition of catalysts such as aluminium trichloride. The striking similarity between these reaction conditions and those that had previously been used for the preparation of the triarylmethyl cations led Meerwein and van Emster to the conclusion that the rearrangement process is initiated by ionization to give a carbocation intermediate. Rearrangement of the short-lived intermediate followed by re-addition of the chloride anion completes the reaction pathway. The importance of this work lies not only in the extension of the carbocation concept to mechanistic chemistry, but also in the departure from the triarylmethyl system.



Scheme 1.1 Rearrangement of camphene hydrochloride **1** to isobornyl chloride **2** via a carbocation intermediate.

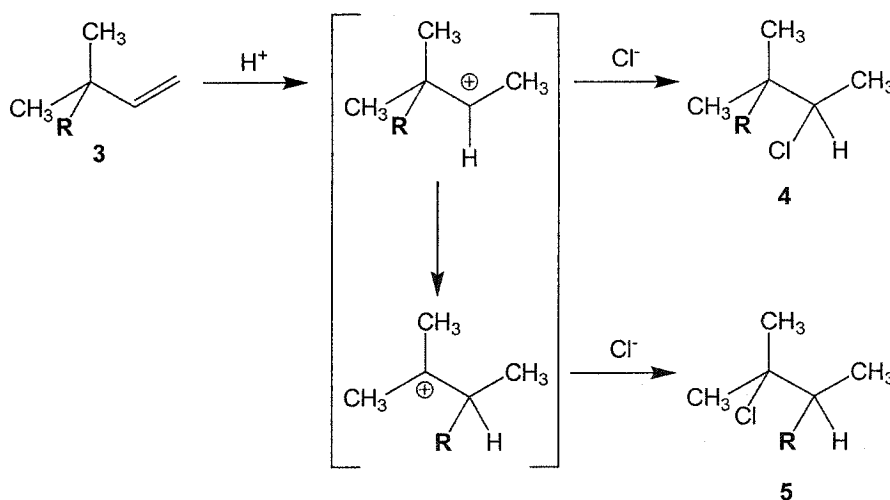
In 1927, Ward observed remarkable differences in the kinetics for solvolysis of 2-chloro-1-phenylethane and 1-chloro-1-phenylethane in basic media.<sup>8</sup> While the 2-chloro derivative underwent a bimolecular reaction that depended on the concentrations of both the alkyl chloride and hydroxide ion, the reaction of the 1-chloro substrate followed a unimolecular rate law that was independent of the concentration of base. A satisfactory explanation for these observations was provided by Ingold, who proposed that the

mechanism of benzyl chloride solvolysis was dependent on the reaction medium – in basic solution the hydroxide ion displaces the chloride, while in acidic media the reaction proceeds *via* prior removal of chloride ion to produce a benzylic carbocation intermediate.<sup>9</sup> Ingold later extended these concepts to the solvolysis of all alkyl substrates containing a leaving group by labelling the two mechanistic extremes  $S_N2$  (bimolecular nucleophilic substitution) and  $S_N1$  (unimolecular nucleophilic substitution).<sup>10</sup> For simple alkyl substrates not containing an aryl group,  $S_N1$  reactions proceed readily for tertiary compounds due to stabilization of the electron-deficient carbocation intermediate through either inductive electron donation or hyperconjugation. In turn, the ionization of secondary or primary substrates proceeds much more slowly, if at all. The reactivity of benzylic substrates in  $S_N1$  reactions, as well as the extremely high stability of the triarylmethyl cations, is attributed to resonance electron donation through the conjugated  $\pi$ -system. Other substituents are capable of stabilizing adjacent carbocations through resonance interactions, including alkenes (*i.e.*, allylic cations) and hydroxyl groups.

The identification of carbocations as intermediate species allowed Whitmore to propose a rationale for the observation of rearrangement products in many organic reactions in 1932.<sup>11</sup> This work also provided a means by which to assess the relative stability of various carbocations. Whitmore used several literature examples to show that following departure of a leaving group in an  $S_N1$  reaction, two possible side reactions can compete with nucleophilic attack on the intermediate carbocation. One side reaction involves removal of a proton from an adjacent carbon to produce a neutral alkene – this mechanism is designated E1 (unimolecular elimination). The second possibility involves



transfer of a substituent to the cationic carbon centre, resulting in a rearranged carbocation of greater stability than the original intermediate. Once formed, the rearranged cation may undergo nucleophilic attack, deprotonation, or further rearrangement. Whitmore emphasized that other reaction pathways involving carbocation intermediates would be subject to similar rearrangements. The addition of hydrochloric acid to 3-methyl-1-butene and 3,3-dimethyl-1-butene, as shown in Scheme 1.2, provide excellent examples of this concept.<sup>12</sup> In these reactions, protonation of the butene **3** results in a secondary carbocation, in accord with Markovnikov's rule for addition to alkenes. Attack of the carbocation intermediate by chloride ion yields the expected product **4**, while rearrangement to the more stable tertiary carbocation leads to the isomeric product **5**. Later studies by Pocker<sup>13</sup> employed gas chromatography to determine the accurate product yields for the reactions: for R = H, 40% **4**, 60% **5**; and for R = CH<sub>3</sub>, 17% **4**, 83% **5**.



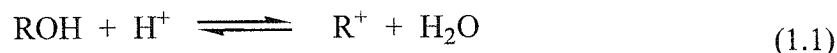
Scheme 1.2 Addition of hydrochloric acid to 3-methyl-1-butene (R = H) and 3,3-dimethyl-1-butene (R = CH<sub>3</sub>), with rearrangement of the carbocation intermediate.

The concepts of  $S_N1/S_N2$  reactivity and simple carbocation rearrangements are now used to provide a foundation for the study of reaction mechanisms in introductory organic chemistry textbooks.<sup>14</sup> However, the early studies of carbocations served as a starting point for an intense research effort designed to understand these species as completely as possible. The results of these investigations have been compiled in advanced organic chemistry textbooks,<sup>15,16,17</sup> literature reviews,<sup>18</sup> and books.<sup>19,20,21</sup> The sections that follow will summarize the important studies of carbocation stability (Section 1.2.2) and reactivity (Section 1.2.3) that have been pursued, with a particular emphasis on the properties of benzylic carbocations that have been studied in the current research projects.

### 1.2.2 Measurements of Carbocation Stability

An early method that was developed for the comparison of carbocation stabilities depends on the equilibrium for cation formation *via* ionization of the corresponding alcohol, Equation 1.1. For all but the most stable cations, however, this reaction will only proceed in strongly acidic solutions. Using the acidity function techniques first developed by Hammett,<sup>22</sup> Deno and co-workers<sup>23</sup> were able to describe the relative stability of a series of carbocations in terms of the  $pK_{R+}$  scale, Equation 1.2. The acidity function  $H_R$  is defined in Equation 1.3, where  $a_{H+}$  and  $a_w$  are the activities for the proton and water, and  $a_{R+}$  and  $a_{ROH}$  are the activity coefficients for the cation and the alcohol. According to this treatment, the formation of a highly stabilized carbocation requires a less acidic solution than does an unstable carbocation, and so the former will have a higher (more positive)  $pK_{R+}$  value. For example, the 4-methoxytriphenylmethyl cation

has a  $pK_{R^+}$  value of -3.4, while the corresponding value for the 4-nitrotriphenylmethyl cation is -9.2. In comparison to the parent triphenylmethyl cation ( $pK_{R^+} = -6.6$ ), these values illustrate the stabilization of the cation by the electron donating methoxy substituent and the destabilization by the electron withdrawing nitro substituent.



$$pK_{R^+} = \log \left( \frac{[R^+]}{[ROH]} \right) + H_R \quad (1.2)$$

$$H_R = -\log \left( \frac{a_{H^+} a_{ROH}^0}{a_{R^+}^0} \right) + \log a_w \quad (1.3)$$

The utility of  $pK_{R^+}$  values is limited by two factors. Firstly, their determination requires quantifying the ratio of cation to unreacted alcohol, typically by UV-Vis spectroscopy. In addition, even the use of very concentrated acid solution only allows access to cations that are reasonably stable. While the triarylmethyl cations mentioned above meet these requirements easily, extension of  $pK_{R^+}$  scales to include the less stable species that form during the course of chemical reactions is problematic.

A technique that has been used with great success to investigate reactions proceeding through benzylic carbocation intermediates is the  $\sigma^+$  scale of substituent constants. The scale was developed by Brown and Okamoto,<sup>24</sup> who compared the rates of ionization for a series of substituted 2-aryl-2-chloropropanes (cumyl chlorides) in 90% aqueous acetone. In comparison to the original Hammett  $\sigma$  scale for the deprotonation of benzoic acids in water,<sup>25</sup> the cumyl chloride system provides a much better assessment of substituent effects for strong  $\pi$ -electron donors (*e.g.*, 4-methoxy). The  $\sigma^+$  scale was obtained using Equation 1.4, where  $k$  and  $k_H$  are the rates of ionization for substituted and

unsubstituted cumyl chlorides, respectively;  $\rho^+$  is -4.54 (determined relative to  $\rho = 1.00$  as defined for the original benzoic acid system), and  $\sigma^+$  is a characteristic of the substituent. The large negative value for the reaction constant  $\rho^+$  indicates that substantial positive charge is developed in the transition state of the ionization process, likely *en route* to a carbocation intermediate. Table 1.1 provides a sample of  $\sigma^+$  values for a variety of meta and para substituents.<sup>26</sup>

$$\log\left(\frac{k}{k_H}\right) = \rho^+ \sigma^+ \quad (1.4)$$

Substituent	$\sigma^+$ (para)	$\sigma^+$ (meta)
OCH <sub>3</sub>	-0.778	0.047
CH <sub>3</sub>	-0.311	-0.066
H	0	0
F	-0.073	0.352
CF <sub>3</sub>	0.612	0.520
CN	0.659	0.562

Table 1.1 Comparison of  $\sigma^+$  values for the solvolysis rates of substituted cumyl chlorides in 90% aqueous acetone.

Although the  $\sigma^+$  scale does not provide a true measure of carbocation stability, it does provide valuable information regarding the development of positive charge in the transition state of a chemical transformation. A close relationship between the stability of a carbocation intermediate and the lowering of the energy barrier leading to its formation is supported by the Hammond postulate, which states (in part) that the best model for the transition state of an endothermic process is the product of the reaction.<sup>27</sup> Thus, for the endothermic formation of a carbocation intermediate, the factors responsible for lowering

the energy of the transition state should be similar to the factors that stabilize the carbocation itself. As Bethel and Gold<sup>28</sup> have pointed out, “kinetic arguments about carbenium ion stabilities [...] cannot be disregarded, for it is precisely on this seemingly insecure evidence that the main structural effects on the stability of simple carbenium ions were first recognized.” Indeed, the kinetic basis of the  $\sigma^+$  scale has not prevented it from being applied with great success to many reactions involving carbocation intermediates. Representative examples are the perchloric acid-catalyzed addition of water to substituted styrenes ( $\rho^+ = -3.53$ ),<sup>29</sup> the bromination of substituted styrenes in acetic acid ( $\rho^+ = -4.5$ ),<sup>30</sup> and the acid-catalyzed elimination of water from substituted 1,2-diphenylethanols in water ( $\rho^+ = -3.77$ ).<sup>31</sup>

Analysis of the ionization potentials of substituted benzyl radicals using  $\sigma^+$  constants gives  $\rho^+ = -20$ .<sup>32</sup> The large (negative)  $\rho^+$  value obtained emphasizes that a substituent's ability to delocalize cationic charge is greatly attenuated in solution relative to in the gas phase. In addition, there is certainly a clear correlation between the kinetic data from solution phase reactions and traditional gas phase thermodynamic measurements of stability. The absolute magnitude of carbocation stabilities calculated from gas phase results may not be representative of solution phase measurements, but the expectation is that *trends* for stability should be similar in both media. Table 1.2 provides a sample of relative carbocation stabilities determined using a variety of experimental techniques: 1) the ionization energy for production of the cation from the corresponding radical in the gas phase;<sup>32</sup> 2) the half-wave oxidation potentials of the corresponding radicals in acetonitrile solution;<sup>33</sup> 3) experimental<sup>34,35</sup> and calculated<sup>36</sup> gas phase hydride affinities; and 4) hydride affinities obtained in acetonitrile solution.<sup>37</sup>

Carbocation	IE <sup>a</sup> (kcal/mol)	E <sub>1/2</sub> (ox) <sup>b</sup> (V)	ΔH <sub>hydride</sub> <sup>c</sup> (kcal/mol)	ΔH <sub>hydride</sub> <sup>d</sup> (kcal/mol)
CH <sub>3</sub> <sup>+</sup>	229	-	314 / -	-
CH <sub>3</sub> CH <sub>2</sub> <sup>+</sup>	202	-	274 / -	-
(CH <sub>3</sub> ) <sub>2</sub> CH <sup>+</sup>	182	-	247 / -	-
(CH <sub>3</sub> ) <sub>3</sub> C <sup>+</sup>	172	-	230 / -	-
4-CH <sub>3</sub> O(C <sub>6</sub> H <sub>4</sub> )CH <sub>2</sub> <sup>+</sup>	158	0.26	- / 227	107
4-CH <sub>3</sub> (C <sub>6</sub> H <sub>4</sub> )CH <sub>2</sub> <sup>+</sup>	172	0.51	- / 236	112
(C <sub>6</sub> H <sub>5</sub> )CH <sub>2</sub> <sup>+</sup>	179	0.73	233 / 238	118
4-F(C <sub>6</sub> H <sub>4</sub> )CH <sub>2</sub> <sup>+</sup>	179	0.73	- / 241	123
4-CN(C <sub>6</sub> H <sub>4</sub> )CH <sub>2</sub> <sup>+</sup>	193	1.08	- / 247	122
(C <sub>6</sub> H <sub>5</sub> )CH <sup>+</sup> CH <sub>3</sub>	-	-	226 / -	-
(C <sub>6</sub> H <sub>5</sub> )C <sup>+</sup> (CH <sub>3</sub> ) <sub>2</sub>	-	0.16	220 / -	-

- a) Ionization energy of corresponding radical in the gas phase, Reference 32.  
b) Oxidation potential of the corresponding radical in acetonitrile versus SCE, Reference 33. c) Hydride ion affinity in the gas phase: experimental values for alkyl cations, Reference 34; benzylic cations, Reference 35; and calculated values, Reference 36. d) Hydride ion affinity in acetonitrile, Reference 37.

Table 1.2      Compilation of measurements for the comparison of carbocation stabilities in the gas phase and in solution.

The tabulated data provide quantitative measurements of the changes in carbocation “stability” that accompany changes in chemical structure. Increasing alkyl substitution leads to decreases in both the ionization energy of carbon-centered radicals

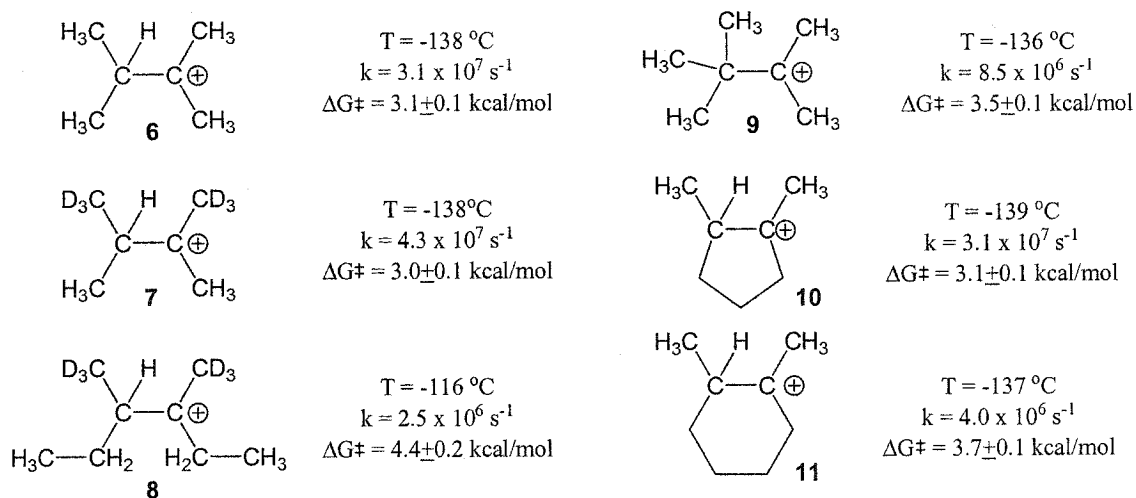
and the heat released by the reaction of the carbocation and hydride ion (note that by convention, hydride affinities are expressed as the *negative* of the enthalpy change). Similar effects are observed for benzylic carbocations with electron donating para substituents. Finally, comparison of the experimental hydride affinities for the benzylic cation in the gas phase (233 kcal/mol) and in acetonitrile solution (118 kcal/mol) emphasizes the important role that polar solvents play in assisting carbocation formation.

The importance of highly ionizing solvents, Lewis acid catalysts, and strong acid solutions for the generation and study of carbocation intermediates was emphasized by Olah, who first employed "superacid" solutions to observe persistent cations in solution.<sup>38,39</sup> The term "superacid" refers to a system that exceeds 100% sulphuric acid in strength, or  $H_0 < -12$  by Hammett's original acidity function.<sup>1</sup> Another important feature of these solvent systems is the absence of good nucleophiles to react with the cation intermediates. Olah's initial studies employed alkyl fluorides dissolved in a mixture of the Lewis acid  $SbF_5$  diluted with  $SO_2ClF$ . In this way the *tert*-butyl cation was prepared and then characterized by a  $^{13}C$  NMR shift of  $\delta = 335.2$  ppm at  $-20^\circ C$ .<sup>40</sup> These techniques were later used for the observation of a wide range of carbocations, including one study in which all of the static (with respect to rearrangement)  $C_3$  to  $C_8$  alkyl cations were completely characterized by  $^{13}C$  NMR.<sup>41</sup> More recently, Arnett and co-workers have determined the heats of ionization for several alcohols and chlorides in superacid solution, thereby providing another quantitative comparison of relative carbocation stabilities.<sup>42</sup>

Superacid solutions not only prolong the lifetimes of carbocations, but also make possible skeletal rearrangements that would not take place in traditional solution studies.

Formation of the 2-butyl cation in superacid solution at temperatures higher than  $-40\text{ }^{\circ}\text{C}$  leads to rapid formation of the more-stable *tert*-butyl cation. For those cations which undergo degenerate rearrangements, temperature-dependent NMR spectra have been observed. The line-broadening of these signals allows an estimation of the rearrangement rate to be calculated using the fast-exchange limit approximation (Equation 1.5), where  $k$  is the rate constant for rearrangement,  $\nu_{AB}$  is the difference between the two averaged signals, and  $\delta\nu$  is the difference between the broadened and natural line width.<sup>38</sup> Saunders<sup>43</sup> has performed the analysis of cations **6-11** in Scheme 1.3; here, the calculated values of  $k$  are shown (using  $\nu_{AB} = 18803\text{ Hz}$  in Equation 1.5), as well as the corresponding activation energies for the rearrangement process.

$$k = \frac{\pi (\nu_{AB})^2}{2 \delta\nu} \quad (1.5)$$

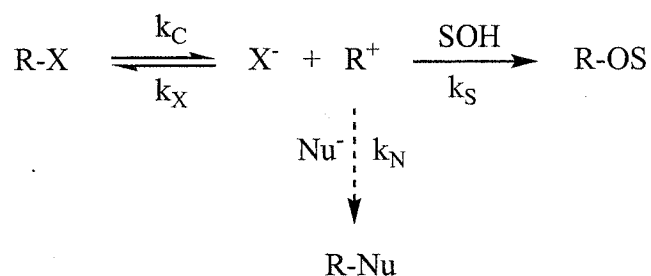


Scheme 1.3 Rates and activation energies for degenerate carbocation rearrangements.



### 1.2.3 Measurements of Carbocation Reactivity

The discussion up to this point has focussed on methods used to study the effect of structure on the ease of carbocation formation and relative thermodynamic stability. However, important consideration must also be given to the reactivity of a given carbocation once it has been formed. The Hammond postulate<sup>27</sup> – employed earlier to support the claim that relative rates of carbocation formation should provide an indication of relative carbocation stabilities – is useful in this regard. The transition state for the attack of a nucleophile on a very reactive carbocation is predicted to more closely resemble the cation itself, compared to attack on a more stabilized carbocation. In turn, the more reactive carbocation will display less selectivity towards a series of nucleophiles than will the stabilized cation – this phenomenon is referred to as the “reactivity-selectivity principle.”



Scheme 1.4 Ionization of generic substrate R-X and formation of solvent adduct R-OS and nucleophile adduct R-Nu.

Scheme 1.4 displays the possible reactions for a carbocation formed by departure of a leaving group  $\text{X}^-$  from a substrate R-X in a nucleophilic solvent SOH, *i.e.*, an  $\text{S}_{\text{N}}1$  reaction. In addition to reaction between the carbocation and the solvent, a second nucleophile  $\text{Nu}^-$  may be added to produce adduct R-Nu. In Scheme 1.4, the first-order rate constant for ionization of R-X to give the carbocation  $\text{R}^+$  is  $k_C$ , the pseudo first-order

rate constant for decay of  $R^+$  by attack of the solvent is  $k_S$ , and the second-order rate constants for reaction of  $R^+$  with  $X^-$  or  $Nu^-$  are given as  $k_X$  and  $k_N$ , respectively.

Although earlier approaches were employed to determine relative carbocation reactivities, the method that ultimately provided the most useful information is that of competition kinetics, where the bimolecular reaction of  $R^+$  with a nucleophile  $Nu^-$  is included (Scheme 1.4). The reaction pathway is now partitioned between reaction with two different nucleophiles, and the ratio between the adducts  $R-Nu$  and  $R-OS$  provides an estimate of the ratio between the rate constants  $k_N$  and  $k_S$  according to Equation 1.6 (recall that  $k_S$  is defined as a pseudo first-order rate constant).

$$\frac{[R-Nu]}{[R-OS]} = \left( \frac{k_N}{k_S} \right) [Nu^-] \quad (1.6)$$

An early competition kinetics study by Schleyer and co-workers<sup>44</sup> surveyed a selection of literature results for the competition reaction between  $H_2O$  ( $SOH$ ) and azide ion  $N_3^-$  ( $Nu^-$ ) for several alkyl chlorides in 80% aqueous acetone. A plot of  $\log(k_{obs})$  versus  $\log(k_N/k_S)$  was linear, suggesting that more stable carbocations (higher rate of ionization,  $k_{obs}$ ) also demonstrated better selectivity between nucleophiles (*i.e.*, the rate of attack by the stronger nucleophile  $N_3^-$  was favoured over attack by  $H_2O$ ). Shortly thereafter Ritchie employed stopped-flow techniques to directly measure the lifetimes of several triarylmethyl cations in aqueous solution, as well as their reactivities towards various nucleophiles.<sup>18</sup> In contrast to the results of Schleyer and co-workers, however, Ritchie observed constant selectivity according to the constant  $N_+$  in Equation 1.7.

$$N_+ = \log \left( \frac{k_N}{k_S} \right) \quad (1.7)$$

The apparent disagreement between Equations 1.6 and 1.7 was resolved by the laboratories of Rappoport<sup>45</sup> and Jencks<sup>46</sup> who proposed that, for many carbocations, attack by the strongly nucleophilic  $\text{N}_3^-$  ion is dependent only on its rate of diffusion in a given solvent – the diffusion-controlled limit. Thus, for the reactive carbocations employed by Schleyer and co-workers,  $k_{\text{N}}$  remains constant while  $k_{\text{S}}$  changes for each substrate, and so the linear correlation is actually between  $\log(k_{\text{obs}})$  and  $-\log(k_{\text{S}})$ . In contrast, the reaction of nucleophiles with the highly stabilized cations studied by Ritchie depends only on the combination of cation and solvent. The diffusion-controlled reactivity of unstable cations ultimately proved to be very helpful for determining rate constants of cation-nucleophile reactions. Competition between azide and a second nucleophile provides a product ratio, and knowledge of an absolute value for  $k_{\text{N}_3}$  allows calculation of the second rate constant.

The use of laser flash photolysis (LFP) has made possible the direct observation of carbocations that are many orders of magnitude more reactive than those investigated by Ritchie using stopped-flow techniques. Although the mechanism for formation of carbocations using this method will not be detailed until later in this report, the general aspects of LFP are important for the current discussion. Excitation of a substrate is achieved using a laser pulse, and subsequent chemistry of the excited state results in formation of the carbocation to be studied. Many different photochemical reactions have been employed to generate carbocations, as well as a variety of other short-lived reactive intermediates. UV-vis absorption spectroscopy is the most common detection system used, and so LFP is restricted to conjugated carbocations (often arylmethyl). In addition, the lifetime of the cation must not be less than the pulse width of the laser used for excitation – currently nanosecond, picosecond, and even femtosecond laser systems are

employed for various experiments. The solvents used for these studies are typical solvolysis systems (*e.g.*, alcohols), although the study of highly reactive species is greatly facilitated by the use of highly ionizing, weakly-nucleophilic alcohol solvents such as 2,2,2-trifluoroethanol (TFE) and 1,1,1,3,3,3-hexafluoroisopropanol (HFIP). The lifetime of the diphenylmethyl cation is increased by a factor of approximately  $1 \times 10^8$  upon changing from 1:1 H<sub>2</sub>O:CH<sub>3</sub>CN to HFIP.

Carbocation	$k_{\text{TFE}} (\text{s}^{-1})$	$k_{\text{HFIP}} (\text{s}^{-1})$
$(\text{C}_6\text{H}_5)_2\text{CH}^+$	$3.2 \times 10^6$	$3 \times 10^2$
$(\text{C}_6\text{H}_5)\text{C}^+(\text{CH}_3)_2$	$> 5 \times 10^7$	$9 \times 10^3$
$4\text{-CH}_3\text{O}(\text{C}_6\text{H}_4)\text{C}^+\text{HCH}_3$	$3.9 \times 10^5$	$2 \times 10^2$
$4\text{-CH}_3\text{O}(\text{C}_6\text{H}_4)\text{CH}_2^+$	$4.3 \times 10^6$	$3 \times 10^2$
$4\text{-CH}_3(\text{C}_6\text{H}_4)\text{C}^+\text{HCH}_3$	$> 5 \times 10^7$	$7 \times 10^4$
$4\text{-CH}_3(\text{C}_6\text{H}_4)\text{CH}_2^+$	$> 5 \times 10^7$	$2 \times 10^6$
$(\text{C}_6\text{H}_5)\text{C}^+\text{HCH}_3$	$> 5 \times 10^7$	$4 \times 10^5$

Table 1.3 Rate constants for the decay of selected arylmethyl carbocations in TFE and HFIP (from Reference 47).

Table 1.3 provides a comparison of the rate constants for decay in TFE and HFIP for a variety of arylmethyl cations as determined by McClelland and co-workers using LFP techniques.<sup>47</sup> The general trends that would be predicted from the carbocation stabilities in Table 1.2 are observed – the more stable cations have smaller rate constants for decay than do the less stable ones. Direct observation of the unsubstituted benzyl

cation has not yet been possible, although estimates place its rate constant for decay in the range of  $5 \times 10^8 - 5 \times 10^9 \text{ s}^{-1}$ .<sup>48</sup> Although simple alkyl cations cannot be directly observed using LFP, estimates of their reactivities in HFIP have been made based on the kinetics for trapping them with the electron-rich (nucleophilic) aromatic 1,3,5-trimethoxybenzene.<sup>49</sup> Electrophilic aromatic addition results in a stabilized cyclohexadienyl cation that can be detected spectroscopically. Using this technique, the values of  $k_{\text{HFIP}}$  for the 2-propyl and 2-adamantyl cations were calculated as  $7.1 \times 10^9 \text{ s}^{-1}$  and  $2.9 \times 10^9 \text{ s}^{-1}$ , respectively.

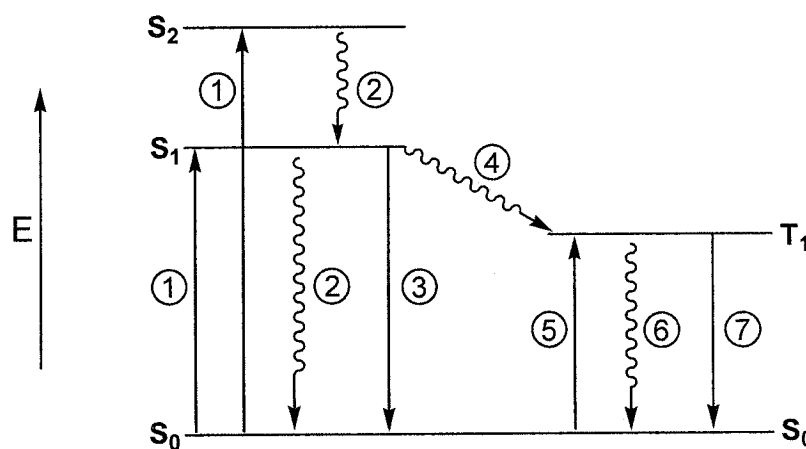
The issues of carbocation stability and reactivity will be addressed at several times in later chapters of this report, but the introductory discussion will now turn to the basic photophysical processes and their relation to photochemical reactions (Section 1.3). In addition, Section 1.3 will also discuss the mechanism of benzylic ester photolysis as an example of a photochemical reaction that generates carbocation intermediates.

## 1.3 Fundamentals of Photochemistry

### 1.3.1 Photophysical Processes

Prior to addressing the chemical reactivity of an excited-state organic compound (*i.e.*, photochemical processes), the factors which influence the interconversion between electronic states of the compound in question (*i.e.*, photophysical processes) must be discussed. Scheme 1.5 displays a simplified energy state diagram – a pictorial representation of the electronic states of a compound.<sup>50,51</sup> The diagram assumes a singlet ground state (all orbitals populated by two paired electrons), designated  $S_0$ . Higher energy singlet states will contain two singly occupied orbitals with paired electrons, and are labelled  $S_1$ ,  $S_2$ , etc. The corresponding triplet states (two singly occupied orbitals

with unpaired electrons) are labelled  $T_1$ ,  $T_2$ , etc. The vertical axis of the energy state diagram represents increasing energy, while the horizontal axis serves only to separate the “manifolds” of singlet states and triplet states. Scheme 1.5 only displays  $S_0$ ,  $S_1$ ,  $S_2$ , and  $T_1$  – higher energy states are not required for the present discussion. The vibrational and rotational energy levels associated with each energy level have also been omitted for simplicity.



Scheme 1.5 A simplified energy state diagram illustrating basic photophysical processes.

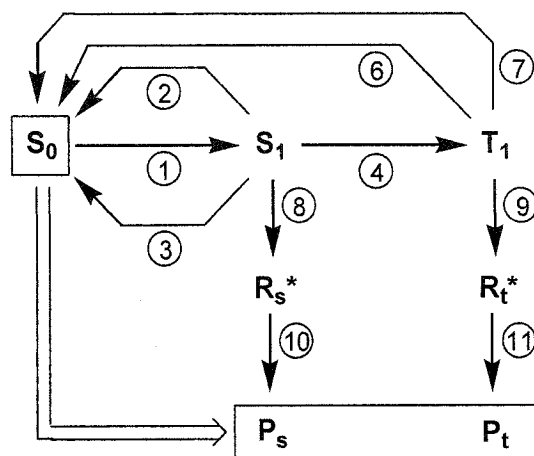
Changes between energy states may involve absorption/emission of light (radiative processes) or heat (non-radiative processes). Scheme 1.5 follows the familiar convention of displaying radiative processes as straight lines and non-radiative processes as wavy lines. The excitation of a molecule from  $S_0$  to a higher singlet state is induced by absorption of an appropriate wavelength photon, process (1). Absorption may lead to population of either  $S_1$  or  $S_2$ , but in the latter case internal conversion (2) is expected to lead to rapid formation of  $S_1$  from the higher state. Internal conversion is favoured for states of similar energy, so the conversion of  $S_2$  to  $S_1$  is generally much faster than the conversion of  $S_1$  to  $S_0$ .<sup>51</sup> Fluorescence (3) involves relaxation of an excited state by

emission of a photon. Due to the rapid internal conversion of  $S_2$  to  $S_1$ , Kasha's rule predicts that fluorescence is generally a  $S_1$  to  $S_0$  process.<sup>51</sup> Deactivation of  $S_1$  may also occur by intersystem crossing to  $T_1$  (4), although the requirement of a concomitant flip of an electron spin makes this "spin-forbidden" process unfavourable for many compounds. For the same reasons, formation of  $T_1$  by absorption from  $S_0$  (5) and the deactivation of  $T_1$  by either intersystem crossing (6) or phosphorescence (7) are all unfavourable processes. These generalizations also account for the fact that  $S_1$  generally decays much faster than  $T_1$ .

### 1.3.2 Photochemical Reactions

The relationship between photophysical processes (Scheme 1.5) and the photochemical reactivity of a compound is shown schematically in Scheme 1.6. The important change is the addition of two new decay pathways, namely chemical reactions from either  $S_1$  (process 8) or  $T_1$  (process 9). These reactions may yield product directly, but often short-lived reactive intermediates (such as carbocations or radicals) are involved in the reaction pathway. Scheme 1.6 implies that the products from the singlet ( $P_s$ ) and triplet ( $P_t$ ) pathways are unique species, but this may not always be the case.

The rate of decay for an unreactive singlet state will depend upon the rates of fluorescence ( $k_f$ ), non-radiative decay by internal conversion ( $k_{ic}$ ), and intersystem crossing ( $k_{isc}$ ). The total rate of decay will then be given by  $k_t$ , the sum of all decay pathways for the state in question. The lifetime of  $S_1$  ( $\tau_s$ ) is defined as the reciprocal of  $k_t$ , Equation 1.8. Lifetimes of singlet excited states are generally on the order of several nanoseconds. However, the availability of a reactive pathway for decay of  $S_1$  will add another term to the expression for  $k_t$ , and the lifetime of the excited state will be reduced.



Symbols	Processes
$S_0$ Ground state singlet	1. Absorption
$S_1$ First singlet excited state	2. Fluorescence
$T_1$ First triplet excited state	3. Radiationless decay
$R_s^*$ Reactive intermediate (singlet pathway)	4. Intersystem crossing
$R_t^*$ Reactive intermediate (triplet pathway)	5. Singlet - triplet absorption (not shown)
$P_s$ Product (singlet pathway)	6. Phosphorescence
$P_t$ Product (triplet pathway)	7. Intersystem crossing
	8. Reaction of first singlet excited state
	9. Reaction of first triplet excited state
	10. Reaction of intermediate (singlet pathway)
	11. Reaction of intermediate (triplet pathway)

Scheme 1.6 A schematic representation of the relationship between photophysical processes and photochemical reactions.

$$\tau_s = \frac{1}{k_t} = \frac{1}{k_f + k_{ic} + k_{isc}} \quad (1.8)$$

An important measure for the efficiency of a photochemical process is the quantum yield  $\phi$ , defined as the fraction of times an event occurs per photon absorbed.<sup>50</sup> For example, the quantum yield of fluorescence  $\phi_f$  is the number of photons emitted divided by the number of photons absorbed from  $S_0$ , Equation 1.9. In the same way, quantum yields for consumption of a substrate or formation of a product can be measured. An alternate expression for the quantum yield of fluorescence is one expressed in rate constants, given by the product of the rate constant for fluorescence and the singlet



lifetime. A critical aspect of the experimental determination of any quantum yield is knowledge of the number of photons emitted by the light source used to excite a substrate – this is done using a reference system with a known quantum yield, *i.e.*, actinometry.

$$\phi_f = \frac{\text{\# of photons emitted}}{\text{\# of photons absorbed}} = \frac{k_f}{k_t} = k_f \tau_s \quad (1.9)$$

An important point to make regarding photochemical reactions is that the structure of a compound will influence the rates of all the deactivation pathways for an excited state, in addition to any subsequent reactions of the reactive intermediate itself. Therefore, the reactivity of a substrate may be very different in the excited state compared to the ground state. However, the chemistry of ground state intermediate species should be the same whether it was generated *via* a ground state reaction or *via* a pathway beginning with an excited state reaction.

### 1.3.3 Generation of Carbocations *via* Photofragmentation

The earliest investigations of photochemically-generated carbocations involved the highly stabilized triarylmethyl cations described in Section 1.2.1. In 1919, Lifshitz<sup>52</sup> observed formation of the characteristically intense crystal violet cation in ethanol solution following irradiation of the uncoloured substrate crystal violet leucocyanide. Later investigations<sup>53</sup> demonstrated the analogous reaction for malachite green leucocyanide, and that quenching of the cation signal with water produced the corresponding alcohol. Finally, in 1957 Holmes<sup>54</sup> made the important observation that irradiation of these substrates in hexanes resulted in decomposition, but the addition of 1,2-dichloroethane as a polar co-solvent allowed formation of the dye cations. Holmes

suggested that more polar solvents promoted heterolytic bond cleavage by stabilization of the ionic intermediates, whereas homolytic cleavage was favoured in less polar solvents. These early studies emphasize some of the key characteristics of photochemical bond cleavage reactions: the formation of various intermediate species, the detection of cations by UV-vis spectroscopy, the quenching of intermediates by added reagents, and the dependence of the reaction pathway on the reaction conditions (solvent) employed.

Another important characteristic of this class of reactions was demonstrated in 1963 by Zimmerman and co-workers.<sup>55</sup> Hückel molecular orbital calculations (results shown in Figure 1.1) were used to determine the resonance contribution of the electron donating methoxy substituent in the ground and excited states (*i.e.*,  $S_0$  and  $S_1$ ). Although the  $S_0$  results were consistent with the well-established electron donation to the ortho and para positions, the  $S_1$  calculations gave the surprising prediction of even greater electron donation to the ortho and meta positions.

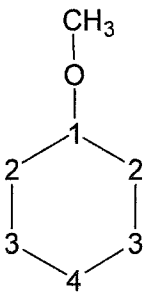
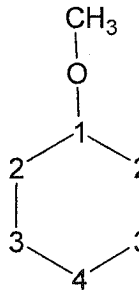
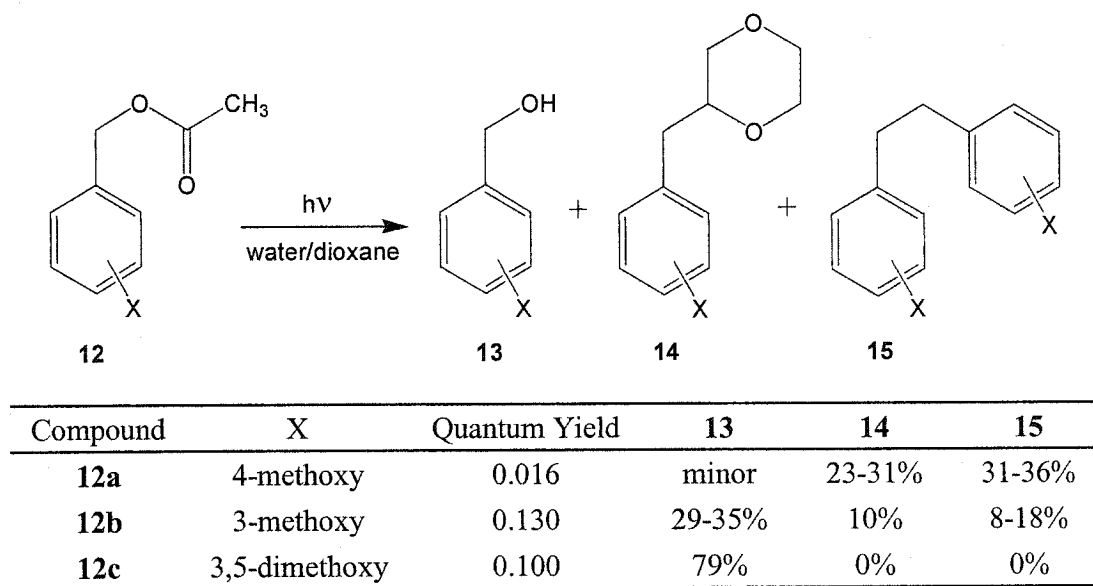
O	1.953 (+0.047)		O	1.762 (+0.238)	
C1	0.972 (+0.028)		C1	0.734 (+0.266)	
C2	1.028 (-0.028)		C2	1.167 (-0.167)	
C3	0.999 (+0.001)		C3	1.204 (-0.204)	
C4	1.021 (-0.021)		C4	0.762 (+0.238)	
Ground State ( $S_0$ )			Excited State ( $S_1$ )		

Figure 1.1 Electron density and formal charges (in parenthesis) for the ground state and first excited state of anisole, calculated using extended HMO theory.



Scheme 1.7 Comparison of product distributions following the irradiation of a series of methoxy-substituted benzyl acetates.

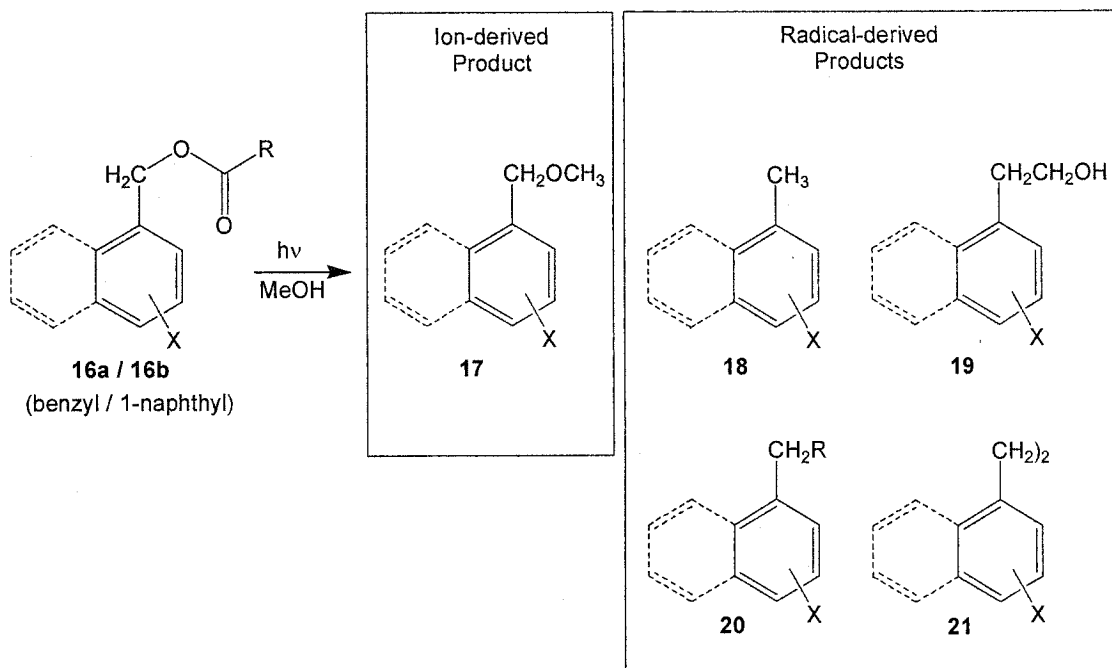
Experimental support for the calculations was provided by irradiation of three methoxy-substituted benzyl acetates (**12a-c**) in 1:1 water/dioxane, Scheme 1.7.<sup>55</sup> The quantum yields for consumption of **12b** and **12c** were nearly an order of magnitude greater than that of **12a**. Furthermore, the cation-derived alcohol **13** was only detected as a minor product following irradiation of the para isomer **12a**, but was formed as the major product for the photolysis of the di-meta substrate **12c**. The yields of radical-derived products **14** and **15** followed the opposite trends. The two distinct classes of products indicated a competition between homolytic cleavage and heterolytic cleavage of the C-O bond. Zimmerman noted that the excited state electron distributions depicted in Figure 1.1 provided an explanation for the photolysis results: electron donation to the meta position in  $S_1$  could facilitate elimination of acetate ion, resulting in high yields of the benzylic carbocation required for formation of **13**. Further support for this line of reasoning was provided by additional calculations, which indicated that the 3-

methoxybenzyl cation was more stable in the excited state than the corresponding 4-methoxybenzyl cation – a trend opposite to ground state observations. Zimmerman later repeated these calculations at higher levels of theory, with essentially the same results.<sup>56</sup> The conclusion reached by these later investigations is that, although adiabatic formation of an excited state benzyl cation *via* heterolytic cleavage is unlikely, heterolytic cleavage of the C-O bond from  $S_1$  is more favourable than homolytic cleavage for the 3,5-dimethoxybenzyl system. In contrast, the opposite is true for the excited state of 4-methoxybenzyl acetate. The term “meta-effect” has been applied to describe the general trend of high reactivity for substrates possessing electron donating substituents in the meta position.

Although the research efforts of Zimmerman provided a clear example of the striking differences in excited state reactivity for different methoxy-substituted benzyl acetates, construction of a complete picture of arylmethyl ester photochemistry was achieved by the efforts of Pincock and co-workers. These experiments involved the study of substituted 1-naphthylmethyl esters<sup>57</sup> and benzyl esters<sup>58</sup> in methanol, Scheme 1.8. As shown in Scheme 1.7 for the irradiations of methoxy-substituted benzyl acetates in water/dioxane, the products indicate the presence of both ionic and radical intermediates in the reaction mixture.

A critical aspect of the investigations by Pincock and co-workers was the variation of not only the aromatic substituents, but also the nature of the ester (‘R’ in Scheme 1.8). In particular, formation of product **20** in the reaction mixture requires a mechanism involving homolytic cleavage of the acetate group, decarboxylation of the resulting oxy-radical, and recombination of the contact radical pair. In a study by Hilborn and Pincock,<sup>59</sup> the yield of the ion-derived product **17b** was found to decrease with increasing

stability of the expected radical intermediate ( $R\cdot$ ). For example, the yield of **17b** was found to be 98% for  $R = \text{CH}_3$ , but only 71% for  $R = (\text{CH}_3)_3\text{C}$  (keeping  $X = \text{H}$ ).



Scheme 1.8 Irradiations of substituted benzyl esters (**16a**) and 1-naphthylmethyl esters (**16b**) in methanol solution.

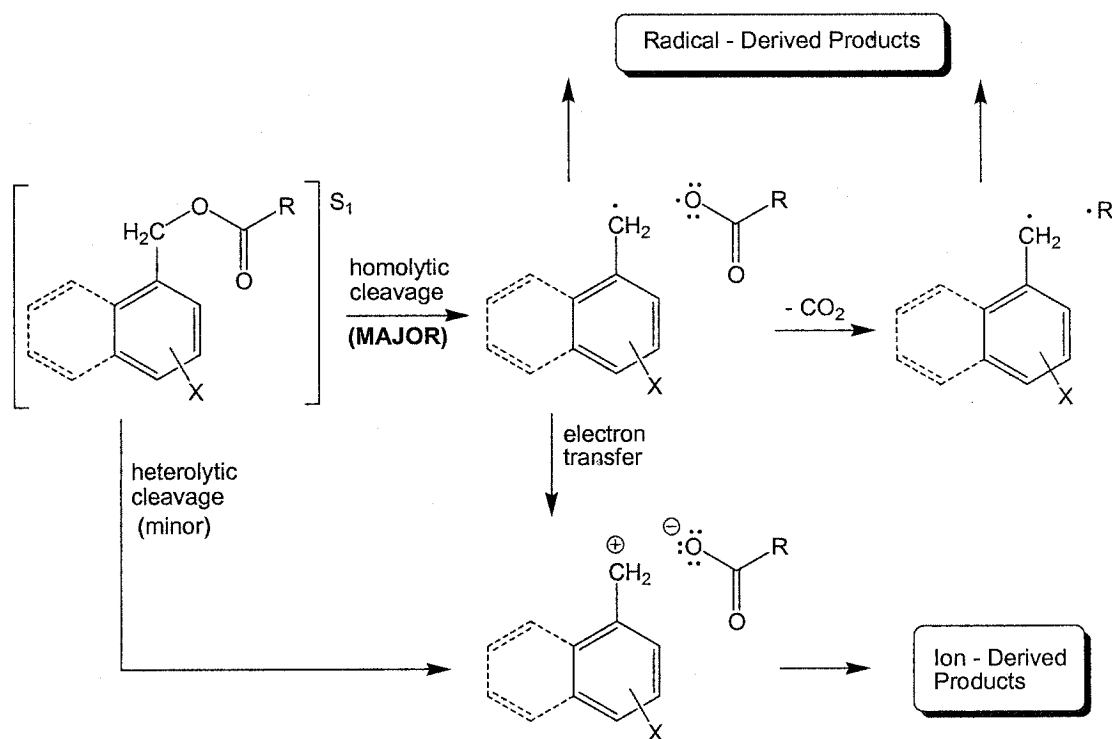
According to DeCosta and Pincock,<sup>57</sup> this important connection between the properties of the *radical* pair and the yield of *ion*-derived product is due to a pathway involving homolytic cleavage followed by electron transfer between the arylmethyl radical ( $\text{ArCH}_2\cdot$ ) and the acyloxy radical ( $\text{RCO}_2\cdot$ ) to give the corresponding ion pair ( $\text{ArCH}_2^+/\text{RCO}_2^-$ ). The stability of  $R\cdot$  governs the rate of decarboxylation of  $\text{RCO}_2\cdot$ , and hence the lifetime of the radical pair that undergoes electron transfer – the ten-fold increase in the rate of decarboxylation upon changing from  $R = \text{CH}_3$  to  $R = (\text{CH}_3)_3\text{C}$  has a measurable impact on the yields of the ion-derived products that depend on the electron transfer pathway for formation of their precursors. Therefore, the differences in the product yields for acetates ( $R = \text{CH}_3$ ) and pivalates ( $R = (\text{CH}_3)_3\text{C}$ ) indicate the presence

of the electron-transfer pathway. Comparison of the ratios of ion-derived product to radical-derived product provided an estimate of the ratio between the rate constants for electron-transfer ( $k_{ET}$ ) and decarboxylation ( $k_{CO_2}$ ). Use of a previously determined value for  $k_{CO_2}$  allowed determination of rate constants for other substrates – this “radical clock” technique is thus analogous to the “azide clock” technique discussed in Section 1.2.3.

Perturbation of the electron-transfer pathway for ion-derived product formation was also observed upon changing the aromatic substituents of the substrates in Scheme 1.8. For a set of substrates with various substituents (X) but with identical R groups, the rate of electron transfer (and therefore the yield of ion-derived product) will depend on the oxidation potential  $E_{1/2}^{OX}$  of the arylmethyl radical. Fortunately, experimental oxidation potentials are available for both benzyl<sup>33</sup> and 1-naphthylmethyl<sup>60</sup> radicals, and so plots of  $\log(k_{ET})$  versus  $E_{1/2}^{OX}$  could be drawn for both sets of compounds. For either class of arylmethyl ester,<sup>57,58</sup> these plots displayed the curvature expected from Marcus’ theory of electron transfer.<sup>61</sup> The key feature of such a treatment is the so-called “inverted region” where the rate of electron transfer actually becomes restricted by the high energy required for solvent and bond reorganization, even though the free energy change for the reaction may be quite favourable. For benzyl acetates, this effect appears to be the source for Zimmerman’s original observation<sup>55</sup> that 3-methoxybenzyl acetate gives a higher yield of ion-derived product than does the 4-methoxy isomer – the latter falls into the inverted region for electron transfer, and so formation of the ion-derived product is suppressed.

The intervention of the homolytic cleavage/electron transfer pathway for the formation of carbocation intermediates clearly runs contrary to Zimmerman’s proposal of a competition between direct homolytic and heterolytic pathways from  $S_1$ . An important

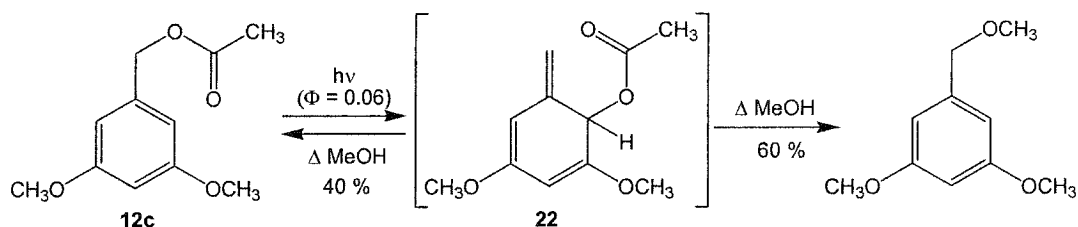
issue is whether or not direct heterolytic cleavage is possible for arylmethyl esters, or if all the ion-derived product results from homolytic cleavage followed by electron transfer. The available results cannot completely rule out the presence of a heterolytic cleavage pathway, but it appears to be only a minor process.<sup>62</sup> Scheme 1.9 displays the current mechanistic interpretation for the mono-substituted arylmethyl ester results, with homolytic and heterolytic cleavage of  $S_1$  labelled as “major” and “minor”, respectively.



Scheme 1.9 Preferred mechanistic pathways for formation of radical-derived and ion-derived products from the photolysis of arylmethyl esters.

Although the mechanism of product formation for the photolysis of mono-substituted arylmethyl esters is more or less resolved, determination of the factors that control the relative product yields for substrates with multiple substituents has been more challenging. In particular, attempts by Pincock and Wedge<sup>63</sup> to extend the above methodology to substrates possessing multiple methoxy substituents resulted in higher-

than-expected values for  $k_{ET}$  (based on experimental oxidation potentials for the corresponding benzyl radicals). The source of the difficulties associated with the analysis appears to be the large differences between the ion-derived product yields for the acetates as compared to the pivalates. Unusually large yields of ion-derived products have also been observed by Itoh and co-workers<sup>64</sup> for the irradiations of ortho methoxy benzyl esters. No satisfactory explanation has been able to account for these discrepancies. Pincock and co-workers<sup>65</sup> have investigated the possibility of alternate reactive intermediates in the photochemistry of 3,5-dimethoxybenzyl acetate **12c** (Scheme 1.7) in methanol. The researchers suspected that coupling of the initially-formed radical pair in the solvent cage could produce the reactive ground state triene **22**, Scheme 1.10. Potential solvolysis of such an intermediate could give the ion-derived product, leading to a significant error in the calculated ratio of heterolytic/homolytic cleavage. However, even though **22** was detected as a viable intermediate for the formation of the methanol-adduct, the quantum yield for the formation of **22** ( $\Phi = 0.06$ ) was too low to account for the exalted yield of ion-derived product in the earlier experiments by Pincock and Wedge.<sup>63</sup>



Scheme 1.10 Formation and reactivity of triene intermediate **22** following irradiation of 3,5-dimethoxybenzyl acetate **12c** in methanol.

At the time of this writing, the factors that contribute to the high yields of ion-derived products from the irradiations of arylmethyl esters possessing multiple methoxy



substituents are not completely understood. However, the fact remains that the 3,5-dimethoxybenzyl acetate system does produce high yields of ion-derived products, and that the quantum yield of the reaction is high. The work described in Chapter 2 represents an effort to utilize these properties for an investigation of subsequent carbocation chemistry.

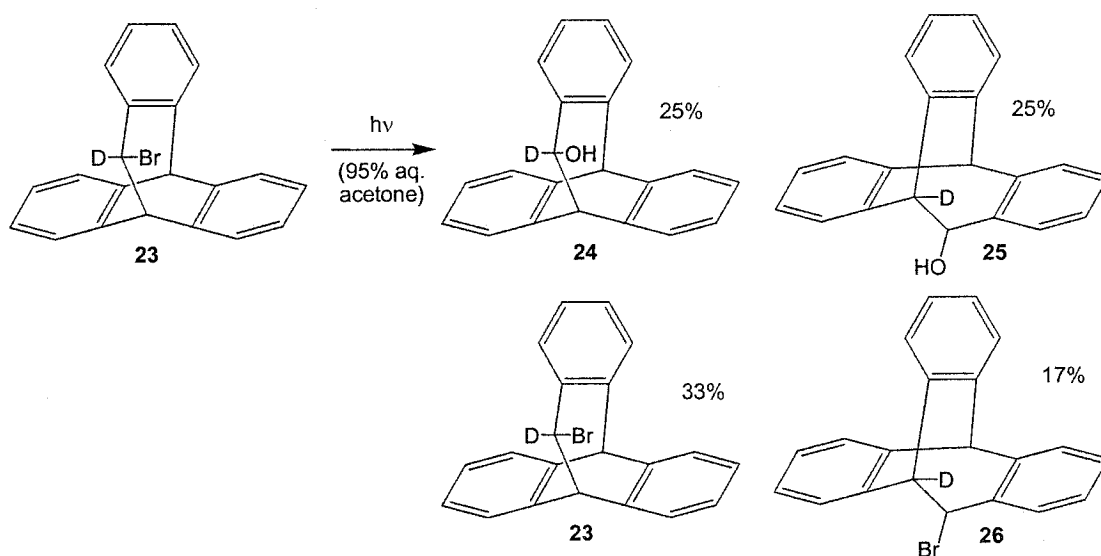
## Chapter 2      Investigations of Rearrangements of Photochemically Generated Carbocations

### 2.1    Introduction

#### 2.1.1   Rearrangements of Photochemically Generated Carbocations

As shown in Section 1.2, the observation of rearrangement products played a key role in the conceptual development of carbocations as short-lived, reactive intermediates. In a similar way, skeletal rearrangements may also serve as indicators of carbocation intermediates in photochemical reactions. However, there are very few reports of such rearrangements in the literature, due to the restrictions involved with the study of photochemically generated carbocations. In particular, photochemical excitation requires a chromophore, almost always a substituted aromatic moiety. Conversion of the excited species to a reactive intermediate, either *via* bond rupture (*vide supra*, Section 1.3.3) or bond formation (*vide infra*, Section 4.1) requires some degree of orbital interaction between the site of carbocation generation and the chromophore. As a result, the majority of photochemically generated carbocations are of the arylalkyl variety. Such species are reasonably stable, and compounds that allow conversion to an even lower energy structure are comparatively rare (excluding “rearrangements” between two resonance forms – allylic cations,<sup>66</sup> for example). This section provides examples of some systems for which such rearrangements have been observed.

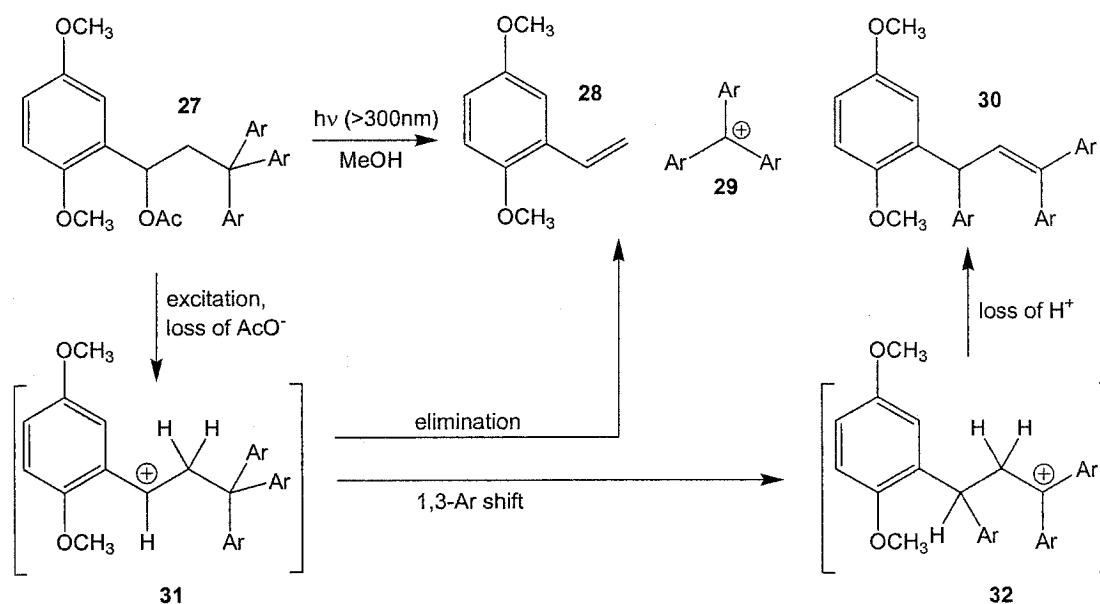
Early examples of rearrangements of photochemically generated carbocations were provided by Cristol and co-workers.<sup>67</sup> As shown in Scheme 2.1, irradiation of the monodeuterated bromohomotriptycene **23** in 95% aqueous acetone lead to the formation of the nucleophile adducts **24** and **25** in addition to a rearranged isomer of the starting material, bromide **26**. The formation of **25** and **26** implies formation of a carbocation from the excited state of **23**, followed by a 1,2-aryl shift and nucleophilic attack. The authors proposed that the 1:1 ratio of **24:25** was consistent with attack on free carbocations, whereas the 2:1 ratio of **23:26** resulted from preferential trapping of the carbocation in the ion pair prior to rearrangement. In the absence of the deuterium label the rearrangement is degenerate, so the stabilities of the two carbocations are expected to be almost identical.



Scheme 2.1 Early observation of photochemical bond cleavage followed by carbocation rearrangement.

Another interesting carbocation/rearrangement system was investigated by Ullman and co-workers<sup>68</sup> (Scheme 2.2). Upon irradiation of the acetate **27** in methanol, the strongly absorbing crystal violet cation **29** was observed. This cation was expected

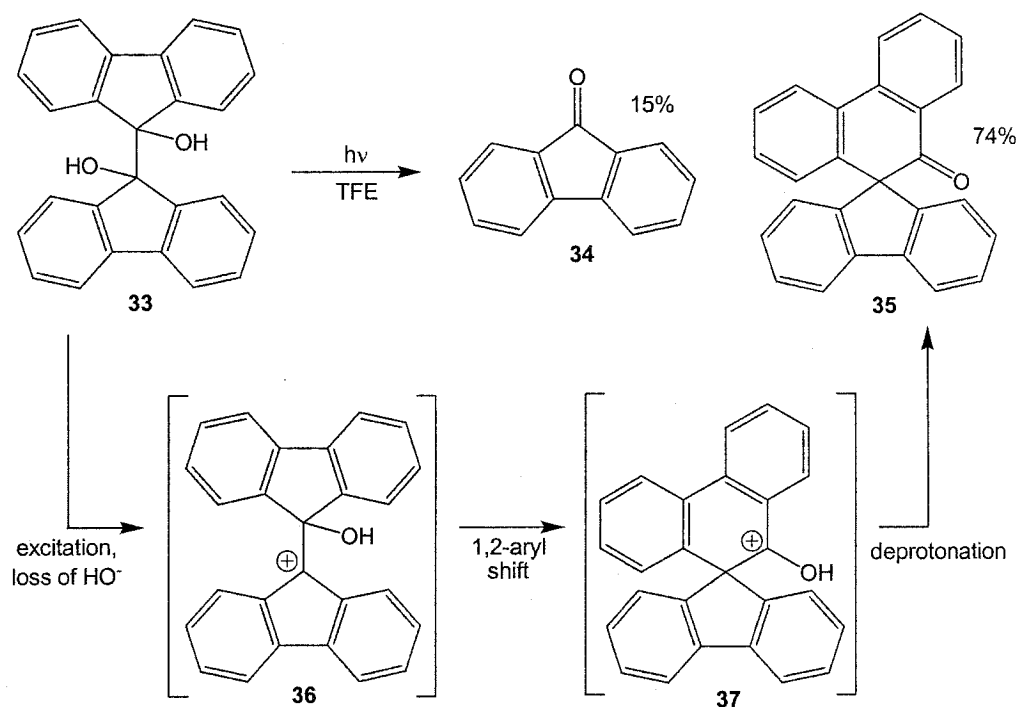
based on a mechanism involving initial formation of carbocation **31**, followed by elimination to give **29** and product **28**. However, the rearrangement product **30** was unexpected – a 1,3-aryl shift of **31** followed by deprotonation of **32** was proposed to account for its formation.



Scheme 2.2 Competition between elimination and rearrangement of photochemically generated carbocation **31**, Ar = 4- $(\text{CH}_3)_2\text{N}(\text{C}_6\text{H}_4)$ .

Two recent studies by Lee-Ruff and co-workers<sup>69,70</sup> have investigated the detection of carbocation rearrangements using laser flash techniques. These efforts focussed on the generation of 9-fluorenyl cations by photolysis of the corresponding 9-fluorenol derivatives. The efficient formation of carbocation intermediates from these substrates has been attributed to possible stabilization of excited state antiaromatic systems (*i.e.*,  $4n \pi$  electrons).<sup>71</sup> The argument follows that such stabilization would favour formation of the cation, even when the reaction proceeds *via* loss of very poor leaving groups (such as hydroxide ion). Lee-Ruff and co-workers<sup>69</sup> designed substrate **33** as a precursor to a “doubly destabilized” di-cation, although photolysis in acetonitrile,

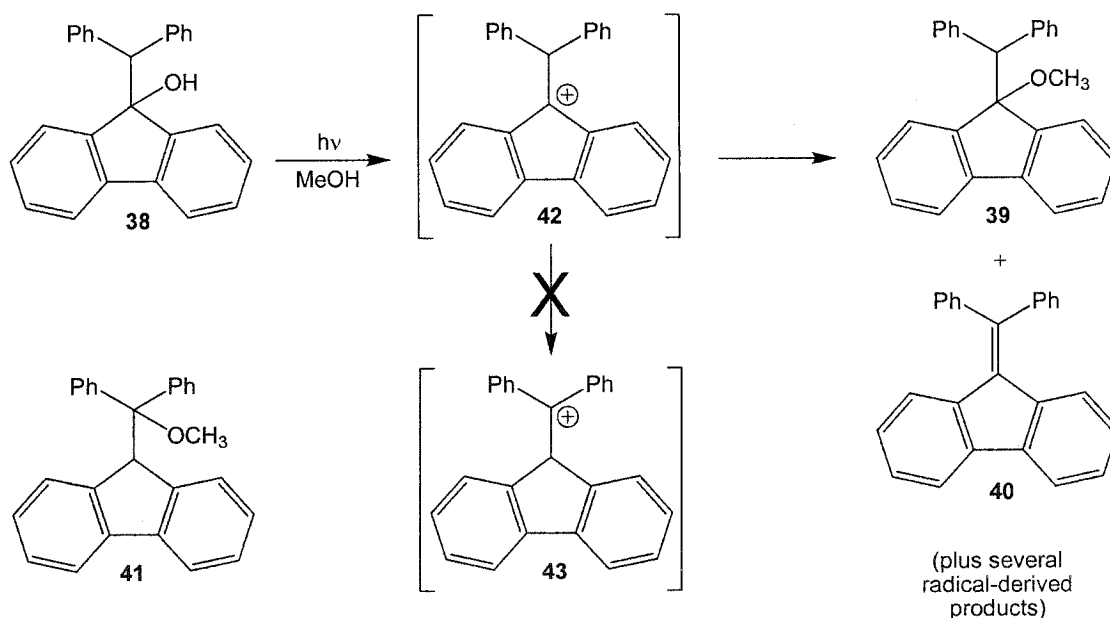
methanol, and TFE gave only the radical-derived product **34** and the rearrangement product **35** (Scheme 2.3). Formation of **35** was proposed to proceed *via* formation of carbocation **36**, followed by a pinacol rearrangement to **37**; this process is favourable due to  $\pi$ -stabilization of **37** by the  $-\text{OH}$  substituent. The cation **36** was observed using LFP, and its unimolecular rearrangement to **37** (which was not detected) was found to have a rate constant of  $5 \times 10^5 \text{ s}^{-1}$  in HFIP.



Scheme 2.3 The formation of ketone **35** *via* the photochemical pinacol rearrangement of carbocation **36**.

The goal of directly observing a carbocation rearrangement using LFP was pursued in a second study by Lee-Ruff and co-workers,<sup>70</sup> this time using substrate **38** (Scheme 2.4). Irradiation of **38** in methanol gave the ether **39** and the elimination product **40**. However, the ether **41** (which would have been formed after a 1,2-hydride shift converting **42** to **43**) was not detected in the reaction mixture. When **38** was subjected to

strong acid conditions at  $-78\text{ }^{\circ}\text{C}$ , **42** was detected spectroscopically, but **43** was not observed until the solution was warmed to room temperature. Quenching of the cold or warmed solution with methanol gave **39** or **41**, respectively. The authors rationalized these observations by suggesting that cation **43** is not formed by a 1,2-hydride shift, but rather by a deprotonation-protonation sequence involving the by-product **40** (a process which is only possible in the strong acid experiments). This hypothesis was supported by high level *ab initio* molecular orbital calculations, which revealed that the hydride shift of **42** to **43** required an activation energy of approximately 27 kcal/mol due to poor overlap of the orbitals required for the rearrangement. Furthermore, the calculations suggested that the energy released by such a rearrangement was only 1.1 kcal/mol, compared to a difference of 9 kcal/mol between the parent diphenylmethyl and 9-fluorenyl cations.<sup>37</sup>



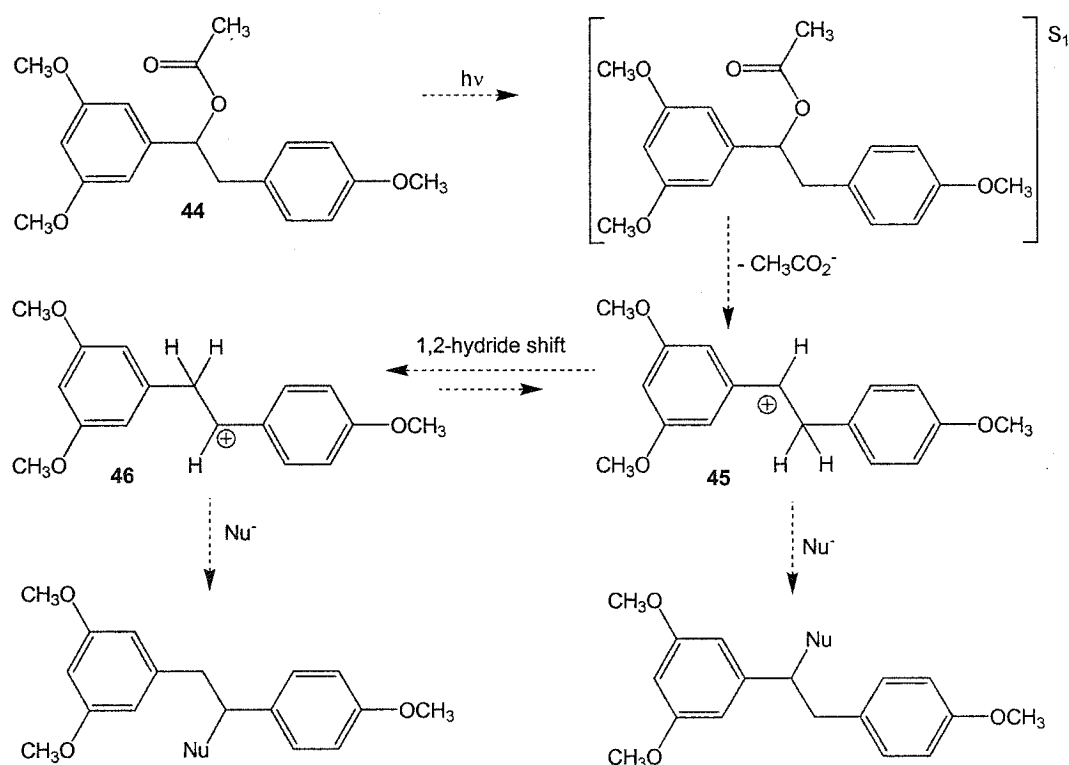
Scheme 2.4 The photochemistry of fluorenol derivative **38** in methanol.

### 2.1.2 Project Proposal

The general goal of the work described in this chapter is to determine the ability of an aromatic substituent to induce a carbocation rearrangement. The compound that was chosen for a preliminary study is 1-(3,5-dimethoxyphenyl)-2-(4-methoxyphenyl)-ethyl ethanoate **44**, shown in Scheme 2.5. The 3,5-dimethoxyphenyl chromophore was envisaged to promote efficient C-O bond cleavage to produce carbocation **45**. As discussed in Section 1.3.3, the exact mechanism of this reaction is still under investigation, but the rapid generation of cations is well established. The yield of ion-derived products from the photolysis of the parent 3,5-dimethoxybenzyl acetate is 60% in methanol, with a quantum yield of 0.37.<sup>65</sup> Rearrangement of cation **45** to cation **46** via a 1,2-hydride shift is expected based on stabilization of **46** by the para methoxy substituent. The degree of rearrangement may be determined using 1) measurement of product ratios that result from trapping of the carbocation intermediates by nucleophiles, or 2) direct observation of the cations by LFP. A variety of 4-methoxyphenyl cations have been investigated in TFE and HFIP with these techniques,<sup>47</sup> so a rate constant for the rearrangement process (in competition with attack by nucleophiles) may be accessible.

Calculation of the expected energy difference between **45** and **46** requires literature values for the hydride affinities of the corresponding benzylic cations. Unfortunately, although  $\Delta H_{\text{hydride}}$  has been measured for the 4-methoxybenzyl cation in acetonitrile, the corresponding measurements for the 3,5-dimethoxybenzyl cation have not been made. However, the relative rates of solvolysis have been determined for a wide variety of substituted benzyl tosylates. The ratio of the rates of solvolysis for 4-methoxybenzyl tosylate and 3-methoxybenzyl tosylate is 83000:1 in 80% aqueous acetone at 25 °C.<sup>72</sup> The same study reported relative rates of 0.96 for 4-chlorobenzyl

tosylate and 1.44 for benzyl tosylate (both compared to 4-methoxybenzyl tosylate). Because these relative rates are roughly the same as that of 3-methoxybenzyl tosylate, the stabilities of the corresponding benzyl cations should be quite similar:  $\Delta H_{\text{hydride}}(4\text{-Cl}) \cong \Delta H_{\text{hydride}}(3\text{-OCH}_3) \cong \Delta H_{\text{hydride}}(\text{unsubs})$ . Solution phase hydride affinities for the 4-chlorobenzyl cation and the unsubstituted benzyl cation have been calculated as 123 kcal/mol and 118 kcal/mol,<sup>37</sup> respectively – these two values will be used as rough estimates for  $\Delta H_{\text{hydride}}(3\text{-OCH}_3)$ . Considering that the corresponding value for the  $\Delta H_{\text{hydride}}(4\text{-OCH}_3)$  is 107 kcal/mol, the difference in stability between the 4-methoxybenzyl cation and the 3-methoxybenzyl cation is estimated as 11-16 kcal/mol. Therefore, the conversion of **45** to **46** may be favourable by a similar magnitude.



Scheme 2.5 Proposed reactivity of substrate **44**: photofragmentation, carbocation rearrangement (**45** to **46**), and trapping by nucleophiles.



The sequence of events outlined in Scheme 2.5 is very similar to the strategy employed by Lee-Ruff and co-workers<sup>70</sup> for substrate **38**: photochemical generation of a relatively unstable cation, rearrangement to a more stable intermediate, trapping of either cation by added nucleophiles, and the prospect of observing the rearrangement directly using LFP. However, the use of **44** appears to present several advantages over the previous system. First, the lack of rearrangement following photolysis of **38** was attributed to a steric interaction between the aromatic rings, which in turn prevented the orbital overlap required for the rearrangement to occur. Cations **45** and **46** should be much less sterically congested, so the barrier for the rearrangement should be considerably lower. Second, the presence of two hydrogens that could potentially undergo hydride shifts should further increase the probability of rearrangement for **44**. Finally, in the case of a successful preliminary study with **44**, a variety of substrates could be synthesized for the investigation of substituent effects on the rearrangement process.

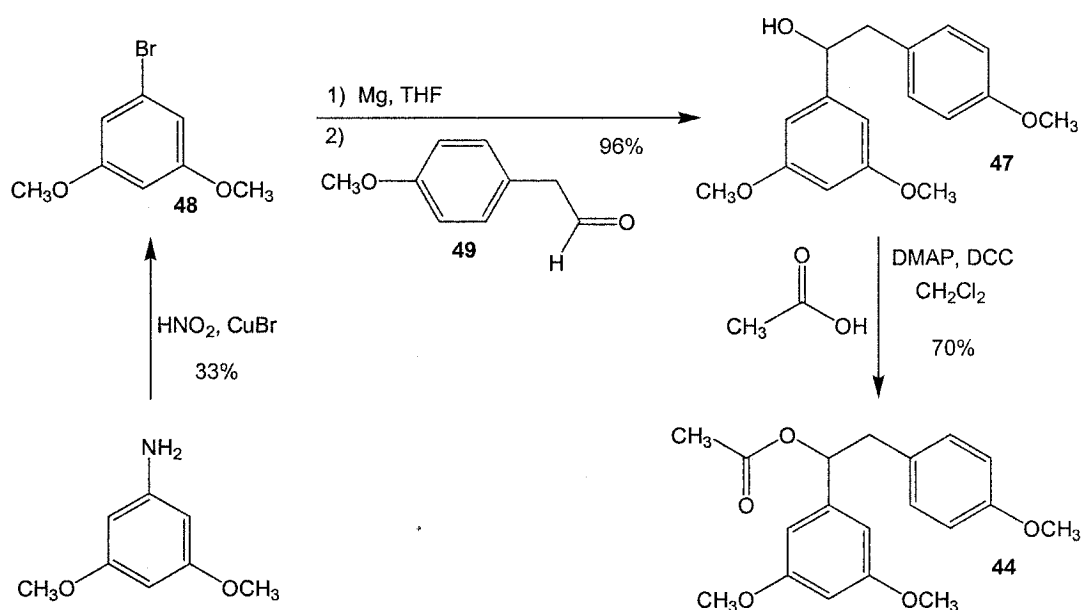
The results described in this Chapter have been published in the Canadian Journal of Chemistry.<sup>73</sup> The complete details of the synthesis and characterization of substrates, methods used for photochemical experiments, and identification of photoproducts are included in Chapter 7 (Experimental Details).

## **2.2 Experimental Results**

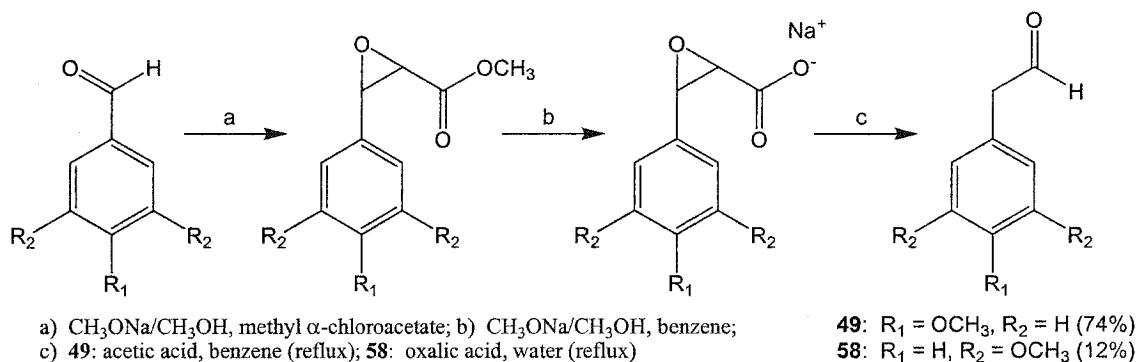
### **2.2.1 Synthesis and Photophysical Characterization of Substrate 44**

Arylmethyl esters such as **44** are easily accessed by esterification of the corresponding alcohols, and therefore alcohol **47** was identified as the direct precursor required for the preparation of **44**. For the synthesis of **47**, a Grignard reaction between 3,5-dimethoxybromobenzene **48** and 2-(4-methoxyphenyl)ethanal **49** was chosen. As

shown in Scheme 2.6, the bromide **48** was synthesized by a Sandmeyer reaction<sup>74</sup> in a low yield that is consistent with literature precedent.<sup>75</sup> The aldehyde **49** was synthesized in 74% yield over three steps by Darzens' sequence from 4-methoxybenzaldehyde as reported by Macchia and co-workers, Scheme 2.7.<sup>76</sup> Grignard coupling of **48** and **49** gave **47** (96% yield), and esterification by the procedure of Steglich and Neises<sup>77</sup> gave the desired ester **44**, 1-(3,5-dimethoxyphenyl)-2-(4-methoxyphenyl)ethyl ethanoate (70% yield).



Scheme 2.6 The synthesis of 1-(3,5-dimethoxyphenyl)-2-(4-methoxyphenyl)ethyl ethanoate **44**.



Scheme 2.7 The synthesis of aldehydes **49** and **58** *via* Darzens' sequence.

A solution of ester **44** in methanol had absorption maxima at 274 nm ( $\epsilon = 3600 \text{ M}^{-1}\text{cm}^{-1}$ ) and 280 nm ( $\epsilon = 3300 \text{ M}^{-1}\text{cm}^{-1}$ ), Figure 2.1-A. Excitation of **44** at 274 nm resulted in fluorescence with  $\lambda_{\text{max}}$  at 298 nm, and the 0,0 band was determined to be 288 nm (415 kJ/mol). Since 3,5-dimethoxybenzyl acetate itself does not fluoresce, this observation is attributed to the 4-methoxyphenyl chromophore, which will absorb competitively with the more reactive portion of the molecule.

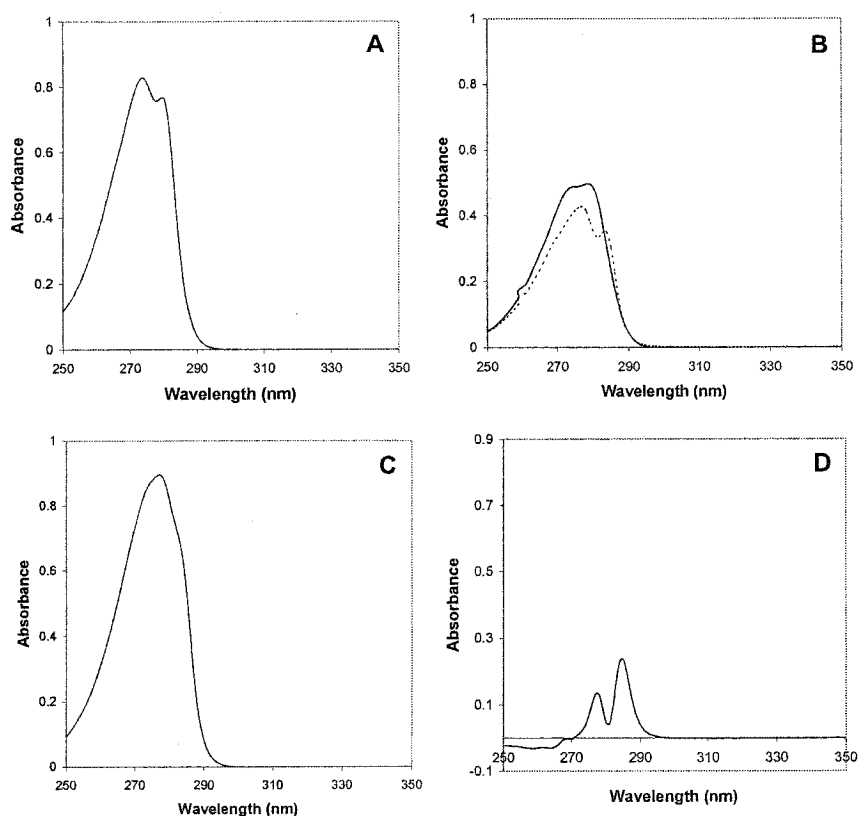


Figure 2.1 Absorption spectra (all solutions  $2.3 \times 10^{-4} \text{ M}$ ). **A.** Ester **44**. **B.** 1-(3,5-dimethoxyphenyl)ethyl ethanoate (solid line) and 4-methylanisole (dashed line). **C.** Summation of spectra in **B**. **D.** Subtraction of experimental spectrum of **44** in **A** from summation spectrum in **C**.

To check for any interaction between the two chromophores, the absorption spectra of 4-methylanisole and 1-(3,5-dimethoxyphenyl)ethyl ethanoate were recorded and normalized (Figure 2.1-B). Summation of the normalized spectra resulted in a

slightly higher absorption than was observed for **44** (Figure 2.1-C). Subtraction of the experimental spectrum of **44** from the summation of the two moieties showed peaks of residual absorption at 277 nm and 285 nm (Figure 2.1-D). No increased absorption was observed at longer wavelengths. Therefore, the competitive absorption between the two chromophores may decrease the quantum yield of any subsequent reactions, but there does not appear to be any strong ground state interaction between them.

### 2.2.2 Photolysis of Ester **44** in Methanol

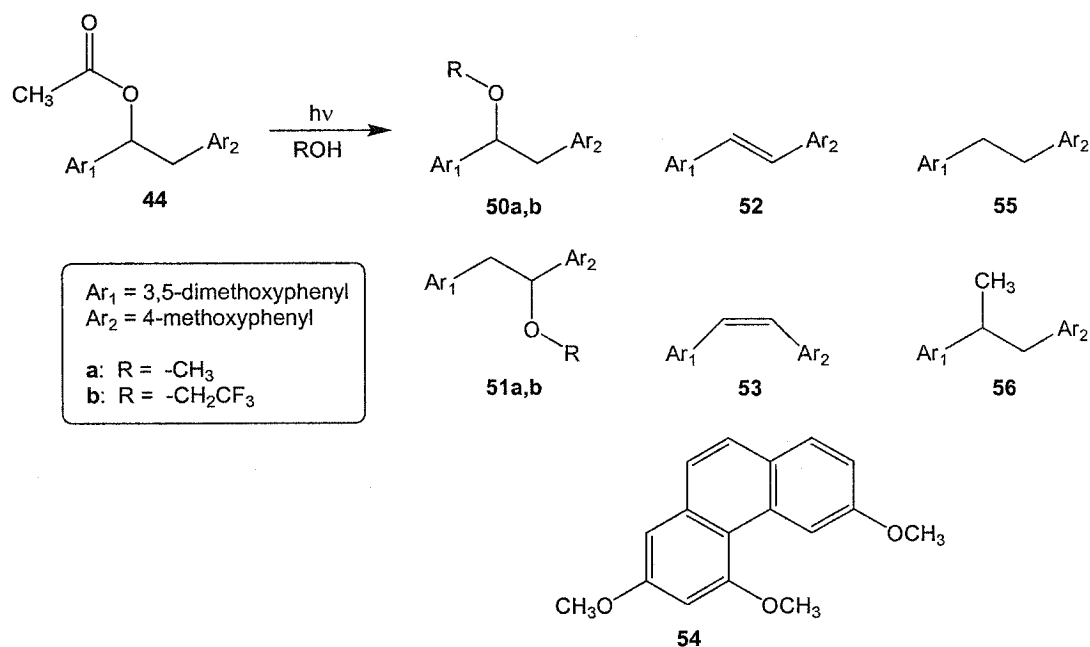
Photolysis of a nitrogen-saturated solution of **44** in methanol using a Rayonet reactor and 254 nm lamps afforded a mixture of seven products after irradiation for one hour, Scheme 2.8. Preliminary identification of the products was made on the basis of their mass spectra, which were recorded using a gas chromatograph with a mass selective detector (GC-MS). Pure samples were obtained either by independent syntheses or by isolation following photochemical reactions (*vide infra*). The reaction was also monitored by gas chromatography with a flame ionization detector (GC-FID). The GC-FID response was calibrated using each of the pure samples, thereby allowing accurate calculation of product yields. The final product yields after one hour are shown in Table 2.1, and Figure 2.2 shows a plot of the normalized product yields as a function of time.

Solvent	% Conversion <sup>a</sup>	<b>50</b> <sup>b</sup>	<b>51</b> <sup>b</sup>	<b>52</b>	<b>53</b>	<b>54</b>	<b>55</b>	<b>56</b>
Methanol (R = CH <sub>3</sub> )	89	42	2	18	19	4	5	10
TFE (R = CH <sub>2</sub> CF <sub>3</sub> )	82	30	27	13	13	5	4	7

a) Product yields are normalized to 100% because mass balances were essentially quantitative.

b) For R = CH<sub>3</sub>, products are designated **50a** and **51a**; for R = CH<sub>2</sub>CF<sub>3</sub>, products are designated **50b** and **51b**.

Table 2.1 Product yields after photolysis of ester **44** for 1 hour in methanol and TFE.



Scheme 2.8 Products formed by photolysis of ester **44** in methanol and TFE.

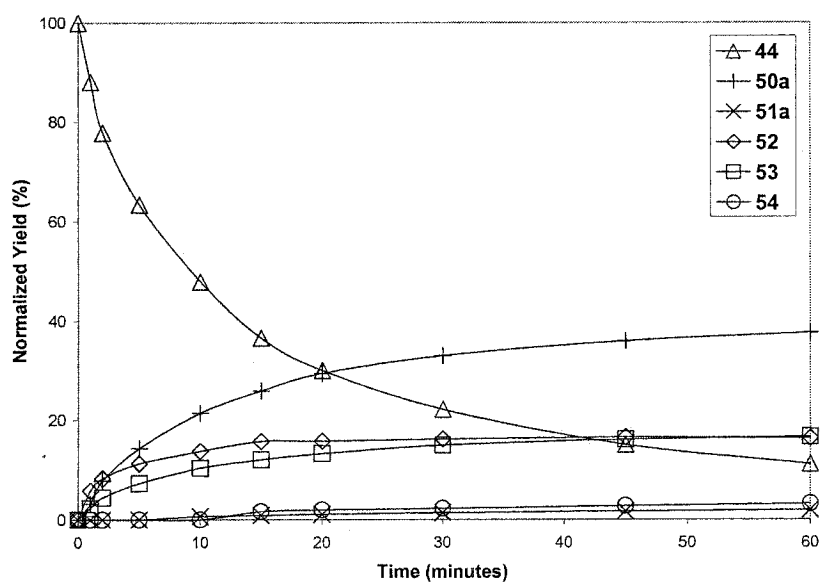
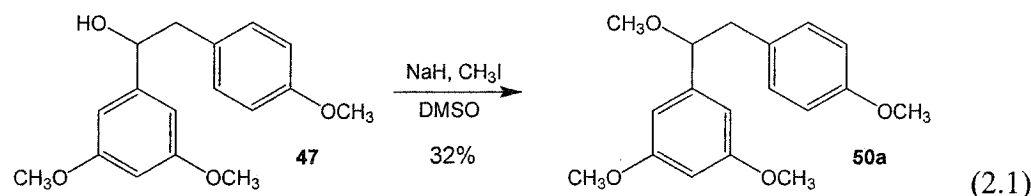


Figure 2.2 Product yields as a function of time for the photolysis of ester **44** in methanol (compounds **55** and **56** have been removed for improved clarity).

As shown in Table 2.2 and Figure 2.1, almost 90% of **44** was consumed after one hour of irradiation, at which point very little change in the relative product yields was

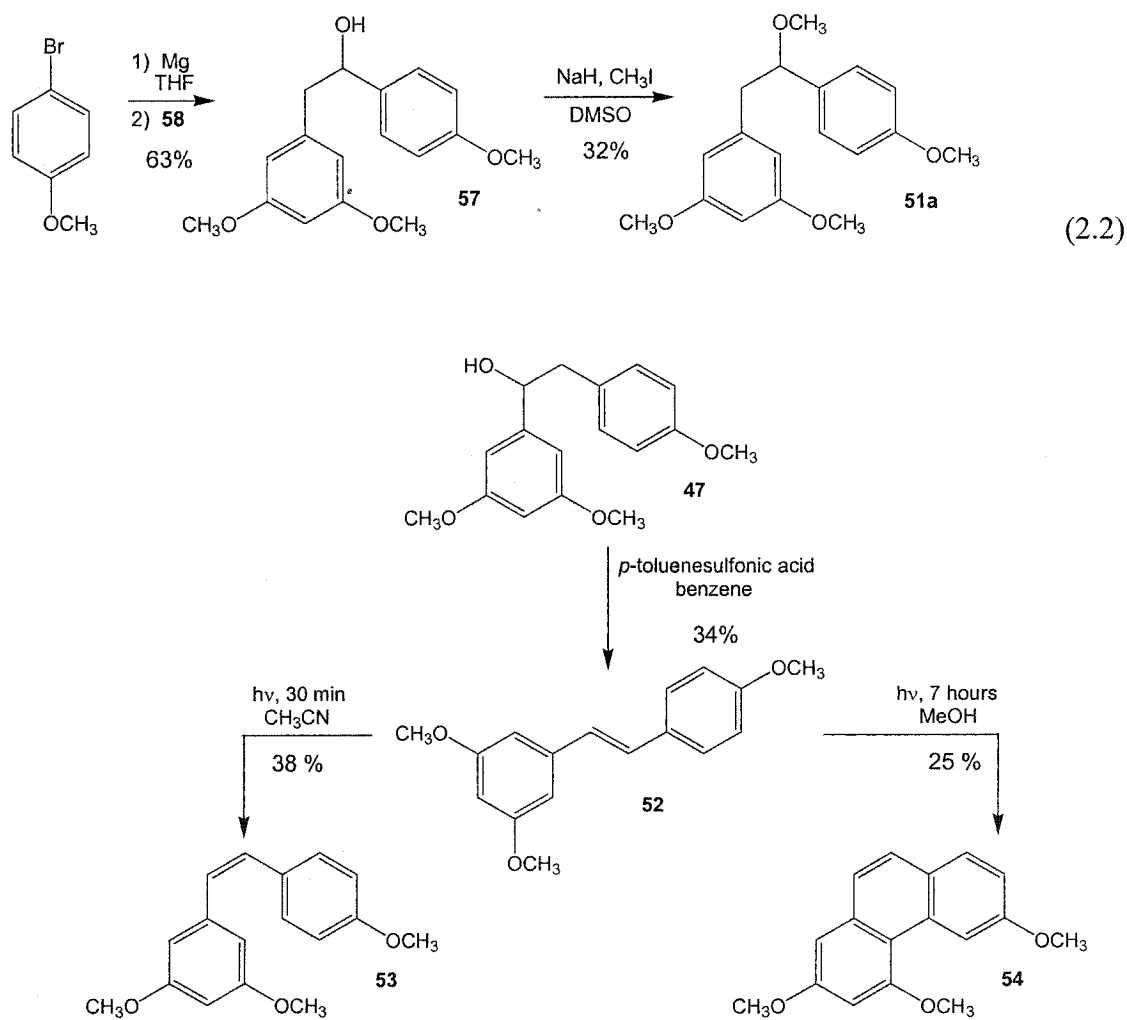
observed over time. For the purposes of the current project, the methyl ethers **50a** and **51a** ( $R = \text{CH}_3$ ) are of the greatest interest, since they are the products that would be formed from nucleophilic attack on carbocations **45** and **46** (Scheme 2.5). Although the yield of **51a** is difficult to measure at low conversions, the ratio of **50a** to **51a** appeared to decrease over the period of irradiation until a steady state ratio of 21:1 was reached; after only 10 minutes, however, **50a:51a** = 33:1.

The substituted stilbenes **52** and **53** are clearly primary photoproducts, but at low conversions the *trans* isomer **52** is formed in higher yield than the *cis* isomer **53** (**52:53** = 2:1 at 2%) conversion. The two isomers appear to photoequilibrate to a ratio of 1:1 at high conversions of **44**. The substituted phenanthrene **54** is likely produced by secondary photochemistry, namely a photochemically allowed conrotatory electrocyclic reaction of the *cis*-stilbene **53**, followed by oxidation of the dihydrophenanthrene intermediate. This reaction is well-established for other electron-rich stilbene derivatives.<sup>78</sup> Finally, products **55** and **56** are radical derived by-products of the reaction, as has been shown for a wide variety of arylmethyl esters (Scheme 1.7).



As noted above, the identification of most products was made by comparison with authentic samples. Ether **50a** was synthesized by reaction of alcohol **47** with sodium hydride and iodomethane, Equation 2.1. In order to produce **51a** *via* a similar alkylation procedure, the required alcohol **57** was synthesized by Grignard coupling of 4-bromoanisole and 2-(3,5-dimethoxyphenyl)ethanal **58**, Equation 2.2. The aldehyde **58**, in turn, was prepared using the Darzens' sequence from 3,5-dimethoxybenzaldehyde,

Scheme 2.7. The substituted *trans*-stilbene **52** was produced by dehydration of the alcohol **47** using *p*-toluenesulfonic acid in refluxing benzene, Scheme 2.9. Photochemical *trans*-*cis* isomerization of **52** in acetonitrile provided access to the substituted *cis*-stilbene **53** in a steady-state ratio of *trans*:*cis* = 1:2 (Pyrex filter, 280 nm cut-off). Finally, irradiation of **52** in an aerated solution of methanol gave the substituted phenanthrene **54** after purification by column chromatography.



Scheme 2.9 Independent synthesis of **52**, **53**, and **54** for comparison with products formed *via* photolysis of ester **44**.

An issue of some concern was whether or not **50a** could react by secondary photochemistry, and thereby revert to carbocation **45**. To this end, a nitrogen-saturated

solution of **50a** in methanol was irradiated. Although the ether was consumed (25% after one hour, 47% after five hours), only the reduction product **55** was detected. This reaction is likely the result of radical (not cation) intermediates. Column chromatography of the reaction mixture after a high-conversion photolysis of **50a** provided a convenient method for isolating larger amounts of **55** than were obtained following photolysis of **44** in methanol. No attempt was made to isolate or synthesize photoproduct **56**, and so its characterization rests solely on the GC-MS results.

### 2.2.3 Photolysis of Ester **44** in TFE

With hopes of prolonging the lifetime of cation **45**, and thereby allowing more time for the rearrangement to **46**, the photochemistry of **44** in TFE was examined under the same conditions as the experiments in methanol. Figure 2.3 shows the normalized product yields as a function of time, and the final product yields are provided in Table 2.1 (*vide supra*). As indicated in Scheme 2.8 and Table 2.1, the same photoproducts were formed as in the methanol photolysis, keeping in mind that the addition of TFE to cations **45** and **46** leads to the ethers **50b** and **51b** (*i.e.*, with  $R = \text{CH}_2\text{CF}_3$ ). The synthesis of pure samples of both trifluoroethyl ethers was accomplished from alcohols **47** and **57** using a modification of the Mitsunobu reaction developed by Falck and co-workers.<sup>79</sup> Attempts to alkylate either **47** or **57** using NaH/DMSO and 2-bromo-1,1,1-trifluoroethane gave no detectable amounts of the desired ethers. Just as in the case of the ether **50a** ( $R = \text{CH}_3$ ), **50b** ( $R = \text{CH}_2\text{CF}_3$ ) was also checked for its photochemical reactivity, this time in TFE. Consumption of the ether was observed, (29% conversion after one hour), but once again **55** was the only product from the reaction. None of the isomeric ether **51b** was detected, confirming that **50b** is not sufficiently reactive to give carbocation intermediates.



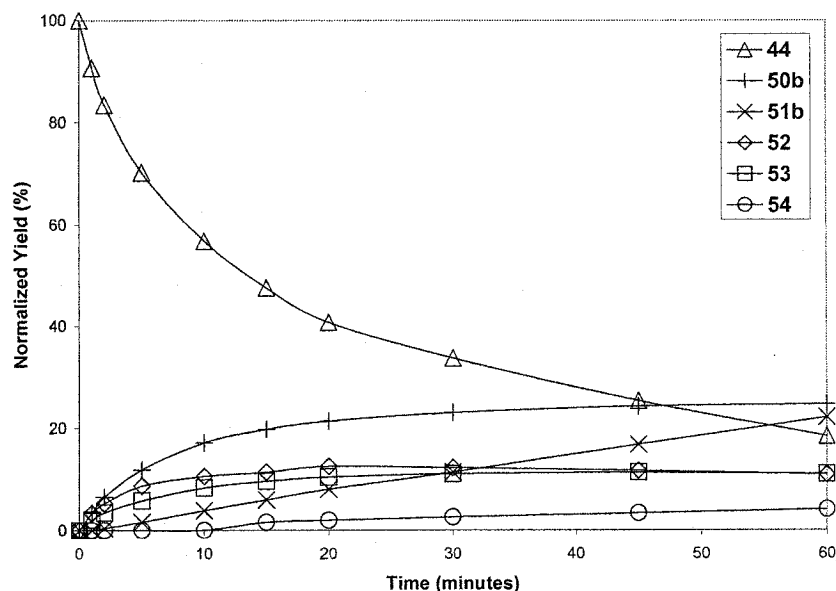


Figure 2.3 Product yields as a function of time for the photolysis of ester **44** in TFE (compounds **55** and **56** have been removed for improved clarity).

Although the percent conversion of **44** over one hour is essentially the same in methanol and TFE (89% *versus* 82%), the product yields do show some significant differences. As discussed earlier for the reaction in methanol ( $R = \text{CH}_3$ ), the ratio of the ether product derived from cation **45** (**50a**) to the product derived from cation **46** (**51a**) is 21:1 after one hour. The analogous ratio for the reaction in TFE ( $R = \text{CH}_2\text{CF}_3$ ) is **50b:51b** = 30:27 (approximately 1:1), supporting the possibility that the less nucleophilic solvent (TFE) perhaps allows more time for the 1,2-hydride shift to occur. However, closer examination of Figure 2.3 reveals that the ratio of **50b:51b** is not constant. In fact, the changes in the relative amounts of the ether products during the photolysis of **44** are much more pronounced in TFE (**50b:51b** = 16:1 after two minutes, 1:1 after one hour) than in methanol (**50a:51a** = 33:1 after ten minutes, 21:1 after one hour).

McClelland and co-workers have observed the 4-methoxyphenethyl cation at 340 nm in TFE and HFIP.<sup>47</sup> With the intention of observing the growth of cation **46** directly,

a solution of the ester **44** in TFE was subjected to LFP at 266 nm. As shown in the representative spectrum (Figure 2.4-A), an intense absorption band was observed from 280 nm (the lowest wavelength used) to 350 nm, with a maximum of approximately 300 nm. Importantly, the signal did not decay over any time window investigated with the laser system (10 ns to 50  $\mu$ s). The same signal was observed in solutions that were purged with either oxygen or nitrogen. To explore the idea that the signal might be due to a transient species that decays over a much longer time period, a solution of **44** in TFE was submitted to 50 laser pulses, and then monitored using a conventional UV-Vis spectrometer. The signal at 300 nm did not decay after 30 minutes, indicating that this signal is not due to a reactive intermediate, but rather to a strongly absorbing photoproduct. Comparison of the laser spectrum with the UV-Vis absorption spectra of the isolated products **50-56** suggests that the substituted *trans*-stilbene **52** ( $\lambda_{\text{max}} = 303$  nm,  $\epsilon_{\text{max}} = 29000 \text{ M}^{-1}\text{cm}^{-1}$ ) is the compound responsible for the absorption, Figure 2.4-B.

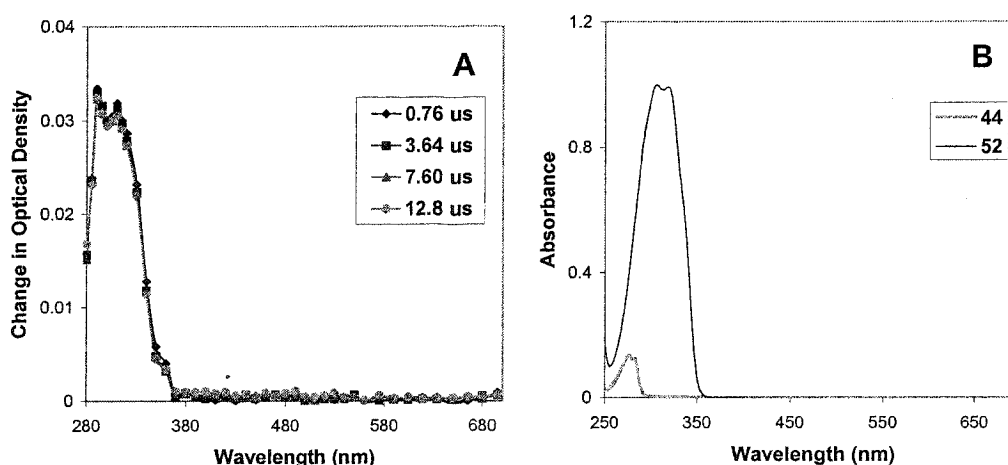


Figure 2.4 **A.** The change in optical density following 266 nm LFP of ester **44** in TFE (0.8  $\mu$ s – 13  $\mu$ s). **B.** Comparison of the absorption spectra of ester **44** and methoxy-substituted *trans*-stilbene **52** (both  $3.45 \times 10^{-5}$  M in methanol).

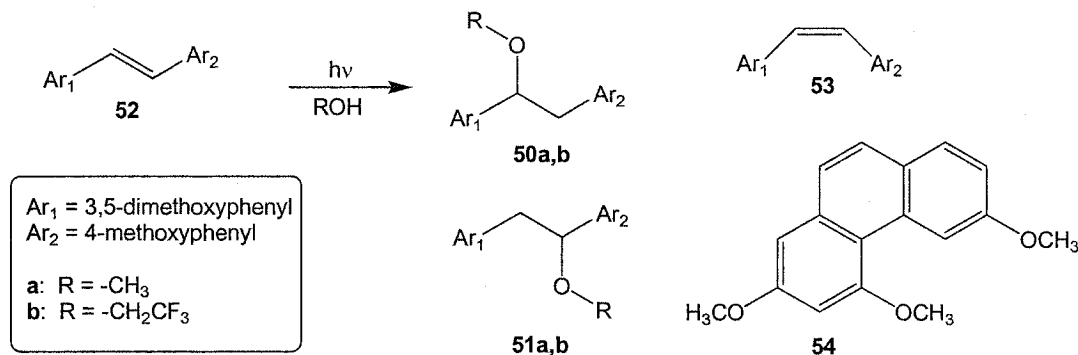
Also shown in Figure 2.4-B is the absorption spectrum of **44**. At the maximum light output of the lamp used for the steady state photolysis experiments ( $\lambda = 254$  nm), the extinction coefficient of **52** ( $\epsilon_{254} = 3030 \text{ M}^{-1}\text{cm}^{-1}$ ) is more than three times larger than that of **44** ( $\epsilon_{254} = 800 \text{ M}^{-1}\text{cm}^{-1}$ ). Furthermore, **52** absorbs much more strongly than **44** at longer wavelengths. This means that when the photolysis of **44** has proceeded to the point that  $[\mathbf{44}] < 3[\mathbf{52}]$ , the majority of the light will be absorbed by **52**. The results from the photolysis of **44** in the two solvents (Figures 2.2 and 2.3) suggest that this condition would be met between 10 and 15 minutes after starting the photolysis.

At this point, an important issue must be addressed. Because the formation of **52** during LFP of **44** makes the direct observation of cations **45** and **46** virtually impossible, the use of product yields in assessing the importance of rearrangement becomes critical. If the excited state of **52** is sufficiently reactive to photochemical addition of the alcohol solvents to give the ethers **50** and **51**, then any conclusions regarding carbocation rearrangements based on product yields will be incorrect. To address this issue, the photochemistry of the methoxy-substituted *trans*-stilbene **52** in methanol and TFE was examined.

#### 2.2.4 Photolysis of Methoxy-Substituted *trans*-Stilbene **52** in Methanol and TFE

The formation of **52** during the photolysis of **44** corresponds to the loss of acetic acid from the parent ester. For this reason, one equivalent of acetic acid was added to the solutions of **52** in each solvent prior to irradiation, so as to reproduce the reaction conditions as accurately as possible. No product formation was observed after stirring the solutions of **52** in methanol or TFE (with added acetic acid) for 48 hours in the dark, thus

confirming that **52** does not react by ground state chemistry during the time frame of the photolysis experiments.



Scheme 2.10 Products detected following the irradiation of the methoxy-substituted *trans*-stilbene **52** in methanol and TFE.

Solvent	Time (hours)	% Conversion <sup>a</sup>	<b>50<sup>b</sup></b>	<b>51<sup>b</sup></b>	<b>53</b>	<b>54</b>
Methanol (R = CH <sub>3</sub> )	1	48	0	4	88	8
Methanol (R = CH <sub>3</sub> )	5	63	0	10	64	26
TFE (R = CH <sub>2</sub> CF <sub>3</sub> )	1	80	4	60	27	9
TFE (R = CH <sub>2</sub> CF <sub>3</sub> )	4	95	2	87	3	8

a) Product yields are normalized to 100% because mass balances were essentially quantitative; see experimental section for complete analysis details; b) For R = CH<sub>3</sub>, products are designated **50a** and **51a**. For R = CH<sub>2</sub>CF<sub>3</sub>, products are designated **50b** and **51b**.

Table 2.2 Product yields after irradiation of methoxy-substituted *trans*-stilbene **52** in methanol and TFE.

Irradiation of **52** in the two solvents gave mixtures of four products, Scheme 2.10. Each of these products had already been observed during the photolysis of **44** (Scheme 2.8), and so calibrated product yields were calculated, Table 2.2. The normalized product yields as a function of time are shown in Figures 2.5-A (methanol) and 2.5-B (TFE). In striking contrast to the ester **44**, which exhibits very similar reactivity in both solvents, **52**

reacts much faster in TFE than in methanol. After one hour, the percent conversion of **52** in methanol is 48%, compared to 80% after the same time in TFE. In both solvents, the substituted stilbene isomers approach a steady state composition of approximately 1:1, and then disappear simultaneously, although the latter process occurs much more rapidly in TFE. The reactivity of **52** in TFE is even greater still when one takes into account the fact that the major product for the reaction in methanol is the *cis*-isomer **53**, whereas the solvent adduct **51b** is the major product in TFE. Another important observation is that the ether products that are formed in these reactions would require the formation of *both* carbocations **45** and **46**, apparently by photochemical protonation of **52**. Furthermore, in contrast to the results for **44**, the ethers produced *via* carbocation **46** (*i.e.*, **51a** and **51b**) are formed in greater yields than their isomeric counterparts (*i.e.*, **50a** and **50b**). In fact, **50a** was not detected even after five hours irradiation in methanol. These results strongly suggest that cations **45** and **46** are formed upon irradiation of **52** in methanol and TFE.

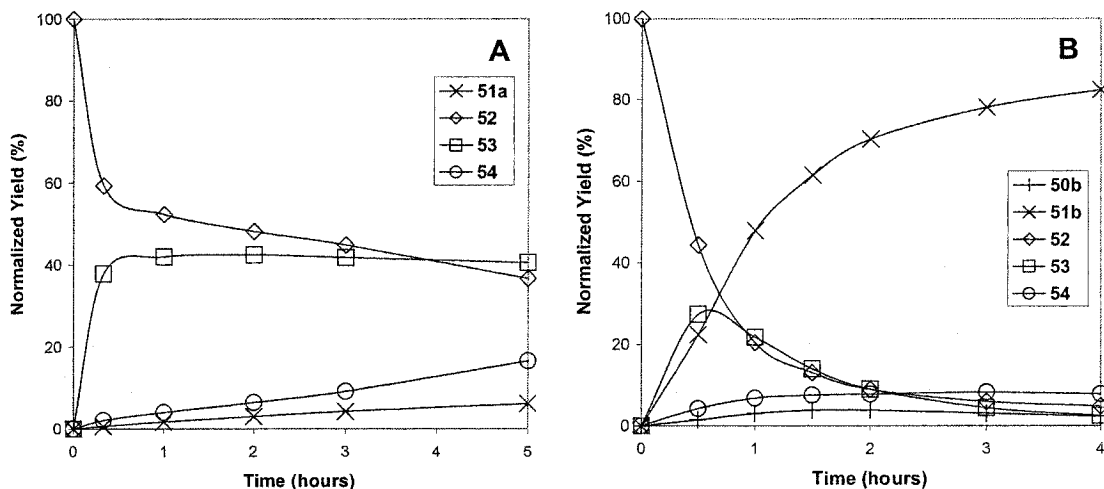


Figure 2.5 Product yields as a function of time for the irradiation of the methoxy-substituted *trans*-stilbene **52** in methanol (A) and TFE (B).

## 2.3 Discussion of Results

### 2.3.1 The Photochemistry of Ester 44

The general mechanism that has been developed for ester photochemistry (Scheme 1.9) seems to hold for ester 44. In the experiments described in Section 2.2.2, both ion- and radical-derived products are formed. The results from the photolysis of 44 in methanol and TFE initially suggested that the desired 1,2-hydride shift was occurring as predicted (Scheme 2.5). This was based on the premise that TFE, being a less nucleophilic solvent, would promote the formation of carbocation 46 from carbocation 45. The difference between the product ratios (50:51) seemed to support this idea. However, closer inspection of the data revealed that this ratio is not constant over the course of the experiment. For the reaction in methanol, 50a:51a = 33:1 after ten minutes and 20:1 after one hour. The change is even more dramatic for the photolysis in TFE: after two minutes 50b:51b = 16:1, but after one hour the ratio is 1:1. The change in the relative amounts of products resulting from nucleophilic attack by the solvents on carbocations 45 and 46 indicates that a secondary photochemical reaction occurs during the steady state photolysis of 44. One possible explanation is that the ethers 50 decay over the course of the photolysis experiments involving 44. Although these ethers were shown to be photochemically active in the control experiments (50a in methanol and 50b in TFE), they appear to react much too slowly to account for the observed changes in the 50:51 ratios. In the case of such a secondary reaction, the yield of the radical-derived product 55 would need to be greater than is observed (4-5%). Furthermore, the presence of several strongly-absorbing compounds (*i.e.*, 52, 53, and 54) in the reaction mixture will make absorption by the ethers 50 even less likely. Indeed, the only experiment in which decay of either 50a or 50b was observed was during the photolysis of 52 in TFE (Figure

2.5-B). In that experiment the yield of **50b** did decrease over the final two hours of irradiation (from 4% to 2%), but only after most of the methoxy-substituted stilbene **52** had been converted to products. Such a slow change in the yield of **50b** should not greatly affect the results of the ester photolysis experiments.

A much more plausible explanation of the observed changes in the **50:51** ratios is that secondary photochemistry provides an alternative pathway for the formation of the products derived from carbocation **46**, specifically the ethers **51**. As shown in the control experiments involving the photolysis of the ethers **50a** and **50b**, there is no active pathway for converting **50** to **51**. Rather, the secondary photochemical reaction is addition of the solvent to the excited state of the methoxy-substituted *trans*-stilbene **52**. As is clearly shown by the irradiations of **52** in methanol and TFE, cation-derived products (*i.e.*, **50** and **51**) can be formed with reasonable efficiency from **52** under the same reaction conditions used for the photolysis of ester **44**. Furthermore, this reaction favours the ethers **51** over **50**, which is the reverse of the regiochemistry observed during the photolysis of **44**. The LFP results demonstrate that **52** is formed rapidly upon irradiation of **44**, and that **52** absorbs competitively with **44** very early in the photolysis experiments involving the ester. Therefore, as **52** accumulates during the photolysis of **44**, the photochemistry of **52** will become more important, and **51** (formed primarily from **52**) will eventually be formed more rapidly than **50** (formed primarily from **44**). Even if the formation of **52** did not make the observation of the benzylic carbocations by LFP impossible (by obscuring the wavelengths of interest), the observation of a signal corresponding to cation **46** would not be conclusive evidence for the rearrangement of interest. Unfortunately, the rapid formation of **52** upon photolysis of **44** makes the ester a poor substrate for the investigation of carbocation rearrangements. These results are

similar to those of Lee-Ruff and co-workers<sup>70</sup> (Scheme 2.4), where the desired cation rearrangement is too unfavourable to compete with rapid quenching by the alcohol solvent (either by nucleophilic attack or by deprotonation). However, the photochemistry of **44** is further complicated by the fact that the by-products themselves are photochemically reactive, which makes reliable assessment of the rearrangement process extremely difficult.

The apparent lack of a 1,2-hydride shift from carbocation **45** to carbocation **46** is supported by ground state experiments described in the literature. Noyce and co-workers investigated the dehydration of several derivatives of 1,2-diphenylethanol in aqueous sulphuric acid.<sup>31,80</sup> They proposed a mechanism involving rapid acid-catalyzed formation of a carbocation intermediate, followed by rate limiting loss of a proton to give the corresponding stilbene product (*i.e.*, an E<sub>1</sub> mechanism). The dehydration of 1,2-diphenylethanol-1d proceeded with complete retention of deuterium, which suggests that scrambling of the protons *via* rapid (degenerate) hydride shifts of the carbocation intermediate *does not* occur. The current results imply that, even with the potential of a strong cation-stabilizing para methoxy substituent, the rearrangement of **45** to **46** is slow relative to other reactions of **45**. That the rearrangement appears to be unfavourable can be rationalized by two arguments. First, the difference in stability between the two carbocations may be significantly less than the 11-16 kcal/mol estimate made in Section 2.2.2. This estimate was made using measurements for *primary* benzylic carbocations, while the intermediates **45** and **46** are both *secondary* benzylic carbocations. Because the influence of aromatic substituents on the stability of primary cations is likely to be greater, the energy difference between **45** and **46** may well be smaller than the estimated value. A second issue is whether or not the minimum-energy conformation of the



carbocation intermediate may preclude the required orbital overlap for the 1,2-hydride shift (as discussed for the results of Lee-Ruff and co-workers, Section 2.1.1). Figure 2.6-A shows a Newman projection for the expected minimum energy conformation of the ester **44**. Following photolytic cleavage of acetate, the resulting carbocation **45** (Figure 2.6-B) will develop a planar geometry – use of molecular models suggests that the dihedral angle between the empty p-orbital and either of the C2 hydrogens would be approximately  $30^\circ$ . This value is quite close to the corresponding angle ( $32.2^\circ$ ) reported by Lee-Ruff and co-workers for high-level calculations of their fluorenyl cation **42**. Although **45** should be somewhat less restricted towards the conformational changes that are needed to attain a geometry which allows hydride transfer from C1 to C2, a further complication is the requirement of orbital overlap between the para methoxy substituent and the developing cationic site at C2 (during conversion of **45** to **46**). In summary, the smaller-than-expected energy difference between **45** and **46**, coupled with the requirement of a very explicit transition state, appear to prevent the 1,2-hydride shift outlined in Scheme 2.5.

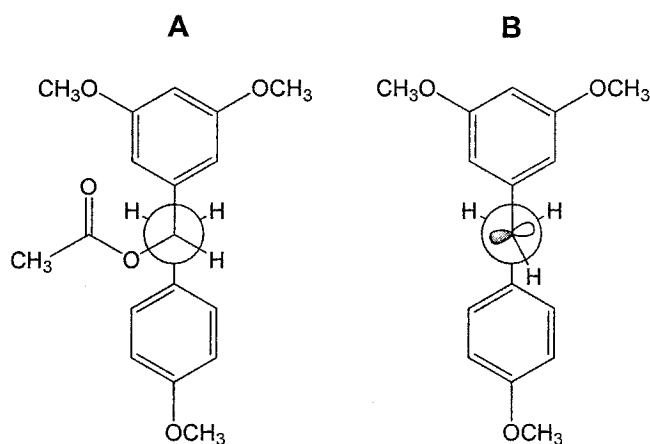


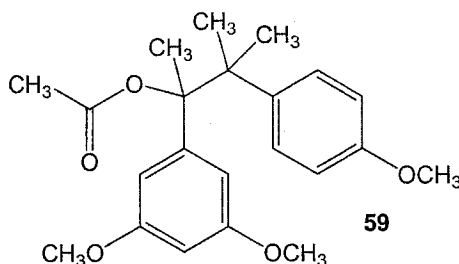
Figure 2.6 Newman projections of ester **44** (A) and carbocation intermediate **45** (B).

A final mechanistic detail that has yet to be resolved is the pathway for formation of the methoxy-substituted *trans*-stilbene **52** *via* photofragmentation of ester **44**. The first possibility is deprotonation of the carbocation intermediate, either by the protic solvents used for the photolysis experiments, or by the acetate ion within the contact ion pair. However, another possibility is hydrogen abstraction by the initially-formed acyloxy radical (*i.e.*, disproportionation). The rapid nature of such a reaction would still be consistent with the inability of oxygen to prohibit the formation of **52** during LFP of **44**. However, neither mechanistic possibility can be ruled out with the available data.

### 2.3.2 Future Directions: Carbocation Rearrangements and Stilbene Photochemistry

With the failure of **44** as a substrate for the direct observation of carbocation rearrangements, other possible rearrangement systems were considered. One option that was entertained involves the slight modification of **44** to the trimethyl derivative **59**. The advantage of this substrate over **44** is that the rearrangement would involve a 1,2-methyl shift, which, as shown by the rearrangements discussed in Scheme 1.2, is slightly more favourable than a 1,2-hydride shift. Also, the formation of a highly conjugated stilbene by-product *via* deprotonation (or hydride abstraction) is impossible for **59**. However, removal of hydrogen *via* either mechanism could result in the formation of an  $\alpha$ -alkyl styrene derivative, which could conceivably be photochemically reactive as well. The additional methyl groups present in substrate **59** would also result in a more stable carbocation following loss of acetate, likely leading to an even smaller energy difference between the two possible carbocations. Finally, the methyl groups would likely increase the steric congestion that restricts the carbocation intermediate from adopting the

geometry required for rearrangement. As a result of these concerns, the synthesis and photochemistry of **59** has not been pursued.



Further modifications of the structures involved in Scheme 2.5 will likely involve substantial changes to the method used for cation formation and/or the rearrangement of interest. A more promising route for the detection of carbocation rearrangements by photochemical techniques may be to focus on those carbocations that are known to undergo rearrangement when generated by ground state methods, and apply known photochemical reactions to produce the same carbocations. The photochemical pinacol rearrangement investigated by Lee-Ruff and co-workers<sup>69</sup> (Scheme 2.3) represents an example of this approach, even though it was not the intended aim of their research.

Although the original goal of this research project has not yet been realized, the investigations described in this chapter uncovered a new area of research that required further investigation – in particular the photochemical addition of alcohols to substituted stilbene derivatives. A survey of the literature indicated that the photochemical addition of methanol to several unhindered stilbene derivatives was first observed by Laarhoven and co-workers.<sup>81</sup> However, the influence of electron-rich substituents in the meta position was never addressed (the only compound examined with meta substituents was the symmetrical 3,3'-dimethylstilbene). The relationship between the photochemistry of **52** and the literature examples was not completely clear. The rapid addition of the solvent

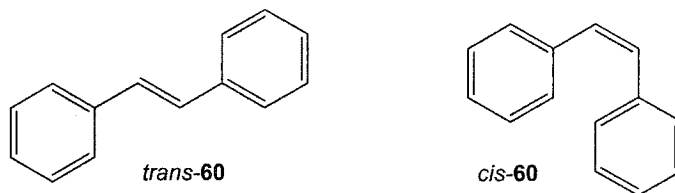
(TFE in particular) appears to be due to the two meta substituents (the 3,5-dimethoxyphenyl ring), while the preferred regiochemistry is governed by the para substituent (the 4-methoxyphenyl ring). In the case that photochemical addition of solvent to **52** involves photochemical protonation to yield carbocations **45** and **46**, a comparison of benzylic carbocation formation *via* *photofragmentation* reactions (methoxy-substituted arylmethyl esters, Section 1.3.3) and *photoaddition* reactions may be possible. Clearly, a larger set of stilbene derivatives was required to confidently assess the factors controlling the reaction. Chapter 3 will provide an introduction to the established photochemistry of stilbene, followed by a study of the photochemical reactivity of several methoxy-substituted stilbene derivatives in polar organic solvents.

## Chapter 3      The Photochemical Addition of Alcohols to Methoxy-Substituted Stilbene Derivatives

### 3.1 Introduction

#### 3.1.1 The Photochemistry of *trans*- and *cis*-Stilbene

The simple structures of the *trans* and *cis* isomers of 1,2-diphenylethene **60** (stilbene) belie their importance as the subjects of many photochemical investigations.<sup>82,83</sup> While *trans*-**60** is essentially planar, *cis*-**60** adopts a bent geometry due to steric repulsion between the ortho hydrogens of the two phenyl rings. These unfavourable non-bonding interactions make *cis*-**60** approximately 2.4 kcal/mol less stable than the *trans* isomer.<sup>82</sup> In addition to stability differences, the geometries of *cis*- and *trans*-**60** lead to quite distinct absorption spectra as a result of changes in  $\pi$ -conjugation. Compared to *trans*-**60** ( $\lambda_{\max} = 295$  nm,  $\epsilon_{\max} = 24000$  M<sup>-1</sup>cm<sup>-1</sup>), the  $S_0 \rightarrow S_1$  transition for *cis*-**60** ( $\lambda_{\max} = 276$  nm,  $\epsilon_{\max} = 10500$  M<sup>-1</sup>cm<sup>-1</sup>)<sup>84</sup> is of both higher energy (*i.e.*, shorter wavelength) and lower intensity.



Much of the interest in the photochemistry of stilbene and its substituted derivatives is a result of the efficient isomerization that occurs upon excitation of either isomer. Figure 3.1 displays the established energy coordinate diagram for *trans*- and *cis*-

**60.**<sup>82</sup> The thermal *trans-cis* isomerization of **60** requires ascending an activation barrier of approximately 48 kcal/mol<sup>85</sup> on the ground state energy surface (process  $t_{S_0} \rightarrow p_{S_0} \rightarrow c_{S_0}$ ). The transition state for isomerization (point  $p_{S_0}$ ) corresponds to a geometry in which the two C-Ph bonds are perpendicular to one another. A second pathway for *trans-cis* isomerization involves photochemical excitation of *trans-60* to its first excited single state (designated  $t_{S_1}$  in Figure 3.1). The  $t_{S_1}$  state displays only very small quantum yields of fluorescence ( $\phi_f = 0.04$ )<sup>86</sup> and intersystem crossing ( $\phi_{isc} = 0.002$ ).<sup>82</sup> The rates of these two deactivation processes are too slow to compete with rapid bond torsion on the  $S_1$  surface, which converts  $t_{S_1}$  to  $p_{S_1}$ . Internal conversion from  $p_{S_1}$  to  $p_{S_0}$  leads to rapid formation of either  $t_{S_0}$  (*trans-60*, no net reaction) or  $c_{S_0}$  (*cis-60*, net *trans-cis* isomerization) with approximately equal probabilities. Excited state bond torsion is the most favourable deactivation pathway for  $t_{S_1}$  at room temperature, as demonstrated by the high quantum yield for *trans-cis* isomerization,  $\phi_{tc} = 0.40$ .

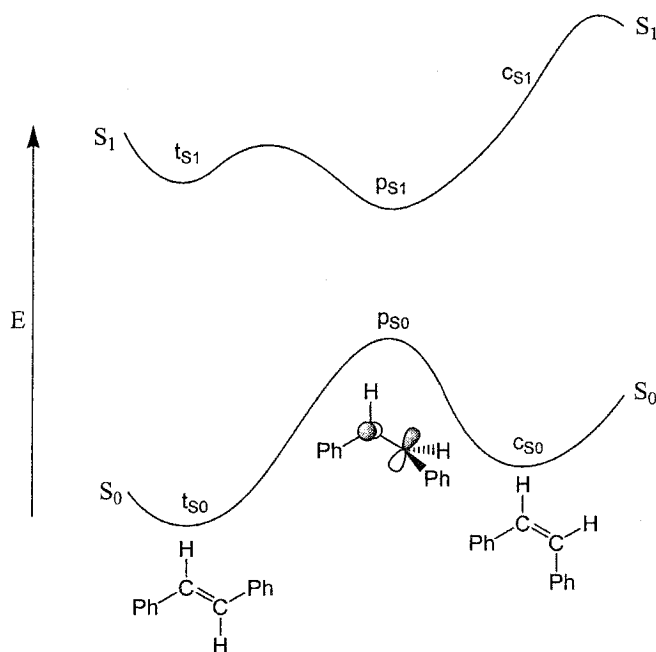
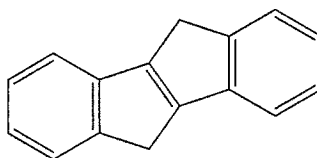


Figure 3.1 The energy-coordinate diagram for stilbene isomerization *via* ground and excited states (not to scale).

The activated process leading from  $t_{S_1}$  to  $p_{S_1}$  has been investigated using a variety of techniques. Most studies of stilbene photochemistry rely on the observation that any restriction to bond torsion results in *lower* quantum yields of isomerization, as well as *higher* quantum yields of fluorescence. In effect, the  $t_{S_1}$  to  $p_{S_1}$  process provides a pathway for deactivating the excited state – changes in the reaction conditions that hinder this process allow fluorescence to become a more important deactivation mechanism. The inverse relationship between  $\phi_{ic}$  and  $\phi_f$  is demonstrated by the dramatically different properties of *trans*-**60** and compound **61**. As shown by Saltiel and co-workers,<sup>87</sup> *trans*-**60** and **61** display similar absorption spectra due to the presence of the same  $\pi$ -system in each case. However, the quantum yield of fluorescence for **61** was found to be unity, compared to 0.04 for *trans*-**60**. The rigid structure of **61** completely inhibits deactivation of  $t_{S_1}$  by bond torsion, and so fluorescence is the dominant  $S_1 \rightarrow S_0$  pathway.

**61**

While the restriction of C=C twisting by covalent bonding clearly results in substantial increases in stilbene fluorescence, a great many studies have focussed on inducing similar changes by altering experimental conditions. Increased values of  $\phi_f$  for *trans*-**60** have been obtained by restricting the solute in high-viscosity solvents ( $\phi_f = 0.15$  in glycerol)<sup>88</sup> or in low-temperature glass matrices ( $\phi_f = 0.75$  in methylcyclohexane/isohexane at 133 K).<sup>89</sup> Values of  $\phi_f$ ,  $\phi_{ic}$ , and  $\tau_s$  have been obtained over a wide range of temperatures for *trans*-**60** in fluid solution (100 K to 300 K in methylcyclohexane/

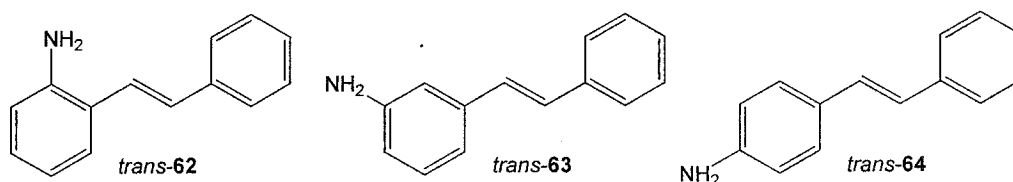
isohexane). An increase in both  $\phi_f$  and  $\tau_s$  was observed as the temperature was lowered, and a concomitant decrease in  $\phi_{tc}$  was also observed. Fitting of the temperature-dependent singlet lifetimes to the Arrhenius equation provided an activation energy of 3.5 kcal/mol for the  $t_{S1} \rightarrow p_{S1}$  process in non-polar solvents.<sup>90</sup> Later investigations in nitrile solvents indicated a slightly lower value (2.6 kcal/mol),<sup>91</sup> which suggests that the transition state for bond rotation is polarizable. A comparison between the reported literature values<sup>92</sup> for the fluorescence quantum yield of *trans*-60 in acetonitrile ( $\phi_f = 0.02$ ) and pentane ( $\phi_f = 0.04$ ) supports this argument.

Excitation of *cis*-60 also results in photochemical isomerization to *trans*-60. In contrast to the 3.5 kcal/mol thermal barrier for bond torsion of  $t_{S1}$ , the  $c_{S1}$  state undergoes essentially barrierless bond rotation to  $p_{S1}$ . The rapid decay of  $c_{S1}$  is demonstrated by the very low fluorescence quantum yield (estimated as  $\phi_f = 0.0001$ )<sup>93</sup> and short singlet lifetime (approximately 1 ps, compared to 70 ps for *trans*-60).<sup>94,95</sup> Moreover, Saltiel and co-workers were able to observe fluorescence from *trans*-60 upon excitation of *cis*-60, and this observation was attributed to partial intervention of a pathway involving adiabatic formation of  $t_{S1}$  followed by emission (*i.e.*,  $c_{S1} \rightarrow p_{S1} \rightarrow t_{S1} \rightarrow t_{S0}$ ). Excitation of *cis*-60 also results in approximately 30% of  $c_{S1}$  decaying *via* an electrocyclic ring closure to give a dihydrophenanthrene intermediate, which results in phenanthrene formation upon oxidation. These cyclization reactions have been reviewed,<sup>96</sup> and will not be discussed to a great extent in the current report.



### 3.1.2 The meta-Amino Effect in Stilbene Photochemistry

A 1997 publication by Lewis and Yang<sup>97</sup> described an unusual observation with respect to the photophysical properties of several amino-substituted stilbene derivatives. Those substrates in which the amino substituent occupied the meta position were found to have higher fluorescence quantum yields and longer singlet lifetimes in comparison to the para isomers. In addition, the isomerization quantum yields of the meta derivatives were markedly smaller than those of the para substrates. The highly fluorescent singlet states of the meta isomers could be quenched by added methanol and, in one case (which will be described in Section 3.1.3), addition of methanol to the alkene double bond was observed. A later publication by Lewis and co-workers<sup>98</sup> outlined many of the important characteristics of this “meta-amino effect” for the three amino-substituted *trans*-stilbenes: *trans*-2-aminostilbene (ortho, *trans*-62), *trans*-3-aminostilbene (meta, *trans*-63), and *trans*-4-aminostilbene (para, *trans*-64).



A comparison of several photophysical parameters for these three substrates (in addition to *trans*-stilbene) is presented in Table 3.1. The clear indication from these data is that the excited states of *trans*-62 and *trans*-63 (ortho and meta) are significantly different than those of *trans*-60 and *trans*-64 (unsubstituted and para). The ortho and meta isomers display longer singlet lifetimes  $\tau_s$  and higher quantum yields of fluorescence  $\phi_f$  than the unsubstituted and para substrates. Furthermore, those substrates for which  $\phi_f$  is high also have exceptionally small quantum yields of isomerization  $\phi_{ic}$ .

These measurements suggest that the presence of strong electron donating substituents in the ortho and meta positions results in an *electronic* restriction of the singlet state bond torsion process (compared to the restrictions imposed by changes in structure, solvent viscosity, and temperature that were discussed in Section 3.1.1).

Substrate	Solvent	$\lambda_{\max}$ (abs) <sup>a</sup> nm	$\epsilon_{\max}$ (abs) <sup>a</sup> M <sup>-1</sup> cm <sup>-1</sup>	$\lambda_{\max}$ (fluor) nm	$\tau_s$ ns	$\phi_f$	$\phi_{tc}$
<i>trans</i> -60	hexane	294, (307, 321)	28000	347	0.07 <sup>b</sup>	0.04 <sup>c</sup>	0.4 <sup>d</sup>
	acetonitrile	294, (308, 320)	29500, (28800, 18200)	347	-	0.02 <sup>e</sup>	0.45 <sup>e</sup>
<i>trans</i> -62	hexane	286, 334	17800, 12900	407	3.7	0.88	0.04
	acetonitrile	291, 346	17800, 12000	445	5.4	0.69	0.12
<i>trans</i> -63	hexane	298, (311, 329)	24000, (19100, 8710)	387	7.5	0.78	0.09
	acetonitrile	300, (312, 332)	25700, (20000, 7940)	446	11.7	0.40	0.23
<i>trans</i> -64	hexane	316, (332)	31600, (29500)	380	0.1	0.05	0.49
	acetonitrile	(318), 336	(30900), 32400	423	0.1	0.03	0.52

a) Values in parentheses correspond to lower intensity shoulders in the absorption band. b) Reference 95.  
c) Reference 86. d) Reference 108. e) Reference 92.

Table 3.1 Photophysical data in hexanes and acetonitrile for *trans*-stilbene (*trans*-60) and three isomeric mono-amino stilbenes *trans*-62, *trans*-63, and *trans*-64.

In contrast to *trans*-60 and *trans*-64, for which the singlet lifetimes increase with decreasing temperature, the singlet lifetimes of *trans*-62 and *trans*-63 were found to be essentially independent of temperature from 298 K down to 80 K in isopentane solution. These results indicated that for *trans*-62 and *trans*-63, the activated bond torsion process ( $t_{S1} \rightarrow p_{S1}$  in Figure 3.1) does not compete with fluorescence. A detailed analysis of the singlet lifetime data for the three aminostilbenes provided estimates of the activation energies for singlet state bond torsion:  $\geq 7$  kcal/mol for both *trans*-62 and *trans*-63, and

3.5 kcal/mol for *trans*-64. The latter value is in accord with the barrier for C=C bond rotation in *trans*-60. However, the significantly larger values for the ortho and meta isomers pointed to an exceptional stabilization of  $t_{S1}$  relative to  $p_{S1}$  for these two substrates. Figure 3.2 provides a graphical comparison of the barriers for singlet state bond torsion for the two classes of compounds.

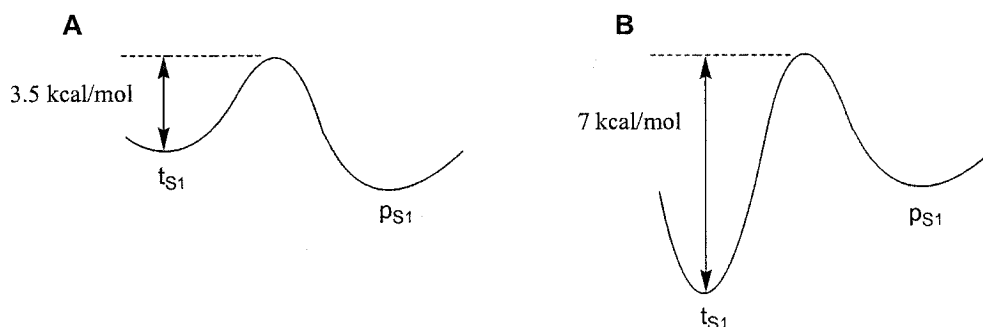


Figure 3.2 The barriers for singlet state bond torsion for **A)** *trans*-60 and *trans*-64; **B)** *trans*-62 and *trans*-63.

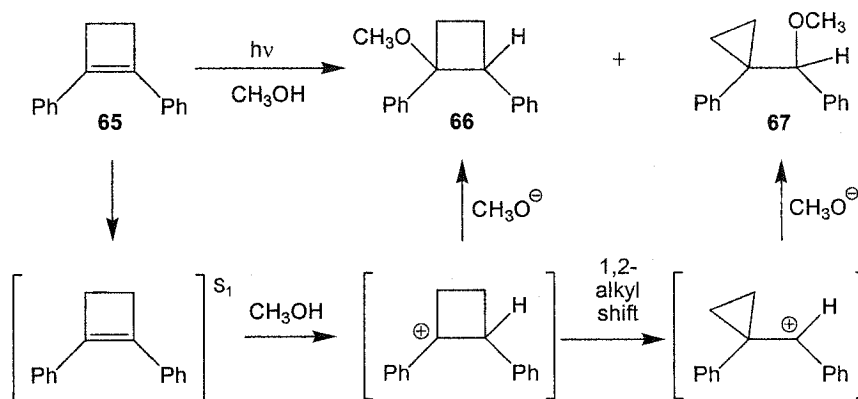
As described above, the temperature-independent lifetimes for *trans*-62 and *trans*-63 indicate that no activated process competes with fluorescence for these two substrates. If this is true, and if the only pathway for *trans-cis* isomerization is on the  $S_1$  surface, then the quantum yields for isomerization should be zero for the ortho and meta substrates. Since this is clearly not the observed behaviour, a second pathway for photoisomerization must be present. Sensitization experiments have shown that the triplet state of *trans*-60 undergoes barrierless twisting to reach the perpendicular geometry on the  $T_1$  surface<sup>82</sup> (using the notation of Figure 3.1, this process would be  $t_{S1} \rightarrow t_{T1} \rightarrow p_{T1}$ ). Thus, Lewis and co-workers concluded that the isomerization mechanism for *trans*-62 and *trans*-63 occurs via intersystem crossing to  $T_1$ , followed by barrierless bond rotation.<sup>98</sup> Isomerization through an intersystem crossing mechanism is well-documented for substrates that undergo exceptionally rapid intersystem crossing (bromo- and nitro-substituted stilbenes

are examples),<sup>82</sup> but in the case of *trans*-**62** and *trans*-**63** the singlet state mechanism is simply too slow to compete with the typical rate of intersystem crossing.

Later studies by Lewis and Kalgutkar investigated the photochemistry of the corresponding *cis*-aminostilbenes.<sup>99</sup> The fluorescence quantum yield and singlet lifetime of *cis*-**63** were both much higher than the values for the unsubstituted stilbene *cis*-**60**, but not nearly as large as any of the *trans*-isomers. The photochemistry of substrates possessing multiple amino substituents<sup>100</sup> and electron withdrawing cyano groups<sup>101</sup> has also been reported. Yang and co-workers have recently published several reports which detail the photochemistry of more complex aminostilbene derivatives.<sup>102,103,104</sup>

### 3.1.3 The Photochemical Addition of Alcohols to Stilbene Derivatives

An early example of the photochemical addition of an alcohol to a stilbene derivative is the addition of methanol to 1,2-diphenylcyclobutene **65**, as reported by Sakuragi and co-workers.<sup>105</sup> This substrate is similar to **62**, where the usual deactivation of the first excited singlet state is prohibited by the bridged structure, and the quantum yield of fluorescence approaches unity. The highly fluorescent singlet state of **65** was quenched by methanol to give products **66** and **67**, Scheme 3.1. The formation of the rearrangement product **67** indicates that the reaction proceeds *via* photochemical protonation of excited **65** to give a cyclobutyl cation, followed by a 1,2-alkyl shift to produce the highly stabilized cyclopropylmethyl cation. Trapping of either cation by solvent is possible, giving **66** (25%) and **67** (43%). The reasonably high yield of product **67** indicates that this system may be useful for future carbocation rearrangement studies designed to avoid the difficulties encountered in Chapter 1.

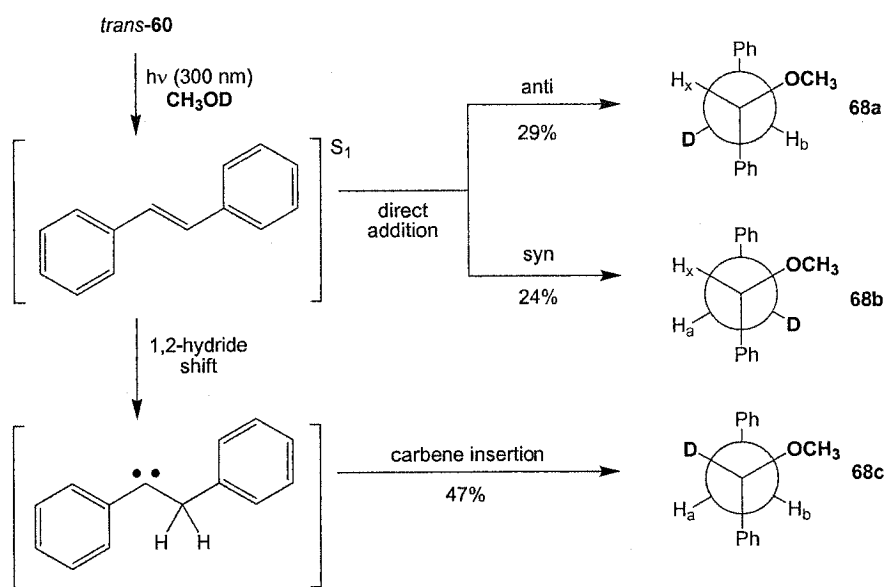


Scheme 3.1 Photochemical addition of methanol to 1,2-diphenylcyclobutene **65**.

As mentioned in Section 2.3.2, the mechanism for the photochemical addition of methanol to *trans*-stilbene (*trans*-**60**) itself was elucidated by Laarhoven and co-workers.<sup>81</sup> Plots of yield versus time for the irradiation of *trans*-**60** at 300 nm ( $4 \times 10^{-4}$  M in methanol) showed rapid equilibration ( $\approx$  five minutes) to a 4:1 ratio of *cis*-**60**:*trans*-**60**, followed by slow formation of phenanthrene and the methanol adduct. The absolute yield of the methanol adduct after two hours of irradiation was approximately 25% (not taking into account unreacted stilbene), and the quantum yield of the reaction was estimated as 0.01. Several other substrates reacted in a similar manner: *trans*-4-methylstilbene, *trans*-4-methoxy-4'-methylstilbene, *trans*-4-methoxystilbene, *trans*-3,3'-dimethylstilbene, *trans*-4,4'-difluorostilbene, and 1,2-diphenylcyclopentene all gave methanol adducts upon irradiation.

The mechanism of the addition reaction was proposed on the basis of several pieces of evidence. Irradiations of *trans*-**60** in methanol with a 20-fold excess of  $\text{H}_2\text{SO}_4$  resulted in identical yields as the experiments in pure methanol. In contrast to the fluorescence quenching observed for 1,2-diphenylcyclobutene **65**, the intensity of *trans*-**60** fluorescence remained unchanged even in 6 M methanolic  $\text{H}_2\text{SO}_4$ . These observations

indicated that the photochemical addition of methanol to the stilbene derivatives did not involve protonation of the excited states. Sensitized irradiation of *trans*-**60** using excess benzophenone resulted in only *trans-cis* isomerization, so a triplet pathway for product formation was also ruled out.

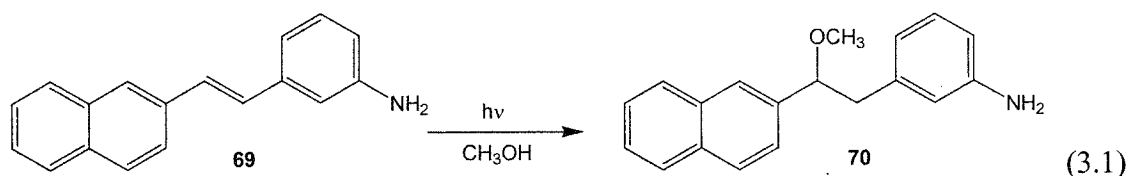


Scheme 3.2 The photochemical addition of methanol to *trans*-**60** via competing mechanisms (direct addition and carbene insertion).

The mechanistic pathway that was proposed by Laarhoven and co-workers to account for the formation of methanol adducts is shown in Scheme 3.2. The critical experiment that led to this scheme was the irradiation of *trans*-**60** in  $\text{CH}_3\text{OD}$ . There are three isomeric products that may be formed in this reaction (**68a-b**) corresponding to the three positions for deuterium incorporation. The three protons are in distinct chemical environments, and so each can be observed separately by  $^1\text{H}$  NMR. The relative amounts of each proton present in the final product mixture can be obtained from the peak areas, and comparison of the spectra from  $\text{CH}_3\text{OD}$  and  $\text{CH}_3\text{OH}$  irradiations allows calculation of the relative yields of **68a-c**. The results indicated that each of the three products was

formed upon irradiation, and a divergent mechanistic pathway was used to explain this observation. The two competing pathways are: 1) direct addition across the central alkene unit to give the anti (**68a**) and syn (**68b**) addition products, and 2) rearrangement of  $t_{S1}$  via a 1,2-hydride shift to give a carbene intermediate, followed by insertion into the O-H bond of the solvent. The presence of the second process was further supported by the observation that product **68c** was formed during the irradiation of 1,1-diphenylethylene in methanol, presumably via a 1,2-phenyl shift to give the same carbene intermediate.

Lewis and Yang have observed the photochemical addition of methanol to amino-substituted stilbene derivatives.<sup>97</sup> Irradiation of 2-(3-aminostyryl)naphthalene **69** in methanol provided the corresponding methanol adduct **70**, Equation 3.1. The reactivity of **69** appears to be due in large part to the meta-amino effect, and the long-lived singlet state of the substrate ( $\tau_s = 12.5$  ns in acetonitrile). By contrast, the para-amino isomer ( $\tau_s = 0.23$  ns in acetonitrile) is unreactive in methanol.



In work that is more closely related to the current project, the photochemistry of several hydroxystilbene isomers has been investigated. Lewis and Crompton<sup>106</sup> reported that whereas *trans*-3-hydroxystilbene ( $\tau_s = 2.0$  ns in tetrahydrofuran) undergoes excited state proton transfer in aqueous solution, *trans*-4-hydroxystilbene ( $\tau_s = 0.03$  ns in tetrahydrofuran) only reacts via isomerization. Again, the more rapid isomerization of the para isomer provides a deactivation pathway that is not available for the meta isomer.

Arai and co-workers<sup>107</sup> later reported that *trans*-3-hydroxystilbene undergoes addition of water to the central alkene unit upon irradiation in a 1:1 H<sub>2</sub>O:CH<sub>3</sub>CN mixture.

### 3.1.4 Project Proposal

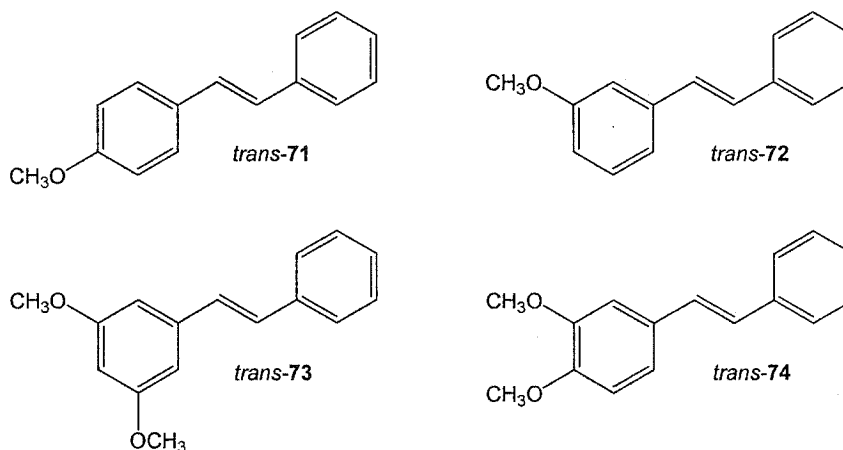
The literature work that has been summarized above clearly demonstrates that changing the position of an electron donating substituent on the stilbene chromophore can dramatically change the photophysical properties of the substrate. In particular, the barriers for bond torsion on the S<sub>1</sub> surface appear to be quite sensitive to the position of the substituent. Larger torsion barriers result in lower quantum yields of isomerization, and competitive deactivation processes begin to play more important roles in the photochemistry of the t<sub>S1</sub> state. Fluorescence, intersystem crossing, deprotonation, and addition of alcohols may then occur, depending on the reaction conditions.

Clearly, the study of these effects has so far been focussed on the very strong electron donating amino substituent. Only very recent work has examined the hydroxystilbene isomers,<sup>106,107</sup> and the methoxystilbenes have hardly been investigated at all. Laarhoven and co-workers<sup>81</sup> did report that *trans*-4-methoxystilbene and *trans*-4-methoxy-4'-methylstilbene underwent photochemical addition of methanol, but no other positional isomers were studied. One publication by Güsten and Klasinc<sup>108</sup> reported the quantum yields of isomerization for *trans*-4-methoxystilbene and *trans*-3-methoxystilbene in cyclohexane as 0.40 and 0.31, respectively. The somewhat unremarkable difference between these values has been taken as evidence that the methoxy substituent is perhaps unable to exert a very strong influence on the photophysical properties of the stilbene chromophore.<sup>98</sup>



However, the photochemistry of methoxy-substituted arylmethyl esters is extremely sensitive to the position of the substituent, particularly for the meta-substituted cases (as discussed in detail in Section 1.3.3). Furthermore, the presence of multiple methoxy substituents induces even greater changes in the photochemistry of these substrates. The effect of multiple amino substituents on the photochemistry of the stilbene chromophore is less clear; *trans*-3,5-diaminostilbene displays a smaller quantum yield of fluorescence ( $\phi_f = 0.10$  in acetonitrile) and a longer singlet lifetime ( $\tau_s = 16.1$  ns in acetonitrile) than the mono-amino derivative *trans*-**63** (data in Table 3.1).<sup>100</sup> The quantum yield of isomerization for the di-amino substrate was not reported in any solvent, so a comparison of  $\phi_{tc}$  values is not possible.

A comprehensive study into the photophysical and photochemical properties of methoxy-substituted stilbene derivatives is attractive for many reasons: 1) providing a clear link between two prominent examples of the photochemical meta effect in two very different systems, 2) comparing the amino and methoxy substituents as determinants of stilbene photoreactivity, 3) the possibility of observing photochemical reactivities (such as TFE addition) that correlate with the photophysical properties (such as  $\phi_f$ ,  $\phi_{tc}$ , and  $\tau_s$ ) for a variety of substrates, 4) elucidating the mechanism of the TFE addition reaction observed for *trans*-**52**, and 5) providing a better understanding of the photochemical addition of alcohols to stilbene and its derivatives. The substrates that were chosen for a preliminary investigation of methoxy-substituted stilbene photochemistry are *trans*-stilbene (*trans*-**60**), *trans*-4-methoxystilbene (*trans*-**71**), *trans*-3-methoxystilbene (*trans*-**72**), *trans*-3,5-dimethoxystilbene (*trans*-**73**), and *trans*-3,4-dimethoxystilbene (*trans*-**74**).



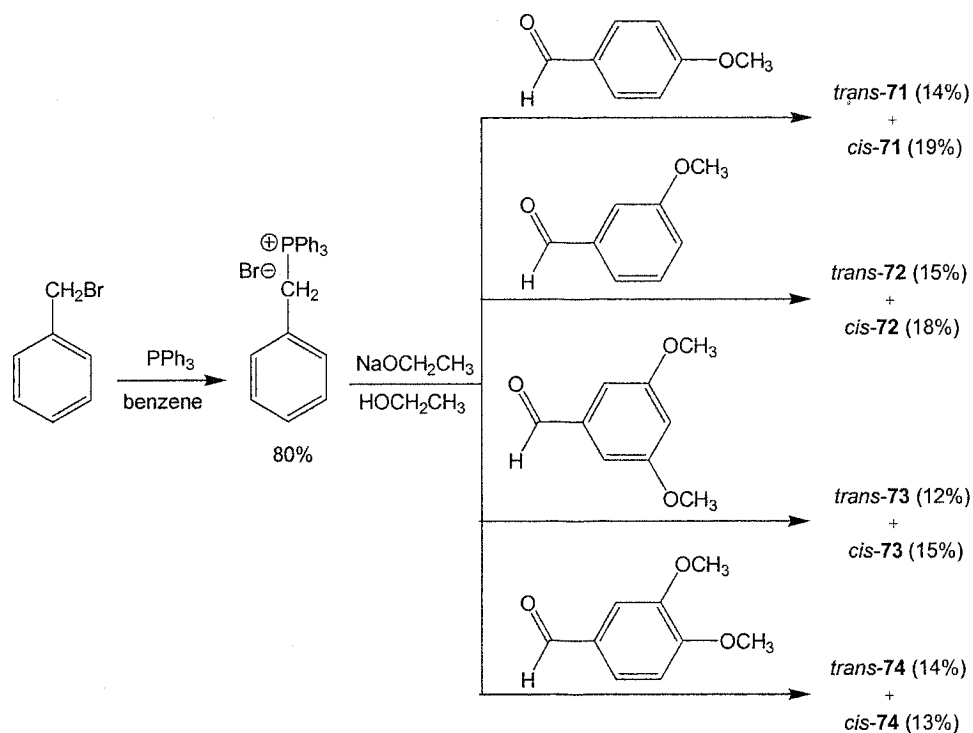
The investigation of *trans*-stilbene and the para and meta methoxy derivatives *trans-71* and *trans-72* are obvious choices for a study of positional substituent effects in stilbene photochemistry. The di-meta derivative *trans-73* will allow a good comparison to benzylic ester photochemistry, where the 3,5-dimethoxyphenyl chromophore is well-known to impart high reactivity. The *trans-74* substrate presents the possibility of observing a direct competition between the effects of para and meta substituents within the same compound. Much of the work presented in this chapter has been published in the Journal of Organic Chemistry,<sup>109</sup> but some of the results that appeared in the publication will not be discussed until Chapter 4.

## 3.2 Experimental Results

### 3.2.1 Synthesis of Methoxy-Substituted Stilbene Derivatives

In Chapter 2, the synthesis of the methoxy-substituted *trans*-stilbene **52** was accomplished by dehydration of the corresponding alcohol. However, the alcohols that would be required for the analogous syntheses of **71-74** are not readily available. A more direct route to the substrates of interest was selected, which employed Wittig coupling of benzyltriphenylphosphonium bromide with the appropriate aldehyde in sodium ethoxide

solution, Scheme 3.3. This procedure provided a mixture of both *trans* and *cis* isomers for all four substrates, but pure samples ( $\geq 97\%$  purity for all *trans* isomers,  $\geq 95\%$  purity for all *cis* isomers) were obtained following column chromatography and distillation or recrystallization. As indicated in Scheme 3.3, the yields of these reactions are rather low, but they are adequate for the purposes of the current studies.



Scheme 3.3 Synthesis of methoxy-substituted stilbene derivatives **71-74**.

### 3.2.2 Photophysical Characterization of Methoxy-Substituted Stilbene Derivatives

A summary of the photophysical data for **60** and **71-74** in acetonitrile is shown in Table 3.2. Included are the absorption data for the *trans*- and *cis*-isomers ( $\lambda_{\text{max}}$  (abs) and  $\epsilon_{\text{max}}$  (abs)), the fluorescence maxima ( $\lambda_{\text{max}}$  (fluor)), the 0,0 band for the lowest energy transition ( $\lambda_{0,0}$ ), the lifetime of the first excited singlet state ( $\tau_s$ ), and the quantum yields for fluorescence and *trans*-*cis* isomerization ( $\phi_f$  and  $\phi_{tc}$ ).

Substrate	$\lambda_{\max}$ (abs) nm	$\epsilon_{\max}$ (abs) $\text{M}^{-1}\text{cm}^{-1}$	$\lambda_{\max}$ (fluor) nm	$\lambda_{0,0}$ nm	$\tau_s$ ns	$\phi_f^a$	$\phi_{tc}^b$
<i>trans</i> - <b>60</b>	295, 307	28500, 27600	350	328	0.07 <sup>c</sup>	0.023 <sup>d</sup>	0.45 <sup>e</sup>
<i>cis</i> - <b>60</b>	275	10300	-	-	-	-	-
<i>trans</i> - <b>71</b>	302, 317	28700, 27700	374	344	<0.5 <sup>f</sup>	0.007	0.53
<i>cis</i> - <b>71</b>	284	13900	-	-	-	-	-
<i>trans</i> - <b>72</b>	295	25800	359	336	0.93	0.164	0.39
<i>cis</i> - <b>72</b>	275	9950	-	-	-	-	-
<i>trans</i> - <b>73</b>	299, 306	30100, 29800	390	341	16.9	0.321	0.28
<i>cis</i> - <b>73</b>	277	11100	-	-	-	-	-
<i>trans</i> - <b>74</b>	301, 321	20600, 24700	385	353	<0.5 <sup>f</sup>	0.035	0.59
<i>cis</i> - <b>74</b>	290	11300	-	-	-	-	-

a) 295 nm excitation, relative to  $\phi_f = 0.0433$  for *trans*-stilbene in hexanes, Reference 86.

b) Determined by steady-state irradiation at 300 nm relative to  $\phi_{tc} = 0.40$  for *trans*-stilbene in cyclohexane, Reference 108. c) Reference 95. d) Literature value 0.016, Reference 92.

e) Literature value 0.45, Reference 92. f) Shorter than the time resolution of the instrument.

Table 3.2 Summary of photophysical data for methoxy-substituted stilbene derivatives in acetonitrile.

The absorption spectra of **71-74** (Figure 3.3) are typical of substituted stilbene derivatives. In all four cases, the  $\lambda_{\max}$  for absorption of the *trans* isomer is at a longer wavelength than the corresponding *cis* isomer, and the *trans* absorption peaks are always of greater intensity (*i.e.*,  $\epsilon_{\max}(\text{trans}) > \epsilon_{\max}(\text{cis})$ ). As discussed in Section 3.1.1, these spectra are consistent with the bent geometry of the *cis* isomers. Closer examination of the  $\lambda_{\max}$  values in Table 3.2 indicates that the para substituted substrates **71** and **74** absorb at slightly longer wavelengths than **72** and **73**, which possess only meta substituents.

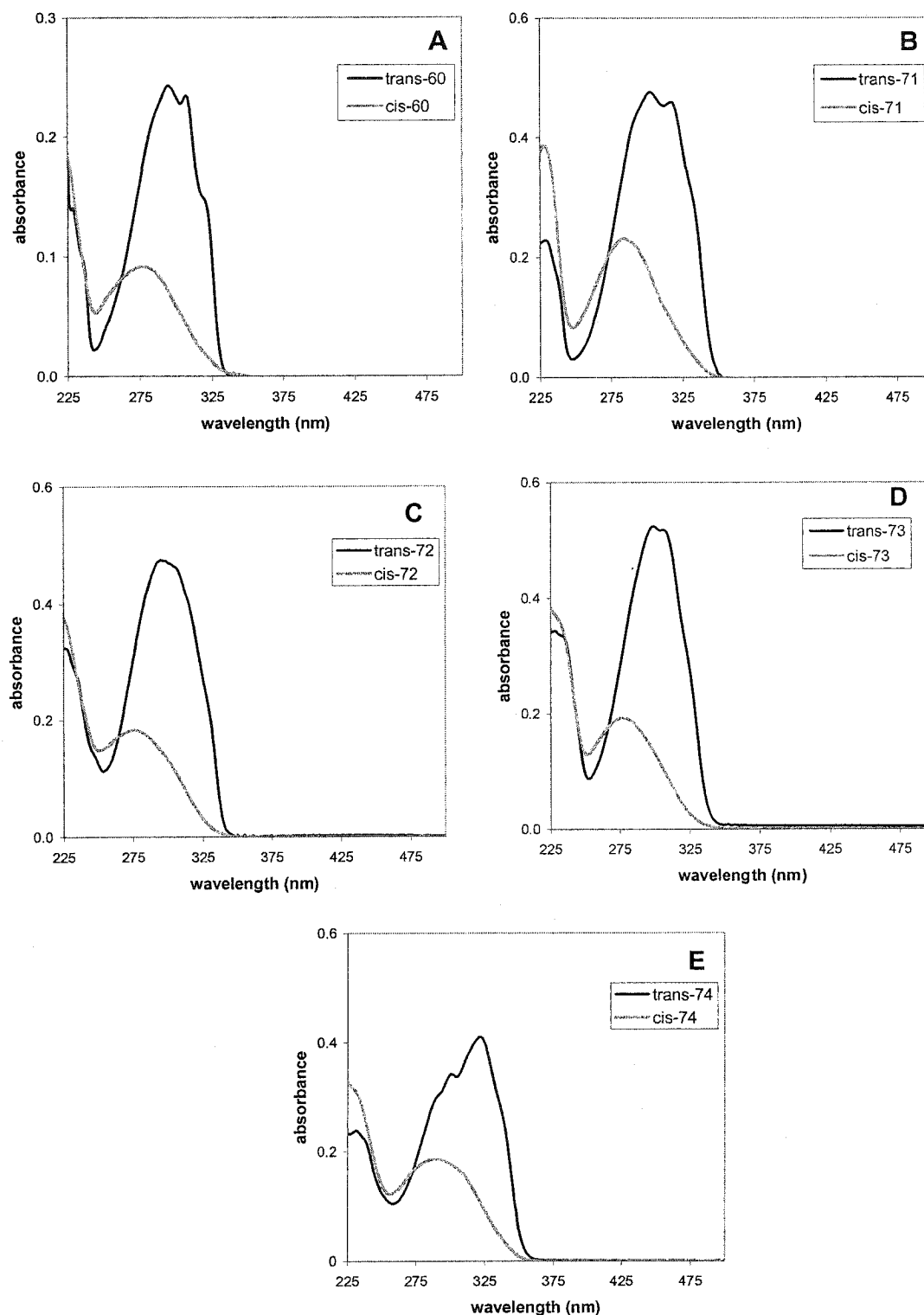


Figure 3.3 Absorption spectra of various stilbene derivatives in acetonitrile. **A)** *trans*-60 and *cis*-60 (both  $8.9 \times 10^{-6}$  M); **B)** *trans*-71 and *cis*-71 (both  $1.7 \times 10^{-5}$  M); **C)** *trans*-72 and *cis*-72 (both  $1.8 \times 10^{-5}$  M); **D)** *trans*-73 and *cis*-73 (both  $1.7 \times 10^{-5}$  M); **E)** *trans*-74 and *cis*-74 (both  $1.7 \times 10^{-5}$  M).

Fluorescence measurements for the *trans* isomers were performed using solutions of equal absorbance (0.25) at the excitation wavelength (295 nm). This wavelength was selected based on the  $\lambda_{\text{max}}$  for absorption of *trans*-stilbene, which was used as a standard for fluorescence quantum yields (*vide infra*). The fluorescence maxima move to longer wavelengths upon increasing the number of methoxy substituents, and a comparison of the mono-substituted compounds shows that the para isomer (*trans*-71) fluoresces at longer wavelength than the meta isomer (*trans*-72). In contrast, the two di-substituted compounds fluoresce at very nearly the same wavelength.

The fluorescence spectra of *trans*-60 and *trans*-71-74 in acetonitrile solution are shown in Figure 3.4. Clearly, the fluorescence behaviour of the *trans* isomers is not uniform – altering the position of the methoxy substituents drastically changes the intensity of fluorescence for the stilbene chromophore. The experimental determination of fluorescence quantum yields was performed by comparing the intensity of fluorescence for a given substrate to the intensity of fluorescence for *trans*-stilbene in hexanes, which was chosen as the reference compound for these studies. Many values of  $\phi_f$  for *trans*-stilbene have appeared in the literature, with slight variations depending on the excitation wavelength, solvent, and temperature. The chosen reference value is  $\phi_f = 0.0433$ , which was obtained by Saltiel and co-workers for *trans*-stilbene in hexane solution at 26.6 °C using an excitation wavelength of 294 nm.<sup>86</sup> The slight differences in excitation wavelength (295 nm *versus* 294 nm) and temperature (25.0 °C *versus* 26.6 °C) should not change the results greatly. For the case of a substrate (a) and a standard (s), the unknown quantum yield of the substrate can be obtained using the simple ratio calculation shown in Equation 3.2, where A is the absorbance at the excitation wavelength, and F is the

integrated intensity of fluorescence over the entire spectrum. This method corrects for differences in the absorbance of the two solutions, but the experimental differences were generally quite small (less than 0.02 absorbance units, or 10%).

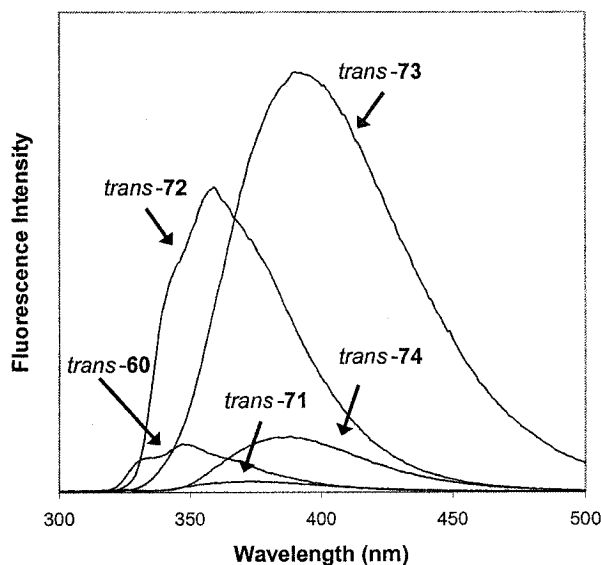


Figure 3.4 Comparison of fluorescence intensity for *trans*-60 and *trans*-71-74 in acetonitrile solution ( $A = 0.25$  at 295 nm for all solutions).

$$\phi_f^a = \phi_f^s \times \frac{F^a}{F^s} \times \frac{A^s}{A^a} \quad (3.2)$$

The  $\phi_f$  values in Table 3.2 do not correlate with either the absorption maxima or the fluorescence maxima. However, the fluorescence quantum yield does appear to increase as the number of meta methoxy substituents is increased: *trans*-73 > *trans*-72 > *trans*-60. In contrast, the presence of para methoxy substituents decreases the fluorescence quantum yield relative to the unsubstituted *trans*-60. Surprisingly, the fluorescence quantum yields of *trans*-60 and *trans*-74 are very similar, perhaps supporting the naïve hypothesis of a “competition” between the effects of the para and meta substituents.

Attempts were made to determine the singlet lifetimes of the *trans* isomers by single photon counting. Unfortunately, *trans*-**72** ( $\tau_s = 0.93$  ns) and *trans*-**73** ( $\tau_s = 16.9$  ns) were the only substrates that were amenable to this technique – the lifetimes of the other three substrates are apparently below the resolution of the lifetime instrument ( $\cong 0.5$  ns). The lifetime of *trans*-**60** has been reported as 0.07 ns in hexane solution,<sup>94</sup> and this value is included in Table 3.2 as a point of reference. The available singlet lifetimes follow the same trend as the fluorescence quantum yields, with meta methoxy substituents providing progressively longer  $\tau_s$  values.

Quantum yields of isomerization were obtained by performing steady state irradiations of the stilbenes in acetonitrile solution. At low conversions (generally < 10%), the increase in the yield of the *cis* isomer was linear in time as determined by GC-FID analysis – the yield versus time plots for these irradiations are shown in Figure 3.5. The slopes of these plots were assumed to be proportional to the quantum yield of isomerization for each substrate. Again, the unsubstituted compound was taken as the reference:  $\phi_{tc} = 0.40$  for *trans*-stilbene in cyclohexane at room temperature using 313 nm excitation.<sup>108</sup> Equation 3.3 provides the simple calculation employed to determine the  $\phi_{tc}$  for a substrate (a) using the standard value for *trans*-**60** in cyclohexane and the slopes of *cis* isomer formation (C) for the standard (s) and the substrate of interest.

$$\phi_{tc}^a = \phi_{tc}^s \times \frac{C^a}{C^s} \quad (3.3)$$



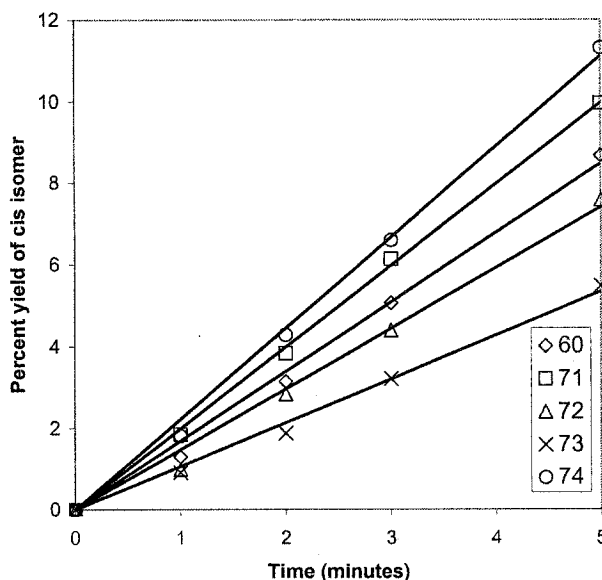


Figure 3.5 Yield *versus* time plots for the irradiation of *trans*-60 and *trans*-71-74 in acetonitrile solution.

The isomerization quantum yields nicely compliment the fluorescence measurements. The two substrates possessing para methoxy substituents display very high quantum yields of isomerization ( $\phi_{tc} = 0.53$  for *trans*-71, 0.59 for *trans*-74), in accord with their low quantum yields of fluorescence. The 3,5-dimethoxy substrate *trans*-73 displays the smallest value of  $\phi_{tc}$  for the five substrates ( $\phi_{tc} = 0.28$ ), as well as the largest values of  $\phi_f$  and  $\tau_s$ .

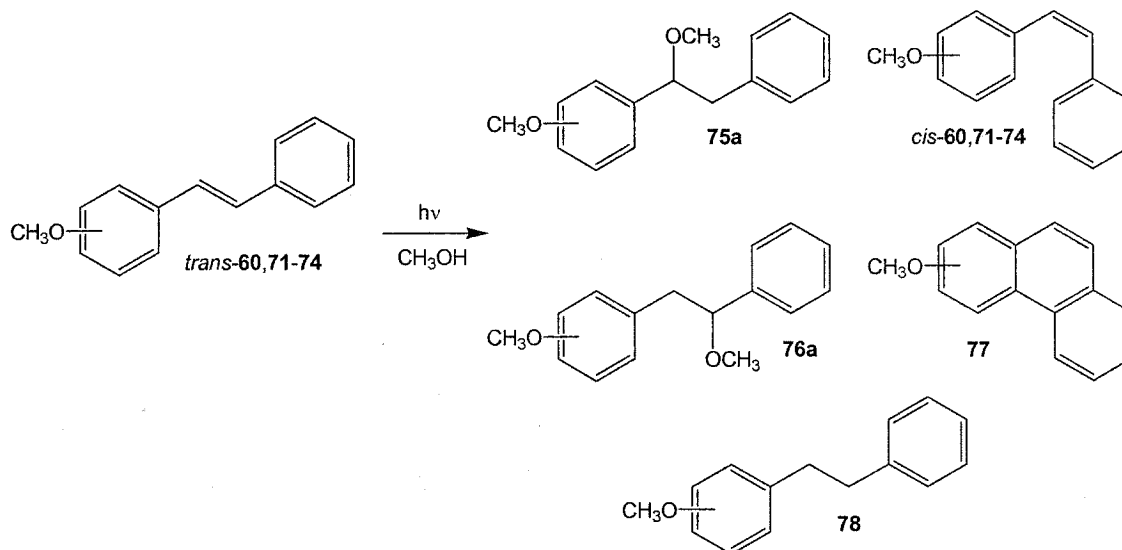
A final note regarding the photophysical measurements is that the *cis* isomers are essentially non-fluorescent. The only *cis* isomer for which fluorescence was observed was *cis*-73 ( $\phi_f = 0.006$  at 384 nm). Because this signal could also be attributed to as little as 2.4% of the highly fluorescent *trans* isomer, this result has not been included in Table 3.2. Lewis and co-workers were able to observe exceptional fluorescence from *cis*-3-aminostilbene, but only at very low temperatures ( $\tau_s = 17.4$  ns at 77 K).<sup>99</sup> Therefore, the lack of any substantial fluorescence of the *cis*-methoxy stilbenes is not surprising.

As a whole, the data presented in Table 3.2 indicate that the five *trans*-stilbenes have remarkably different photophysical properties in acetonitrile solution. In particular, the long-lived, highly fluorescent excited state of *trans*-**73** suggests that the meta effect observed by Lewis and co-workers<sup>97-101</sup> for aminostilbenes is quite important for methoxystilbenes as well. The following sections will determine whether or not these differences in photophysical properties translate into differences in photochemical reactivity when the substrates are irradiated in alcohol solvents.

### 3.2.3 Irradiation of *trans*-**60** and *trans*-**71-74** in Methanol

The irradiations of the five *trans*-stilbenes were performed using 300 nm lamps, in contrast to the irradiations performed using 254 nm lamps in Chapter 1. This change in the reaction conditions takes advantage of the longer-wavelength absorption maxima of the *trans*-stilbene substrates. The observed products are shown in Scheme 3.3, and the yields are listed in Table 3.3. Clearly, the products illustrated in Scheme 3.3 are analogous to those formed by irradiation of *trans*-**52** in either methanol or TFE (Scheme 2.10, Chapter 2). Addition of solvent to the central alkene bond provides the methanol adducts **75a** and **76a** – note that as in Chapter 2, ‘a’ is used to designate products formed by the addition of methanol, while ‘b’ will be used for TFE adducts (see below, Section 3.2.4). Mechanistic pathways for formation of the other products are presumably the same as were discussed in Chapter 2, namely trans-cis isomerization (*cis*-**60**, *cis*-**71-74**), electrocyclic reaction of the cis isomers (**77**), and radical cleavage of the ethers **75a** and **76a** (**78**). Specific references to products **75-78** will be made using an extra hyphenated numeral, which refers to the stilbene starting material. For example, the product **75a**

formed by irradiation of *trans*-stilbene (*trans*-**60**) will be designated **75a-0**, while the analogous product formed from the para methoxy substrate *trans*-**71** will be **75a-1**.



Scheme 3.3 Products detected following 300 nm irradiation of *trans*-**60** and *trans*-**71-74** in methanol.

	% conv. ( <i>trans</i> only)	% conv. ( <i>trans</i> & <i>cis</i> )	<b>75a</b>	<b>76a</b>	<b>77<sup>a</sup></b>	<b>78</b>
<i>trans</i> - <b>60</b>	92	14	76	-	24	0
<i>trans</i> - <b>71</b>	86	9	79	0	19	1
<i>trans</i> - <b>72</b>	90	29	12	31	49	8
<i>trans</i> - <b>73</b>	92	56	2	17	73	8
<i>trans</i> - <b>74</b>	82	15	52	4	43	0

a) Yield is the sum of two possible isomers.

Table 3.3 Percent conversions and product yields following one hour irradiation of *trans*-**60** and *trans*-**71-74** in methanol (300 nm).

A complicating feature of these reactions is the interconversion of the *trans* and *cis* isomers. The *trans*-*cis* isomerization reaction is by far the most rapid process that

occurs upon irradiation of the substituted *trans*-stilbenes – as a result, the percent conversions of the *trans* isomers are very similar after the one hour irradiation period (see Table 3.3, first numerical column). This point is more clearly illustrated by the yield versus time plots in Figure 3.6, where all five substrates are converted to the *cis* isomers in 80-85% yield *after only two minutes irradiation*. However, just as was observed for the experiments involving the methoxy-substituted *trans*-stilbene **52** (Chapter 2), the mixture of stilbene isomers decays over time to yield the other reaction products (**75-77**). Two explanations are possible for this phenomenon: 1) Secondary photochemistry of the *cis* isomers is the only route for product formation – the *trans* isomer would then serve only as a photochemical precursor for the more reactive *cis* isomer. 2) The *trans* isomer is responsible for product formation, but the competitive *trans*-*cis* isomerization process decreases the quantum yields of the other reactions. Product formation *via* the second pathway would likely depend on a cyclic *trans* → *cis* → *trans* process to reform the reactive *trans* isomer. These two possibilities may not be mutually exclusive – the mechanism for formation of the phenanthrene product **77** is well established<sup>96</sup> to be a reaction of substituted *cis*-stilbene derivatives, and so it likely falls into the first category. However, the pathway for formation of the ethers **75** and **76** is much less clear. As a result of the uncertainty in the “reactive” stilbene’s identity, Table 3.3 also shows the percent conversions of *the mixture of stilbene isomers*, which provides a much better indication of the reactivity of each substrate. Thus, the order of reactivity for the substrates in methanol is *trans*-**71** < *trans*-**60**  $\cong$  *trans*-**74** < *trans*-**72** < *trans*-**73**. Importantly, this order of increasing reactivity is identical to the order of increasing fluorescence quantum yields for the substrates in acetonitrile (*vide supra*, Table 3.2).

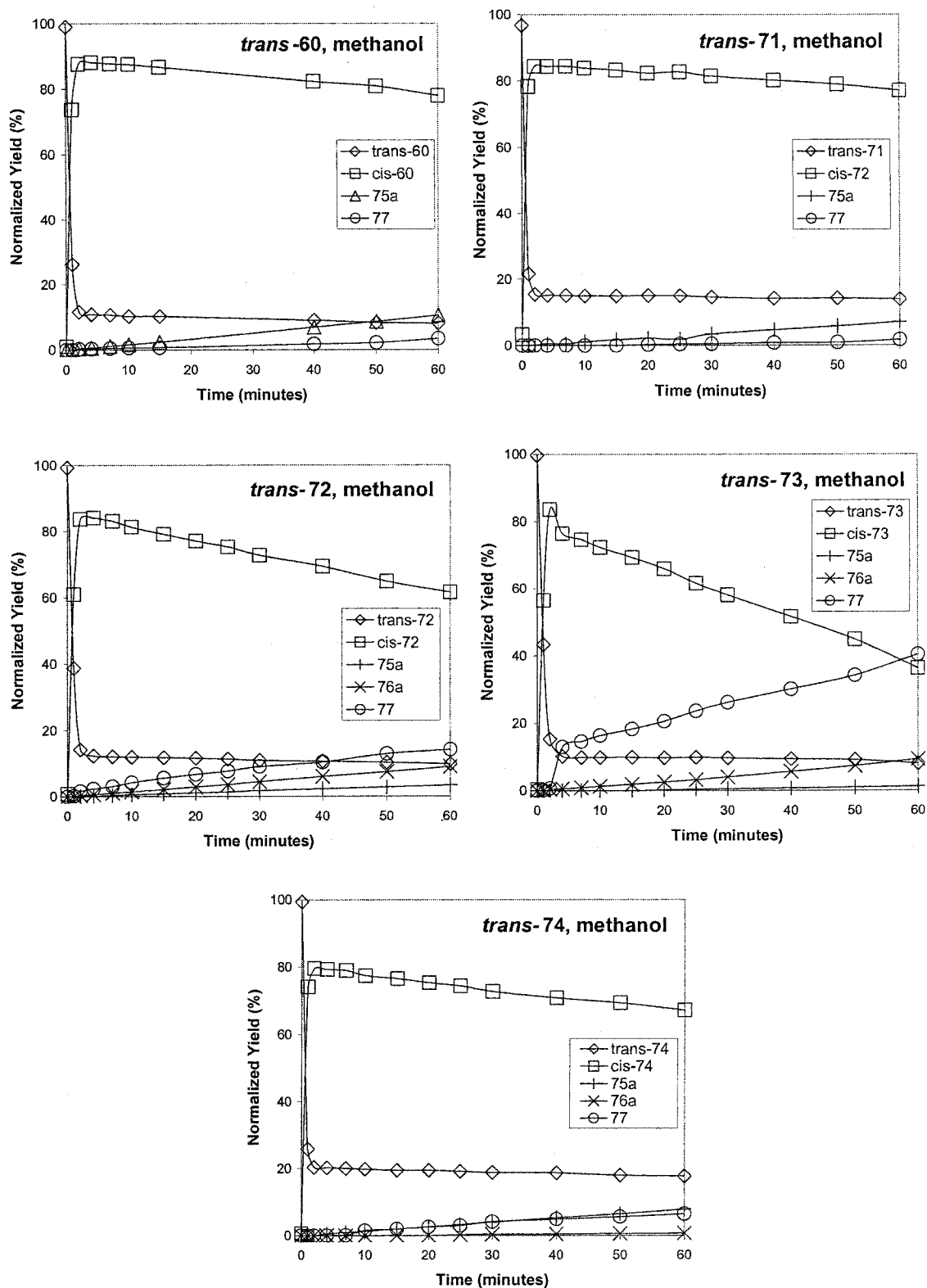


Figure 3.6 Yield versus time plots for 300 nm irradiation of *trans*-60 and *trans*-71-74 in methanol (product 78 has been omitted for improved clarity).

One final point must be made regarding the identification of the products from these experiments. Whereas the products from the irradiations performed in Chapter 2 were characterized following isolation or synthesis of the authentic compounds, the products in Scheme 3.3 (and from the irradiations that follow) have been assigned mainly on the basis of their GC-MS spectra. Although this may not be a rigorous method for structural analysis, the products from these reactions lend themselves particularly well to GC-MS. To demonstrate the usefulness of this method, the GC-MS spectra of all compounds encountered during the photolysis of *trans*-**73** in methanol are shown in Figure 3.7 along with the expected major fragmentation patterns for the compounds resulting from solvent addition. The mass spectra of *trans*-**73**, *cis*-**73**, and the substituted phenanthrene **77-3** are all characterized by their stable molecular ions ( $m/z$  240 for **73**,  $m/z$  238 for **77-3**); the two isomeric stilbenes are differentiated by their known GC-MS retention times. Identification of the isomeric methanol adducts **75a-3** and **76a-3** is made on the basis of the preferred fragmentation pathway for each compound. The expected molecular ion ( $m/z = 272$ ) is observed for **76a-3**, but not for **75a-3**. Fortunately, the base peaks in both mass spectra ( $m/z$  181 for **75a-3** and  $m/z$  121 for **76a-3**) are characteristic of the regiochemistry of the methanol addition for both products. These ions are formed *via* fragmentation of the diphenylethane molecular ions to generate the arylmethyl cations that are alkoxy-substituted, presumably due to the enhanced stability of these ions over the alternatives. The same fragmentation selectivity was observed for the corresponding addition products in Chapter 2, where the structures were unambiguously assigned by independent syntheses. As a result of these favourable fragmentation pathways, GC-MS provides a very powerful tool for the rapid identification of the irradiation products.

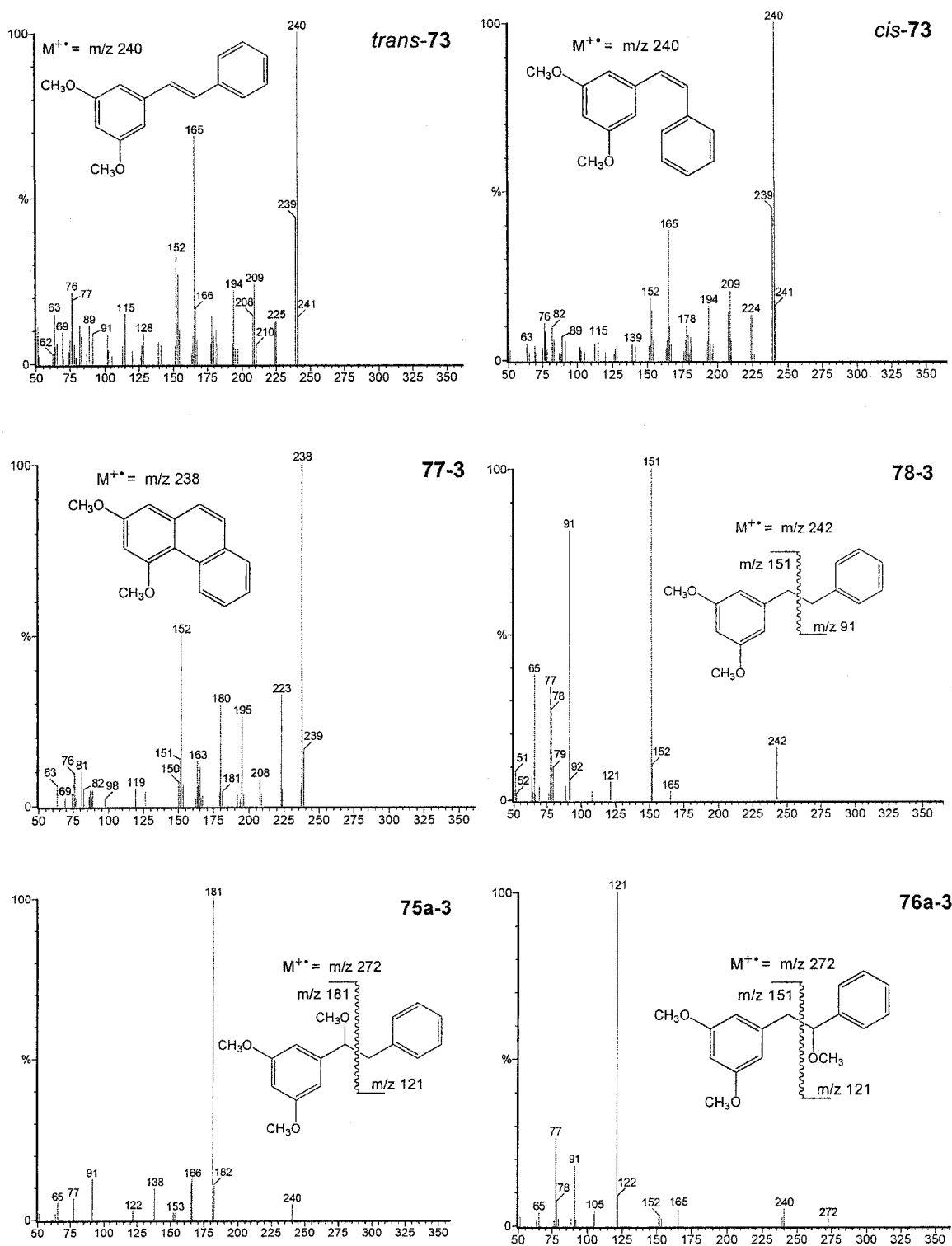
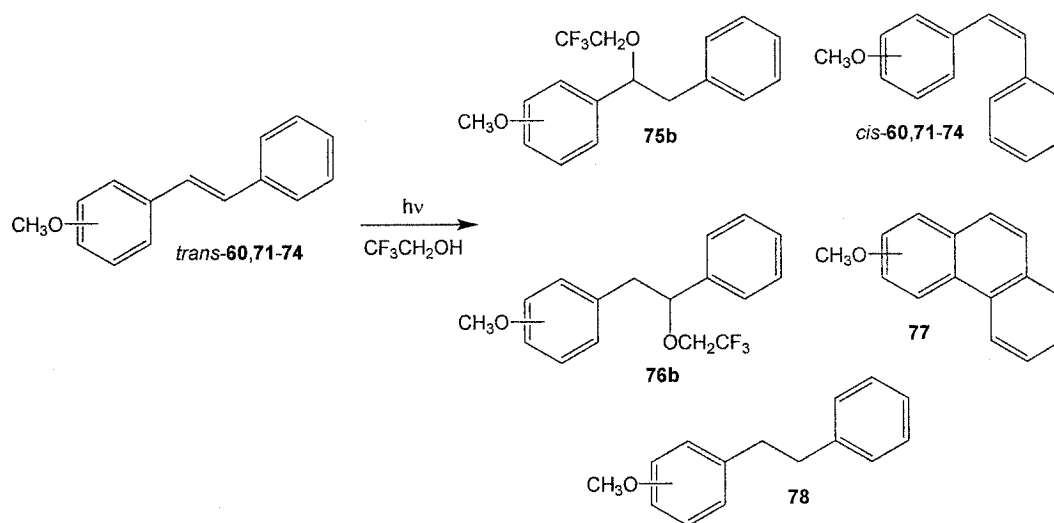


Figure 3.7 GC-MS spectra of compounds present in irradiation mixture of *trans*-73 (*trans*-73, *cis*-73, 77-3, 78-3, 75a-3, and 76a-3).

### 3.2.4 Irradiation of *trans*-60 and *trans*-71-74 in TFE

In Chapter 2, photochemical conversion of the methoxy-substituted *trans*-stilbene **52** to solvent adducts proceeded more rapidly in TFE than in methanol. In order to compare the reactivity of *trans*-**60** and *trans*-**71-74** in a similar fashion, irradiations of these new stilbene substrates at 300 nm were performed in TFE solution. The products identified from these reaction mixtures are shown in Scheme 3.5, the product yields are given in Table 3.4, and yield *versus* time plots for these reactions are shown in Figure 3.8.



Scheme 3.5 Products detected following 300 nm irradiation of *trans*-**60** and *trans*-**71-74** in TFE.

	% conv. ( <i>trans</i> & <i>cis</i> )	<b>75b</b>	<b>76b</b>	<b>77<sup>a</sup></b>	<b>78</b>
<i>trans</i> - <b>60</b>	21	84	-	16	0
<i>trans</i> - <b>71</b>	22	83	0	16	1
<i>trans</i> - <b>72</b>	69	13	74	12	1
<i>trans</i> - <b>73</b>	100	14	82	2	1
<i>trans</i> - <b>74</b>	33	57	34	9	0

a) Yield is the sum of two possible isomers.

Table 3.4 Percent conversions and product yields following irradiation of *trans*-**60** and *trans*-**71-74** for ten minutes in TFE (300 nm).



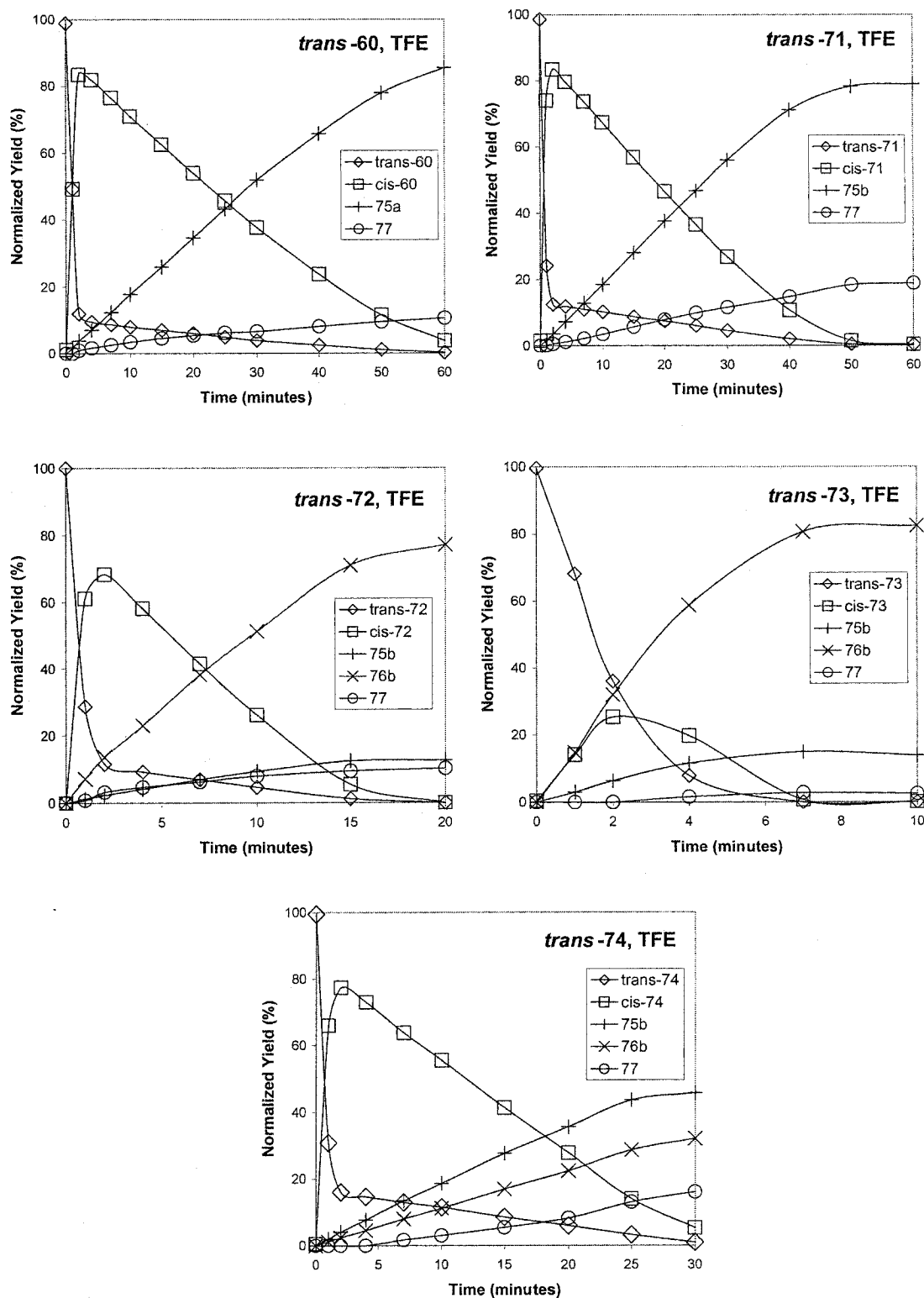


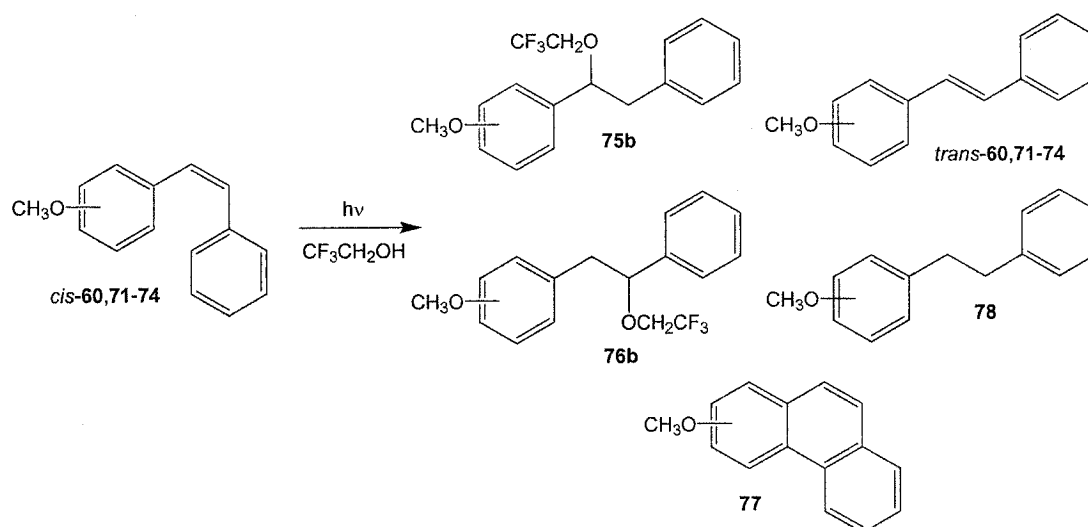
Figure 3.8 Yield *versus* time plots for 300 nm irradiation of *trans*-60 and *trans*-71-74 in TFE (product 78 has been omitted for improved clarity).

The products detected in the TFE reaction mixtures (Scheme 3.5) are essentially the same as the products observed in the methanol irradiations (Scheme 3.4), with the exception that addition of solvent to the substrates yields the TFE ethers **75b** and **76b**. Again, the GC-MS analysis techniques described in Section 3.2.2 allow confident identification of the reaction products. As shown by the percent conversion values in Table 3.4, the substrates are much more reactive in TFE than in methanol (*c.f.*, Table 3.3). In fact, *trans*-**73** and *cis*-**73** are completely consumed after only ten minutes irradiation in TFE. Due to the very high reactivity of the substrates in TFE, the percent conversions and product yields shown in Table 3.4 are given after only ten minutes irradiation (rather than after one hour, as was the case for the methanol reactions in Table 3.3). In addition, note that the yield *versus* time plots for the TFE reactions (Figure 3.8) are shown only up to the time when the *cis* and *trans* isomers are completely converted to products, as opposed to the uniform time of one hour for the methanol plots in Figure 3.6.

The order of reactivity for the TFE irradiations (*trans*-**60**  $\cong$  *trans*-**71** < *trans*-**74** < *trans*-**72** < *trans*-**73**) is almost the same as for the methanol irradiations, except that the reactivity of *trans*-**60** in TFE is slightly attenuated relative to the other substrates. The TFE irradiations also give much higher yields of solvent adducts **75** and **76** compared to the methanol irradiations. In the case of *trans*-**73** (the most reactive substrate in both solvents), the major product following irradiation in methanol is phenanthrene **77-3** (73% after one hour), while solvent adduct **76b-3** is the major product in TFE (82% after ten minutes). These results suggest that the excited states of the methoxy-substituted stilbene derivatives are more susceptible to addition of TFE and less reactive towards methanol – in the latter solvent the major products result from intramolecular cyclization.

### 3.2.5 Irradiation of *cis*-60 and *cis*-71-74 in TFE

In order to check for differences in the reactivity of the methoxy-substituted *cis*- and *trans*-stilbenes, solutions of *cis*-60 and *cis*-71-74 in TFE were irradiated under the same conditions as the *trans* isomers (Section 3.2.3). The products detected following these irradiations are shown in Scheme 3.6, the product yields are given in Table 3.5, and the yield *versus* time plots for the irradiations are presented in Figure 3.9.



Scheme 3.6 Products detected following 300 nm irradiation of *cis*-60 and *cis*-71-74 in TFE.

	% conv. ( <i>trans</i> & <i>cis</i> )	75b	76b	77 <sup>a</sup>	78
<i>cis</i> -60	21	85	-	15	0
<i>cis</i> -71	18	89	0	11	0
<i>cis</i> -72	64	14	75	12	0
<i>cis</i> -73	96	15	81	3	1
<i>cis</i> -74	24	58	34	8	0

a) Yield is the sum of two possible isomers.

Table 3.5 Percent conversions and product yields following one hour irradiation of *cis*-60 and *cis*-71-74 in TFE (300 nm).

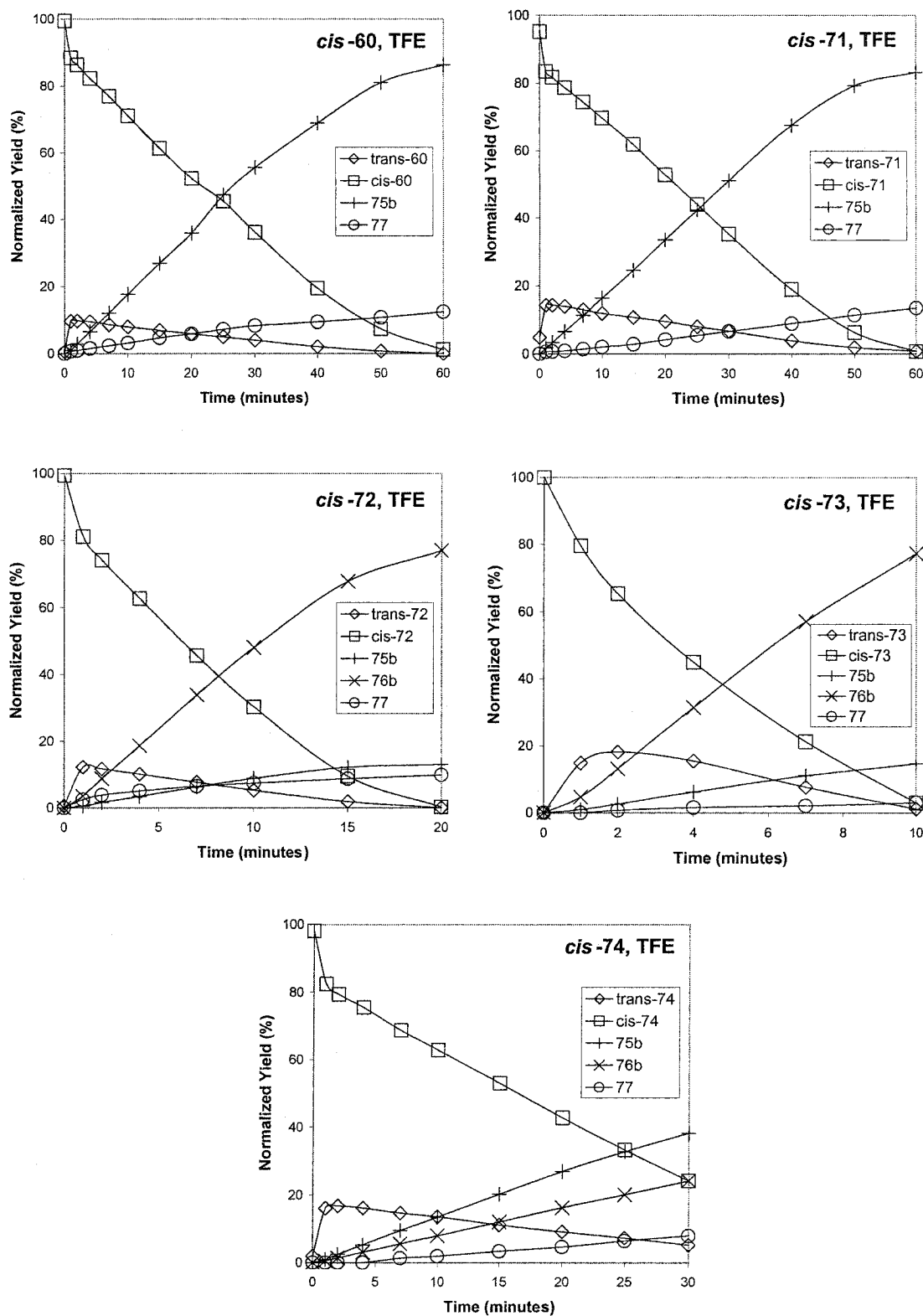


Figure 3.9 Yield versus time plots for 300 nm irradiation of *cis*-60 and *cis*-71-74 in TFE (product 78 has been omitted for improved clarity).

The products from the irradiation of *cis*-**60** and *cis*-**71-74** in TFE are the same as the products detected following irradiation of the corresponding *trans* isomers. Indeed, the product yields in Table 3.5 (*cis* starting materials) are virtually identical to the values in Table 3.4 (*trans* starting materials). In a similar fashion, after the short period of time ( $\approx$  two minutes) required for equilibration of the *cis* and *trans* isomers, the yield *versus* time plots in Figures 3.8 and 3.9 show the same product mixtures in all five cases. These experiments emphasize the importance of the *trans*-*cis* and *cis*-*trans* isomerization reactions during the steady state irradiations.

### 3.2.6 Quenching of *trans*-**73** Fluorescence by TFE

The bimolecular reaction that results in efficient formation of TFE adducts upon irradiation of the methoxy-substituted stilbenes demands closer study; the isomer responsible for product formation and the identity of the excited state are clearly of interest. The high fluorescence quantum yield of the 3,5-dimethoxy substrate *trans*-**73** makes it an attractive candidate for quenching studies, especially in light of the very high reactivity of the compound in TFE. In order to probe the interaction of the fluorescent excited state of *trans*-**73** with TFE, the fluorescence quantum yield of the substrate was determined in various mixtures of acetonitrile and TFE. In addition, the same experiments were repeated in mixtures of acetonitrile and mono-deuterated TFE ( $\text{CF}_3\text{CH}_2\text{OD}$ , TFE-OD). The results of these experiments are given in Table 3.6, and a plot of  $\phi_f$  versus percent alcohol is shown in Figure 3.10.

% TFE in acetonitrile	$\phi_f$ (TFE)	$\phi_f$ (TFE-OD)	$\phi_f^o/\phi_f$ (TFE)	$\phi_f^o/\phi_f$ (TFE-OD)
0	0.321	0.321	1.00	1.00
10	0.311		1.03	
20	0.310	0.315	1.04	1.02
30	0.284		1.13	
40	0.260	0.303	1.23	1.06
50	0.217		1.48	
60	0.148	0.266	2.17	1.20
70	0.098		3.28	
80	0.069	0.183	4.65	1.75
90	0.045		7.14	
100	0.029	0.079	11.11	4.08

Table 3.6 Quantum yields of fluorescence  $\phi_f$  for *trans*-73 in various mixtures of acetonitrile and TFE or TFE-OD, and Stern-Volmer ratios  $\phi_f^o/\phi_f$ .

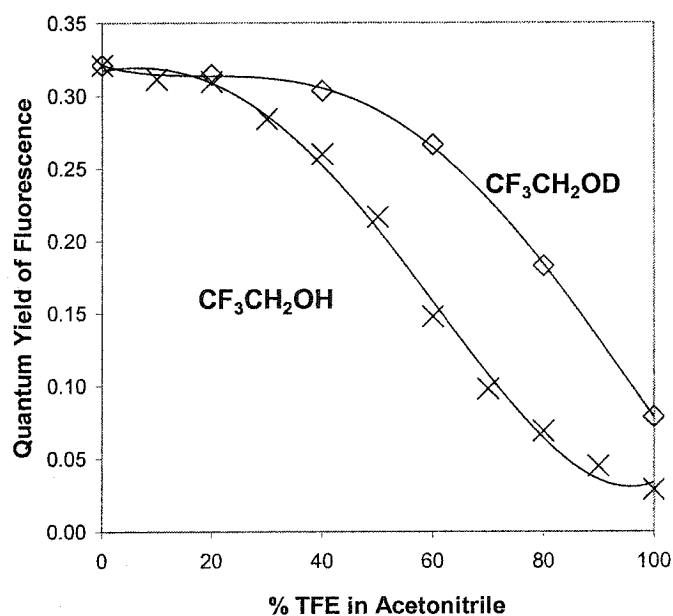


Figure 3.10 Fluorescence quantum yield  $\phi_f$  of *trans*-73 in mixtures of acetonitrile and either TFE (crosses) or TFE-OD (diamonds).

The data in Table 3.6 indicate that the fluorescent excited state of *trans*-73 is quenched by both TFE and TFE-OD. There appear to be two plateau regions in Figure 3.10: a low-quenching region (0-20% TFE) where  $\phi_f \approx 0.3$ , and a high-quenching region (80-100% TFE) where  $\phi_f \approx 0.03$ . The transition between these two regions (30-70% TFE) moves smoothly through an inflection point where the decrease in  $\phi_f$  with increasing percentage of TFE is most obvious. The onset of this steep decrease in  $\phi_f$  is observed at higher concentrations of TFE-OD (40% TFE-OD *versus* 20% TFE), and so the high-quenching plateau is not observed for the deuterated solvent. In contrast to the efficient quenching by TFE, the fluorescence quantum yield of *trans*-73 in pure methanol ( $\phi_f = 0.30$ ) is only slightly lower than in acetonitrile ( $\phi_f = 0.32$ ).

Studies of fluorescent excited states and their bimolecular interactions with added quenchers often involve the use of the Stern-Volmer relationship, Equation 3.4.<sup>50</sup> In this formulation,  $\phi_f^0$  is the quantum yield of fluorescence in the absence of any quenching molecules,  $\phi_f$  is the quantum yield of fluorescence with a quencher added,  $k_q$  is the bimolecular rate constant for the bimolecular quenching reaction,  $\tau_s$  is the lifetime of the unquenched excited state, and  $[Q]$  is the concentration of the quencher. A plot of  $\phi_f^0/\phi_f$  versus  $[Q]$  will be linear with an intercept of one and a slope of  $k_q\tau_s$  – if  $\tau_s$  is known, then  $k_q$  can be calculated. With the  $\phi_f^0/\phi_f$  ratios for *trans*-73 (Table 3.6), a pseudo Stern-Volmer plot was constructed using percent alcohol in acetonitrile rather than concentration, Figure 3.11. The strong upwards curvature of the plots for both TFE and TFE-OD indicate that the quenching mechanism does not follow a simple bimolecular process. Using a value of 13.7 M for the concentration of pure TFE and  $\tau_s = 16.9$  ns (Table 3.2) allows  $k_{\text{TFE}}$  to be estimated as  $9 \times 10^6 \text{ M}^{-1}\text{s}^{-1}$  in the low-quenching region and

$1 \times 10^8 \text{ M}^{-1}\text{s}^{-1}$  in the high-quenching region (see calculations, Section 7.3.4). Similar calculations give a quenching ratio of  $k_{\text{TFE}}/k_{\text{TFE-OD}} = 3:1$ .

$$\frac{\phi_f^0}{\phi_f} = k_q \tau_s [\text{Q}] + 1 \quad (3.4)$$

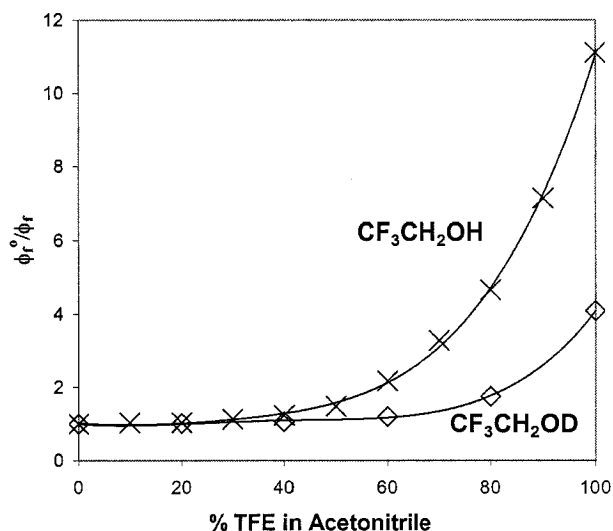


Figure 3.11 Stern-Volmer plot for the quenching of *trans*-**73** in mixtures of acetonitrile and either TFE (crosses) or TFE-OD (diamonds).

In order to provide evidence for a connection between the quenching of *trans*-**73** fluorescence by TFE (Table 3.6) and the high yield of TFE adducts upon steady state irradiation (Table 3.4), the irradiation of *trans*-**73** was repeated in a series of TFE/acetonitrile mixtures. Figure 3.12 shows a plot of the combined yields of the stilbenes *cis*- and *trans*-**73** and the combined yields of the TFE-adducts **75b-3** and **76b-3** after ten minutes of irradiation in several mixtures of TFE and acetonitrile. For low concentrations of TFE (< 40%), the ethers are not formed, and the stilbenes are the major components in the reaction mixture (inclusion of the yield of phenanthrene **77** with the stilbenes **73** brings the mass balance to 100%). As the percentage of TFE in the solvent mixture is increased, the yield of the ethers **75b-3** and **76b-3** increases at the expense of



the stilbenes **73**. The complimentary trends in Figures 3.10 and 3.12 indicate that the process responsible for quenching the fluorescence of *trans*-**73** also leads to formation of TFE adducts. In addition, these experiments establish the excited state TFE addition process as a reaction of the singlet manifold.

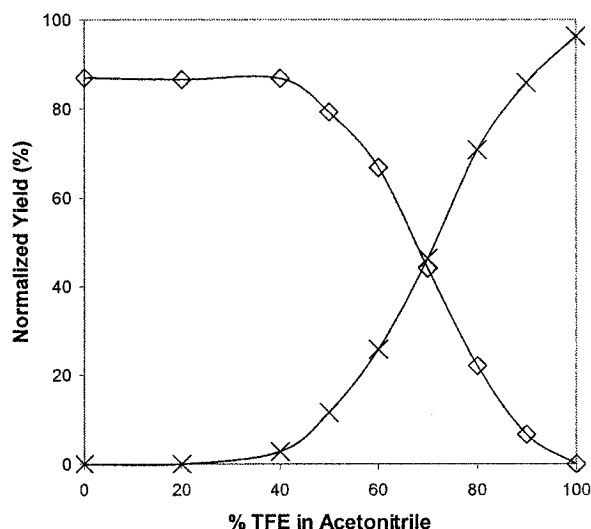


Figure 3.12 The combined yields of *cis*- and *trans*-**73** (diamonds) and the combined yields of TFE-adducts **75b-3** and **76b-3** (crosses) after ten minutes irradiation, plotted as a function of percent TFE in acetonitrile.

### 3.3 Discussion of Results

#### 3.3.1 Reliability of the Photophysical Measurements

A critical aspect of the photophysical measurements is the reliability of the values obtained. This point is particularly important given the extensive measurements that have been made on stilbene and its substituted derivatives.<sup>82</sup> Changes in solvent, temperature, concentration, and excitation wavelength can all have major effects on many of the measurements. The values for  $\lambda_{\text{max}}$  (abs) should be quite reliable, given that the purity of the *trans* substrates was determined by GC-FID to be greater than 97% in all cases. The high purity of the substrates also means that the largest source of error in the  $\epsilon_{\text{max}}$  values

should be in the measurements of masses and volumes. The measurements of  $\lambda_{0,0}$  and  $\lambda_{\text{max}}$  (fluor) should be correct to within  $\pm 2$  nm – the uncertainty is due to instrument noise in some of the fluorescence spectra. The singlet lifetimes were determined using a typical nanosecond single photon counting apparatus, which reproduced literature lifetime values with reasonable accuracy (see Chapter 4 for examples).

However, the values of  $\phi_f$  and  $\phi_{\text{ic}}$  were determined in relation to literature standards. Choosing appropriate standards was somewhat difficult, given that so many values have been reported in the literature using many different experimental conditions. As was discussed in Section 3.2.2, the reference value of  $\phi_f = 0.0433$  for *trans*-stilbene in hexane was obtained under experimental conditions that are very similar to those used for the current studies.<sup>86</sup> Therefore, the experimental error in the  $\phi_f$  values in Table 3.2 should be quite low, especially given the corrections for the very slight differences in the absorbance of the solutions. Furthermore, the fluorescence spectra of all four methoxy-substituted *trans*-stilbenes were obtained using solutions that were degassed using three freeze-pump-thaw cycles, which should eliminate the possibility of quenching the excited states by gaseous impurities.

While the experimental work described in this chapter was being performed, Majima and co-workers<sup>110</sup> published an account of the photophysical parameters of several of the same methoxy-substituted stilbene derivatives – the data are displayed in Table 3.7. Many of the reported values are in obvious conflict with the results of the current work (Table 3.2). Although the absorption and fluorescence maxima are in reasonable agreement, the extinction coefficients differ by a significant amount. The singlet lifetime for *trans*-73 reported by Majima and co-workers (4 ns) is over ten

nanoseconds shorter than the value in Table 3.2 (16.9 ns). Finally, the fluorescence quantum yields reported in Table 3.6 are in serious disagreement with the current results – the  $\phi_f$  values for *trans*-**73** differ by more than an order of magnitude.

Substrate	$\lambda_{\max}$ (abs) nm	$\epsilon_{\max}$ (abs) $\text{M}^{-1}\text{cm}^{-1}$	$\lambda_{\max}$ (fluor) nm	$\tau_s$ ns	$\phi_f^a$
<i>trans</i> - <b>60</b>	307	33000	349	-	0.016
<i>trans</i> - <b>71</b>	317	25000	373	-	0.003
<i>trans</i> - <b>73</b>	308	29000	392	4	0.023
<i>trans</i> - <b>74</b>	325	29000	384	-	0.008

a) Relative to  $\phi_f = 0.016$  for *trans* -**60**, Reference 92.

Table 3.7 Summary of photophysical data for methoxy-substituted stilbene derivatives in acetonitrile, taken from Reference 110.

A complete assessment of the reasons for the significant differences between the measurements performed in the current studies and those of Majima and co-workers is clearly impossible, but some theories may be advanced. The disagreement between the  $\epsilon_{\max}$  values must be due to errors in solution preparation. Although either party could be guilty of such errors, comparison of the  $\epsilon_{\max}$  values for *trans*-stilbene in acetonitrile (current work:  $28500 \text{ M}^{-1}\text{cm}^{-1}$ , Majima:  $33000 \text{ M}^{-1}\text{cm}^{-1}$ ) to the value obtained by Lewis and co-workers ( $29500 \text{ M}^{-1}\text{cm}^{-1}$ ) supports the measurements reported herein. The large differences in the fluorescence quantum yields are more difficult to explain, especially given the lack of detailed experimental procedures reported by Majima and co-workers. In particular, the excitation wavelengths used for the fluorescence measurements are not reported, and the issue of matching the absorbance of the sample and standard is not

discussed. Although the standard employed for calculating the fluorescence quantum yields ( $\phi_f = 0.016$  for *trans*-stilbene in acetonitrile, excitation at 315 nm)<sup>92</sup> is slightly less than the value obtained in the current report ( $\phi_f = 0.023$ , excitation at 295 nm), the changes that result from scaling either set of results do not eliminate the discrepancies between them. A problem that may have lead to errors in the results of Majima and co-workers is the trans-cis isomerization process. In the current work, great care was taken to ensure that isomerization of the fluorescence samples did not occur to a large extent – performing too many experiments with the same sample could allow the trans isomer to undergo substantial isomerization to the less-fluorescent cis isomer. If Majima and co-workers did not appreciate this difficulty, their fluorescence quantum yields would be lower than those obtained in the current work (as is the case). Unfortunately, these problems would not account for the large differences in the values of  $\tau_s$  obtained for *trans*-73. A general comment is that low values of  $\tau_s$  can result from quenching of the excited states by unknown impurities, and therefore the higher values reported herein are more likely to be correct. In summary, despite the fact that many of the values in Table 3.2 are clearly inconsistent with the results reported by Majima and co-workers, I remain confident in the reliability of my own measurements.

In contrast to the determination of  $\phi_f$ , where the experimental procedures used in the current work were essentially the same as those employed for the literature standard, the  $\phi_{tc}$  values have been determined using quite different techniques. The literature value<sup>108</sup> of  $\phi_{tc} = 0.40$  for *trans*-stilbene in cyclohexane was obtained by comparing the absorbance spectrum before and after irradiation at 313 nm. In contrast, the values in Table 3.2 were obtained from the slopes of the low-conversion yield *versus* time plots

(Figure 3.5) following irradiation in a Rayonet reactor. A potential pitfall in this technique is the high temperature (240 °C) of the injection port in the gas chromatograph used to obtain the product yields – if thermal isomerization of either the cis or trans isomers is possible, then the isomerization quantum yields (and all of the yield *versus* time plots) will be in error. However, the observation that injection of any of the ten pure stilbenes (cis or trans) allowed the calculation of sample purities greater than 95% in all cases indicates that such thermal reactions do not occur to any great extent.

The reliability of the  $\phi_{tc}$  values listed in Table 3.2 is established by several observations. First, the measured value of  $\phi_{tc} = 0.45$  for *trans*-stilbene in acetonitrile matches the reported<sup>92</sup> value exactly. These results agree with the expectation<sup>83</sup> that the quantum yield of isomerization will be higher in more polar solvents. A comparison of the literature values<sup>108</sup> for the isomerization quantum yields of *trans*-4-methoxystilbene (*trans*-71,  $\phi_{tc} = 0.40$ ) and *trans*-3-methoxystilbene (*trans*-72,  $\phi_{tc} = 0.31$ ) in cyclohexane with the measurements in acetonitrile from this work ( $\phi_{tc} = 0.53$  for *trans*-71, 0.39 for *trans*-72) indicates an analogous solvent effect for substituted stilbene derivatives. Second, as was noted in Section 3.2.2, the  $\phi_{tc}$  values complement the  $\phi_f$  measurements. The substrates with the *higher* quantum yields of isomerization (the 4-methoxy substrate *trans*-71 and the 3,4-dimethoxy substrate *trans*-74) displayed *smaller* quantum yields of fluorescence. In contrast, the substrates with the *smaller* quantum yields of isomerization (the 3-methoxy substrate *trans*-72 and the 3,5-dimethoxy substrate *trans*-73) displayed *higher* quantum yields of fluorescence. The unsubstituted compound *trans*-60 has properties that are intermediate between these two extremes. Finally, the quantum yields of isomerization for *trans*-71 and *trans*-72 were determined in cyclohexane solution as

part of the investigations described in Chapter 4. The excellent agreement between these values ( $\phi_{tc} = 0.39$  for *trans*-71, 0.32 for *trans*-72) and those of Güsten and Kasinc ( $\phi_{tc} = 0.40$  for *trans*-71, 0.31 for *trans*-72)<sup>108</sup> provides strong support for the accuracy of the current results.

### 3.3.2 The Photophysics of Methoxy-Substituted Stilbene Derivatives

The effects of electron donating methoxy substituents on the photophysical properties of the stilbene chromophore appear to be similar to those of amino substituents. In particular, the presence of either substituent in the meta position prolongs the lifetime of the excited singlet state ( $\tau_s$ ), resulting in higher quantum yields of fluorescence. Lewis and co-workers determined that, in the case of *trans*-3-aminostilbene (*trans*-63), these changes resulted from an increase in the barrier for excited state bond torsion relative to *trans*-stilbene itself (Figure 3.2). Thus, the increased quantum yields of fluorescence  $\phi_f$  were accompanied by small quantum yields of isomerization  $\phi_{tc}$ . The available data for the methoxystilbenes (Table 3.2) indicate a similar connection between  $\tau_s$ ,  $\phi_f$ , and  $\phi_{tc}$ . For example, the substrate with two meta-methoxy substituents (*trans*-73) displays an exceptionally high quantum yield of fluorescence ( $\phi_f = 0.32$ ), a very low quantum yield of isomerization ( $\phi_{tc} = 0.28$ ), and (to the best of my knowledge) the longest singlet lifetime that has been reported for an unconstrained stilbene derivative at ambient temperature in a non-viscous solvent ( $\tau_s = 16.9$  ns). These results provide convincing evidence that although the methoxy substituent does not have as large an influence on *trans*-stilbene photophysics as the

amino substituent does, its presence does induce substantial changes in the properties of the excited singlet states.

The fluorescence data for the other substrates clearly depends on the position of the methoxy substituents. The second-highest values of  $\phi_f$  and  $\tau_s$  belong to *trans*-72, the 3-methoxy substrate. In contrast, the fluorescence quantum yield of the 4-methoxy substrate *trans*-71 ( $\phi_f = 0.007$ ) is substantially less than that of *trans*-stilbene itself ( $\phi_f = 0.023$ ). This observation may be taken to imply that the presence of para methoxy substituents influences the photophysics in a manner *opposite* to that of the meta methoxy substituents: smaller quantum yields of fluorescence and higher quantum yields of isomerization. The high  $\phi_{tc}$  values for *trans*-4-methoxystilbene (*trans*-71,  $\phi_{tc} = 0.53$ ) and *trans*-3,4-dimethoxystilbene (*trans*-74,  $\phi_{tc} = 0.59$ ) seem to support this idea. Furthermore, the observation that the quantum yield of fluorescence for the 3,4-dimethoxy substrate *trans*-74 ( $\phi_f = 0.035$ ) is intermediate between the values for the 3-methoxy substrate (*trans*-72,  $\phi_f = 0.16$ ) and the 4-methoxy substrate (*trans*-71,  $\phi_f = 0.007$ ) suggests a competition between the conflicting effects of the two substituents. For the most part, the results give trends that agree with the established inverse correlation between  $\phi_{tc}$  and  $\phi_f$ . The only exception to this relationship is the 3,4-dimethoxy substrate *trans*-74, which displays the highest quantum yield of isomerization ( $\phi_{tc} = 0.59$ ) but only an intermediate quantum yield of fluorescence ( $\phi_f = 0.035$ ).

### 3.3.3 Addition of Alcohols to the Excited States of Methoxy-Substituted Stilbene Derivatives

Irradiation of the five *trans*-stilbene derivatives (*trans*-60 and *trans*-71-74) results in formation of the same types of products as in the irradiation of the trimethoxy-

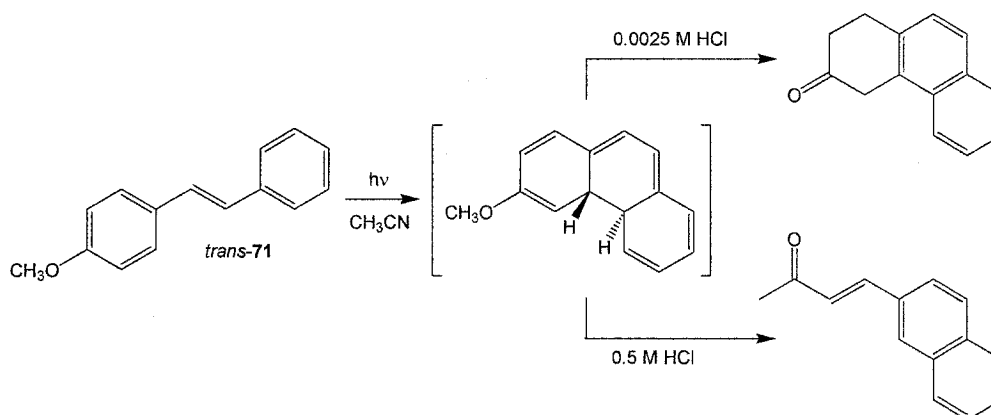
substituted *trans*-stilbene **52** in Chapter 2. The *trans*-*cis* isomerization reaction is the most rapid reaction for all substrates in either TFE or methanol, and so photostationary states of the two isomers are produced very early in the steady state experiments. As a result of these rapid *trans*-*cis* (and *cis*-*trans*) isomerization reactions, the percent conversions are listed by taking into account the consumption of *both* isomers. The rapid photochemical equilibration between two isomers of a given substrate greatly complicates the elucidation of mechanistic pathways for formation of the other reaction products. However, the experiments described in this chapter provide a basic understanding of some of the principles that determine the outcomes of the irradiation experiments.

There are two significant differences between the irradiations performed in methanol and those performed in TFE: 1) The percent conversions of all five substrates are greater in TFE than in methanol; 2) The solvent adducts **75** and **76** are formed in much higher yields in the TFE irradiations. Clearly the rapid photochemical addition of TFE is responsible for the higher conversions of the stilbenes in that solvent. The slower rate of methanol addition to the stilbene excited states allows formation of the phenanthrene product **77** (through secondary photochemistry of the *cis* isomers) to become a viable reaction pathway. Thus, the yields of **77** are higher for the reactions performed in methanol than in TFE.

The most controversial issue regarding the results of the irradiation experiments is the identity of the photochemical precursor for the solvent adducts **75** and **76**. The observation that the phenanthrenes are major products in methanol while the addition products are major products in TFE might lead to the proposal that the two types of products are formed from a common source. Conceivably, the dihydrophenanthrene intermediate, which is required for formation of **77**, could be susceptible to attack by



TFE. Ho and co-workers<sup>111</sup> have reported that the phenanthrene intermediate formed by photocyclization of *trans*-4-methoxystilbene can be intercepted by acids, and that the structure of the final product depends on the concentration of acid, Scheme 3.7. However, the addition products detected in the current experiments are formed more rapidly in TFE than are the phenanthrene products in methanol, making a common precursor unlikely. Moreover, such a pathway would not be consistent with the quenching of the *trans*-73 fluorescence described in Section 3.2.6.



Scheme 3.7 Switching of the final product by irradiation of *trans*-4-methoxystilbene (*trans*-71) in different concentration of hydrochloric acid in acetonitrile (Reference 111).

With the dihydrophenanthrene intermediate ruled out as the precursor to the solvent adducts, the excited states of the *cis*- and *trans*-stilbene derivatives become the most likely candidates. As was discussed in Section 3.2.3, such a process could involve one or both of the two isomers. Initial inspection of the yield *versus* time plots for the reactions beginning with the *trans* isomers (Figure 3.8) appears to support the theory that the *trans* isomers serve only as the photochemical precursor for the *cis* isomers, which then react to give the solvent adducts. Indeed, the behaviour expected for a two-step consecutive reaction is very similar to the plots observed in Figure 3.8.<sup>112</sup> However, the

yield *versus* time plots for the cis isomers (Figure 3.9) display *slower* formation of the solvent adducts at low conversions – this is most obvious when comparing the plots for *trans*-73 (Figure 3.8) and *cis*-73 (Figure 3.9). Thus, the cis isomers are not more reactive than the trans isomers under the reaction conditions (as would be required by a consecutive  $\text{trans} \rightarrow \text{cis} \rightarrow \text{adduct}$  mechanism), and the question then arises as to whether or not the cis isomers are capable of ether formation at all.

The quenching of the strong *trans*-73 fluorescence by TFE (Section 3.2.6) supports the idea that the excited states of the trans isomers react with TFE. These experiments also provide evidence that the non-fluorescent  $p_{S1}$  state is *not* responsible for ether formation. The similarity between the trends observed for fluorescence quenching (Figure 3.10) and product yields (Figure 3.12) as a function of percent TFE in acetonitrile strongly indicates that quenching of the trans isomer excited state ( $t_{S1}$ ) results in formation of the solvent adducts. The lack of fluorescence from any of the cis isomers prevents similar quenching studies. However, based on studies performed for stilbene itself<sup>94,94</sup> and for the aminostilbenes,<sup>98,99</sup> the lifetimes of the *cis*-methoxystilbenes are expected to be at least an order of magnitude less than the corresponding trans isomers. Therefore, the rate constants for the interaction of TFE with the  $c_{S1}$  state would need to be an order of magnitude *larger* than for the corresponding reaction with the trans isomers. Given that such large differences in reactivity for the excited states of two structural isomers is unlikely, the cis isomers are concluded to be less reactive than the trans isomers. Although large quantities of the cis isomers are formed rapidly during the steady state irradiations, eventual cis-trans isomerization is expected to provide a route to return to the reactive trans isomer. Thus, the trans-cis isomerization process serves only as a

competitive deactivation pathway for the reactive  $t_{S1}$  state, and not as the first step in a consecutive reaction.

The singlet lifetimes of the *trans* isomers may provide a rationale for the order of substrate reactivity. Although the lifetimes of the *trans* substrates possessing 4-methoxy substituents (*trans*-71 and *trans*-74) are shorter than the resolution of the available instrument, the lifetime of *trans*-stilbene has been reported in the literature ( $\tau_s = 0.07$  ns)<sup>94</sup> and the lifetimes of *trans*-3-methoxystilbene (*trans*-72,  $\tau_s = 0.93$  ns) and *trans*-3,5-dimethoxystilbene (*trans*-73,  $\tau_s = 16.9$  ns) have been determined in the current work. The longer singlet lifetimes of *trans*-72 and *trans*-73 are a result of the meta effect, which apparently results in a larger barrier for the  $t_{S1} \rightarrow p_{S1}$  process (as discussed in Section 3.1.2 for the amino-stilbenes). The order of available singlet lifetimes for the methoxy-substituted *trans*-stilbenes matches the order of their reactivity in TFE. A longer lifetime for the reactive excited state would likely increase the probability of interception by a molecule of TFE. Whether or not the lifetime of the  $t_{S1}$  state is the determining factor in the solvent addition reaction will require further investigation.

Up until this point in the discussion, the regiochemistry of the solvent addition reactions has not been addressed. Traditionally, the two possible products that result from addition of an alcohol to an alkene moiety are labelled as the Markovnikov and anti-Markovnikov products, which in modern mechanistic terms refer to the products that result from attack of a nucleophile on the more- and less-stable carbocation intermediates, respectively. If the products of the addition reactions are formed *via* carbocation intermediates, then the major products can be referred to as Markovnikov ethers. Such nomenclature is based on the order of carbocation stabilities described in Chapter 1,

keeping in mind that meta methoxy substituents would have a destabilizing effect on a benzylic carbocation. However, given that the mechanism for formation of the solvent adducts is yet to be determined, such labels are somewhat premature. Indeed, the studies by Laarhoven and co-workers described in Section 3.1.3 have indicated that carbocation intermediates are *not* involved in the addition of methanol to *trans*-stilbene itself.

However, the addition of TFE to methoxy-substituted stilbene derivatives could follow a different mechanism. The purpose of using TFE as a solvent for the photolysis studies in Chapter 2 was to employ a polar, ionizing solvent of low nucleophilicity that is capable of stabilizing carbocation intermediates. Furthermore, the generation and observation of carbocation intermediates was accomplished by McClelland and co-workers<sup>47</sup> by irradiating a variety of substituted styrene derivatives in TFE. The mechanism for this reaction, which involves photochemical protonation of the styrene excited state, could also provide a pathway for formation of TFE adducts observed in the current study. The work described in Chapter 4 of this thesis will describe efforts to fully elucidate the mechanism of the TFE addition reactions.

## Chapter 4                      Mechanistic Aspects of the Photochemical Addition of Alcohols to Methoxy-Substituted Stilbenes, Styrenes, and 1-Arylpropenes

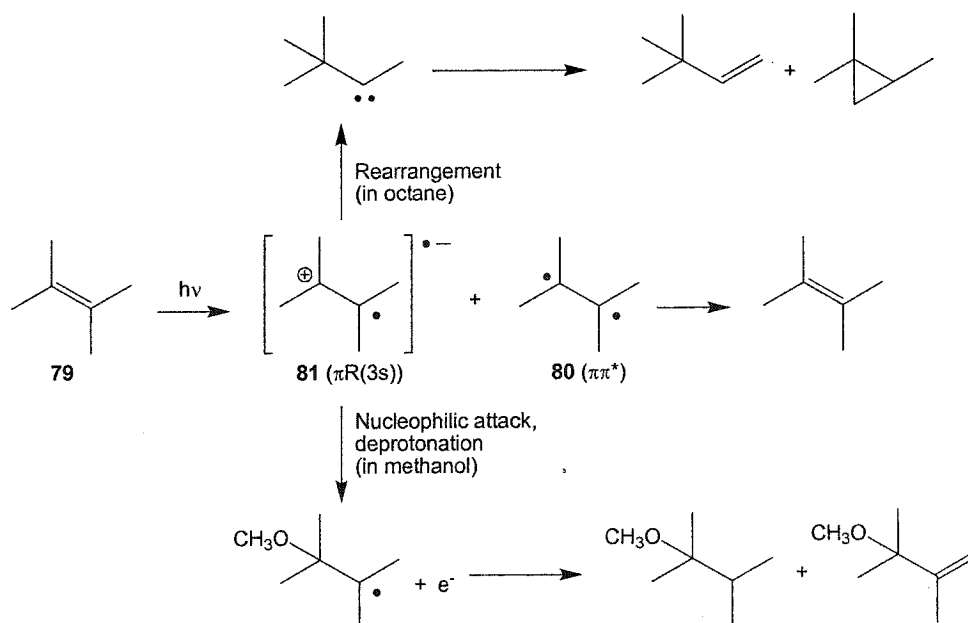
### 4.1 Introduction

#### 4.1.1 Early Examples of the Photochemical Addition of Alcohols to Alkenes

The focus of the current research was initially directed towards those photochemical reactions which proceed *via* carbocation intermediates, in particular the photofragmentation reactions investigated in Chapter 2. When considering the TFE addition reactions described in Chapter 3, there is a certain bias towards accepting carbocations as the reactive intermediates *a priori*, without also considering other mechanistic pathways. However, there are several examples where the photochemical addition of an alcohol to an alkene has been concluded to occur *without* the involvement of carbocation intermediates, or by a mechanism that *does not* proceed by protonation of an excited state. This section will briefly discuss some representative examples of these reactions, followed by a more complete examination of those reactions where the photochemical addition of alcohols to alkenes *does* proceed directly through carbocation intermediates.

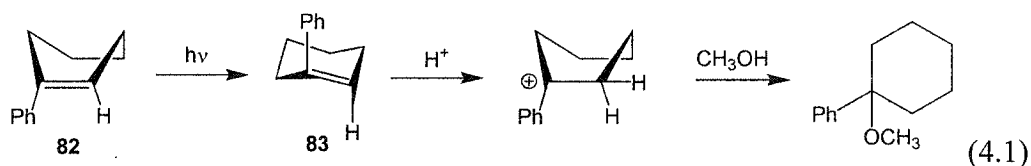
The photochemistry of simple alkyl-substituted alkenes is quite complex.<sup>113</sup> Upon direct irradiation of 2,3-dimethyl-2-butene **79**, two excited states are formed: the usual

$\pi, \pi^*$  state **80**, as well as the  $\pi, R(3s)$  Rydberg state **81** (Scheme 4.1). The  $\pi, \pi^*$  state undergoes bond torsion, which results in re-formation of the ground state alkene – this process is analogous to the deactivation of excited state stilbene derivatives discussed in Chapter 3. Rydberg states of simple alkenes are described as resulting from promotion of a  $\pi$  electron to an orbital with the dimensions of a helium 3s orbital.<sup>50</sup> Thus, **81** reacts by processes that are characteristic of radical cations. In alkane solvents, the observed products are rationalized by a pathway involving rearrangement of **81** to a carbene intermediate, followed by either deprotonation or intramolecular C-H bond insertion. In contrast, the decay of the  $\pi, R(3s)$  state in methanol proceeds by nucleophilic attack by the solvent, followed by hydrogen abstraction or disproportionation.<sup>114</sup> In some cases, the addition of methanol may also occur *via* O-H bond insertion by the carbene intermediate.<sup>115</sup> The latter mode of reactivity was postulated by Laarhoven and co-workers to occur upon irradiation of stilbene in methanol (*vide supra*, Section 3.1.2).<sup>81</sup>

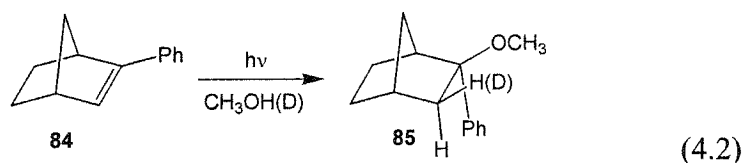


Scheme 4.1 Products resulting from the irradiation of 2,3-dimethyl-2-butene **79** in either octane or methanol.

The addition of methanol to simple alkenes through a mechanism involving a Rydberg state is a singlet process, and therefore is only available upon direct excitation of a substrate. In contrast, many cyclic alkenes undergo addition of methanol when excitation is achieved both by direct irradiation and by triplet sensitization. These addition reactions are most favourable for cyclohexenes and cycloheptenes – compounds possessing smaller or larger rings add methanol only *via* the (singlet) Rydberg mechanism described above.<sup>113</sup> The addition reaction also occurs more readily as the pH of the solution is lowered. Following LFP of *cis*-1-phenylcyclohexene **82**, Jousset-Dubien and co-workers<sup>116</sup> identified a transient species with an absorption maximum at 380 nm and a lifetime of 9  $\mu$ s in methanol. The intermediate was assigned as the strained isomer, *trans*-1-phenylcyclohexene **83**. Thus, the mechanism for methanol addition proceeds *via* photochemical isomerization of **82**, protonation of the ground state of the highly unstable *trans* isomer **83**, and finally trapping of the carbocation intermediate by nucleophilic methanol, Equation 4.1. The dependence of this mechanism on the size of the ring is clearly due to the requisite formation of an unstable *trans* isomer; larger rings are reasonably stable and are therefore less reactive towards acids, while smaller rings prevent photochemical isomerization altogether.<sup>117</sup> Furthermore, the process outlined in Equation 4.1 can be accessed by either singlet or triplet isomerization pathways, in accord with experimental observations.



In light of the mechanisms described above for the photochemical addition of methanol to substituted alkenes, the reaction of 2-phenyl-2-norbornene **84** (Equation 4.2) was initially quite surprising.<sup>118</sup> The ring structure of **84** should prevent the cis-trans isomerization process that would be required for the reaction to proceed through an unstable trans isomer. No formation of the product **85** was observed upon triplet sensitization, and so a singlet process was postulated – the quenching of the fluorescence of the analogous 2-phenyl-2-bornyl derivative by methanol supported this idea. However, irradiation of **84** in CH<sub>3</sub>OD produced the methanol adduct possessing deuterium on the adjacent carbon – addition of methanol *via* the carbene mechanism outlined in Scheme 4.1 would require incorporation of hydrogen. In order to account for these observations, Kropp proposed a mechanism involving direct protonation of a polarized excited singlet state followed by nucleophilic trapping of a carbocation intermediate. Similar methanol addition reactions have been observed for several substituted  $\beta$ -(*tert*-butyl)styrenes,<sup>119</sup> *trans*-1-(2-methoxyphenyl)propene,<sup>120</sup> and for a series of 1-phenylcyclobutenes.<sup>121</sup>

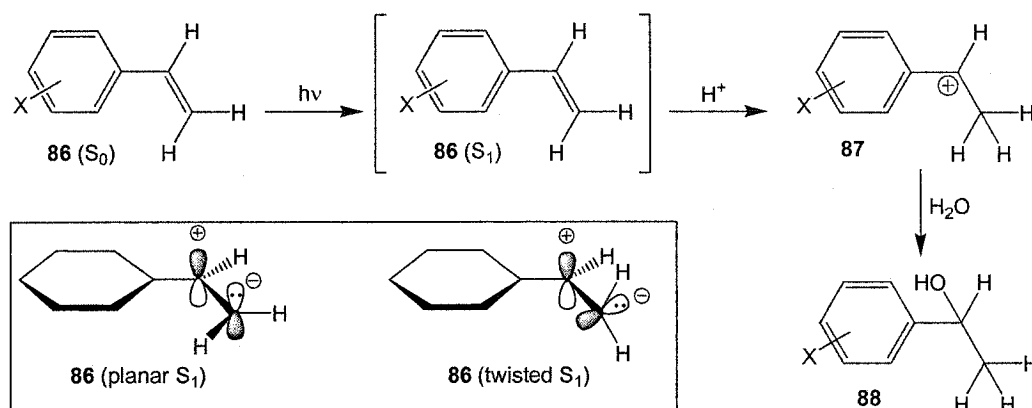


#### 4.1.2 The Photochemical Addition of Water and Alcohols to Substituted Styrenes

The addition of water<sup>122</sup> and methanol<sup>123</sup> to a variety of phenylacetylenes and diphenylacetylenes was first observed by Roberts and co-workers. The final product of the water addition reaction is the corresponding ketone, just as in the ground state hydration reaction. Using this work as a conceptual starting point, Yates and co-workers



carried out more thorough investigations of the photochemical hydration of a number of ring-substituted phenylacetylenes and styrenes.<sup>124</sup> The current discussion will focus on the properties of the styrene derivatives, although the reactivity of the phenylacetylenes is similar in many respects.

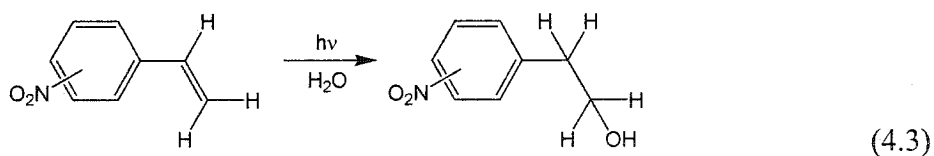


Scheme 4.2 Photohydration of a substituted styrene derivative, with two possible electronic structures for the reactive excited state species.

The mechanism for the photohydration of substituted styrenes is shown in Scheme 4.2. Excitation of the ground state styrene derivative **86** results in a  $\pi,\pi^*$  transition to form the first excited singlet state  $S_1$ . The change in electron distribution that accompanies this transition endows  $S_1$  with enhanced basicity relative to  $S_0$ , and therefore proton donors are capable of quenching **86** ( $S_1$ ) to give the ground state carbocation intermediate **87**. The observation of slower reaction rates in deuterated media support the idea of proton (deuterium) transfer to the excited state. The preferred regiochemistry of the addition product **88** (Markovnikov) indicates that C2 is the site of protonation due to increased electron density in  $S_1$ . Two geometries of the reactive  $S_1$  species were considered: one in which the structure remains planar, and a second in which the C1-C2 bond has undergone a  $90^\circ$  twist (Scheme 4.2). On the basis of the quenching of  $S_1$

fluorescence at lower pH and the concomitant increase in the yield of hydration product **88**, Yates and co-workers identified the planar geometry as the reactive state.<sup>124</sup> The twisted geometry is analogous to the perpendicular  $p_{S_1}$  state described earlier for the excited state of stilbene (*vide supra*, Section 3.1.1), and as such would likely undergo rapid internal conversion to  $S_0$ . Moreover, recent evidence indicates that the barrier for bond torsion on the  $S_1$  surface of styrene may be much higher than that of stilbene (*vide infra*, Section 4.3.2).

The mechanism outlined in Scheme 4.2 is operative for a wide variety of substituents: the parent styrene ( $X = H$ ), along with alkyl, methoxy, or fluoro derivatives (para or meta for each) all gave the hydration product **88** upon irradiation.<sup>124</sup> The chloro and bromo derivatives were somewhat reactive, but a competing Ar-X homolytic bond cleavage reaction complicated the product analysis. The trifluoromethyl and cyano substituted styrenes were unreactive towards photohydration. In contrast, the meta and para nitrostilbenes did undergo photohydration, but with opposite regiochemistry, Equation 4.3. Furthermore, the quantum yield for product formation from the nitrostyrenes was independent of the pH of the solution. Sensitization experiments indicated that the reaction is actually a triplet state process, with the mechanism involving *nucleophilic* attack by water on the electron-deficient C2.<sup>125</sup>



Using the Stern-Volmer techniques discussed in Section 3.2.6, McEwen and Yates were able to determine the rate constants  $k_{H^+}$  for the quenching of the  $S_1$  state by  $H^+$  in water, Table 4.1.<sup>126</sup> These values agree with the expectations 1) that electron donating

substituents accelerate the rate of protonation, and 2) that in the excited state, the meta-substituted compounds exhibit greater reactivity than the para isomers. Thus, the rate constant for the quenching of  $S_1$  by  $H^+$  is greatest for 3-methoxystyrene ( $k_{H^+} = 7.23 \times 10^8 M^{-1}$ ). These rate constants, and those for the analogous quenching of excited state phenylacetylene derivatives, were employed to obtain a structure-activity relationship in the form of the Hammett equation (*vide supra*, Section 1.2.3), as shown in Equation 4.4. Using the phenylacetylene series as a reference ( $\rho^{hv} = -1.0$ ), a value of  $\rho^{hv} = -1.24$  was obtained for the styrene series – the values of  $\sigma^{hv}$  are provided in Table 4.1. The  $\sigma^{hv}$  values were also found to give good correlations ( $r^2 \geq 0.95$ ) when plotted versus the results of several other excited state reactions, such as the photosolvolysis of benzyl alcohols<sup>127</sup> ( $\rho^{hv} = -0.76$ ) and the quenching of excited state 9-arylxanthyl cations by water<sup>128</sup> ( $\rho^{hv} = -1.44$ ).

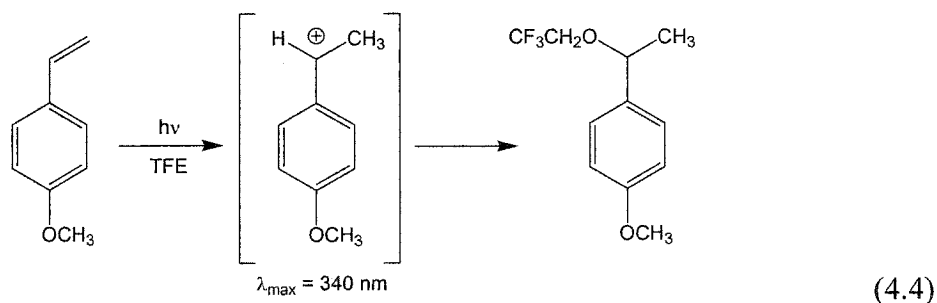
Substituent	$k_{H^+} (M^{-1})$	$\sigma^{hv}$
H	$8.1 \times 10^6$	0
4-F	$6.1 \times 10^6$	0.18
3-F	$1.4 \times 10^7$	-0.37
4-CH <sub>3</sub>	$3.4 \times 10^7$	-0.53
3-CH <sub>3</sub>	$4.2 \times 10^7$	-0.79
4-OCH <sub>3</sub>	$2.7 \times 10^8$	-1.17
3-OCH <sub>3</sub>	$7.2 \times 10^8$	-1.48

Table 4.1      Rate constants for the quenching of excited state styrene derivatives by hydronium ion ( $k_{H^+}$ ) and substituent constants for the  $\sigma^{hv}$  scale.

#### 4.1.3 Direct Observation of Carbocations Formed *via* Photoprotonation

The direct observation of a carbocation intermediate produced *via* photoprotonation was first reported by McClelland and co-workers.<sup>129</sup> Following

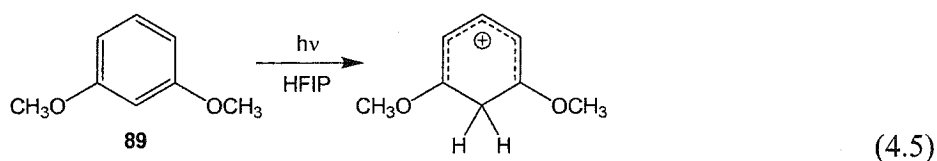
irradiation of a solution of 4-methoxystyrene in TFE with a 20 ns laser pulse at 248 nm, a transient species with an absorption maximum of 340 nm was observed. The rate constant for decay for the transient was found to be  $4 \times 10^5 \text{ s}^{-1}$  in pure TFE, and the addition of nucleophiles such as azide ion accelerated the rate of decay. Furthermore, the sole product formed upon 254 nm steady state irradiation of the styrene in TFE was the corresponding Markovnikov adduct.<sup>130</sup> The failure of oxygen to prevent formation of either the transient or the solvent adduct indicated that the reaction does not involve triplet states or radical species. The results were explained by the mechanism shown in Equation 4.4: the excited state ( $S_1$ ) of the styrene is quenched by protonation from TFE to yield the 4-methoxyphenethyl cation, and subsequent nucleophilic attack by the solvent provides the final product. This reaction is essentially the same process as was outlined in Scheme 4.2 for the photoprotonation of substituted styrene derivatives in the presence of aqueous acid.



The ability of an alcohol (TFE) to function as the source of “H<sup>+</sup>” in a photoprotonation reaction is attributed to a combination of factors. First, as was noted in Section 4.1.2, the excited state styrene possesses exceptionally high basicity relative to the ground state compound – the increase in reactivity that accompanies excitation of these substrates has been estimated as approximately eight orders of magnitude.<sup>124</sup> Second, the ability of TFE to act as a proton donor is enhanced by the inductive electron

withdrawing effect of the fluorine substituents – the acidity of TFE ( $pK_a = 12.4$ ) is greater than ethanol ( $pK_a = 15.9$ ), methanol ( $pK_a = 15.5$ ), or water ( $pK_a = 15.7$ ).<sup>131</sup> The properties that provide TFE with increased acidity also lead to a lower nucleophilicity and a higher ionizing power than other alcohols, thus allowing the solvent to stabilize carbocation intermediates.

The mechanism shown in Equation 4.4 is not unique to 4-methoxystyrene; subsequent studies allowed the characterization of many other aryl-substituted phenethyl cations *via* photoprotonation of the appropriate substrates.<sup>47,48</sup> The analogous procedure has been employed to the study phenylvinyl cations, which are formed by photoprotonation of the corresponding phenylacetylenes. Unfortunately, the rate constants for decay of highly reactive carbocations are often so large as to prevent their observation in TFE. These difficulties have been resolved by the use of 1,1,1,3,3,3-hexafluoroisopropanol (HFIP), a solvent which exhibits an even lower nucleophilicity than TFE. The strength of HFIP as a photoprotonation agent is indicated by its ability to protonate the excited states of simple methoxy-substituted aromatic compounds.<sup>132</sup> As shown for the case of 1,3-dimethoxybenzene **89** (Equation 4.5), these reactions provide cyclohexadienyl cation intermediates, which can be observed directly by LFP.

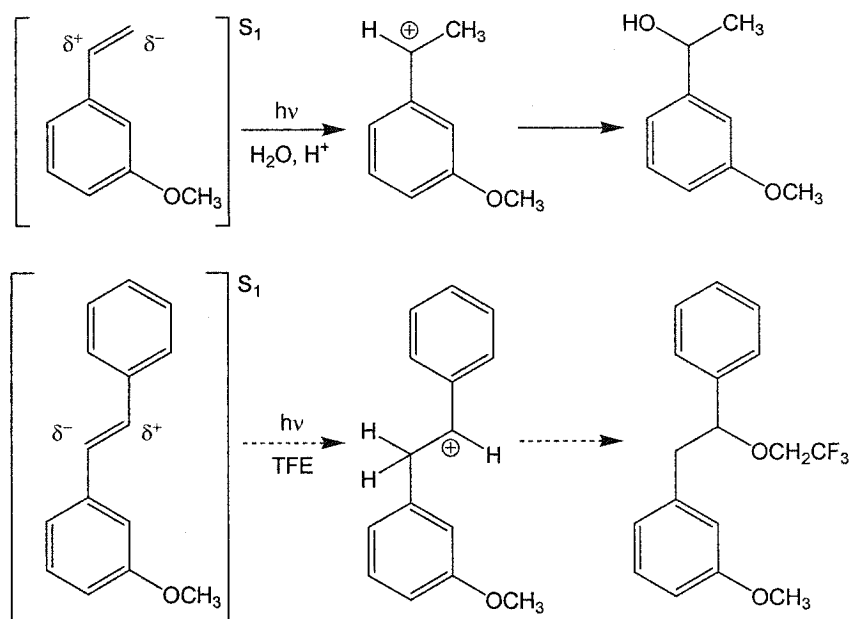


#### 4.1.4 Project Proposal

The mechanism described above for the photoprotonation of substituted styrene derivatives offers a suitable explanation for the TFE photoaddition reactions described in

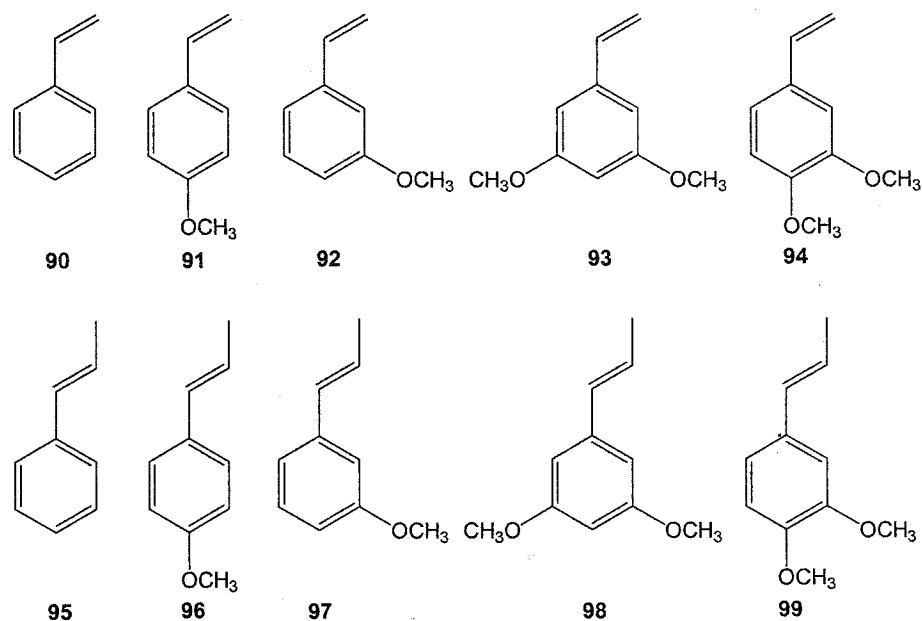
Chapter 3. Both reactions result in addition across the alkene double bond, and the fluorescence experiments indicate that both reactions occur from the singlet manifold. The enhanced acidity and ionizing power of TFE (compared to methanol) may explain the high reactivity of the methoxy-substituted stilbene derivatives in TFE. The quenching of *trans*-73 fluorescence by TFE and TFE-OD supports the concept of excited state protonation. Finally, the observation that both reactions occur more rapidly for meta-methoxy substrates is also encouraging.

However, there are several points that need to be addressed prior to accepting the photoprotonation mechanism as the preferred mode of reactivity for the stilbene substrates. In particular, the investigations of Laarhoven and co-workers concluded that the addition of methanol to a variety of substituted stilbene derivatives *does not* proceed via a photoprotonation mechanism (*vide supra*, Section 3.1.3). Another problem concerns the regiochemistry of the addition reactions: 3-methoxystyrene undergoes photoprotonation to yield the 3-methoxyphenethyl cation – this mechanism is supported by the structure of the isolated product, and also by the direct observation of the 3-methoxyphenethyl cation upon LFP of 3-methoxystyrene in HFIP ( $\lambda_{\text{max}} = 335 \text{ nm}$ ,  $k_{\text{HFIP}} = 5 \times 10^5 \text{ s}^{-1}$ ).<sup>47</sup> In contrast, the major product formed by TFE addition to *trans*-3-methoxystilbene (*trans*-72) indicates that the 3-methoxyphenethyl cation is *not* formed, Scheme 4.3. In other words, although both compounds exhibit increased reactivity towards excited state protonation (compared to the unsubstituted and 4-methoxy analogues), the site of protonation is different in the two cases. Because the site of protonation should indicate the location of increased electron density following excitation, these differences in reactivity are intriguing.



Scheme 4.3 Comparison of the mechanism for photohydration of 3-methoxystyrene with the supposed mechanism for photochemical TFE addition to *trans*-72.

Clearly, a more thorough assessment of the factors governing the addition of TFE to aryl alkenes is required. To this end, the properties of the five stilbene substrates introduced in Chapter 3 (*trans*-60 and *trans*-71-74) have been compared with the identically-substituted styrenes (90-94) and *trans*-1-arylpropenes (*trans*-95-99). The five styrene derivatives are obvious choices for comparison with the stilbenes, given that much of the literature on photoprotonation reactions (in either aqueous or fluorinated media) has focussed on the properties of substituted styrenes. In contrast, the reactivity of *trans*-1-arylpropene derivatives towards photoprotonation is not well established, aside from a report regarding the photochemical addition of methanol to *trans*-(2-methoxyphenyl)propene.<sup>120</sup> However, the photophysical properties of several *trans*-1-arylpropenes have been studied in detail by Lewis and co-workers.<sup>133</sup> In addition, arylpropenes 95-99 will allow a comparison of the photoisomerization behaviour, and as such should provide a useful link between the properties of the styrenes and stilbenes.



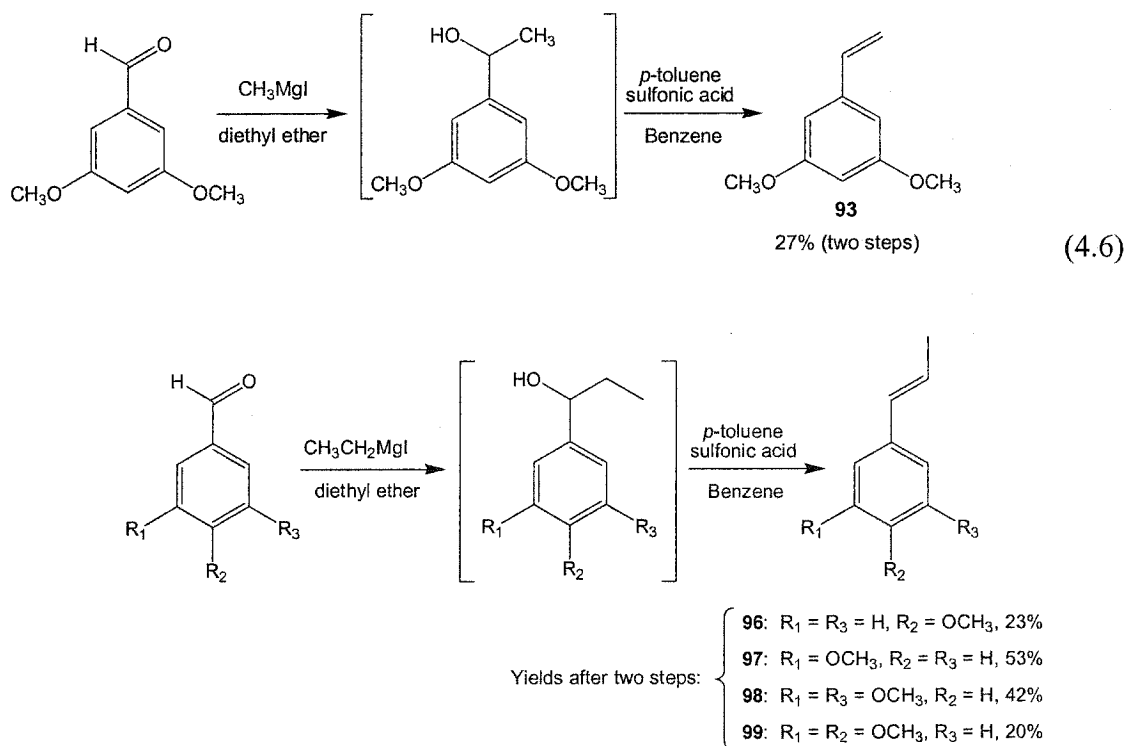
The approach to these investigations has taken the form of a wide range of experiments. Following a description of the synthesis of those substrates that were not commercially available (Section 4.2.1), the photophysical properties of the ten substrates shown above will be presented (Section 4.2.2). An important aspect of this work has been the comparison of the photophysical properties of the three sets of compounds in solvents of varying polarity (Section 4.2.3). The reactivity of the ten new compounds in steady state TFE irradiations has been investigated (Section 4.2.4), and a comparison of the fluorescence quantum yields and singlet lifetimes in acetonitrile and TFE has been made for all 15 substrates (Section 4.2.5). Attempts have been made to use LFP to directly observe the carbocation intermediates that would be formed following photoprotonation of the four methoxy-substituted *trans*-stilbenes (Section 4.2.6). Finally, irradiations in TFE and TFE-OD have provided information regarding the regiochemistry and stereochemistry of the photochemical addition reactions (Section 4.2.7).



## 4.2 Experimental Results

### 4.2.1 Synthesis of Methoxy-Substituted Styrenes and *trans*-1-Arylpropenes

Of the five styrene derivatives selected for the current investigations, only 3,5-dimethoxystyrene **93** was not commercially available. This compound was produced by combination of the methylmagnesium iodide Grignard reagent with 3,5-dimethoxybenzaldehyde, followed by dehydration of the alcohol intermediate, Equation 4.6. The unsubstituted *trans*-1-phenylpropene **95** was also commercially available. The syntheses of the four methoxy-substituted *trans*-1-arylpropenes were accomplished using the same route as for **93**, but using ethylmagnesium iodide with the appropriate methoxyphenyl aldehydes, Scheme 4.4. Separation of the *trans*-1-arylpropenes from their *cis* isomers by chromatographic techniques was not possible, but fortunately GC-FID analysis indicated that the reaction mixtures contained  $\geq 90\%$  of the *trans* isomers in all cases.



Scheme 4.4 Syntheses of methoxy-substituted *trans*-1-arylpropenes *trans*-**96-99**.

#### 4.2.2 Photophysical Properties of Methoxy-Substituted Styrenes and *trans*-1-Arylpropenes

The following pages contain the photophysical characterization data for styrenes **90-94** and *trans*-1-arylpropenes *trans*-**95-99** in acetonitrile solution. Tables 4.2 (styrenes) and 4.3 (*trans*-1-arylpropenes) provide summaries of the results, including absorption maxima, extinction coefficients, fluorescence maxima, singlet lifetimes, and fluorescence quantum yields. Also provided are the actual absorption spectra (Figure 4.1 – styrenes, Figure 4.2 – arylpropenes) and fluorescence spectra (Figure 4.3 – styrenes, Figure 4.4 – arylpropenes). The fluorescence data were obtained using an excitation wavelength of 254 nm, and the fluorescence quantum yields were determined using styrene in cyclohexane as an external standard ( $\phi_f = 0.25$ ).<sup>134</sup> In order to facilitate comparison of the current results with literature values, data for styrene (**90**) in cyclohexane<sup>135</sup> and *trans*-1-phenylpropene (*trans*-**95**) in hexanes<sup>133</sup> were also obtained.

The experimental singlet lifetimes for **90** ( $\tau_s = 12.7$  ns) and *trans*-**95** ( $\tau_s = 12.6$  ns) are both very similar to the literature values ( $\tau_s = 13.5$  ns<sup>135</sup> and 12.7 ns,<sup>133</sup> respectively). These results indicate that the measurements of  $\tau_s$  reported in Tables 4.2 and 4.3 (and elsewhere in this thesis) are reliable. The experimentally determined fluorescence quantum yield of *trans*-**95** ( $\phi_f = 0.34$ ) is also in fair agreement with the literature value ( $\phi_f = 0.30$ )<sup>133</sup> when using the same solvent, excitation wavelength, temperature, and reference value. In addition, the quantum yield of fluorescence has been reported for *trans*-(4-methoxyphenyl)propene (*trans*-**96**) upon 254 nm excitation in hexane solution ( $\phi_f = 0.38$ )<sup>133</sup> – this value is in good agreement with the current measurement in acetonitrile ( $\phi_f = 0.36$ ).

Compound <sup>a</sup>	$\lambda_{\max}$ (abs) <sup>b</sup> nm	$\epsilon_{\max}$ <sup>b</sup> M <sup>-1</sup> cm <sup>-1</sup>	$\lambda_{\max}$ (fluor) <sup>c</sup> nm	$\tau_s$ <sup>c</sup> ns	$\phi_f$ <sup>c,d</sup>
<b>90</b> (cyclohexane)	248, 282, 291	14400, 780, 540	304	12.7 <sup>e</sup>	0.25 <sup>d</sup>
<b>90</b>	247, 281, 290	14400, 780, 540	304	13.1	0.25
<b>91</b>	259, (290), (302)	19000, (2500), (1500)	323	6.4	0.33
<b>92</b>	249, 295	9400, 2300	333	7.7	0.40
<b>93</b>	256, 299	9800, 2000	349	6.8	0.24
<b>94</b>	261, 293, (309)	14300, 5300, (3300)	334	3.2	0.46

a) In acetonitrile unless otherwise noted. b) Shoulders of spectra given in parentheses.

c) Using 254 nm excitation. d) Relative to  $\phi_f = 0.25$  for styrene in cyclohexane, Reference

134. e) Literature value 13.5 ns, Reference 135.

Table 4.2 Summary of photophysical data for methoxy-substituted styrenes **90-94** in acetonitrile.

Compound <sup>a</sup>	$\lambda_{\max}$ (abs) <sup>b</sup> nm	$\epsilon_{\max}$ <sup>b</sup> M <sup>-1</sup> cm <sup>-1</sup>	$\lambda_{\max}$ (fluor) <sup>c</sup> nm	$\tau_s$ <sup>c</sup> ns	$\phi_f$ <sup>c,d</sup>
<b>95</b> (hexanes)	249, 283, 292	16300, 1100, 700	310	12.6 <sup>e</sup>	0.34 <sup>f</sup>
<b>95</b>	250, 283, 292	17100, 1100, 690	310	11.6	0.35
<b>96</b>	258, (292), (305)	19800, (2100), (1200)	331	8.6	0.36
<b>97</b>	252, 293	11800, 2400	328	6.2	0.34
<b>98</b>	257, 296	12100, 1900	339	2.8	0.08
<b>99</b>	259, 290, (308)	16300, 5200, (3200)	334	3.8	0.41

a) In acetonitrile unless otherwise noted. b) Shoulders of spectra given in parentheses.

c) Using 254 nm excitation. d) Relative to  $\phi_f = 0.25$  for styrene in cyclohexane, Reference

134. e) Literature value 12.7 ns, Reference 133. f) Literature value 0.30, Reference 133.

Table 4.3 Summary of photophysical data for arylpropenes *trans*-**94-99** in acetonitrile.

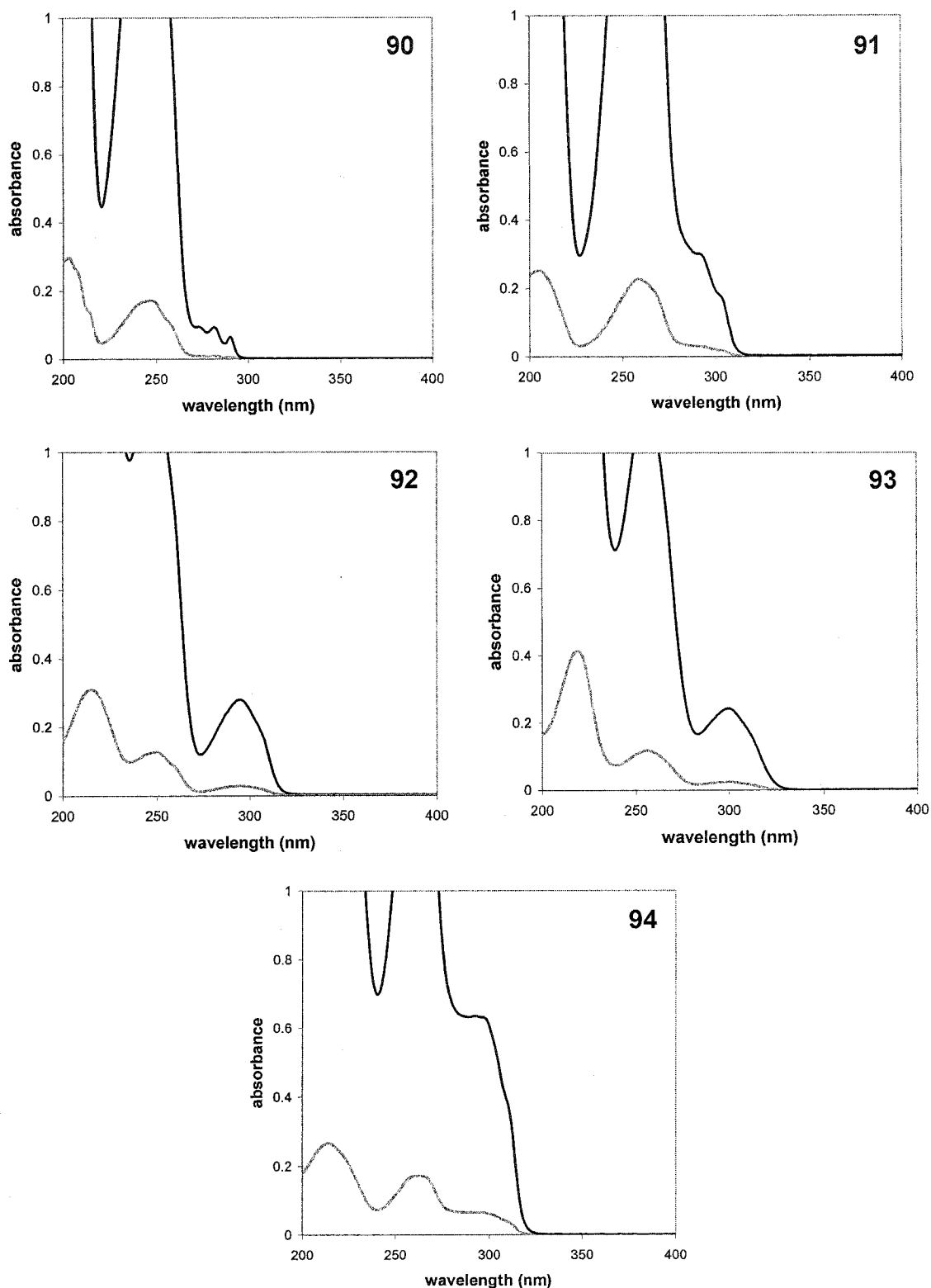


Figure 4.1 Absorption spectra of methoxy-substituted styrenes **90-94** in acetonitrile. Each plot provides a spectrum taken at  $1.2 \times 10^{-4}$  M (dark line) and  $1.2 \times 10^{-5}$  M (pale line).

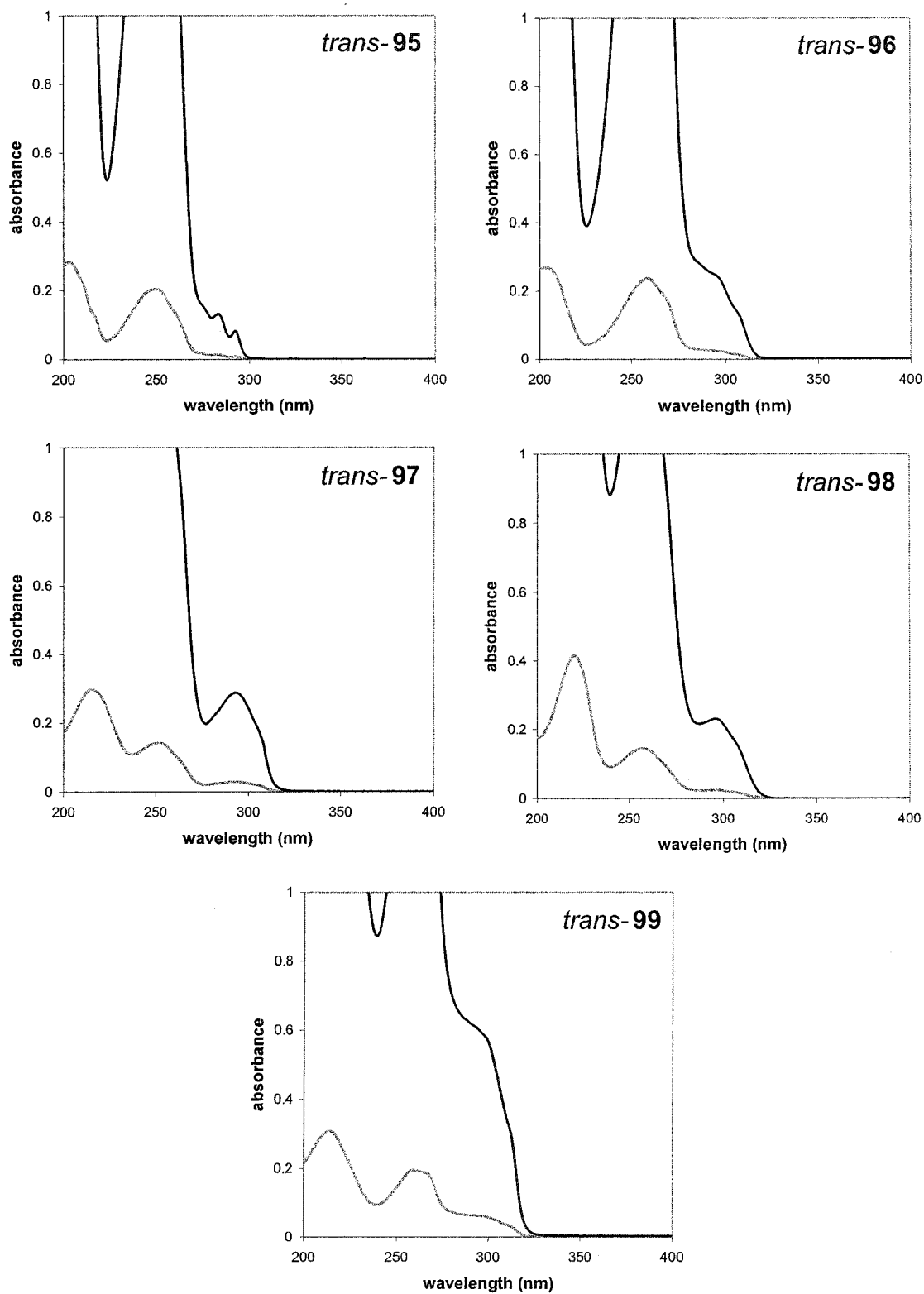


Figure 4.2 Absorption spectra of arylpropenes *trans*-95-99 in acetonitrile. Each plot provides a spectrum taken at  $1.2 \times 10^{-4}$  M (dark line) and  $1.2 \times 10^{-5}$  M (pale line).

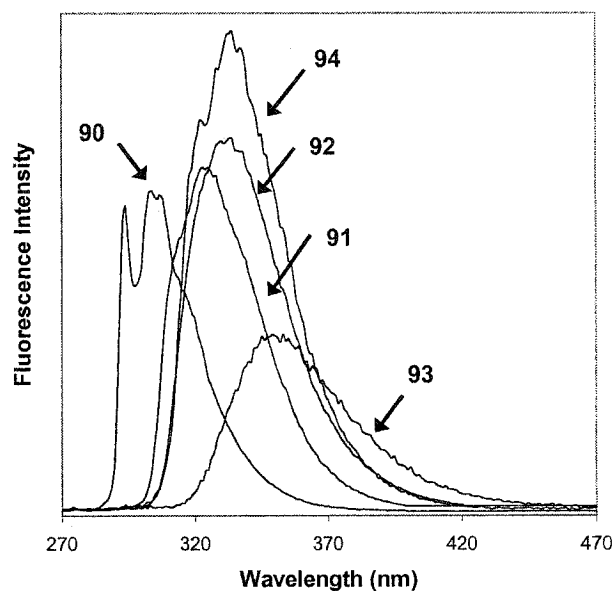


Figure 4.3 Comparison of fluorescence intensity for methoxy-substituted styrenes **90-94** in acetonitrile solution ( $A = 0.25$  at 254 nm for all solutions).

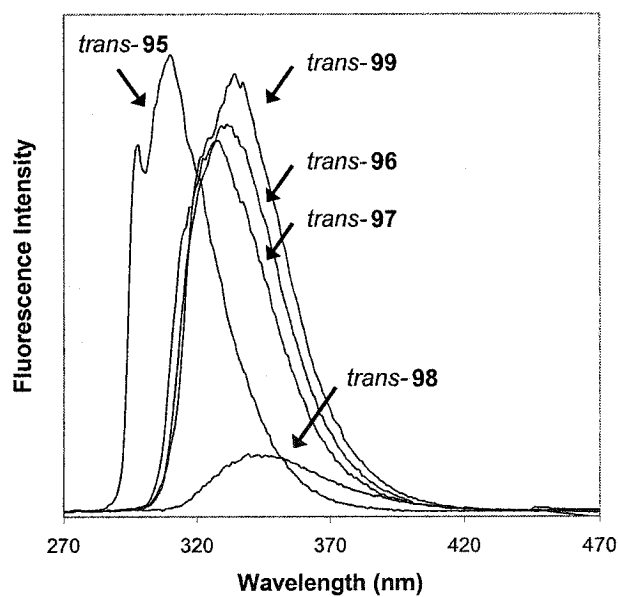


Figure 4.4 Comparison of fluorescence intensity for arylpropenes *trans*-**95-99** in acetonitrile solution ( $A = 0.25$  at 254 nm for all solutions).

The absorption spectra of the styrenes **90-94** (Figure 4.1) and the arylpropenes *trans*-**95-99** (Figure 4.2) are quite different than the spectra of the stilbenes *trans*-**60** and

*trans*-71-74 (*vide supra*, Figure 3.3). The  $S_0 \rightarrow S_1$  transitions for the ten new substrates are all observed at shorter wavelengths than the corresponding stilbene derivatives – the absorption spectra for the unsubstituted compounds **90** and *trans*-95 do not even extend past 300 nm. In addition, the extinction coefficients for the  $S_0 \rightarrow S_1$  transitions of the arylalkenes are about an order of magnitude lower in intensity than those of the methoxy-substituted stilbene derivatives. These observations are all consistent with the extended  $\pi$ -conjugation that is present in the stilbenes but not in the arylalkenes. However, an important observation is that the changes in  $\lambda_{\text{max}}$  (abs) and  $\epsilon_{\text{max}}$  induced by each substituent pattern are roughly the same for all three types of compounds.

The fluorescence spectra of the new substrates also deserve some discussion. The order of fluorescence maxima across the set of the styrenes **90-94** is quite similar to the arylpropenes *trans*-95-99, but neither set of substrates follows the same order of  $\lambda_{\text{max}}$  (fluor) values as the analogous stilbenes from Chapter 3. Furthermore, the order of fluorescence quantum yields for the ten new substrates is quite different from that of the substituted stilbene derivatives. The spectra in Figure 4.3 and 4.4 clearly show that in both cases, the 3,5-dimethoxy substrates **93** and *trans*-98 display the *lowest* fluorescence intensities for either set of compounds. In contrast, the fluorescence of *trans*-3,5-dimethoxystilbene (*trans*-73) was the *highest* of the five stilbenes investigated (*vide supra*, Figure 3.4). Apart from the low fluorescence quantum yields of the 3,5-dimethoxy substrates, the methoxystyrenes and *trans*-1-arylpropenes show remarkably similar fluorescence intensities. Such behaviour is a significant departure from the methoxy-substituted *trans*-stilbene fluorescence quantum yields, which spanned nearly two orders of magnitude (*vide supra*, Table 3.3).

#### 4.2.3 Photophysical Properties of Methoxy-Substituted Styrenes, Arylpropenes, and Stilbenes in Solvents of Varying Polarity

The effect of solvent polarity on the isomerization efficiency of *trans*-stilbene was introduced in Chapter 3. In particular, the observation that the barrier for C=C bond torsion on the  $S_1$  surface changes from 3.5 kcal/mol in alkane solvents to 2.4 kcal/mol in nitrile solvents has been taken as evidence that the barrier is polarizable.<sup>83</sup> The results of Mazzucato appear to confirm this idea, as demonstrated by *trans*-*cis* isomerization quantum yields ( $\phi_{tc}$  = 0.43 in hexane, 0.45 in acetonitrile) and fluorescence quantum yields ( $\phi_f$  = 0.04 in hexane, 0.02 in acetonitrile).<sup>92</sup> In order to understand how these concepts might relate to the current investigations, a variety of photophysical properties were measured in solvents ranging from cyclohexane (low polarity) to acetonitrile (high polarity). Results for the methoxystyrenes and *trans*-1-arylpropenes will be presented first, followed by those for the stilbene derivatives.

Table 4.4 displays values for the fluorescence maxima, fluorescence quantum yields, and singlet lifetimes for methoxy-substituted styrenes **91-94** in cyclohexane and acetonitrile. The same data for the methoxy-substituted *trans*-1-arylpropenes in hexanes and acetonitrile are provided in Table 4.5. The absorption spectra of these substrates did not show significant variations from the results in Tables 4.2 and 4.3, and so they have not been included with the current data. In order to allow comparison with the results for the methoxy-substituted *trans*-stilbenes (*vide infra*), the fluorescence measurements reported in Tables 4.4 and 4.5 were obtained using excitation at 295 nm (rather than 254 nm), and *trans*-stilbene in hexanes was used the reference value for the fluorescence quantum yield measurements. Unfortunately, neither of the unsubstituted compounds (**90**



or *trans*-95) absorb appreciably at 295 nm, and so both substrates were excluded from the current investigations.

Compound	Solvent	$\lambda_{\max}$ (fluor) <sup>a</sup> nm	$\phi_f^{a,b}$	$\tau_s^a$ ns
<b>91</b>	cyclohexane	322	0.33	6.6
	acetonitrile	323	0.21	6.3
<b>92</b>	cyclohexane	327	0.32	6.8
	acetonitrile	330	0.28	7.8
<b>93</b>	cyclohexane	341	0.12	3.8
	acetonitrile	350	0.15	6.9
<b>94</b>	cyclohexane	331	0.32	3.3
	acetonitrile	334	0.29	3.2

a) Using 295 nm excitation. b) Relative to  $\phi_f = 0.0433$  for *trans*-stilbene in hexane, Reference 86.

Table 4.4 Comparison of photophysical properties for methoxy-substituted styrenes **91-94** in cyclohexane and acetonitrile.

Compound	Solvent	$\lambda_{\max}$ (fluor) <sub>a</sub> nm	$\phi_f^{a,b}$	$\tau_s^a$ ns
<i>trans</i> - <b>96</b>	hexanes	328	0.35	7.9
	acetonitrile	330	0.27	8.7
<i>trans</i> - <b>97</b>	hexanes	325	0.31	5.9
	acetonitrile	327	0.24	6.5
<i>trans</i> - <b>98</b>	hexanes	338	0.04	1.5
	acetonitrile	343	0.05	2.9
<i>trans</i> - <b>99</b>	hexanes	334	0.35	3.7
	acetonitrile	333	0.28	4.0

a) Using 295 nm excitation. b) Relative to  $\phi_f = 0.0433$  for *trans*-stilbene in hexane, Reference 86.

Table 4.5 Comparison of photophysical properties for methoxy-substituted arylpropenes *trans*-**96-99** in hexanes and acetonitrile.

The data in Tables 4.4 and 4.5 indicate that changes in solvent polarity lead to only very slight changes in the photophysical properties of the methoxy-substituted styrenes and *trans*-1-arylpropenes. There are general trends of longer-wavelength emission, smaller fluorescence quantum yields, and longer singlet lifetimes in acetonitrile, but in many cases the changes are so small that it is difficult to rule out experimental error as the source of the differences. The singlet lifetime of *trans*-1-(4-methoxyphenyl)propene (*trans*-96) has been reported as 8.5 ns in hexane and 7.2 ns in acetonitrile (281 nm excitation).<sup>133</sup> These values are quite similar to those given in Table 4.5, but the trend is opposite – this emphasizes the degree of error that may exist in the lifetime measurements. However, the 3,5-dimethoxy substituted compounds **93** and *trans*-98 appear to display significant differences in the two solvents. The red shifts in the fluorescence maxima of these substrates is larger than for the other substrates (5-11 nm upon changing to acetonitrile), and the singlet lifetimes of both compounds are significantly longer in the more polar solvent.

In addition to the results in Tables 4.4 and 4.5, the quantum yields of isomerization have been measured in hexanes and acetonitrile for the *trans*-1-arylpropenes. These values were obtained using the same technique as for the methoxy-substituted *trans*-stilbene derivatives in Chapter 3 (by performing steady state irradiations at 300 nm and comparing the rate of reaction to that of *trans*-stilbene in cyclohexane,  $\phi_{tc} = 0.40$ ).<sup>108</sup> The unsubstituted substrate *trans*-95 does not absorb significantly at 300 nm, and so it was not included in these experiments. As indicated in Table 4.6, increases in polarity lead to only small increases in the magnitude of  $\phi_{tc}$  for *trans*-96-99. The quantum yield of isomerization for *trans*-1-(4-methoxyphenyl)propene (*trans*-96) upon

excitation at 281 nm has been reported as 0.12 in hexane and 0.13 in acetonitrile.<sup>133</sup> The excellent agreement between the literature values and those obtained in the current work indicates that the results in Table 4.6 should be quite reliable.

Compound	$\phi_{tc}^a$ (hexanes)	$\phi_{tc}^a$ (acetonitrile)
<i>trans</i> - <b>96</b>	0.10	0.12
<i>trans</i> - <b>97</b>	0.07	0.10
<i>trans</i> - <b>98</b>	0.03	0.05
<i>trans</i> - <b>99</b>	0.12	0.14

a) Determined by steady-state irradiation at 300 nm, relative to  $\phi_{tc} = 0.40$  for *trans* - stilbene in cyclohexane, Reference 108.

Table 4.6 Quantum yields of isomerization  $\phi_{tc}$  for the methoxy-substituted *trans*-1-arylpropenes *trans*-**96-99** in hexanes and acetonitrile.

In contrast to the methoxy-substituted styrenes and *trans*-1-arylpropenes, the excited states of the *trans*-stilbene derivatives are quite responsive to the polarity of the solvent. The five methoxy-substituted *trans*-stilbenes were investigated in a series of six solvents: cyclohexane, di-*n*-butyl ether, diethyl ether, ethyl acetate, 2-propanol, and acetonitrile. The absorption spectra of the five substrates do not show significant differences between any of the six solvents listed above. In contrast, the fluorescence maxima display significant bathochromic shifts with increasing solvent polarity, Table 4.7. The fluorescence quantum yields and singlet lifetimes (which are also solvent-dependent) will be discussed in due course following a complete analysis of the solvent-induced shifts in the fluorescence maxima.

Solvent	<i>trans</i> -60	<i>trans</i> -71	<i>trans</i> -72	<i>trans</i> -73	<i>trans</i> -74
cyclohexane	349	364	358	364	372
dibutyl ether	349	367	358	372	375
diethyl ether	349	366	357	374	373
ethyl acetate	349	366	358	382	382
2-propanol	348	365	357	382	374
acetonitrile	350	374	359	390	385

Table 4.7 The fluorescence maxima (in nanometers) for the methoxy-substituted *trans*-stilbenes in a series of six solvents.

The solvatochromic behaviour displayed by some of the methoxy-substituted *trans*-stilbenes in Table 4.7 has been observed for many other substrates. In those cases, researchers have successfully analysed the results by using the Lippert-Mataga treatment, Equation 4.7.<sup>98</sup> In this expression,  $\nu_{\text{ex}}$  and  $\nu_{\text{fluor}}$  are the maxima of the excitation and fluorescence spectra (in wavenumbers); the difference between these maxima is the Stokes' shift of the observed emission. The dipole moment of the ground state is given by  $\mu_g$ , and the dipole moment of the emissive excited state is given by  $\mu_e$ . The parameter  $\Delta f$  provides a measurement of solvent polarity – as shown in Equation 4.8,  $\Delta f$  is a function of the dielectric constant  $\epsilon$  and the refractive index  $n$ . Table 4.8 displays literature values of  $\epsilon$  and  $n$  for the six solvents employed in the current investigations, as well as values of  $\Delta f$  calculated using Equation 4.8. The remaining constants in Equation 4.7 are  $\pi$ ,  $\epsilon_0$  (the permittivity of a vacuum),  $h$  (Planck's constant),  $c$  (the speed of light), and  $a$  (the solvent cavity radius for the compound in question).

$$\bar{\nu}_{\text{ex}} - \bar{\nu}_{\text{fluor}} = \frac{\mu_e(\mu_e - \mu_g) \Delta f}{2\pi\epsilon_0 h c a^3} \quad (4.7)$$

$$\Delta f = \left[ \frac{\epsilon - 1}{2\epsilon + 1} - \frac{1}{2} \left( \frac{\eta^2 - 1}{2\eta^2 + 1} \right) \right] \quad (4.8)$$

Solvent	$\epsilon$	$\eta$	$\Delta f$
cyclohexane	2.023	1.426	0.1008
dibutyl ether	3.100	1.398	0.1945
diethyl ether	4.340	1.352	0.2561
ethyl acetate	6.000	1.372	0.2920
isopropanol	18.300	1.380	0.3661
acetonitrile	37.500	1.340	0.3936

Table 4.8 Literature values for the dielectric constant  $\epsilon$  and the refractive index  $\eta$ , as well as values for the solvent parameter  $\Delta f$  (calculated using Equation 4.8).

The analysis of Stokes' shift data using the Lippert-Mataga equation is performed by plotting  $(\nu_{\text{ex}} - \nu_{\text{fluor}})$  versus  $\Delta f$  for a series of solvents. The linear slope of the plot allows calculation of  $\mu_{\text{e}}$ , provided that reasonable estimates of  $\mu_{\text{g}}$  and  $a$  can be made. This technique has been employed to calculate the dipole moments of excited state species that are thought to possess substantial charge transfer character (*vide infra*, Section 5.1). The involvement of similar charge transfer excited states may play an important role in the photochemistry of the methoxy-substituted *trans*-stilbenes, so the Lippert-Mataga treatment of *trans*-60 and *trans*-71-74 was pursued.

Table 4.9 provides the Stokes' shifts of the five stilbene derivatives in all six solvents. Note that these shifts are expressed as  $(\lambda_{\text{max}}(\text{fluor}) - \lambda_{\text{max}}(\text{ex}))$ , and are given in nanometers rather than wavenumbers. The same values in wavenumber units are provided in Chapter 7. Figure 4.5 shows plots of the Stokes' shifts (in nanometers) versus the solvent parameter  $\Delta f$  for all five substrates.

Solvent	<i>trans</i> -60	<i>trans</i> -71	<i>trans</i> -72	<i>trans</i> -73	<i>trans</i> -74
cyclohexane	41	42	42	51	43
dibutyl ether	40	46	41	60	47
diethyl ether	41	45	43	61	45
ethyl acetate	40	43	41	69	53
2-propanol	39	44	42	71	49
acetonitrile	42	52	43	79	57

Table 4.9 Stokes' shifts (in nanometers) for the fluorescence of *trans*-60 and *trans*-71-74 in a series of six solvents.

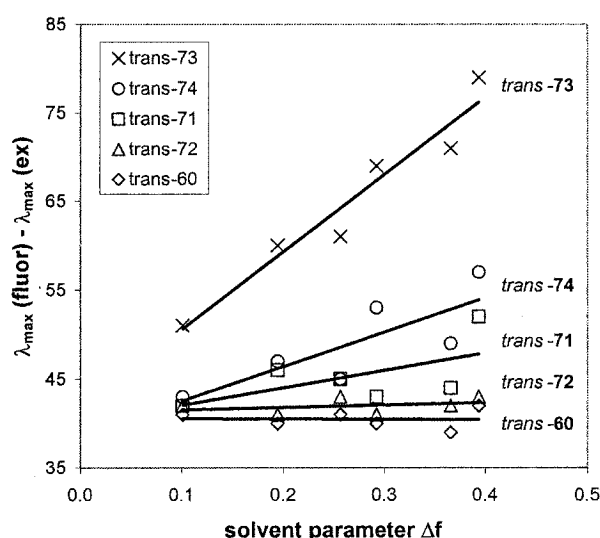


Figure 4.5 Plot of the solvent induced Stokes' shifts ( $\lambda_{\max}(\text{fluor}) - \lambda_{\max}(\text{ex})$ ) versus the solvent parameter  $\Delta f$  for five methoxy-substituted *trans*-stilbenes.

Although there is significant scatter in the data, Figure 4.5 indicates that solvent polarity does alter the position of the fluorescence maxima for the stilbene substrates. In order to determine dipole moments for the emissive excited states, the slope and intercepts of the linear least-squares plots were converted to wavenumber units, Table 4.10. The Gaussian 98 software package was employed to calculate ground state (B3LYP/6-31G(d), optimized geometries) and excited state (TDDFT/6-31G(d), at the ground state geometry, *i.e.*, vertical excitation) dipole moments for *trans*-60 and *trans*-71-

74. The experimental dipole moments of the emissive excited states ( $\mu_e$ ) were determined from Equation 4.7 using the solvatochromic slopes and the calculated ground state dipole moments ( $\mu_g$ ). A solvent cavity radius of  $a = 5 \times 10^{-10}$  m was used for all five substrates – this same value was used by Lewis and co-workers for the calculation of  $\mu_e$  for several amino-substituted stilbene derivatives.<sup>98</sup>

Compound	slope <sup>a</sup>	intercept <sup>a</sup>	$r^2$	$\mu_g$ (calculated) <sup>b</sup>	$\mu_e$ (calculated) <sup>b</sup>	$\mu_e$ (experimental) <sup>c</sup>
	cm <sup>-1</sup>	cm <sup>-1</sup>		D	D	D
<i>trans</i> -60	-53	3800	0.002	0	0	-
<i>trans</i> -71	1400	3500	0.36	1.6	2.0	6.8
<i>trans</i> -72	260	3600	0.11	1.3	1.1	3.2
<i>trans</i> -73	6400	3800	0.94	1.3	1.4	13.2
<i>trans</i> -74	2900	3200	0.65	0.6	1.1	8.7

a) Parameters from plots of Stoke's shift in cm<sup>-1</sup> versus solvent parameter  $\Delta f$ . b) Calculated using the Gaussian software package (see experimental for details). c) Calculated using Equation 4.7 with a solvent cavity radius of  $5 \times 10^{-10}$  m in all cases.

Table 4.10 Analysis of the solvatochromic behaviour of *trans*-60 and *trans*-71-74 using the Lippert-Mataga treatment (Equation 4.7).

The results in Table 4.10 indicate that the emissive excited states of *trans*-71-74 have much larger dipole moments than the corresponding ground states. The disagreement between the calculated and experimental values of  $\mu_e$  can be attributed to relaxation of the initially formed Frank-Condon state to a state possessing some degree of charge transfer character. The latter species are likely to play a role in the reactivity of these substrates in TFE. Indeed, the most reactive compound in TFE (the 3,5-dimethoxy substrate *trans*-73) also displays the highest excited state dipole moment ( $\mu_e = 13.2$  D). However, there is not a perfect correlation between  $\mu_e$  and reactivity in TFE – the 3-methoxy substrate *trans*-72 reacts quite quickly in TFE, but also displays a comparatively

low excited state dipole moment ( $\mu_e = 3.2$  D). Clearly there are additional factors that determine the efficiency of the TFE addition reactions.

As was mentioned earlier, other photophysical properties of the methoxy-substituted *trans*-stilbenes can be modified by changes in solvent polarity. Table 4.11 shows the fluorescence quantum yields for the substrates in the six solvents investigated above, and Figure 4.6 shows a plot of the data versus the solvent parameter  $\Delta f$ .

Solvent	<i>trans</i> -60	<i>trans</i> -71	<i>trans</i> -72	<i>trans</i> -73	<i>trans</i> -74
cyclohexane	0.034	0.020	0.16	0.17	0.048
dibutyl ether	0.038	0.018	0.18	0.23	0.039
diethyl ether	0.032	0.013	0.16	0.24	0.040
ethyl acetate	0.029	0.012	0.16	0.27	0.036
2-propanol	0.027	0.010	0.13	0.25	0.032
acetonitrile	0.021	0.006	0.15	0.29	0.028

Table 4.11 Fluorescence quantum yields for *trans*-60 and *trans*-71-74 in a series of six solvents.

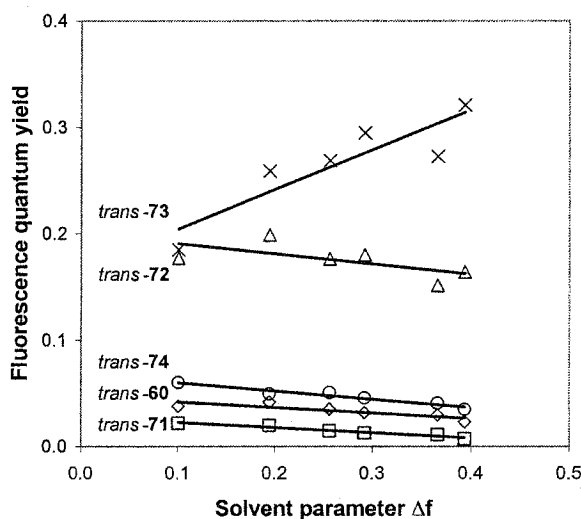


Figure 4.6 Plot of fluorescence quantum yields *versus* the solvent parameter  $\Delta f$  for five methoxy-substituted *trans*-stilbenes.



The plots in Figure 4.6 display some intriguing trends. For instance, four of the five substrates become slightly less fluorescent with increasing solvent polarity, and the slopes of the  $\phi_f$  versus  $\Delta f$  plots appear to be quite similar. Also, *trans*-72 displays a much higher fluorescence quantum yield than *trans*-60, *trans*-71, or *trans*-74. While this in itself is not unusual, the fact that solvent polarity has a very similar influence on the weakly fluorescent compounds as on *trans*-72 is peculiar. Finally, the observed increase in the fluorescence of *trans*-73 with increasing solvent polarity is remarkable. In low-polarity cyclohexane, the fluorescence quantum yield of *trans*-73 ( $\phi_f = 0.17$ ) is almost the same as that of *trans*-72 ( $\phi_f = 0.16$ ). However, while the fluorescence of *trans*-72 decreases slightly upon changing to high-polarity acetonitrile ( $\phi_f = 0.15$ ), the fluorescence of *trans*-73 increases substantially ( $\phi_f = 0.32$ ).

The singlet lifetimes of *trans*-72 and *trans*-73 are also influenced by solvent polarity. Unfortunately, the lifetimes of the other three substrates are too short to be measured by single photon counting ( $\tau_s < 0.5$  ns). Table 4.12 provides the singlet lifetimes for *trans*-72 and *trans*-73, and Figure 4.7 shows a plot of  $\tau_s$  versus solvent parameter  $\Delta f$ . The variations in the singlet lifetime of *trans*-72 with changing solvent polarity are only very slight, and may only be due to error in the measurement. In contrast, the monoexponential singlet lifetime of *trans*-73 increases dramatically with increasing polarity, from cyclohexane ( $\tau_s = 3.7$  ns) to acetonitrile ( $\tau_s = 16.9$  ns). Although the fluorescence quantum yields of *trans*-72 and *trans*-73 are very nearly the same in cyclohexane (*vide supra*), the lifetime of *trans*-73 in cyclohexane ( $\tau_s = 3.7$  ns) is clearly larger than that of *trans*-72 ( $\tau_s = 0.7$  ns)

Solvent	<i>trans</i> -72 <sup>a</sup>	<i>trans</i> -73 <sup>a</sup>	<i>trans</i> -73 (fast) <sup>b</sup>	<i>trans</i> -73 (slow) <sup>b</sup>
cyclohexane	0.7	3.7	0.9	4.0
dibutyl ether	0.7	6.7	1.6	7.6
diethyl ether	0.8	9.0	1.7	9.6
ethyl acetate	0.6	11.5	2.1	12.9
2-propanol	0.7	12.6	2.0	13.8
acetonitrile	0.9	16.9	3.9	18.5

a) Fit to a monoexponential decay. b) Fit to a biexponential decay.

Table 4.12 Monoexponential singlet lifetimes for *trans*-72 and *trans*-73 in a series of six solvents, as well as the fast and slow components for the biexponential decay of *trans*-73.

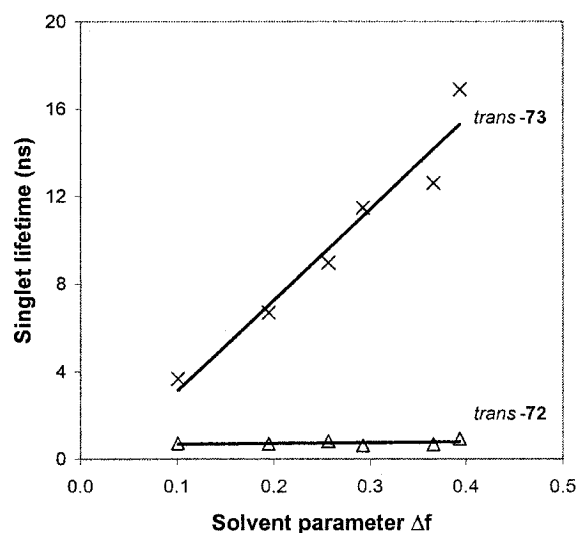


Figure 4.7 Plot of monoexponential singlet lifetimes for *trans*-72 and *trans*-73 versus the solvent polarity function  $\Delta f$ .

A very interesting aspect of the singlet lifetime data for the 3,5-dimethoxy substrate *trans*-73 has been ignored up to this point in the report. The computer analysis of the fluorescence decay of *trans*-73 in acetonitrile using a monoexponential kinetic fit is provided in Figure 4.8. Although a monoexponential fit reproduces most characteristics of the experimental data, there are slight deviations in the very early portion of the plot

(Figure 4.8-A). The error in the monoexponential fit is most easily seen in the plot of residuals (Figure 4.8-B); the distinct curvature in the residual plot indicates that additional parameters are required to fit the data. Figure 4.9 shows the fitting of the same data to a biexponential decay model. The data are reproduced more faithfully by the biexponential fit (Figure 4.9-A), and the systematic error in the residual plot has been removed (Figure 4.9-B). Furthermore, the  $r^2$  correlation coefficient for the fit is improved from 0.988 (monoexponential) to 0.998 (biexponential). The long and short lifetimes of the *trans*-73 excited state are given in Table 4.12 (*vide supra*), and are plotted versus the solvent parameter  $\Delta f$  in Figure 4.10.

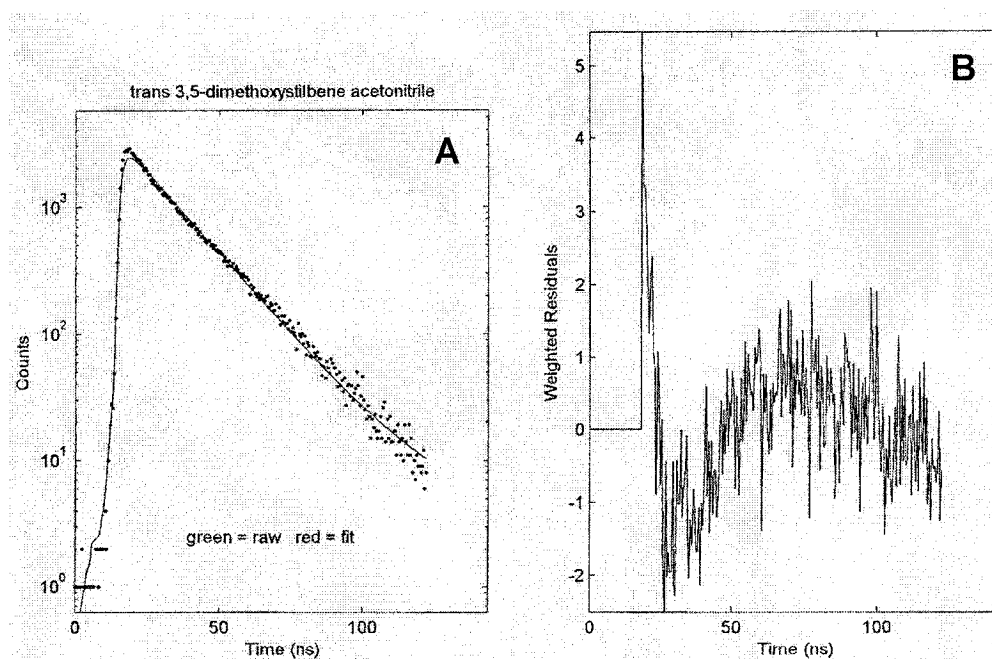


Figure 4.8 Analysis of the fluorescence decay of *trans*-73 using a monoexponential kinetic fit. **A.** Experimental data (points) and fitting curve (line). **B.** Weighted residuals (experimental - fit).

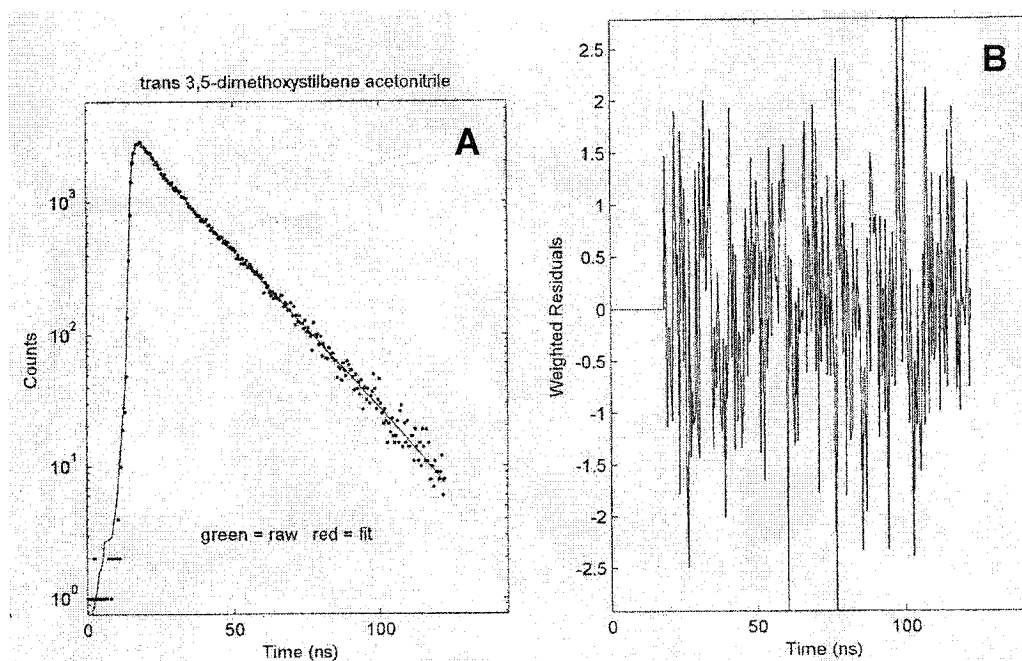


Figure 4.9 Analysis of the fluorescence decay of *trans*-73 using a biexponential kinetic fit. **A.** Experimental data (points) and fitting curve (line). **B.** Weighted residuals (experimental - fit).

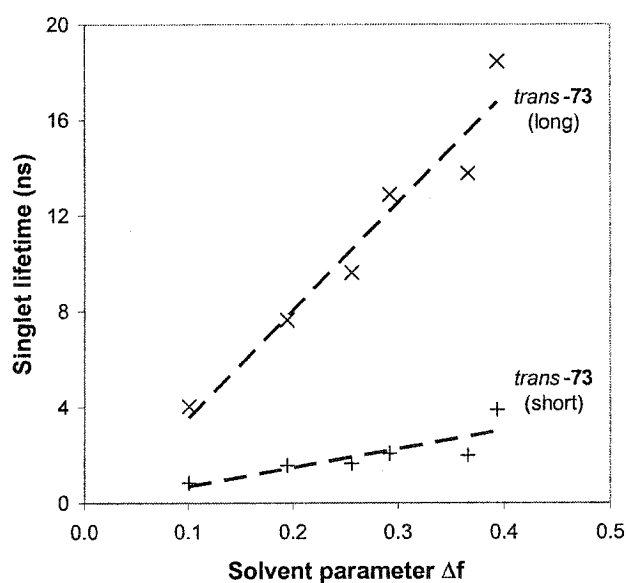


Figure 4.10 The two components of the biexponential lifetime of *trans*-73 versus the solvent parameter  $\Delta f$  for a series of six solvents.

The observation that the fluorescence of *trans*-73 decays biexponentially requires further consideration. In essence, this means that the observed fluorescence is due to *two* emitting species. Furthermore, the plots in Figure 4.10 demonstrate that lifetimes of both species are longer in more polar solvents. Biexponential fluorescence decay was not observed for *trans*-72 (the only other stilbene derivative that could be studied by single photon counting) or for any of the methoxy-substituted styrenes or *trans*-1-arylpropenes. Thus, from all the substrates investigated in the current report, biexponential singlet lifetimes are apparently unique to *trans*-73. This unusual behaviour will be more fully addressed in the discussion (Section 4.3) and particularly in Chapter 5.

The dependence of the quantum yields of isomerization on solvent polarity was also investigated for the methoxy-substituted *trans*-stilbenes, Table 4.13. The very good agreement between the values of  $\phi_{ic}$  obtained for in cyclohexane *trans*-71 and *trans*-72 in the current studies and those reported in the literature<sup>108</sup> was discussed earlier (*vide supra*, Section 3.3.1). The results in Table 4.6 indicated that the *trans*-1-arylpropenes display only very slight increases in  $\phi_{ic}$  upon changing from low-polarity hexanes to high-polarity acetonitrile. In contrast, many of the methoxystilbenes display much larger quantum yields of isomerization in acetonitrile than in cyclohexane. The only stilbene substrate for which  $\phi_{ic}$  is not greater in acetonitrile is *trans*-73. This observation is of particular note given very strong influence of solvent polarity on the Stokes' shift, fluorescence quantum yield, and singlet lifetime of *trans*-73. The excited state behaviour *trans*-3,5-dimethoxystilbene (*trans*-73) is clearly unique in comparison to the methoxy-substituted styrenes, *trans*-1-arylpropenes, and even the other *trans*-stilbene derivatives.

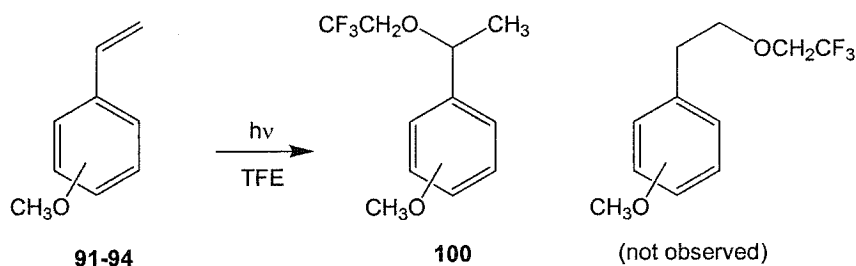
Compound	$\phi_{tc}^a$ (cyclohexane)	$\phi_{tc}^a$ (acetonitrile)
<i>trans</i> -60	0.40	0.45
<i>trans</i> -71	0.39	0.53
<i>trans</i> -72	0.32	0.39
<i>trans</i> -73	0.29	0.28
<i>trans</i> -74	0.41	0.59

a) Determined by steady-state irradiation at 300 nm, relative to  $\phi_{tc} = 0.40$  for *trans*-stilbene in cyclohexane, Reference 108.

Table 4.13 Quantum yields of isomerization for the methoxy-substituted stilbenes *trans*-60 and *trans*-71-74 in cyclohexane and acetonitrile.

#### 4.2.4 Irradiations of 91-94 and *trans*-96-99 in TFE

In order to completely assess the photochemistry of the methoxystyrenes and *trans*-1-arylpropenes, irradiations in TFE were performed. The very low absorbance of the unsubstituted compounds (styrene **90** and *trans*-1-phenylpropene *trans*-95) at the maximum output of the lamps (300 nm) once again prevented detailed investigations of these substrates. As expected, the major product detected following irradiation of styrenes **91-94** in TFE was the corresponding Markovnikov ether **100** (Scheme 4.5). Yield *versus* time plots for the styrene irradiations are provided in Figure 4.11.



Scheme 4.5 Products detected following irradiation of methoxy-substituted styrenes **91-94** in TFE.

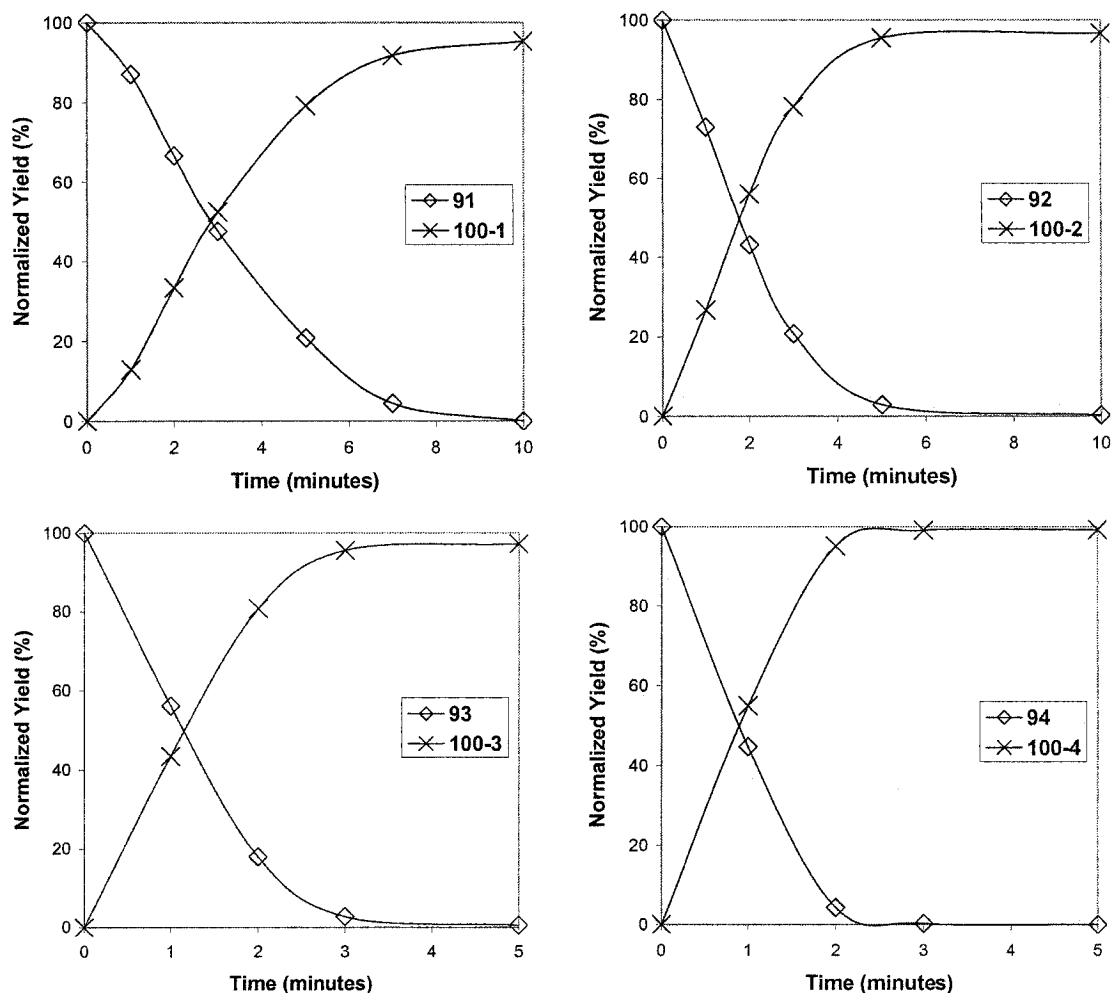


Figure 4.11 Yield *versus* time plots for the irradiation of methoxy-substituted styrenes in TFE (91 and 92 for *ten* minutes, 93 and 94 for *five* minutes).

The anti-Markovnikov TFE adduct was not observed following irradiation of 91-94, but small amounts (<5%) of other products were detected in some reaction mixtures. The GC retention times of these products were much longer than those of the starting styrenes or TFE adducts, and GC-MS indicated masses in excess of  $m/z$  300. The unidentified compounds are tentatively assigned as dimers or oligomers of the styrenes. As a result of the difficulty in making confident structural identifications of these by-products, they have not been included in the yield *versus* time plots in Figure 4.11. The

percent conversions for **91-94** in TFE are given in Table 4.14, keeping in mind that the major product from all four irradiations is the TFE ether **100**. The nomenclature for **100** will follow the same trend as for the products in Chapter 3; **100-1** corresponds to the ether derived from **91**, and so forth.

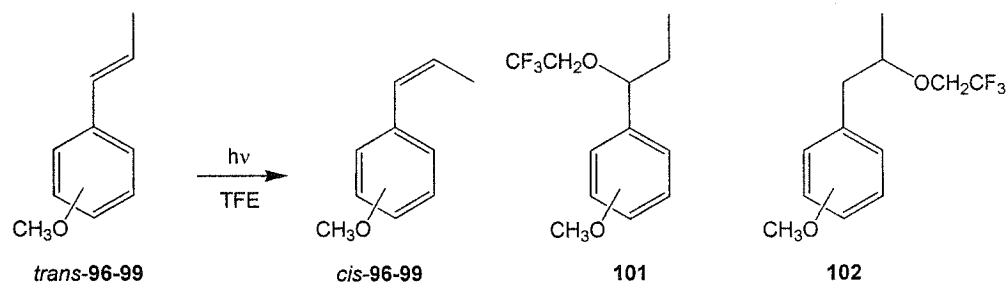
Compound	% Conversion <sup>a</sup>
<b>91</b>	33
<b>92</b>	57
<b>93</b>	82
<b>94</b>	96

a) The Markovnikov TFE adduct **100** was formed in greater than 90% yield from all four substrates.

Table 4.14    Percent conversions of the methoxy-substituted styrenes **91-94** after two minutes of 300 nm irradiation in TFE.

Irradiations of arylpropenes *trans*-**96-99** in TFE were also performed. As indicated in Scheme 4.6, these reactions produce the isomers *cis*-**96-99** in addition to the TFE adducts **101** and **102** (small amounts of possible dimeric products were also detected by GC). The yield versus time plots for these reactions (Figure 4.12) show that, unlike the case for the corresponding *trans*-stilbene derivatives, the photochemistry of the *trans*-arylpropenes is not dominated by the *trans*-*cis* isomerization reaction (*c.f.*, Figure 3.8). This observation is supported by the much lower quantum yields of isomerization of *trans*-**96-99** (Table 4.6) compared to *trans*-**71-74** (Table 4.13).





Scheme 4.6 Products detected following irradiation of methoxy-substituted *trans*-arylpropenes *trans*-96-99 in TFE.

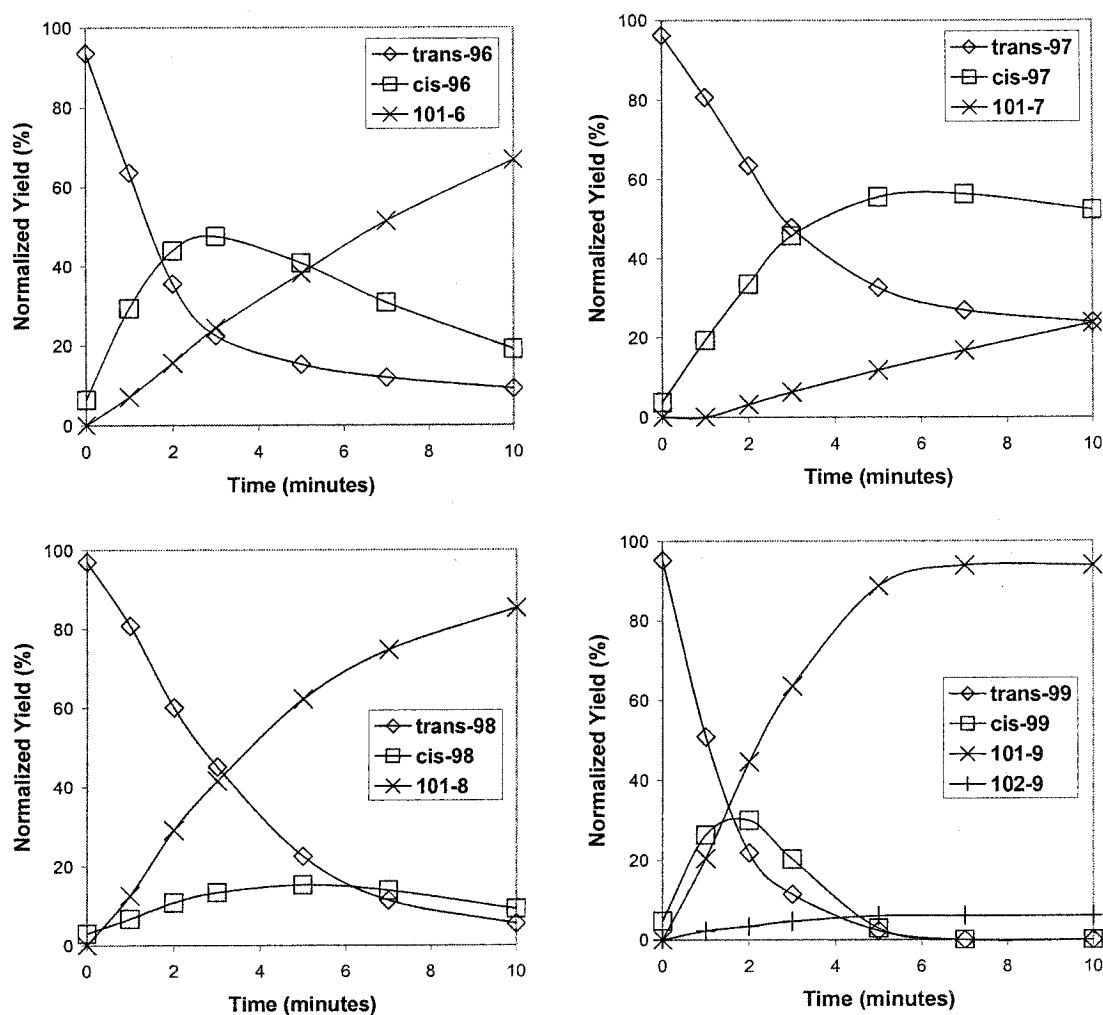


Figure 4.12 Yield *versus* time plots for the irradiation of methoxy-substituted *trans*-arylpropenes in TFE (ten minutes for all four compounds).

The major product detected following irradiation of *trans*-**96-99** (aside from the cis isomers) is the Markovnikov solvent adduct **101**. Surprisingly, the regioisomer **102** was observed following irradiation of the 3-methoxy substrate *trans*-**97** or the 3,4-dimethoxy substrate *trans*-**99**. The GC-MS identification of **102** is based on observation of either molecular ion ( $m/z$  248 for **102-7** or  $m/z$  278 for **102-9**) as well as peaks corresponding to the required benzylic cations ( $m/z$  121 or  $m/z$  151). In the case of *trans*-**97**, **102-7** was observed only in trace amounts (**101-7**:**102-7** = 45:1 after ten minutes), and therefore this product has not been included in the yield *versus* time plots. However, irradiation of *trans*-**99** resulted in much higher amounts of **102-9** (**101-9**:**102-9** = 16:1 after ten minutes). Values for the percent conversions of the trans isomers only and of the combined trans and cis isomers together are given in Table 4.15. One of the most intriguing aspects of these reactions is the very low reactivity of *trans*-**97** compared to the other substrates. In addition, the order of reactivity of the *trans*-1-arylpropenes in TFE is different than the order for either the *trans*-stilbene derivatives (*vide supra*, Table 3.4) or the styrene derivatives (Table 4.14).

Compound	% Conversion <sup>a</sup>	% Conversion <sup>b</sup>
<i>trans</i> - <b>96</b>	64	20
<i>trans</i> - <b>97</b>	19	3
<i>trans</i> - <b>98</b>	40	29
<i>trans</i> - <b>99</b>	78	48

a) Conversion of trans isomer *only*. b) Conversion of trans *and* cis isomers combined (>90% of product yield is TFE adduct from all four substrates).

Table 4.15     Percent conversions of the arylpropenes *trans*-**96-99** after two minutes of 300 nm irradiation in TFE.

#### 4.2.5 Quenching of Fluorescence and Singlet Lifetimes by TFE

The three classes of substrates (stilbenes, styrenes, and 1-arylpropenes) display very different orders of reactivity upon irradiation in TFE solution. In order to assess the ability of TFE to react directly with the excited state of each substrate, measurements of fluorescence quantum yields and singlet lifetimes were performed in TFE, and compared to the same values in acetonitrile. The experimentally determined values of  $\phi_f$  and  $\tau_s$  are provided in Table 4.16 (stilbenes *trans*-60 and *trans*-71-74), Table 4.17 (styrenes 91-94), and Table 4.18 (arylpropenes *trans*-96-99).

Compound	$\phi_f$ (AcN) <sup>a</sup>	$\phi_f$ (TFE) <sup>a</sup>	$\phi_f$ ratio <sup>b</sup>	$\tau_s$ (AcN) <sup>c</sup>	$\tau_s$ (TFE) <sup>c</sup>	$\tau_s$ ratio <sup>b</sup>
<i>trans</i> -60	0.023	0.01	2.3	< 0.5 <sup>d</sup>	< 0.5 <sup>d</sup>	-
<i>trans</i> -71	0.007	0.006	1.1	< 0.5 <sup>d</sup>	< 0.5 <sup>d</sup>	-
<i>trans</i> -72	0.16	0.08	1.9	0.93	0.63	1.5
<i>trans</i> -73	0.32	0.029	11.1	16.9	1.64	10.3
<i>trans</i> -74	0.035	0.026	1.4	< 0.5 <sup>d</sup>	< 0.5 <sup>d</sup>	-

a) Excitation at 295 nm, in relation to  $\phi_f = 0.0433$  for *trans*-stilbene in hexane, Reference 86.

b) AcN/TFE. c) Excitation at 295 nm, measured at fluorescence maximum. d) shorter than the time resolution of the instrument.

Table 4.16 Quenching of fluorescence quantum yields  $\phi_f$  and singlet lifetimes  $\tau_s$  by TFE for stilbenes *trans*-60 and *trans*-71-74.

Compound	$\phi_f$ (AcN) <sup>a</sup>	$\phi_f$ (TFE) <sup>a</sup>	$\phi_f$ ratio <sup>b</sup>	$\tau_s$ (AcN) <sup>c</sup>	$\tau_s$ (TFE) <sup>c</sup>	$\tau_s$ ratio <sup>b</sup>
91	0.21	0.02	12.2	6.3	< 0.5 <sup>d</sup>	> 12.6
92	0.28	0.15	1.8	7.8	4.6	1.7
93	0.15	0.02	9.6	6.9	0.9	8.1
94	0.29	0.05	6.4	3.2	0.7	4.5

a) Excitation at 295 nm, in relation to  $\phi_f = 0.0433$  for *trans*-stilbene in hexane, Reference 86.

b) AcN/TFE. c) Excitation at 295 nm, measured at fluorescence maximum. d) shorter than the time resolution of the instrument.

Table 4.17 Quenching of fluorescence quantum yields  $\phi_f$  and singlet lifetimes  $\tau_s$  by TFE for styrenes 91-94.

Compound	$\phi_f(\text{AcN})^a$	$\phi_f(\text{TFE})^a$	$\phi_f \text{ ratio}^b$	$\tau_s(\text{AcN})^c$	$\tau_s(\text{TFE})^c$	$\tau_s \text{ ratio}^b$
<i>trans</i> -96	0.27	0.20	1.4	8.7	6.6	1.3
<i>trans</i> -97	0.24	0.23	1.0	6.5	6.3	1.0
<i>trans</i> -98	0.05	0.03	1.8	2.9	2.3	1.3
<i>trans</i> -99	0.28	0.20	1.4	4.0	3.1	1.3

a) Excitation at 295 nm, in relation to  $\phi_f = 0.0433$  for *trans*-stilbene in hexane, Reference 86.

b) AcN/TFE. c) Excitation at 295 nm, measured at fluorescence maximum.

Table 4.18 Quenching of fluorescence quantum yields  $\phi_f$  and singlet lifetimes  $\tau_s$  by TFE for arylpropenes *trans*-96-99.

For those cases where both quantum yields and singlet lifetimes are available in acetonitrile and TFE, the quenching ratios determined by either method are remarkably consistent for a given substrate. Taking the stilbenes as an example, the ratios determined by fluorescence quantum yields (1.9 for *trans*-72 and 11.1 for *trans*-73) are quite close to those determined using singlet lifetimes (1.5 for *trans*-72 and 10.3 for *trans*-73). This implies that the quantum yield ratios should be reliable for those substrates possessing very short singlet lifetimes ( $<0.5$  ns). In addition, the order of quenching ratios for the methoxystilbenes *trans*-71-74 matches the order of product formation upon steady-state irradiation in TFE.

Unfortunately, the quenching ratios determined for the styrenes and arylpropenes do not match the order of reactivity from the steady state irradiations. 4-Methoxystyrene 91 reacted the *slowest* of the styrene derivatives (33% after 2 minutes of irradiation, Table 4.14) but displays the *highest* quenching ratio (12.2 by fluorescence quantum yields). In contrast, the *trans*-1-arylpropenes produced TFE adducts at quite different rates (Table 4.15), but the ratios in Table 4.18 indicate very similar quenching by TFE for all four

substrates. That the quenching ratios agree with the very low reactivity of *trans*-**97** is somewhat of a consolation.

There may be several reasons for the disagreement between the measurements of substrate reactivity in TFE (in terms of adduct formation) and the quenching of excited states by TFE. First, even if the sole quenching pathway involves a photoprotonation mechanism, the carbocation intermediate may react in some way that *does not* lead to adduct formation – deprotonation to re-form the arylalkene starting material, for example. Alternatively, TFE may interact with the excited substrates through a variety of different mechanisms, not all of which yield the solvent adducts. An example of the latter possibility was described for 1,3-dimethoxybenzene **89** in Section 4.1.3 – direct aryl photoprotonation by HFIP does involve quenching an excited state, but does not lead to product formation. In order to evaluate these issues, LFP experiments were carried out.

#### 4.2.6 LFP of Methoxy-Substituted Stilbenes *trans*-**71-74**

With hopes of directly observing the reactive intermediates involved in the photochemical addition of TFE to *trans*-**71-74**, these four substrates were subjected to excitation at 308 nm using a XeCl excimer laser. Based on the previous steady state irradiations and the fluorescence quenching experiments, the 3,5-dimethoxy substrate *trans*-**73** is the most reactive of the four compounds. Thus, initial LFP studies were directed towards this substrate. The major product detected following irradiation of *trans*-**73** in TFE (**76b-3**) would be formed *via* the phenethyl cation, rather than the alternative 3,5-dimethoxyphenethyl cation. McClelland and co-workers have previously observed the phenethyl cation following LFP of styrene in HFIP.<sup>47</sup> The transient cation was found to have an absorption maximum of 315 nm, and the rate constant for decay of

the signal was  $k_{\text{HFIP}} = 4 \times 10^5 \text{ s}^{-1}$ . Based on these data, initial efforts to detect the intermediate involved in the rapid addition of TFE to *trans*-73 were focussed at 315 nm.

A representative kinetic trace of the change in optical density ( $\Delta\text{OD}$ ) at 315 nm following 308 nm excitation of *trans*-73 in TFE is provided in Figure 4.13. The intense bleaching at this monitoring wavelength is attributed to the efficient *trans*-*cis* isomerization process. As indicated by the absorption spectra in Figure 3.3 (vide supra), the extinction coefficient of *trans*-73 is much greater than that of *cis*-73 at 315 nm. This bleaching effect, which is general to all four methoxy-substituted stilbene derivatives, greatly complicates the use of LFP for these substrates. Each sample could only be exposed to one or two laser flashes before a fresh solution was required. Clearly the substituted styrenes employed by McClelland and co-workers were much better suited to LFP studies – any isomerization would have resulted in re-formation of the starting material, and so no bleaching was observed at the detection wavelength.

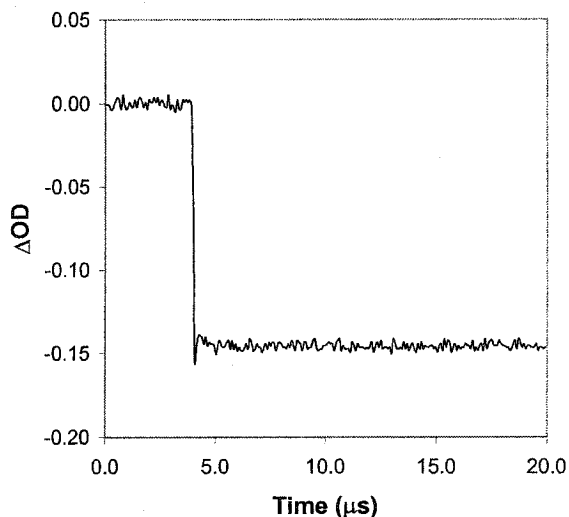


Figure 4.13 Kinetic trace at 315 nm following LFP of *trans*-73 in TFE.

The failure to observe transient cations following LFP of *trans*-73 in TFE was unfortunate, but not surprising. Indeed, the original investigations of the phenethyl cation *required* the use of HFIP as the solvent – presumably the rate constant for decay of the transient in TFE is simply too large to allow sufficient quantities of the cation for observation ( $k_{\text{TFE}} > 5 \times 10^7 \text{ s}^{-1}$ ). With HFIP as the solvent, LFP of *trans*-73 gave more promising results, as shown by the kinetic trace in Figure 4.14. The bleaching of the initial absorbance that was observed in TFE is still present, but an additional decay is observed between 1 and 3  $\mu\text{s}$ . In the range of 310 nm to 340 nm, the intensity of this transient was found to be greatest at 320 nm. Kinetic modelling of the data indicated that the first-order rate constant for decay of the transient signal is  $1.7 \times 10^6 \text{ s}^{-1}$ . As indicated by the second trace in Figure 4.14, a preliminary experiment revealed that the presence of strongly nucleophilic azide ion accelerates the decay of the transient, giving a rate constant of  $4.6 \times 10^6 \text{ s}^{-1}$ .

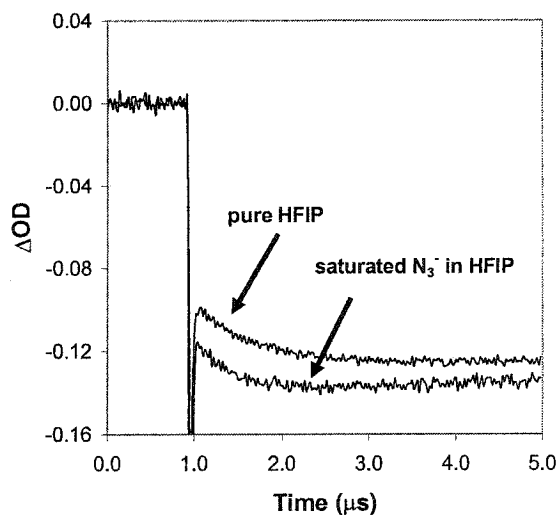


Figure 4.14 Kinetic trace at 320 nm following LFP of *trans*-73 1) in pure HFIP, and 2) in HFIP saturated with sodium azide.

Weakly absorbing transients were also observed following LFP of either *trans*-72 ( $k_{\text{HFIP}} = 1.8 \times 10^6 \text{ s}^{-1}$  at 315 nm) or *trans*-74 ( $k_{\text{HFIP}} = 6.7 \times 10^5 \text{ s}^{-1}$  at 345 nm) in HFIP solution. In contrast, *trans*-71 gave a much longer-lived transient signal, with an absorption maximum of 340 nm, Figure 4.15. Preliminary quenching studies demonstrated that the rate constant for decay of the 340 nm transient changes from  $3.5 \times 10^3 \text{ s}^{-1}$  in pure HFIP to  $1.4 \times 10^5 \text{ s}^{-1}$  in an HFIP solution saturated with sodium azide.

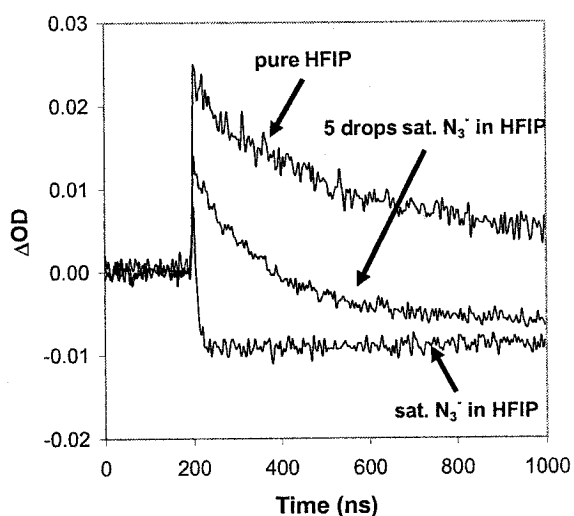


Figure 4.15 Kinetic trace at 340 nm following LFP of *trans*-71 1) in pure HFIP, 2) in HFIP with a small amount of sodium azide added, and 3) in HFIP saturated with sodium azide.

In Section 4.1.3, the ring-protonation of 1,3-dimethoxybenzene **89** in HFIP was discussed.<sup>132</sup> Because the same 1,3-dimethoxy substitution pattern is present in *trans*-73, this substrate was checked for a similar cyclohexadienyl cation by monitoring the change in optical density at 380 nm. As shown in Figure 4.16, a very weak transient signal was observed at 380 nm. However, virtually the same signal was observed when the monitoring wavelength was increased to 500 nm, and was also observed in either HFIP or TFE. These characteristics suggest that the broad signal is unlikely to be due to a



transient formed by direct ring-protonation of *trans*-73. Instead, this transient is attributed to the radical cation of *trans*-73. Majima and co-workers were able to produce this intermediate by two-photon excitation of the neutral precursor in acetonitrile solution.<sup>110</sup> The exceptionally long singlet lifetime of the substrate lends itself to such a process, and the spectrum of the transient radical cation extends to 525 nm (the spectrum is still intense at 425 nm, but the short-wavelength edge of the signal was not shown in the literature report). The intensity of irradiation employed by Majima and co-workers (200 mJ per pulse) compared to that of the current research (75 mJ per pulse) explains the low intensity of the signal in Figure 4.15. Note that, even if this assignment is correct and the radical cation of *trans*-73 is formed during the laser experiments, the formation of such an intermediate during the steady-state irradiations is quite unlikely. The light output from the lamps is much lower than that of the laser, and so radical cations are unlikely to be involved in the photochemical addition of TFE to the substituted stilbenes.

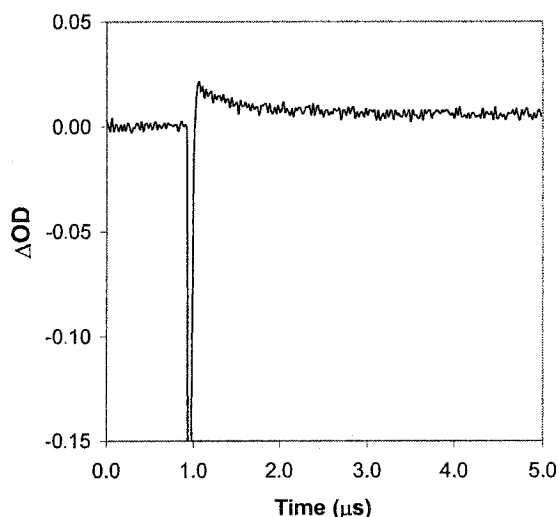


Figure 4.16 Kinetic trace at 380 nm following LFP of *trans*-73 in HFIP.

#### 4.2.7 The Photochemical Addition of Deuterated TFE to Methoxy-Substituted Aryl Alkenes and Stilbenes

The photochemical addition of methanol to *trans*-stilbene was discussed earlier in Section 3.1.3. A key aspect of the original studies by Laarhoven and co-workers<sup>81</sup> was the use of methanol-*O-d* as a probe for the mechanism of alcohol addition. In particular, the observation that deuterium is incorporated on the same carbon as the methoxy nucleophile provided good evidence for a mechanism involving carbene insertion into the O-H(D) bond of the solvent (*vide supra*, Scheme 3.2). However, the results described in the current report are consistent with a mechanism involving excited state protonation by TFE, followed by nucleophilic attack on a short-lived carbocation. In order to evaluate the possibility that carbene intermediates might be formed during the addition of TFE to the aryl alkenes, the reactivity of the substrates in TFE and TFE-OD (CF<sub>3</sub>CH<sub>2</sub>OD) was investigated.

The results obtained for the styrenes **91-94** provide a good starting-point for the current discussion – 3,5-dimethoxystyrene **93** is typical of the four methoxystyrenes. The <sup>1</sup>H NMR spectrum of the product obtained from the photochemical addition of TFE to **93** (Figure 4.17) supports the original GC-MS identification of the solvent adduct **100-3** as the major product. The quartet at 4.5 ppm (1H) and the doublet at 1.5 ppm (3H) are consistent with the A<sub>3</sub>X coupling pattern in the aliphatic side chain. The strong singlet at 3.8 ppm (6H) from the two methoxy substituents, and the signals between 7 and 6 ppm (3H) indicate that the aromatic portion of the molecule is unchanged from the starting material. The complex coupling pattern at 3.7 ppm (2H) corresponds to the methylene unit in the trifluoroethoxy side chain, in which the two protons are in a diastereotopic relationship due to the stereocenter at C1.

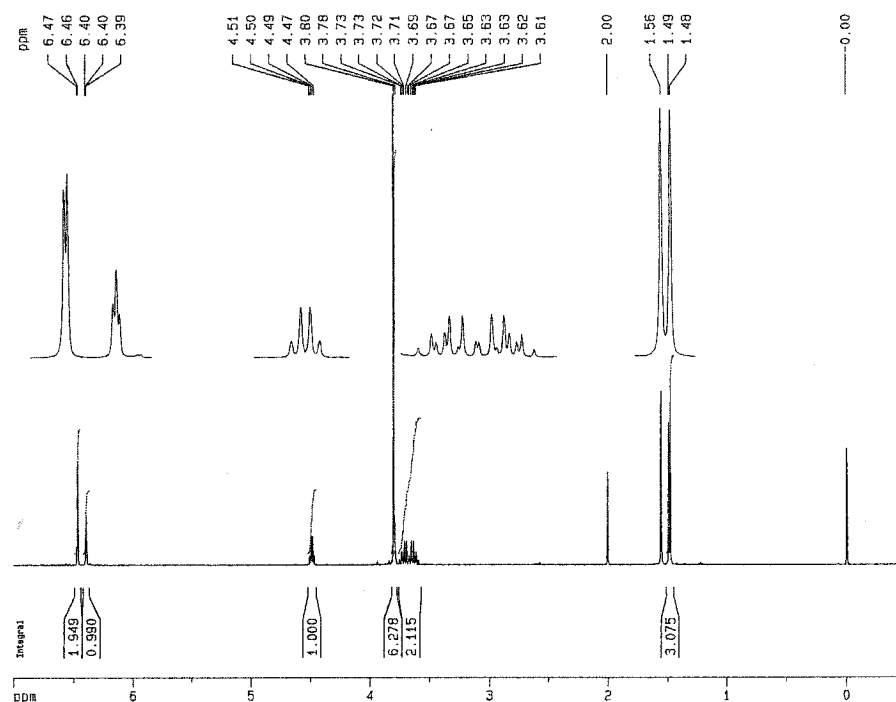


Figure 4.17  $^1\text{H}$  NMR spectrum of 1-(trifluoroethoxy)-1-(3,5-dimethoxyphenyl)ethane **100-3** following irradiation of 3,5-dimethoxystyrene **93** in TFE.

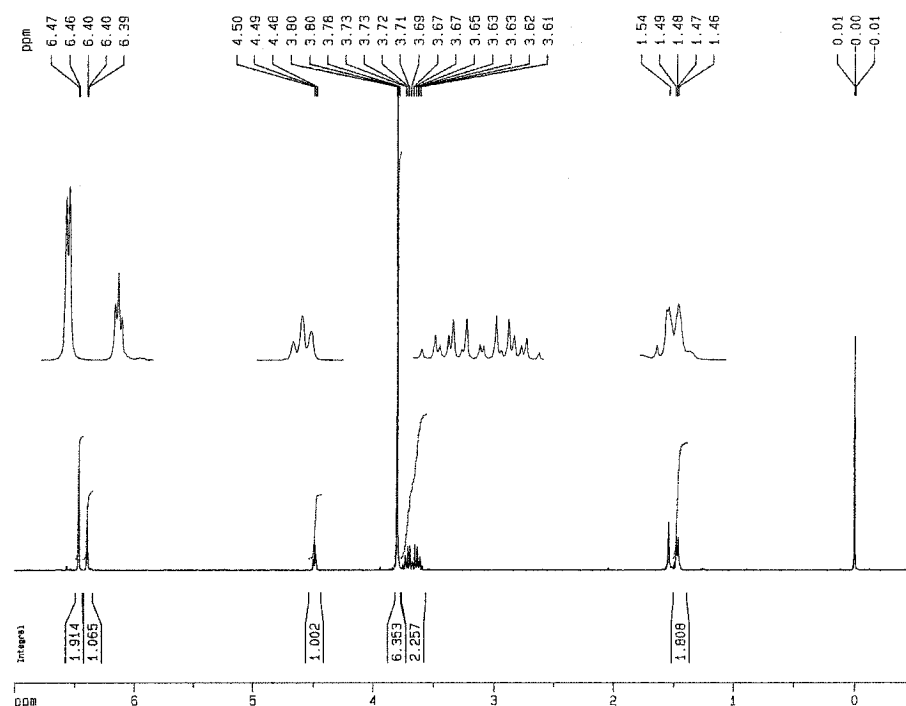


Figure 4.18  $^1\text{H}$  NMR spectrum of 1-(trifluoroethoxy)-1-(3,5-dimethoxyphenyl)-2-deuterioethane **100-3d** following irradiation of 3,5-dimethoxystyrene **93** in TFE-OD.

The  $^1\text{H}$  NMR spectrum obtained following irradiation of **93** in TFE-OD (Figure 4.18) is virtually unchanged relative to the original results, with two important exceptions. First, the signal at 4.5 ppm has been reduced in multiplicity from a quartet to a triplet. Second, the doublet at 1.5 ppm now integrates for two hydrogens instead of three. Taken together, these changes indicate deuterium incorporation at C2 but not at C1. This hypothesis is further supported by the GC-MS spectra of **100-3** and **100-3d**. Whereas the molecular ions of the products appear with  $m/z$  264 (TFE) and  $m/z$  265 (TFE-OD), the benzylic carbocations formed *via* fragmentation of either product have the identical mass,  $m/z$  249. Therefore, fragmentation results in loss of the portion of the compound where deuterium is incorporated. The  $^1\text{H}$  NMR and GC-MS results are in complete agreement with the established mechanism for the addition of TFE to substituted styrene derivatives: protonation (or deuteration) at C2, followed by attack of nucleophilic solvent on the benzylic cation at C1.

Further inspection of the results for **100-3** and **100-3d** provides even more detailed information regarding the photoprotonation of **93**. Comparison of the low-field regions in the two  $^1\text{H}$  NMR spectra (Figures 4.17 and 4.18) indicates that deuterium incorporation does not occur directly on the aromatic ring – this conclusion is consistent with the GC-MS results described in the preceeding paragraph. Furthermore, the LFP studies in HFIP (*vide supra*) found no evidence of direct aryl photoprotonation of *trans*-**73**, the stilbene with the same 3,5-dimethoxy substitution as **93**. Taken together, these results suggest that the alkene bond is the unique site of photoprotonation for these substrates.

A compilation of the  $^1\text{H}$  NMR results for the irradiations of methoxystyrenes **91-94** in TFE and TFE-OD is presented in Table 4.19. The relative integrations of  $\text{H}_\text{A}$  were calculated using the signal from  $\text{H}_\text{X}$  as a reference value of one. The data show that the

observations described above for **93** are general for the four styrene substrates: the relative integration of  $H_A$  changes from a value of three (following irradiation in TFE) to a value of two (following irradiation in TFE-OD). Again, the results corroborate the general mechanism for styrene photoprotonation.

Substrate	Product	TFE <sup>a</sup>		TFE-OD <sup>a</sup>	
		$H_X$	$H_A$	$H_X$	$H_A$
<b>91</b>	<b>100-1</b>	1	3.1	1	2.0
<b>92</b>	<b>100-2</b>	1	3.1	1	1.9
<b>93</b>	<b>100-3</b>	1	3.0	1	1.8
<b>94</b>	<b>100-4</b>	1	3.0	1	2.2

a) Integrations are relative to  $H_X = 1$ .

Table 4.19  $^1\text{H}$  NMR results for the  $A_3X$  coupling pattern of the solvent adducts following irradiation of styrenes **91-94** in TFE or TFE-OD.

A summary of the information collected using GC-MS is given in Table 4.20 for the TFE irradiations and in Table 4.21 for the TFE-OD irradiations. These data show that the molecular ions of the products from the TFE-OD experiments are all one mass unit larger than those derived from TFE. However, in all cases the benzylic fragment ions *do not* show the same increase in mass. By process of elimination, then, deuterium incorporation occurs solely at the terminal carbon (C2). The two data tables also display the relative intensities of the  $M+1$  peaks for the molecular ions and the benzylic fragment ions. In table 4.20, the percentages match the values that are expected based on the natural abundance of 1.1%  $^{13}\text{C}$  (about 11-12% for a  $\text{C}_{11}$  or  $\text{C}_{12}$  substrate). However, the same values in Table 4.21 are somewhat larger in many cases. These results may be explained by a reaction pathway involving deprotonation of the carbocation intermediate – if not all carbocations generated by photoprotonation carry on to yield the solvent

adduct **100**, then deuterated styrene may be formed in the course of the irradiation experiment. Reprotonation of the same molecule could potentially lead to solvent adducts in which more than one deuterium has been incorporated. This argument is supported by the observation that the order of secondary deuterium incorporation *increases* as the expected stability of the carbocation intermediate *decreases*. This trend is important, because it is consistent with the idea that a less stable carbocation will be less selective with regards to its mode of reactivity.

Substrate	Product	Molecular ion (m/z)	Intensity of M+1 <sup>a</sup>	Major fragment ion (m/z)	Intensity of M+1 <sup>b</sup>
<b>91</b>	<b>100-1</b>	234	11%	219	10%
<b>92</b>	<b>100-2</b>	234	11%	219	10%
<b>93</b>	<b>100-3</b>	264	12%	249	11%
<b>94</b>	<b>100-4</b>	264	13%	249	11%

a) Calculated relative to a molecular ion of 100% relative abundance.

b) Calculated relative to a benzylic fragment ion of 100% relative abundance.

Table 4.20 GC-MS data for the solvent adducts produced following irradiation of styrenes **91-94** in TFE.

Substrate	Product	Molecular ion (m/z)	Intensity of M+1 <sup>a</sup>	Major fragment ion (m/z)	Intensity of M+1 <sup>b</sup>
<b>91</b>	<b>100-1d</b>	235	15%	219	10%
<b>92</b>	<b>100-2d</b>	235	24%	219	10%
<b>93</b>	<b>100-3d</b>	265	42%	249	12%
<b>94</b>	<b>100-4d</b>	265	21%	249	12%

a) Calculated relative to a molecular ion of 100% relative abundance.

b) Calculated relative to a benzylic fragment ion of 100% relative abundance.

Table 4.21 GC-MS data for the solvent adducts produced following irradiation of styrenes **91-94** in TFE-OD.

Irradiations in TFE and TFE-OD were also performed for the *trans*-1-arylpropene derivatives *trans*-96-99. The GC-MS results for these substrates are provided in Tables 4.22 (TFE reactions) and 4.23 (TFE-OD reactions). As was the case for the styrene reactions, the molecular ions of the solvent adducts produced by irradiation of the *trans*-1-arylpropenes in TFE-OD are one mass unit larger than the same products from the TFE reactions. Comparison of the results in Tables 4.22 and 4.23 also indicates that the major benzylic fragment ions are not the most likely location of deuterium incorporation during the addition reaction – the masses of these ions are the same for a given product, irrespective of the solvent. However, the data in Table 4.23 do indicate some extra incorporation of deuterium into the products, as evidenced by larger M+1 ion intensities for the molecular ion peaks. Furthermore, the relative M+1 intensities of the molecular ions are the same as the relative M+1 intensities of the benzylic fragment ions. This implies that, in contrast to the reactions of the styrene substrates, some extra deuterium incorporation in the *trans*-1-arylpropene photoproducts *does* occur in the portion of the product that becomes the benzylic fragment ion. The most likely position for such deuterium incorporation is at C1, and so these substrates may actually react through pathways other than photoprotonation. Unfortunately, the reaction mixtures obtained from the *trans*-1-arylpropene derivatives are not as clean as those of the methoxystyrenes, and so analysis of the solvent adducts by  $^1\text{H}$  NMR spectroscopy is much more difficult. Another factor that complicates the NMR analysis of these substrates is the additional coupling interaction of the terminal methyl group. Although future efforts may allow confident analysis of the *trans*-1-arylpropene photoproducts by  $^1\text{H}$  NMR spectroscopy, this was not the case at the time of this writing.

Substrate	Product	Molecular ion (m/z)	Intensity of M+1 <sup>a</sup>	Major fragment ion (m/z)	Intensity of M+1 <sup>b</sup>
<i>trans</i> -96	<b>101-6</b>	248	12%	219	10%
<i>trans</i> -97	<b>101-7</b>	248	10%	219	10%
<i>trans</i> -98	<b>101-8</b>	278	14%	249	15%
<i>trans</i> -99	<b>101-9</b>	278	13%	249	13%

a) Calculated relative to a molecular ion of 100% relative abundance.

b) Calculated relative to a benzylic fragment ion of 100% relative abundance.

Table 4.22 GC-MS data for the solvent adducts produced following irradiation of arylpropenes *trans*-96-99 in TFE.

Substrate	Product	Molecular ion (m/z)	Intensity of M+1 <sup>a</sup>	Major fragment ion (m/z)	Intensity of M+1 <sup>b</sup>
<i>trans</i> -96	<b>101-6d</b>	249	14%	219	11%
<i>trans</i> -97	<b>101-7d</b>	249	21%	219	23%
<i>trans</i> -98	<b>101-8d</b>	279	17%	249	16%
<i>trans</i> -99	<b>101-9d</b>	279	18%	249	16%

a) Calculated relative to a molecular ion of 100% relative abundance.

b) Calculated relative to a benzylic fragment ion of 100% relative abundance.

Table 4.23 GC-MS data for the solvent adducts produced following irradiation of arylpropenes *trans*-96-99 in TFE-OD.

The irradiations of the methoxy-substituted stilbenes *trans*-60 and *trans*-71-74 in TFE and TFE-OD provided a great deal of information regarding the mechanism of the addition reactions. The GC-MS results from the irradiations of the five stilbenes in TFE and TFE-OD were consistent with the important aspects of the reactions of the styrenes and *trans*-1-arylpropenes. In particular, the incorporation of deuterium occurs on the carbon that does not bear the trifluoroethoxy substituent – this is shown by masses of the major benzylic fragment ions (and their M+1 peaks), which are the same for the products



following irradiation in either TFE or TFE-OD. Unfortunately, fragmentation to give these ions is so favourable that the M+1 peaks for the molecular ions are too weak to be observed, and so a complete analysis of deuterium incorporation by GC-MS was not possible. However, careful analysis of the 500 MHz  $^1\text{H}$  NMR spectra of the stilbene reaction mixtures provided substantial information regarding the photoaddition mechanism. These results are summarized in Table 4.24 – complete analysis details are provided in Chapter 6, but the following discussion provides a good overall picture of the rationale involved.

Substrate	Product	TFE <sup>a,b</sup>			TFE-OD <sup>b,c</sup>			% insertion <sup>d</sup>	% anti	% syn
		H <sub>X</sub>	H <sub>B</sub>	H <sub>A</sub>	H <sub>X</sub>	H <sub>B</sub>	H <sub>A</sub>			
<i>trans</i> -60	<b>75a-0</b>	1	1.05	1.08	1	0.60	1.04	39	22	39
<i>trans</i> -60	<b>75b-0</b>	1	1.04	1.10	1	0.36	0.78	12	28	60
<i>trans</i> -71	<b>75b-1</b>	1	1.03	1.06	1	0.46	0.51	0	47	53
<i>trans</i> -72	<b>76b-2</b>	1	1.06	1.13	1	0.31	0.76	6	27	67
<i>trans</i> -73	<b>76b-3</b>	1	0.96	1.04	1	0.27	0.75	2	26	73
<i>trans</i> -74	<b>75b-4</b>	1	0.68	0.65	1 <sup>e</sup>	0.23	0.30	0 <sup>e</sup>	43	57
<i>trans</i> -74	<b>76b-4</b>		0.42	0.47		0.16	0.32		33	67

a) In methanol for product **75a-0**. b) Integrations are relative to H<sub>X</sub> = 1. c) In methanol-*O-d* for product **75a-0**.

d) Highest possible percentage of insertion mechanism, see text. e) The two products from irradiation of *trans*-74 display overlapping H<sub>X</sub> signals, so the percentage of carbene insertion product cannot be determined.

Table 4.24 Summary of the  $^1\text{H}$  NMR spectra of the products derived from irradiation of the stilbenes *trans*-60 and *trans*-71-74 in TFE and TFE-OD.

The results for the unsubstituted substrate (*trans*-60) in TFE and TFE-OD provide a good example for discussion; these data are given in the second row of Table 4.24. The product from this reaction (the solvent adduct **75b-0**) possesses three chemically distinct protons: H<sub>X</sub>, H<sub>B</sub>, and H<sub>A</sub>. Figure 4.19 displays a Neuman projection of the preferred conformation for the compound, where the two large phenyl rings have a dihedral angle of 180°. Also provided are the chemical shifts and coupling constants for the three

protons, as well as the relevant portions of the  $^1\text{H}$  NMR spectra for the product formed by irradiation in either TFE or TFE-OD.

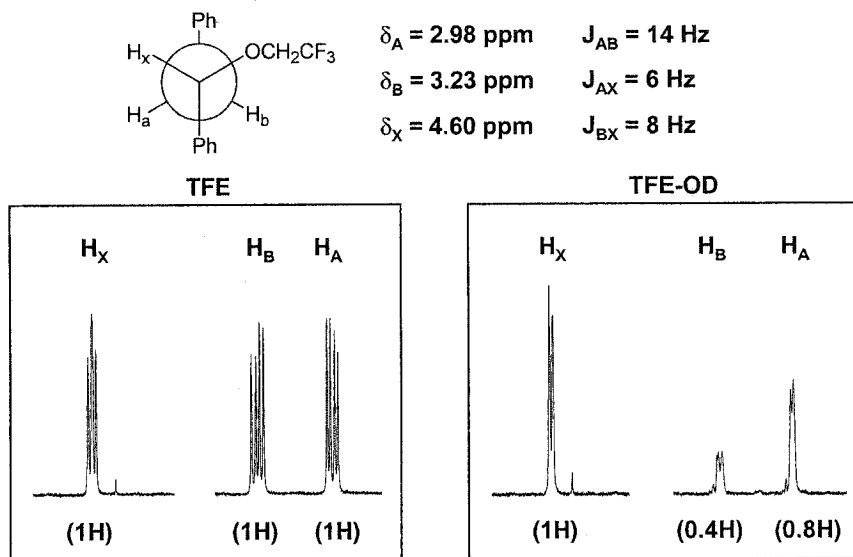


Figure 4.19 Neuman projection for photoproduct **75b-0**, and analysis of the ABX coupling pattern following irradiation in TFE or TFE-OD.

The  $^1\text{H}$  NMR spectrum for **75b-0** is a good example of an ABX coupling pattern. The presence of the electron-withdrawing oxygen moves the signal for  $\text{H}_x$  to a much lower frequency than either  $\text{H}_B$  or  $\text{H}_A$ . The two latter protons are diastereotopic, and therefore present slightly different chemical shifts. Coupling between all three protons is observed, and the coupling constants are consistent with the conformation shown. All of the chemical shifts and coupling constants that were determined through the course of this work were consistent with previous  $^1\text{H}$  NMR studies of 1,2-diphenylethanol by Kingsbury and Thornton.<sup>136</sup> The product from the TFE irradiation gives the expected 1:1:1 ratio for the integrations of the three protons.

Following irradiation in TFE-OD, the  $^1\text{H}$  NMR spectrum of **75b-0** is significantly modified. The signals of all three protons are reduced to doublets, and the integrations

are altered as well. These changes indicate that incorporation of deuterium does occur, but also that the location of incorporation is not always the same. As was discussed in Section 3.1.3 for the addition of methanol-*O-d* to styrene, any one of the three protons in **75b-0** could be "replaced" by deuterium. The three isomers for deuterated **75b-0** are shown in Figure 4.20.

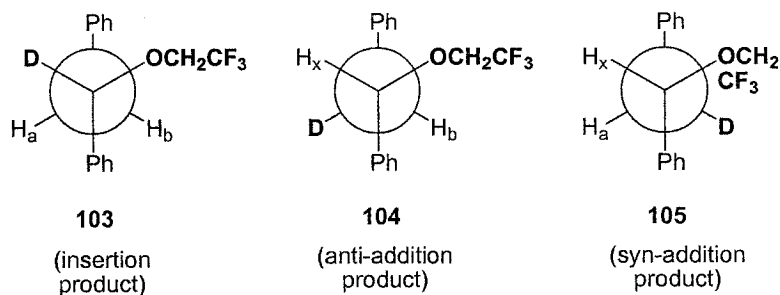


Figure 4.20 The three possible isomers of **75b-0** that may be formed by addition of TFE-OD to stilbene (*trans*-**60**).

In mechanistic terms, **103** is the product that would result from a rearrangement-carbene insertion mechanism, while **104** and **105** represent either anti or syn addition of TFE-OD across the alkene bond of the *trans* isomer. That the experimentally-determined integration of  $H_A$  (0.8H) is larger than that of  $H_B$  (0.4H) indicates a preference for syn addition, *i.e.*, the ratio between the integrations of  $H_A$  and  $H_B$  provides a numerical measurement of the more favoured mechanism. However, the relative amount of **103** is more difficult to assess. For all of the reactions that have been investigated by  $^1\text{H}$  NMR, the integrations of  $H_A$  and  $H_B$  have been determined by setting the integration of  $H_X$  equal to one. In the case that **103** is formed to some extent, then the integrations will be in error. In order to compensate for this problem, the assumption has been made that the total integration of the three protons in the deuterated product should equal two. A total integration greater than two indicates that the intensity of  $H_X$  (the reference) has been

overestimated, and that **103** actually is formed during the reaction. Using this rationale, the relative importance of carbene insertion, anti addition, and syn addition products have been calculated for all reactions, and the values are compiled in Table 4.24. The somewhat indirect method of determining the amount of carbene insertion product means that the relative importance of this pathway may in fact be overestimated – the values in Table 4.24 are therefore best viewed as upper limits for the insertion mechanism.

The first entry in Table 4.24 shows the data from the reaction of *trans*-stilbene in methanol and methanol-*O-d*, the very same reaction studied by Laarhoven and co-workers in their original study.<sup>81</sup> The spectra obtained from this reaction were easily the most difficult to analyse of all the experiments – the very low yield of the solvent adduct and the overlapping signal from product **78-0** (bibenzyl) makes the reliable integration of the important peaks quite problematic. In spite of these difficulties, the calculated percentages of the three reaction pathways (39% insertion, 22% anti addition, 39% syn addition) are in fact very close to the values of Laarhoven and co-workers (47% insertion, 24% anti addition, 29% syn addition). The reasonable agreement between these results is an excellent vote of confidence for the measurements reported in the current work, especially given the fact that the spectra obtained for the TFE/TFE-OD irradiations are far superior to those from the methanol reactions.

The results for the irradiations in TFE-OD support all aspects of the likely mechanism for addition of the solvent to the substituted stilbene derivatives. The relative importance of the carbene insertion reaction is much lower for the unsubstituted *trans*-**60** in TFE-OD (12%) than in methanol-*O-d* (39%). The calculated amount of carbene insertion product is even less for the methoxy-substituted compounds *trans*-**71-74** (6-0%), and is probably within the error involved with determining accurate integrations for the

three peaks. Therefore, the carbene insertion mechanism appears to be of lesser importance in TFE solution. This solvent dependence may be attributed to the ability of TFE to act as a photoprotonation reagent, and thereby react with an excited substrate prior to the 1,2-hydride shift that initiates the carbene insertion mechanism. The relationship between the relative amounts of syn and anti addition products and the position of the methoxy substituent is also very interesting. In particular, the relative amount of syn addition is lower for the substrates possessing para methoxy substituents compared to those with meta methoxy substituents. For example, syn = 53% for *trans*-**71** (4-methoxy) and 73% for *trans*-**73** (3,5-dimethoxy). Importantly, *trans*-**74** yields two products with *different* amounts of syn addition: 57% for **75b-4** and 67% for **76b-4**. These apparent substituent effects provide compelling evidence for the mechanism of TFE addition to these substrates, as will be described in Section 4.3.

A final note regarding the experiments involving TFE and TFE-OD is that the conversion of starting material to product was significantly slower when the deuterated solvent was used. This isotope effect was observed for all substrates investigated, and the effect varied depending on the position of the methoxy substituent and the type of chromophore. Unfortunately, the solutions employed for the reactions in TFE-OD were quite small (5 mL), so not many samples were taken for GC analysis. Thus, a rigorous examination of the difference in reactivity is difficult. Nevertheless, the ratio between the percent conversion of starting material for two samples taken after the same time of irradiation in TFE and TFE-OD does provide an estimate of the effect. These values are provided in Table 4.25 for all thirteen substrates. That all substrates show  $k_H/k_D > 1$  supports the claim that all of the TFE addition reactions involve protonation as the initial step in the reaction.

Stilbene	Time (min.) <sup>a</sup>	$k_H/k_D$ <sup>b</sup>	Styrene	Time (min.) <sup>a</sup>	$k_H/k_D$ <sup>b</sup>	Arylpropene	Time (min.) <sup>a</sup>	$k_H/k_D$ <sup>b</sup>
<i>trans</i> -60	60	1.3						
<i>trans</i> -71	60	2.1	91	10	3.2	<i>trans</i> -96	30	2.2
<i>trans</i> -72	30	1.7	92	10	2.7	<i>trans</i> -97	60	3.7
<i>trans</i> -73	10	1.2	93	5	1.5	<i>trans</i> -98	30	2.8
<i>trans</i> -74	30	2.1	94	5	2.0	<i>trans</i> -99	30	1.2

a) Time of irradiation in TFE or TFE-OD. B) Ratio of percent conversion in TFE to percent conversion in TFE-OD.

Table 4.25 Estimates of the solvent isotope effect  $k_H/k_D$  for irradiations of the stilbenes, styrenes, and *trans*-1-arylpropenes in TFE and TFE-OD.

## 4.3 Discussion of Results

### 4.3.1 Summary of Chapter 4 Experiments

A large number of different experiments (and a great many compounds) have been investigated in Section 4.2. Prior to a detailed discussion of the mechanistic information that has been gained from this work, this section will provide a brief summary of the salient features of the experiments described above. Recall that the main goal of these studies was to provide a more complete picture of the mechanism for the TFE addition reactions that were first investigated for five methoxy-substituted *trans*-stilbene derivatives in Chapter 3. A key factor in these reactions is clearly the position of the methoxy substituents, and their influence on the underlying photophysical properties of the stilbene chromophore. While the photochemical addition of alcohols to substituted stilbene derivatives has only been reported in a few publications,<sup>81,97,107</sup> investigations of similar reactions for substituted styrenes have been extensively studied in aqueous media,<sup>124</sup> and the presence of carbocation intermediates in these reactions has been confirmed by LFP in TFE and HFIP solutions.<sup>47</sup> Therefore, a comparison of the

photophysical properties of similarly-substituted stilbenes and styrenes seemed useful for a better understanding of 1) the addition of alcohols to the stilbene derivatives, and 2) the effect of changing substituent position. The *trans*-1-arylpropene derivatives were included in the study so as to determine whether the ability of the methoxy substituent to influence the isomerization efficiencies of arylalkenes is a general effect for arylalkenes.

Preliminary characterization of the photophysical properties of the methoxy-substituted styrenes (**91-94**) and *trans*-arylpropenes (*trans*-**96-99**) provided values that were consistent with literature precedent (Section 4.2.2). Unfortunately, the unsubstituted compounds (styrene **90** and *trans*-1-phenylpropene *trans*-**95**) do not absorb significantly at 300 nm, so a direct comparison of their properties with those of the stilbene derivatives could not be carried out. In general, the photophysical properties ( $\lambda_{\text{max}}$ ,  $\tau_s$ ,  $\phi_f$ ) of the styrenes and arylpropenes are quite uniform, in that a value for a given styrene is similar to the value of the *trans*-1-arylpropene with the same methoxy substituents. In comparison to the stilbene derivatives, the new compounds have shorter wavelength fluorescence maxima ( $\approx 300\text{-}350$  nm), longer singlet lifetimes ( $\approx 1\text{-}9$  ns), and larger fluorescence quantum yields ( $\approx 0.1\text{-}0.35$ ). Also, the *trans*-1-arylpropenes display much smaller isomerization quantum yields ( $\approx 0.03\text{-}0.14$ ) than do the substituted stilbenes. In addition, the properties of the styrenes and *trans*-1-arylpropenes in cyclohexane solution are only slightly different from those in acetonitrile (Section 4.2.3). In most cases the use of a more polar solvent induces small increases in  $\lambda_{\text{max}}$  (fluor) and  $\phi_{\text{tc}}$ , along with small decreases in  $\phi_f$  (the values of  $\tau_s$  are generally unchanged). One interesting observation is that the two 3,5-dimethoxy substrates (**93** and *trans*-**98**) display unusually small values of  $\phi_f$  and  $\tau_s$  relative to the other substrates.

Section 4.2.3 also investigated the effects of solvent polarity on the photophysical properties of the five stilbene derivatives. Analysis of the fluorescence maxima of the substrates in a series of six solvents allowed calculation of the dipole moment of the emitting state,  $\mu_e$ . In all cases, these values were greater than those obtained by Gaussian calculations of the excited states at the same geometries as the optimized ground states. Most of the substituted stilbenes also displayed significant decreases in  $\phi_f$  and increases in  $\phi_{tc}$  upon changing to progressively more polar solvents, but the results for the 3,5-dimethoxy substrate *trans*-**73** were quite different. This compound, for which an excited state dipole moment of 13.2 D was determined, showed significant increases in  $\phi_f$  and  $\tau_s$  in more polar solvents. In addition, the best fit of the fluorescence decay of *trans*-**73** was found by using a biexponential decay model.

The irradiations of the methoxy-substituted styrenes and *trans*-1-arylpropenes in TFE were presented in Section 4.2.4. All four styrenes reacted very quickly, providing the Markovnikov solvent adduct **100** in greater than 90% yield for all cases. The *trans*-1-arylpropenes gave the corresponding solvent adduct **101** at a slower rate, apparently due to the competitive trans-cis isomerization process. Small amounts of the anti-Markovnikov product **102** was observed during the irradiation of *trans*-**97** and *trans*-**99**. Surprisingly, the relative order of reactivity determined in the steady state irradiations of the methoxy-substituted *trans*-stilbenes, styrenes, and *trans*-1-arylpropenes in TFE did not match the order of reactivity that was determined by fluorescence quenching experiments (Section 4.2.5).

Preliminary LFP experiments were performed in the hopes of identifying transient carbocation intermediates derived from the methoxy-substituted stilbenes *trans*-**71-74**



(Section 4.2.6). The intense bleaching of the initial absorption (due to photochemical trans-cis isomerization) makes these experiments more challenging than for the corresponding styrene derivatives. Although transient species were not observed in TFE, the use of HFIP provided signals at the appropriate wavelengths for the expected carbocations. Quenching of the transients derived from *trans*-71 and *trans*-73 was observed following addition of the strongly nucleophilic azide ion. In addition, efforts to observe the cyclohexadienyl cation formed by direct aryl photoprotonation of *trans*-73 were negative.

Section 4.2.7 employed GC-MS and  $^1\text{H}$  NMR to analyze reaction mixtures following irradiation of the substrates in both TFE and TFE-OD. The GC-MS results indicated that, in all cases, incorporation of deuterium occurs preferentially at the carbon that does not include the trifluoroethoxy group. A small amount of secondary deuterium incorporation was detected for the styrene derivatives, presumably due to a protonation/deprotonation sequence that provides a pathway for deuteration of the starting material.  $^1\text{H}$  NMR analysis of the products from the styrene reactions added further support for the location of deuterium incorporation. The  $^1\text{H}$  NMR spectra of the stilbene reaction mixtures were even more informative. The carbene insertion mechanism, which has been reported in the literature as the major pathway for addition of methanol to stilbene,<sup>81</sup> was found to be much less important in TFE. Furthermore, the data provided relative amounts of syn and anti addition of the trifluoroethoxy nucleophile and deuterium to the alkene bond. Finally, a preference for syn addition was observed for the products derived from the meta methoxy stilbenes.

#### 4.3.2 Photophysical Properties of Methoxy-Substituted Arylalkenes

The preferred deactivation pathway for excited state *trans*-stilbene is trans-cis isomerization. However, the typical quantum yield for this process (0.40 in cyclohexane) is actually misleading with respect to the importance of this pathway relative to other deactivation processes. Recall from the discussion in Section 3.1.1 that isomerization involves the excited state of the trans isomer  $t_{S1}$  moving through activated bond torsion, and reaching a perpendicular geometry  $p_{S1}$ . Internal conversion allows decay of  $p_{S1}$  to  $p_{S0}$  on the ground state surface. Most researchers make the assumption that approximately half of the  $p_{S0}$  population provides  $c_{S0}$  (net trans-cis isomerization) and the other half provides  $t_{S0}$  (net reformation of trans starting material).<sup>82</sup> In other words, the quantum yield for deactivation of  $t_{S1}$  by *bond torsion* is actually  $\phi_{tc} \times 2 = 0.80$ . In comparison, the other modes for deactivation of  $t_{S1}$  are much lower ( $\phi_f = 0.04$ ,  $\phi_{isc} = 0.002$ ).<sup>93,87</sup>

Analysis of the temperature dependence of  $\phi_{tc}$ ,  $\phi_f$ , and  $\tau_s$  for *trans*-stilbene in alkane solvents provided a value of 3.5 kcal/mol for the barrier involved in the  $t_{S1} \rightarrow p_{S1}$  bond torsion process.<sup>82</sup> This barrier is inferred to be polarizable, based on the observation that this barrier is somewhat lower in polar nitrile solvents (2.4 kcal/mol).<sup>91</sup> As a result of this change in the height of the barrier, *trans*-stilbene in acetonitrile solution displays a larger quantum yield of isomerization ( $\phi_{tc} = 0.45$ ) and a smaller quantum yield of fluorescence ( $\phi_f = 0.02$ ).<sup>92</sup>

The height of the thermal barrier for excited state bond torsion was also found to be the determining factor in the photophysical properties of *trans*-aminostilbenes. Lewis and co-workers calculated a lower limit for the barrier of *trans*-3-aminostilbene (*trans*-**63**) as 7.5 kcal/mol – the unusually high barrier endows this substrate with a very low quantum

yield of isomerization ( $\phi_{tc} = 0.09$ ) and a very high quantum yield of fluorescence ( $\phi_f = 0.78$ ) in cyclohexane solution.<sup>98</sup> However, the effect of solvent polarity on the photophysics of *trans*-**63** is the same as for *trans*-stilbene itself; in acetonitrile, the quantum yield of isomerization for *trans*-**63** is increased ( $\phi_{tc} = 0.23$ ) and the quantum yield of fluorescence is reduced ( $\phi_f = 0.40$ ).

The results obtained through the course of the current work indicate that methoxy substituents also play a critical role in altering the height of the barrier for excited state bond torsion, and in turn the photophysical properties, of the *trans*-stilbene chromophore. A comparison between the photophysical properties of the 4-methoxy substrate (*trans*-**71**) and the 3-methoxy substrate (*trans*-**72**) is quite informative. In cyclohexane solution, *trans*-**71** displays photophysical properties ( $\phi_{tc} = 0.39$ ,  $\phi_f = 0.02$ ) that are quite similar to those of unsubstituted *trans*-stilbene. Furthermore, these properties change in the expected ways when a polar solvent such as acetonitrile is employed ( $\phi_{tc} = 0.53$ ,  $\phi_f = 0.006$ ). The meta methoxy substrate *trans*-**72** displays quantum yields of isomerization ( $\phi_{tc} = 0.32$  in cyclohexane,  $0.39$  in acetonitrile) that are slightly lower than those of the para methoxy substrate in either solvent. More surprising, however, is the observation that *trans*-**72** displays a very large quantum yield of fluorescence ( $\phi_f = 0.16$ ) and a long singlet lifetime ( $\tau_s = 0.7$  ns). Furthermore, these values are largely unaffected by solvent polarity. The unusual properties of *trans*-**72** indicate that methoxy substituents are capable of a meta effect that is similar to that of the amino substituents. As a result of this effect, the barrier for  $t_{S1} \rightarrow p_{S1}$  process is larger for *trans*-**72** than for either *trans*-stilbene or *trans*-**71**. Unfortunately, the exact height of the barrier for *trans*-**72** cannot be determined without additional measurements. However, the very large effect of the meta

amino substituent on the quantum yield of isomerization for *trans*-**63** ( $\phi_{tc} = 0.09$ )<sup>98</sup> likely indicates that the barrier for this substrate (estimated as 7.5 kcal/mol) is significantly larger than that of *trans*-**72**. The observation of solvent-independent properties for the meta methoxy substrate is intriguing in comparison to the properties of the meta amino substrate, where the properties undergo significant changes with solvent polarity. A possible explanation for these differences may lie in the experimentally determined excited state dipole moments ( $\mu_e = 11.9$  D for *trans*-**63**,<sup>98</sup>  $\mu_e = 3.2$  D for *trans*-**72**). Assuming that similar differences in polarization may exist for the excited state torsional barriers of these two substrates, solvent polarity should have a greater effect on the barrier for *trans*-**63**.

The 3,4-dimethoxy substrate (*trans*-**74**) appears to be more similar to *trans*-**71** than to *trans*-**72**. The effects of solvent polarity on  $\phi_{tc}$  (0.41 in cyclohexane, 0.59 in acetonitrile) and on  $\phi_f$  (0.05 in cyclohexane, 0.03 in acetonitrile) for this substrate more closely resemble those of the para methoxy substrate. The calculated excited state dipole moment of *trans*-**74** ( $\mu_e = 8.7$  D) is higher than that of either *trans*-**71** ( $\mu_e = 6.8$  D) or *trans*-**72** ( $\mu_e = 3.2$  D). An intriguing trend is shown by the compilation of data in Table 4.26: those substrates which display the *highest* excited state dipole moments  $\mu_e$  also give the *largest increases* in  $\phi_{tc}$  upon changing from non-polar cyclohexane to polar acetonitrile. This trend supports the somewhat naïve hypothesis given above that substrates with larger excited state dipoles should also possess more polarizable torsional barriers. As shown in Figure 4.21, the plot of the difference in the isomerization quantum yields *versus*  $\mu_e$  is linear, with a surprisingly high correlation coefficient of  $r^2 = 0.961$  (removing *trans*-**60** from the data set further improves the correlation to  $r^2 = 0.997$ ).

Although the exact mathematical relationship that governs this correlation is not yet clear, the data do suggest that  $\mu_e$  does dictate the influence of solvent on the isomerization process.

Compound	$\mu_e$ (D) <sup>a</sup>	$\phi_{tc}$ (Cyc) <sup>b</sup>	$\phi_{tc}$ (AcN) <sup>b</sup>	$\phi_{tc}$ (AcN) - $\phi_{tc}$ (Cyc)
<i>trans</i> - <b>60</b>	0	0.40	0.45	0.05
<i>trans</i> - <b>71</b>	6.8	0.39	0.53	0.14
<i>trans</i> - <b>72</b>	3.2	0.32	0.39	0.07
<i>trans</i> - <b>74</b>	8.7	0.41	0.59	0.18
<i>trans</i> - <b>73</b>	13.2	0.29	0.28	0.00

a) Calculated based on solvatochromic data, see Table 4.9. b) Relative to  $\phi_{tc} = 0.40$  for *trans*-stilbene in cyclohexane, Reference 108.

Table 4.26 Excited state dipole moments  $\mu_e$  and the quantum yields of isomerization  $\phi_{tc}$  for the methoxy-substituted *trans*-stilbene derivatives in cyclohexane (Cyc) or acetonitrile (AcN).

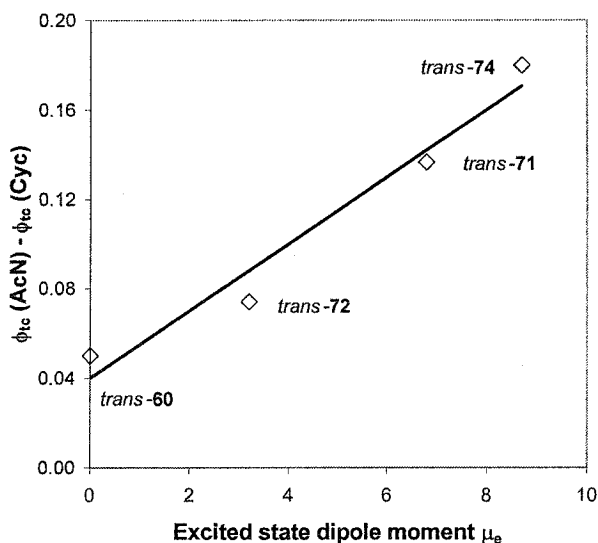


Figure 4.21 Plot of the difference between isomerization quantum yields  $\phi_{tc}$  in acetonitrile and cyclohexane versus the excited state dipole moment  $\mu_e$  for *trans*-60, *trans*-71, *trans*-72, and *trans*-74.

The one caveat in the data analysis discussed above is that the 3,5-dimethoxy substrate *trans*-73, which behaves differently in almost all respects from the other stilbenes, has not been included in Figure 4.21. Although this substrate has the highest dipole moment of the five compounds ( $\mu_e = 13.2$  D), the quantum yield of isomerization is the same in cyclohexane or acetonitrile ( $\phi_{ic} = 0.28$ ). Furthermore, the excited state of *trans*-73 becomes more fluorescent in polar solvents ( $\phi_f = 0.17$  in cyclohexane, 0.32 in acetonitrile). The observed biexponential fluorescence decay is also unique to *trans*-73. Given these very different results, the failure of *trans*-73 to fit the trend in Figure 4.21 is not surprising. The very large values of  $\mu_e$ ,  $\phi_f$ , and  $\tau_s$  that have been measured for *trans*-73 are characteristics that have been observed for compounds that possess charge transfer excited states. A more thorough discussion of the photophysical properties *trans*-73 (and those of several related derivatives) will be presented in Chapter 5.

Some discussion of the photophysical properties of the methoxy-substituted styrenes and *trans*-1-arylpropenes is also required. Lewis and co-workers have determined the barriers for excited state bond torsion of styrene (6.6 kcal/mol in methylcyclohexane)<sup>135</sup> and *trans*-1-phenylpropene (8.8 kcal/mol in hexane, 8.0 kcal/mol in acetonitrile).<sup>133</sup> The larger barriers for excited state bond torsion in these substrates decrease the importance of the singlet state as the route for excited state isomerization (compared to *trans*-stilbene). Instead, isomerization occurs to a large extent by intersystem crossing to the triplet state ( $t_{S1} \rightarrow t_{T1}$ ), followed by barrierless bond torsion ( $t_{T1} \rightarrow p_{T1}$ ). Although the rate constants of intersystem crossing for *trans*-stilbene ( $k_{isc} = 3.9 \times 10^7 \text{ s}^{-1}$ )<sup>82</sup> and *trans*-1-phenylpropene ( $k_{isc} = 4.7 \times 10^7 \text{ s}^{-1}$ )<sup>133</sup> are very similar, the

much larger barrier for bond rotation in *trans*-1-phenylpropene makes intersystem crossing the major decay pathway for this compound ( $\phi_{isc} = 0.60$ ).

The effects of various aryl substituents on the photophysical properties of the *trans*-arylpropenes have also been determined. The presence of either electron donating or electron withdrawing substituents appears to lower the barrier, particularly in polar solvents; *trans*-1-(4-methoxyphenyl)propene (5.6 kcal/mol in hexane, 4.2 kcal/mol in acetonitrile) and *trans*-1-(4-cyanophenyl)propene (5.6 kcal/mol in hexane, 2.6 kcal/mol in acetonitrile) are representative examples.<sup>133</sup> In addition, the relative importance of the singlet isomerization pathway increases as the temperature is raised. To the best of my knowledge, the effects of substituents on the photophysical properties of the styrene chromophore have not been reported.

The photophysical measurements involving the methoxy-substituted styrenes and *trans*-1-arylpropenes are consistent with most aspects of the literature results described in the preceeding paragraphs. As a result of the larger torsional barriers that these substrates should possess, the singlet lifetimes, quantum yields of fluorescence, and quantum yields of isomerization are more uniform than those of the stilbene derivatives. In general, these substrates display longer singlet lifetimes, larger quantum yields of fluorescence, and (in the case of the *trans*-1-arylpropenes) smaller quantum yields of isomerization. The minimal effect of solvent polarity on these properties is another consequence of the larger barriers for excited state bond torsion.

One interesting observation that is not explained by the literature data is the unusually low quantum yields of fluorescence for the 3,5-dimethoxy substrates (**93** and *trans*-**98**). For the arylpropenes, most substrates displayed quite strong fluorescence in

either hexanes or acetonitrile ( $0.35 \geq \phi_f \geq 0.24$ ) except for *trans*-**98** ( $\phi_f = 0.05$ ). This large difference is particularly intriguing, given that the 3,5-dimethoxy substrate in the stilbene series (*trans*-**73**) displayed the *highest* quantum yield of fluorescence ( $\phi_f = 0.32$ ) of those five substrates. In addition to the low fluorescence displayed by *trans*-**98**, the substrate also gives the smallest isomerization quantum yield of the *trans*-1-arylpropenes. Taken together, these observations may imply that the 3,5-dimethoxy system undergoes a deactivation process that results in return to the ground state for the styrene and arylpropene systems, but instead forms a highly fluorescent excited state in the presence of a second phenyl ring (*i.e.*, in the stilbene system). Unfortunately, these ideas are little more than speculation given the available data.

#### 4.3.3 The Mechanism of the TFE Addition Reactions

In TFE solution, the methoxy-substituted styrenes react *via* protonation of the excited singlet states to yield carbocation intermediates – this mechanism is already quite well established based on the LFP studies by McClelland and co-workers.<sup>47</sup> The differences in the relative reactivity of the four styrenes investigated in this work (**91**-**94**) are actually quite small, and all of them are completely consumed within ten minutes of irradiation in TFE. Given the similar rates of product formation, the very different susceptibilities of the excited states towards quenching by TFE was somewhat surprising. In particular, although the percent conversion values after two minutes in TFE are 33% for **91** (4-methoxy) and 57% for **92** (3-methoxy), the quenching of fluorescence is much larger for **91** ( $\phi_f(\text{AcN}) / \phi_f(\text{TFE}) = 12$ ) than for **92** ( $\phi_f(\text{AcN}) / \phi_f(\text{TFE}) = 2$ ). These results imply that either 1) the quenching of **91** occurs by some mechanism that does not involve photoprotonation, or 2) the carbocation derived from **91** may not always carry on



to give the solvent adduct **100-1**. Several arguments against the latter possibility may be advanced. The LFP studies by McClelland and co-workers have shown that, upon 248 nm LFP of 4-methoxystyrene (**91**), the bleaching of the styrene (below 300 nm) does not return to baseline.<sup>47</sup> In other words, deprotonation of the transient carbocation to reform the starting styrene does not occur to any great extent for the 4-methoxy substrate. Indeed, the GC-MS analysis of the products formed by photochemical addition of TFE-OD to the substrates (*vide supra*, Tables 4.20 and 4.21) indicated that although some deprotonation of the carbocation intermediates may occur, this reaction is actually more favourable for the meta methoxy substrates. In light of these results, the efficient quenching of the excited state of **91** is attributed to a pathway that *does not* involve photoprotonation. Similar quenching mechanisms may exist for the other substrates (styrenes, *trans*-1-arylpropenes, or *trans*-stilbenes), so the ratios in Tables 4.16-18 are probably less useful than was originally hoped.

With the exception of the very unreactive *trans*-**97**, the percent conversions of the *trans*-1-arylpropenes in TFE are even less varied than the methoxystyrenes. An important observation is that the *trans*-1-arylpropenes are all less reactive than the corresponding styrenes. This difference is presumably due to the excited state bond torsion process, which leads to *trans*-*cis* isomerization of the propenes, but results in reformation of the starting material in the case of the styrenes. Although both processes are non-productive (in terms of solvent adduct formation), the isomerization of the *trans*-1-arylpropenes yields a species with different photophysical properties than the original *trans* isomer. Specifically, the singlet lifetimes of the *cis* isomers are likely to be shorter than those of the *trans* isomers; *cis*-1-phenylpropene has a lifetime of  $\tau_s = 2.6$  ns in

hexane solution, while *trans*-1-phenylpropene has a lifetime of  $\tau_s = 11.8$  ns under the same conditions.<sup>133</sup> The slower conversion of the *trans*-1-arylpropenes to TFE adducts (compared to the methoxystyrenes) is likely due to the shorter lifetimes of the *cis* isomers, which in turn makes the interception of their excited states by TFE less probable. In essence, the formation of the less-reactive *cis* isomers of the *trans*-1-arylpropenes leads to a significant decrease in the rate of TFE addition. These ideas are essentially the same as those presented in Section 3.3 to explain the reactivity of the methoxy-substituted stilbene derivatives.

As indicated in Section 4.3.1, the main goal of the mechanistic investigations described in this chapter was to determine the pathway for the formation of TFE-stilbene adducts. The available data are fully consistent with a mechanism involving photoprotonation of the excited stilbenes, followed by nucleophilic attack by solvent on a carbocation intermediate. Some of the results presented in Chapter 3 are quite useful for establishing this mechanism. The clear increase in the yield of solvent adducts for the irradiations in TFE compared to those in methanol indicated that a polar, ionizing solvent is important to the photoaddition mechanism. Also, the quenching of the *trans*-73 fluorescence by TFE and TFE-OD suggested that proton transfer occurs early in the reaction sequence.

However, the work described in this chapter provides a much clearer picture of the steps that lead from reagent to product. The connection between the rate of product formation and the lifetime of the substrate in question appears to be general for all three classes of substrates. The styrenes are the most reactive of the compounds studied, apparently due in large part to the fact that excited state C=C bond torsion results only in

deactivation of the excited state. In contrast, the cis isomers of the *trans*-1-arylpropenes and *trans*-stilbenes have much shorter singlet lifetimes, which should greatly inhibit their ability to undergo solvent addition chemistry. Although the lifetimes of the cis isomers have not been experimentally determined, a comparison of the available data for the trans and cis isomers of stilbene and 1-phenylpropene suggests that the short lifetimes of the cis isomers should be a general phenomenon. The differences between typical values for the excited state lifetimes and quantum yields of isomerization of the *trans*-stilbenes and *trans*-1-arylpropenes accounts for the lower reactivity of the stilbenes. An important corollary to these ideas is that studies of the trans isomers only should still provide valid information regarding the mechanism of the addition reactions.

Attempts to use LFP techniques to directly observe the transient carbocations derived from highly reactive *trans*-**73** were unsuccessful in TFE. This difficulty is consistent with literature precedent,<sup>47</sup> where arylethyl cations not possessing a stabilizing para methoxy substituent could only be observed in HFIP solution. The same was found to be true for the current studies, and transient intermediates were successfully detected upon excitation of the substrates in HFIP using a 308 nm laser. The structures of the proposed cation intermediates are provided in Figure 4.22, along with their absorption maxima and rate constants for decay in HFIP.

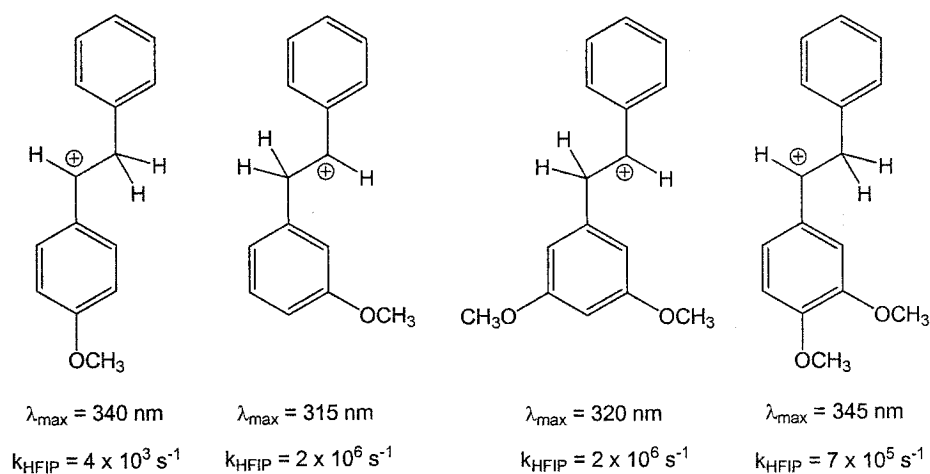


Figure 4.22 Cation intermediates detected following 308 nm LFP of *trans*-71-74 in HFIP.

The absorption maxima of the transients depicted in Figure 4.22 are consistent with literature precedent for the analogous arylethyl cations in HFIP. However, the rate constants for decay of these transients are all larger than the established literature values.<sup>47</sup> These differences are attributed to the presence of residual water that may be present in the HFIP used for these investigations. In addition, the kinetic traces used for the determination of  $k_{\text{HFIP}}$  are likely to be of much lower quality than those obtained from the styrene precursors. Despite the disagreement between the current results and the literature values, the order of cation reactivity agrees with the expected stabilities of the cations:  $k_{\text{HFIP}}(\textit{trans}\text{-}73) = k_{\text{HFIP}}(\textit{trans}\text{-}72) > k_{\text{HFIP}}(\textit{trans}\text{-}74) > k_{\text{HFIP}}(\textit{trans}\text{-}71)$ .

In addition to observing the expected transient absorptions, the LFP studies were also able to establish the reactivity of the cations with nucleophiles. Preliminary experiments using a solution of saturated sodium azide in HFIP accelerated the decay of the transients derived from *trans*-71 and *trans*-73. For *trans*-73, attempts to observe the cyclohexadienyl cation that would be produced by aryl ring protonation were negative. A weak transient absorption that was observed at wavelengths higher than 380 nm was

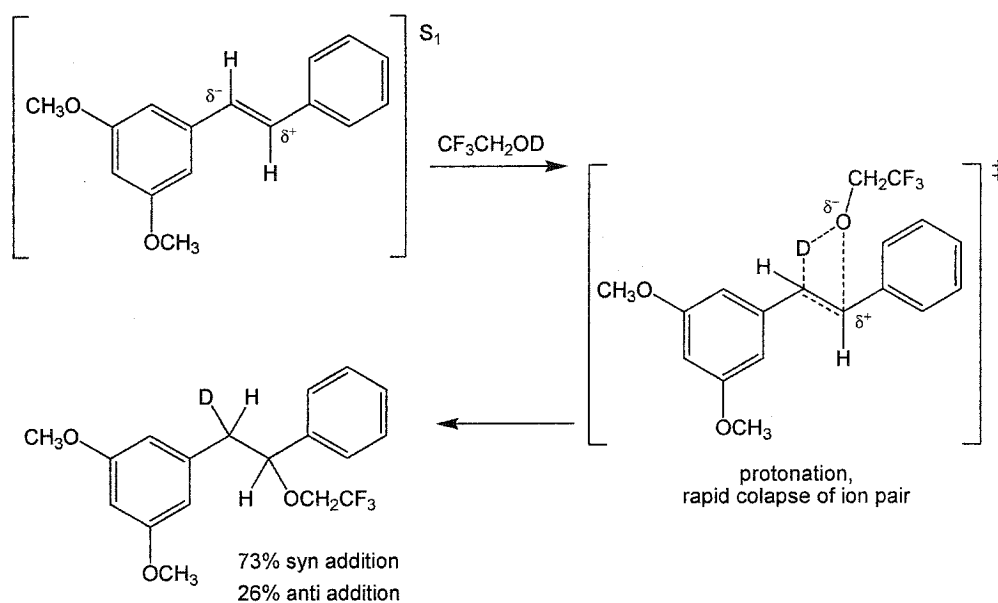
assigned to the radical cation of *trans*-73, which has been reportedly formed by two photon ionization of the neutral substrate. However, as was mentioned earlier, radical cation formation is much less likely to occur during the steady state irradiations. A final comment regarding the laser experiments is that the results are based on preliminary explorations. The work will be re-examined in the future to ensure the reproducibility of the rate constants, and to provide a more thorough characterization of the reactivity of the transients with nucleophiles.

The GC-MS and  $^1\text{H}$  NMR analysis of the reaction mixtures formed following irradiation in TFE and TFE-OD has provided many helpful pieces of information. The strong preference of all substrates to incorporate the trifluoroethoxy nucleophile and the proton (deuteron) of the solvent on adjacent carbons is a good indicator of the photoprotonation mechanism. Furthermore, the decrease in reaction rate in TFE-OD compared to TFE (as expressed by the  $k_{\text{H}}/k_{\text{D}}$  values in Table 4.25) emphasizes the importance of the proton transfer step.

The use of  $^1\text{H}$  NMR spectra to determine the location of deuterium incorporation in the solvent adducts proved to be an extremely important mechanistic tool. As was shown in Section 4.2.7, each of the three possible proton resonances can be identified, and peak integrations allow the relative importance of different mechanistic pathways to be determined. The results in Table 4.24 provided the relative percentages of products resulting from syn addition, anti addition, and carbene insertion during the incorporation of TFE-OD into the methoxy-substituted *trans*-stilbenes. Irradiation of *trans*-stilbene in methanol-*O-d* gave results that were consistent with the carbene insertion mechanism proposed by Laarhoven and co-workers.<sup>81</sup> However, the importance of this pathway in

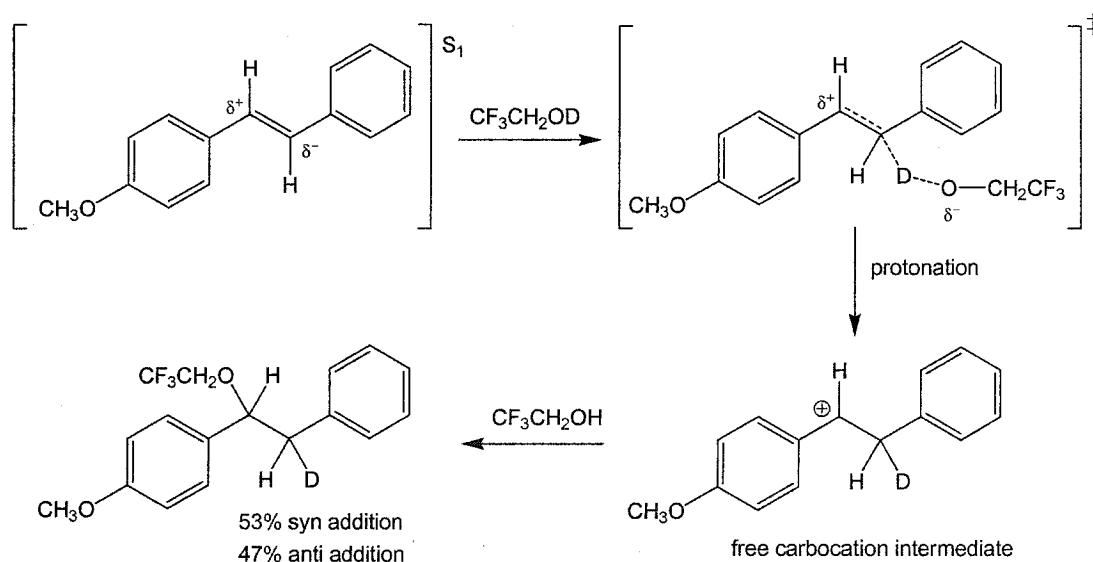
TFE-OD was found to be much lower for *trans*-stilbene itself (12% in TFE-OD *versus* 39% in methanol-*O-d*), and almost negligible for the methoxy-substituted compounds.

As indicated in Section 4.2.7, the syn:anti ratio for the TFE-OD addition reactions is larger for meta methoxy substrates than for para methoxy substrates. This observation is in complete agreement with the photoprotonation mechanism for solvent addition. Delivery of deuterium and the trifluoroethoxy nucleophile to the same face of a *trans*-stilbene derivative (*i.e.*, syn addition) should be favoured for those cases where the carbocation intermediate is quite unstable. Using established terminology, the reaction proceeds through an early transition state, where protonation and nucleophilic attack occur in quick succession. As a result of this mechanism, there is a strong preference for attack by the anionic nucleophile derived from the original molecule of TFE-OD. In the contact ion pair, the attachment of  $\text{CF}_3\text{CH}_2\text{O}^-$  occurs on the same face of the substrate as the original deuteration event. This type of reaction is shown in Scheme 4.7, using the reaction of *trans*-73 to give 76b-3 as a representative example (73% syn, 26% anti).



Scheme 4.7 Mechanism for the addition of TFE-OD to the excited state of *trans*-73.

The mechanism described above is not unique to *trans*-**73**; all products derived from the same short-lived phenethyl cation give similar results: **76b-0** (60% syn, 28% anti), **76b-2** (67% syn, 27% anti), and **76b-4** (67% syn, 33% anti). In contrast, those products that would be formed *via* a 4-methoxyphenethyl cation or a 3,4-dimethoxyphenethyl cation give very similar amounts of syn and anti addition: **75b-1** (53% syn, 47% anti) and **75b-4** (57% syn, 43% anti). The extra stabilization provided by the para methoxy substituent extends the lifetimes of the carbocation precursors for these products. These cations are more resistant to attack by solvent, and are less likely to react quickly within the contact ion pair. The similar amounts of syn and anti addition products support the idea that the intermediates react as free carbocations. This mechanism is shown in Scheme 4.8, using the reaction of *trans*-**71** as an example.



Scheme 4.8 Mechanism for the addition of TFE-OD to the excited state of *trans*-**71**.

A final issue that must be addressed is the relative reactivity of the methoxy-substituted stilbene derivatives. The results obtained in these studies indicate that there are likely to be several factors that determine the ability of a given substrate to produce

the TFE adducts. Certainly the degree to which trans-cis isomerization contributes to the decay of the excited state will be important; those substrates with higher quantum yields of isomerization generally give lower yields of products. Indeed, the differences in the reactivity of the styrenes, *trans*-1-arylpropenes, and *trans*-stilbenes appears to be due to the characteristics of their isomerization reactions.

The other important factor that controls the rate of solvent addition is the dipole moment of the excited state. The importance of  $\mu_e$  in determining reactivity is demonstrated by comparing unsubstituted *trans*-stilbene (*trans*-**60**, 21% conversion after ten minutes in TFE) and the 3,4-dimethoxy substrate *trans*-**74** (33% conversion after 10 minutes in TFE). Although *trans*-**60** has a lower quantum yield of isomerization ( $\phi_{tc} = 0.45$ ) compared to *trans*-**74** ( $\phi_{tc} = 0.59$ ), the higher dipole moment of the latter compound ( $\mu_e = 0.0$  D for *trans*-**60**, 8.7 D for *trans*-**74**) makes it the more reactive substrate in TFE.

The photochemical addition of TFE to the methoxy-substituted stilbene derivatives provides the Markovnikov ethers as the major products in all cases. This preference does not appear to be the result of protonation followed by a 1,2-hydride shift that equilibrates to the more stable cation intermediate. If such a mechanism were operating, it would provide another pathway for formation of the “carbene insertion” product in the TFE-OD experiments; that this product is not observed is good evidence that no rearrangement occurs following protonation. Indeed, the inferred lack of rearrangement is consistent with the results presented in Chapter 2, where the detection of carbocation rearrangements was actually the *goal* of the research.

The observation that two different regioisomers are observed from many of the addition reactions raises an interesting question: are both products formed from the same



excited state, or is each product the result of a unique electronic isomer? This issue is particularly interesting in light of the observed biexponential decay of the *trans*-73 fluorescence. Unfortunately, generalizations are difficult because *trans*-73 is the only substrate for which this behaviour was observed; *trans*-72 is the only other stilbene derivative for which a singlet lifetime could be measured (0.9 ns in acetonitrile). In order to provide more information regarding the unique properties of the *trans*-3,5-dimethoxystilbene chromophore, Chapter 5 describes the investigations of a set of substituted derivatives of *trans*-73.

## Chapter 5                      Intramolecular Charge Transfer States in the Photochemistry of Methoxy-Substituted Stilbene Derivatives

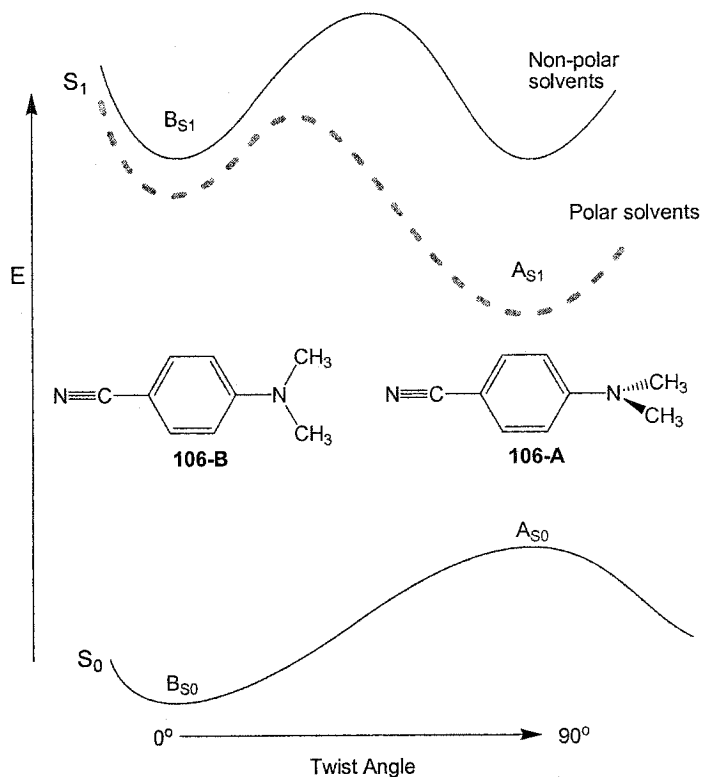
### 5.1 Introduction

#### 5.1.1 Twisted Intramolecular Charge Transfer (TICT) States

Highly polarized excited states, such as those detected through the course of the investigations in Chapter 4, have been observed by other researchers for a wide variety of chemical systems. Substrates that possess these Internal Charge Transfer (ICT) excited states are comprised of an electron donor (D) which is coupled to an electron acceptor (A).<sup>137</sup> Typically, D and A correspond to substituents and/or heteroatoms that are electron releasing or electron accepting according to the usual trends in organic chemistry. Often, ICT excited states may adopt a geometry that is quite different from that of the ground state. The simple aromatic substrate 4-*N,N*-dimethylaminobenzonitrile **106** is a classic example of a compound possessing a Twisted ICT state, commonly referred to as a “TICT” state.<sup>138</sup> As indicated in Scheme 5.1, the ground state conformation for this substrate ( $B_{S_0}$ ) is the planar geometry **106-B** that is expected for a substituted aniline derivative. Following  $B_{S_0} \rightarrow B_{S_1}$  excitation of **106** in non-polar solvents such as hexane, emission from  $B_{S_1}$  is observed at 350 nm. However, upon changing to a solvent of higher polarity, a second emission band is detected at

approximately 410 nm. In acetonitrile, only the long-wavelength emission is produced.

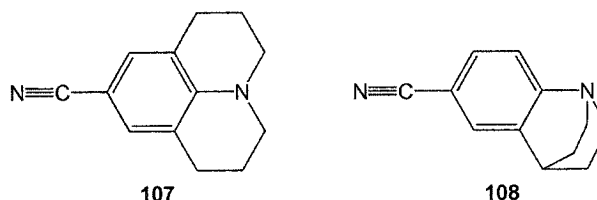
In solvents of intermediate polarity, both fluorescence maxima are observed.



Scheme 5.1 The energy-coordinate diagram for 4-*N,N*-dimethylaminobenzonitrile **106** in non-polar solvents (solid line) or polar solvents (dashed line).

The reasons for the “dual fluorescence” behaviour displayed by **106** are outlined in Scheme 5.1. In non-polar solvents, the usual  $B_{S1} \rightarrow B_{S0}$  is the main deactivation mechanism for the excited state. However, in more polar solvents, the barrier for excited state Ar-N bond torsion is lowered. This activated process allows formation of a second excited state  $A_{S1}$ , where the plane of the dimethylamino substituent has been twisted perpendicular to the plane of the aryl ring, structure **106-A**.<sup>139</sup> The excited state dipole moment of  $A_{S1}$  ( $\mu_e = 16$  D) is much greater than that of  $B_{S1}$  ( $\mu_e = 6$  D), and so the former species is favoured in polar solvents. Comparisons have been drawn between the effect

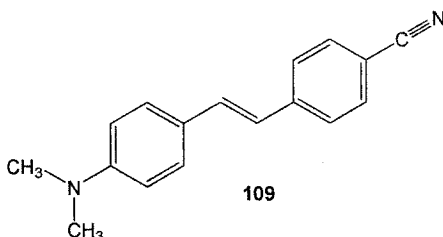
of polar solvents on the twisting motion for **106** and on the bond torsion for the excited state of *trans*-stilbene.<sup>140</sup> Compelling evidence for the twisted geometry of  $A_{Si}$  is provided by the bridged analogues **107** and **108**. The structure of **107** completely inhibits the  $B_{Si} \rightarrow A_{Si}$  twisting process – this substrate displays only B-type emission, even in highly polar solvents. In contrast, **108** more closely resembles the twisted structure of **106-A**, and so only A type emission is produced.<sup>139</sup>



### 5.1.2 Formation of ICT States *via* Excitation of Donor-Acceptor Stilbenes

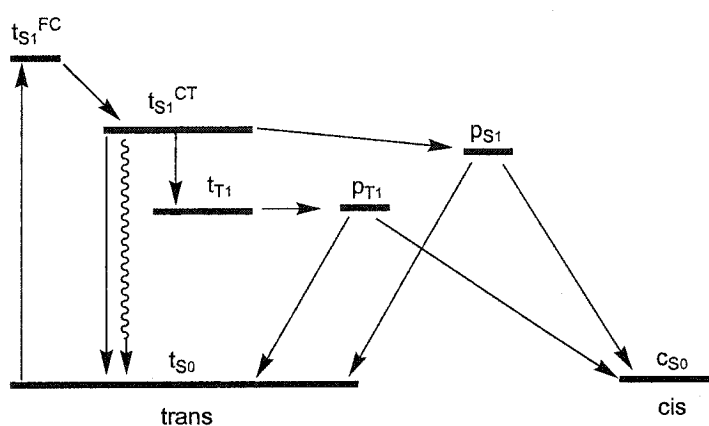
The donor-acceptor stilbene *trans*-4-*N,N*-dimethylamino-4'-cyanostilbene **109** has been extensively studied for many years.<sup>141</sup> From a conceptual viewpoint, **109** represents the same donor and acceptor moieties that were present in **106**, but with a different conjugated connection. However, the photochemistry of **109** is much more complex, due mainly to the fact that the substrate is essentially a substituted *trans*-stilbene derivative. Early research efforts explored the idea that **109** might exhibit TICT emission from twisting of the dimethylamino substituent. Although the emission of **109** does move to longer wavelengths with increasing solvent polarity ( $\lambda_{\max}$  (fluor) = 441 nm in methylcyclohexane, 532 nm in acetonitrile),<sup>101</sup> the effect is due to a *shift* in the emission band rather than to formation of a second emitting state. Thus, the emitting species is likely a highly polarized state that becomes *progressively* more stable in more polar solvents. Bridged analogues of **109** (similar to **107** and **108**) displayed the same emission

properties as the original substrate, thereby providing additional evidence that the excited state of **109** does not resemble **106-A**.<sup>142</sup> However, bridging of other bonds in the chromophore of **109** revealed that the excited state species may exhibit some degree of rotation about the aniline-cyanostyrene bond.



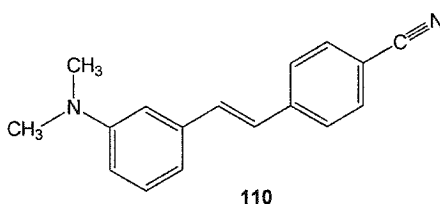
Further investigations of the photophysical properties of **109** have yielded much information regarding the highly polarized excited state of this substrate. The quantum yield of fluorescence of **109** increases from  $\phi_f = 0.03$  in cyclohexane to 0.13 in acetonitrile, and the quantum yield of isomerization is only slightly affected by solvent polarity ( $\phi_{ic} = 0.40$  in cyclohexane, 0.45 in acetonitrile).<sup>101</sup> Using the solvatochromic techniques described in Section 4.2.3, Zachariasse and co-workers were able to determine that the dipole moment of the initial Frank-Condon excited state ( $\mu_e^{FC} = 13$  D) is larger than that of the ground state ( $\mu_g = 7$  D), but the dipole moment of the fluorescent charge transfer state is even higher still ( $\mu_e^{CT} = 21$  D).<sup>143</sup> Furthermore, the temperature-dependence of the singlet lifetime of **109** provided values for the height of the  $t_{S_1} \rightarrow p_{S_1}$  barrier: 3.3 kcal/mol in *n*-heptane and 5.4 kcal/mol in acetonitrile. Therefore, although the values of  $\phi_{ic}$  for **109** are quite similar to those of *trans*-stilbene, the other characteristics of **109** are more unusual (*i.e.*, the increase in both  $\phi_f$  and the barrier for excited state bond torsion with increasing solvent polarity).

The generally accepted model for **109** and several other donor-acceptor stilbenes is shown in Scheme 5.2. Upon excitation of the initial trans isomer of **109**, an initial Frank-Condon state is formed,  $t_{S1}^{FC}$ . Relaxation of the initial state occurs *via* internal charge transfer to produce a highly polarized state,  $t_{S1}^{CT}$ . The highly polarized nature of the latter state is demonstrated by the solvatochromic behaviour and the large excited state dipole moment ( $\mu_e^{CT} = 21$  D). Attempts to observe the  $t_{S1}^{FC} \rightarrow t_{S1}^{CT}$  process by laser techniques have been pursued,<sup>144</sup> but the identity of the transients observed by these methods is somewhat controversial.<sup>145</sup> The exact structure of  $t_{S1}^{CT}$  has also been debated, and a variety of twisted structures have been proposed. Whatever the structure of the CT excited state, the barrier for the singlet state trans-cis isomerization process ( $t_{S1}^{CT} \rightarrow p_{S1}$ ) is increased substantially compared to substituted stilbene derivatives that are unable to form charge transfer states. As a result of this change in the barrier for torsional motion, isomerization of donor-acceptor stilbenes such as **109** occurs predominantly *via* intersystem crossing ( $t_{S1}^{CT} \rightarrow t_{T1}$ ) followed by barrierless bond rotation to the perpendicular geometry ( $t_{T1} \rightarrow p_{T1}$ ).



Scheme 5.2 Simplified energy state diagram for the excited state behaviour of donor-acceptor stilbene derivatives.

There are clearly many similarities between the photochemistry of donor-acceptor stilbenes and the meta aminostilbenes that have been the focus of much research by Lewis and co-workers. In both cases the barrier for excited state C=C bond torsion is increased, leading to higher quantum yields of fluorescence as well as isomerization *via* a triplet pathway. In order to investigate the possibility that meta aminostilbenes might also function as donor-acceptor systems, Lewis and Weigel examined the photochemistry of *trans*-3-N,N-dimethylamino-4'-cyanostilbene **110**, the meta isomer of **109**.<sup>101</sup> As indicated by the values in Table 5.1, although the charge transfer dipoles of **109** and **110** are similar, many of their photophysical properties are quite different. An increase in fluorescence quantum yield with increasing solvent polarity is observed for **109**, but the fluorescence of **110** is decreased dramatically. In addition, the values of  $\phi_{tc}$  and  $\tau_s$  show very different responses to solvent polarity for each substrate. In summary, **110** displays photophysical properties that are more closely related to *trans*-3-aminostilbene (*trans*-**63** – *vide supra*, Table 3.1) than to **109**.



Substrate	Solvent	$\lambda_{\text{max}}$ (abs) nm	$\lambda_{\text{max}}$ (fluor) nm	$\phi_f$	$\phi_{tc}$	$\tau_s$ ns	$\mu_e^{\text{CT}}$ D
<b>109</b>	cyclohexane	382	441	0.03	0.45	0.09	21
	acetonitrile	383	532	0.13	0.40	0.52	
<b>110</b>	methylcyclohexane	364	443	0.64	0.11	13.3	21.8
	acetonitrile	368	546	0.05	0.24	13.5	

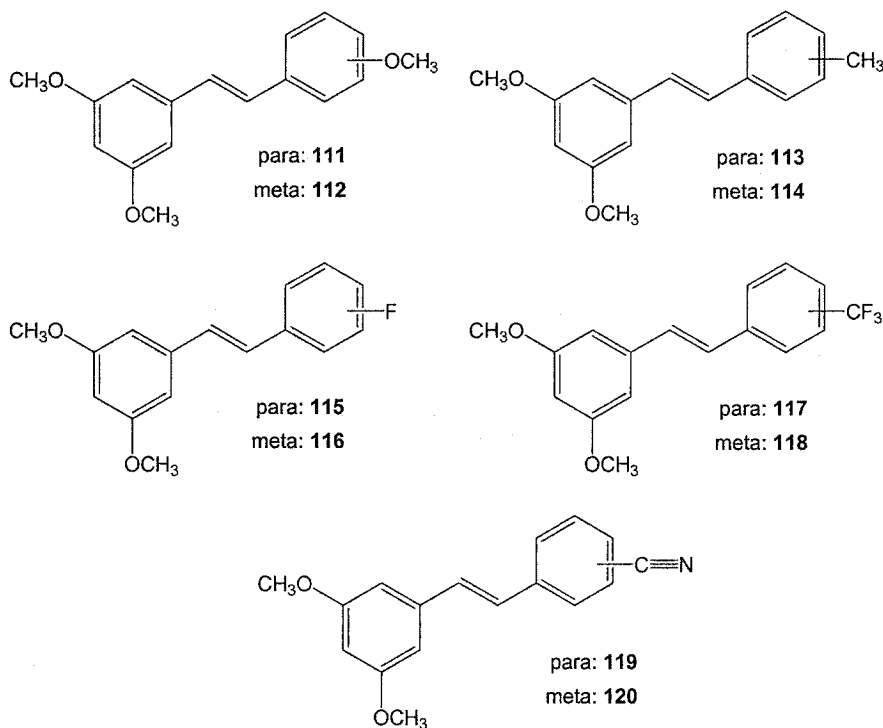
Table 5.1 Photophysical data for donor-acceptor stilbenes **109** and **110** (data from Reference 101).

### 5.3 Project Proposal

The work reported in Chapter 4 indicated that *trans*-3,5-dimethoxystilbene (*trans*-73) is different from the other methoxy-substituted stilbene derivatives in many ways. Upon changing to more polar solvents, the fluorescence maximum of *trans*-73 is shifted to longer wavelengths, the quantum yield of fluorescence increases, and the singlet lifetime increases. The quantum yield of isomerization is unaffected by solvent polarity. These trends are exactly the same as those displayed by the well-studied donor acceptor stilbene 109. These similarities are particularly intriguing given that *trans*-73 does not possess the strong amino donor substituent, nor a traditional acceptor substituent of any kind. A preliminary hypothesis for these observations is that the 3,5-dimethoxyphenyl system acts as a potent electron donor to the connected styrene unit. This process, which should be more favourable in polar solvents, yields a highly fluorescent, long-lived ICT state. If these suggestions are valid, then the biexponential decay of the *trans*-73 excited state may be an extremely important observation. In order to determine the generality of the photophysical properties displayed by *trans*-73, a series of substituted derivatives *trans*-111-120 was targeted for further investigations. These substrates were selected so as to span the range of electron donating (methoxy) to electron withdrawing (cyano) substituents. The nitro substituent was not employed because of the increased quantum yields of intersystem crossing that have been observed for other nitro-substituted stilbenes.<sup>146</sup> In addition to providing valuable information regarding the novel photophysical properties of the 3,5-dimethoxystilbene chromophore, *trans*-111-120 were envisaged as a new set of compounds for which the TFE addition reactions could be explored. Note that, in the results to follow, the discussion will refer to some substrates according to the substituent on the ring that is *not* 3,5-dimethoxy-substituted. In these



cases, “unsubstituted”, “4’-methoxy”, or “3’-methoxy” will refer to *trans*-73, *trans*-111, or *trans*-112, respectively. This point is important, because similar labels have been used in previous chapters for *trans*-60 (unsubstituted), *trans*-71 (4-methoxy) and *trans*-72 (3-methoxy). In the case that these latter substrates are discussed, efforts have been taken to ensure that the structure in question is clear to the reader.

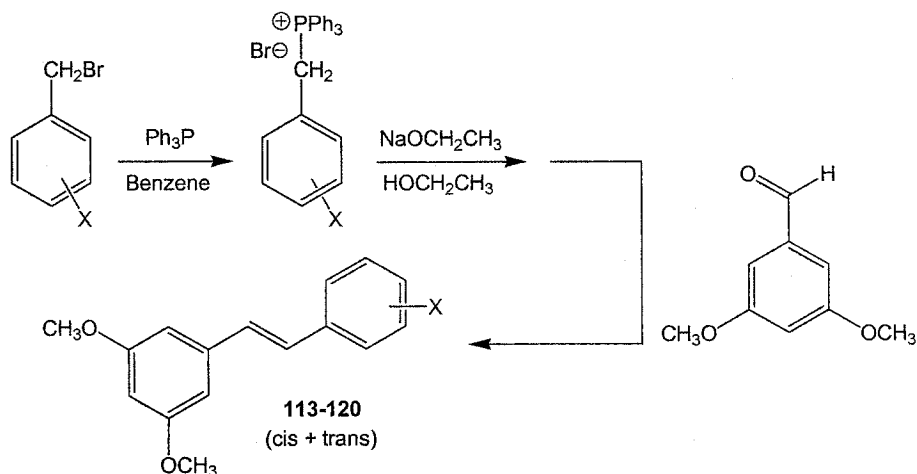


## 5.2 Experimental Results

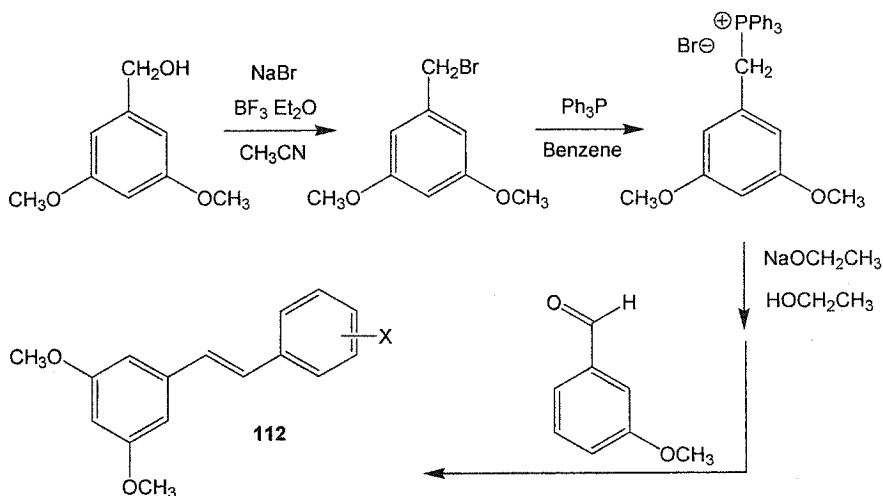
### 5.2.1 Synthesis of *trans*-111-120

The syntheses of the ten new substrates were accomplished using the same Wittig chemistry that was employed for the production of the methoxy-substituted stilbene derivatives in Chapter 3. For these reactions, the aryltriphenylphosphonium bromide salts were prepared from the corresponding benzyl bromide derivatives, and the salts were then reacted with 3,5-dimethoxybenzaldehyde in sodium ethoxide solution. The exceptions to

this scheme are the methoxy-substituted derivatives **111** and **112**. The 4-methoxy substrate **111** was synthesized earlier in the Chapter 2 experiments, Scheme 2.9. Note that this substrate was previously given the label **52**, but it will now be referred to as **111** in order to retain the numbering system of the current chapter. The 3-methoxy substrate **112** was synthesized by the sequence of reactions in Scheme 5.3.



Scheme 5.2 Syntheses of **113-120** (cis and trans isomers for each).



Scheme 5.3 Synthesis of **112** (both cis and trans isomers).

### 5.2.2 Photophysical Properties of *trans*-111-120 in Acetonitrile Solution

A summary of the important photophysical properties for the ten substituted *trans*-3,5-dimethoxystilbenes is provided in Table 5.2. All fluorescence measurements ( $\lambda_{\max}$  (fluor),  $\phi_f$ ,  $\tau_s$ ) were obtained using 295 nm excitation, and *trans*-stilbene in hexanes was employed as the standard for fluorescence quantum yields ( $\phi_f = 0.0433$ ).<sup>86</sup> The isomerization quantum yields were determined by steady state irradiations using *trans*-stilbene in cyclohexane as a standard ( $\phi_{tc} = 0.40$ ).<sup>108</sup>

Substrate	Substituent	$\lambda_{\max}$ (abs) nm	$\epsilon_{\max}$ $M^{-1}cm^{-1}$	$\lambda_{\max}$ (fluor) nm	$\phi_f^a$	$\phi_{tc}^b$	$\tau_s$ (fast)	$\tau_s$ (slow)
<i>trans</i> -111	4'-OCH <sub>3</sub>	306	30800	374	0.007	0.60	<0.5 <sup>c</sup>	<0.5 <sup>c</sup>
<i>trans</i> -112	3'-OCH <sub>3</sub>	304	26800	390	0.29	0.29	1.9	16.0
<i>trans</i> -113	4'-CH <sub>3</sub>	303	30900	385	0.08	0.44	0.7	7.0
<i>trans</i> -114	3'-CH <sub>3</sub>	303	29900	389	0.26	0.29	2.6	15.6
<i>trans</i> -73	H	299	30100	390	0.32	0.28	3.9	18.5
<i>trans</i> -115	4'-F	298	27700	390	0.25	0.23	3.7	16.8
<i>trans</i> -116	3'-F	307	28300	402	0.34	0.18	6.4	24.2
<i>trans</i> -117	4'-CF <sub>3</sub>	310	30000	418	0.26	0.24	5.5	22.7
<i>trans</i> -118	3'-CF <sub>3</sub>	298	26200	410	0.34	0.22	7.3	24.2
<i>trans</i> -119	4'-CN	321	25000	441	0.16	0.39	4.4	20.6
<i>trans</i> -120	3'-CN	302	26400	414	0.30	0.29	4.8	18.0

a) 295 nm excitation, relative to  $\phi_f = 0.0433$  for *trans*-stilbene in hexanes, Reference 86. b) Determined by steady-state irradiation at 300 nm relative to  $\phi_{tc} = 0.40$  for *trans*-stilbene in cyclohexane, Reference 108.

c) Shorter than the time resolution of the instrument.

Table 5.2 Summary of photophysical data for the substituted derivatives of *trans*-3,5-dimethoxystilbene in acetonitrile.

The absorption spectra of the new substrates display the same intense transitions ( $\epsilon_{\max} \approx 25000 - 30000 M^{-1}cm^{-1}$ ) that are typical of substituted stilbene derivatives, and so experimental spectra themselves have not been included in the current report. The absorption maxima are observed at slightly longer wavelengths for substrates with

electron withdrawing substituents, but virtually all compounds display high absorption in the range of 290-315 nm. The fluorescence spectra in acetonitrile solution are all comprised of a single broad, structureless band – the actual spectra are not displayed in the current section, but Section 5.2.3 provides the spectra of all 11 substrates in a series of four different solvents.

The fluorescence maxima are shifted to longer wavelengths for substrates bearing electron withdrawing substituents, and the effect is larger for the para substituents. The smallest value of  $\lambda_{\text{max}}$  (fluoro) is observed for the 4'-methoxy substrate *trans*-**111** (375 nm), while the 4'-cyano substrate *trans*-**119** displays the longest wavelength emission (441 nm). In contrast to the methoxy-substituted stilbene derivatives investigated in Chapters 3 and 4, the new substrates *trans*-**111-120** all have fairly large quantum yields of fluorescence ( $\phi_f \approx 0.25 - 0.34$ ). The 4'-cyano substrate *trans*-**119** is slightly less fluorescent ( $\phi_f = 0.16$ ) than the majority of the compounds in Table 5.2, while *trans*-**113** (4'-methyl,  $\phi_f = 0.08$ ) and *trans*-**111** (4'-methoxy,  $\phi_f = 0.007$ ) both have very weak emission spectra compared to the other substrates. The quantum yields of isomerization displayed by the 11 compounds are all lower than that of *trans*-stilbene in acetonitrile ( $\phi_{\text{tc}} = 0.45$ ), with the exception of the 4'-methoxy substrate *trans*-**111** ( $\phi_{\text{tc}} = 0.60$ ). Finally, as was the case for *trans*-**73** (*vide supra*, Section 4.2.3), the best fits for the fluorescence decay of *trans*-**112-120** are obtained using a biexponential model. The two components for this decay are of about the same magnitude as for *trans*-**73**; a short component in the range of 1-7 ns, and a long component in the range of 16-24 ns. Unfortunately, the lifetime for *trans*-**111** was below the time resolution of the instrument.

In general, the data in Table 5.2 indicate that the main characteristics of the *trans*-3,5-dimethoxystilbene chromophore are preserved in most of the substituted derivatives. In comparison to *trans*-stilbene itself, most substrates display longer-wavelength fluorescence maxima, much higher fluorescence quantum yields, smaller isomerization quantum yields, and biexponential singlet lifetimes. However, the 4'-methoxy substrate *trans*-111 has properties that are more typical of traditional stilbene derivatives: a large quantum yield of isomerization ( $\phi_{ic} = 0.60$ ), a very small quantum yield of fluorescence ( $\phi_f = 0.007$ ), and a singlet lifetime that is below 0.5 ns.

### 5.2.3 Solvent Dependence of the Photophysical Properties of *trans*-111-120

A key aspect of the investigations in Chapter 4 was the dependence of the photophysical properties on solvent polarity. Clearly, the analogous studies for *trans*-111-120 should provide valuable information regarding the proposed charge transfer excited state of the 3,5-dimethoxystilbene chromophore. This section describes the trends observed for the Stokes' shifts, fluorescence quantum yields, singlet lifetimes, and isomerization quantum yields for the ten new substrates. To begin this section, the experimental fluorescence spectra of the 11 substrates in four different solvents (cyclohexane, diethyl ether, ethyl acetate and acetonitrile) are provided in Figures 5.1-11. The same data have also been obtained in di-*n*-butyl ether and isopropyl alcohol, but these spectra have not been included in the figures due to space limitations. Note also that the vertical axis of the plots have arbitrary fluorescence units; although all spectra were recorded using solutions of equal absorbance ( $A = 0.25$  at 295 nm), comparisons *between* two figures should not be made.

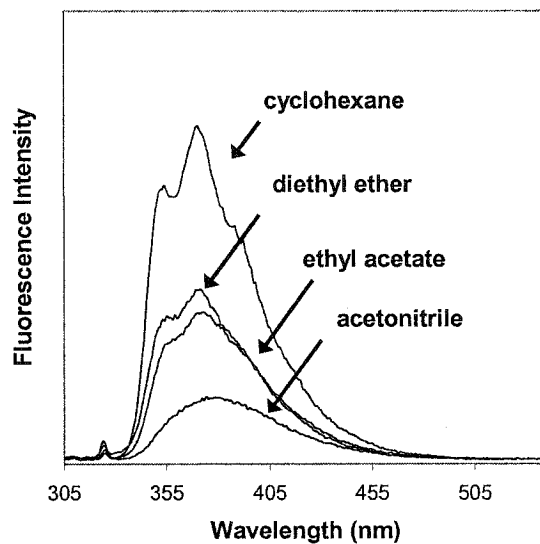


Figure 5.1 Fluorescence spectra of *trans*-111 (4'-methoxy) in a series of four solvents.

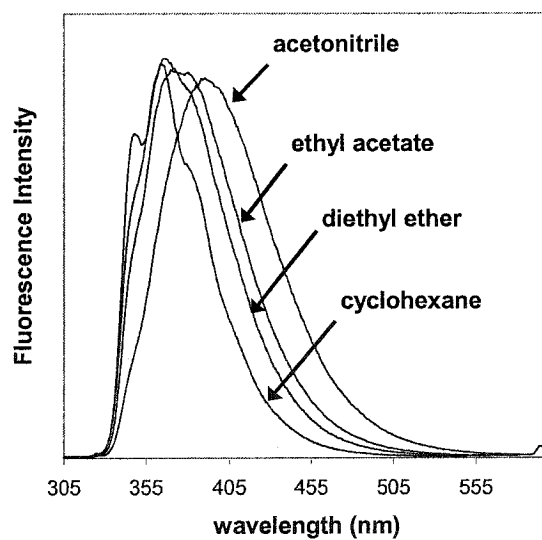


Figure 5.2 Fluorescence spectra of *trans*-112 (3'-methoxy) in a series of four solvents.

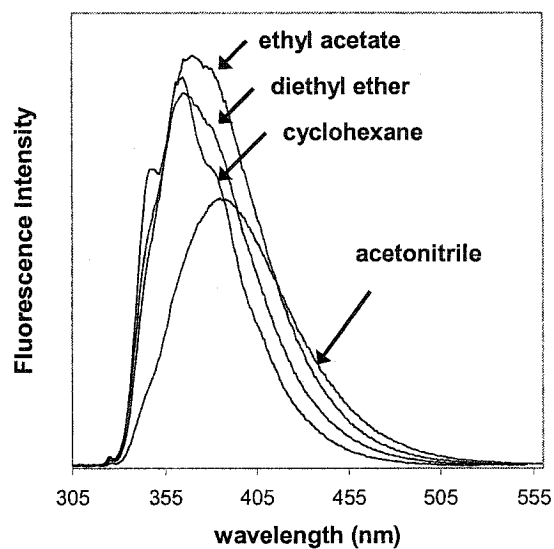


Figure 5.3 Fluorescence spectra of *trans*-113 (4'-methyl) in a series of four solvents.

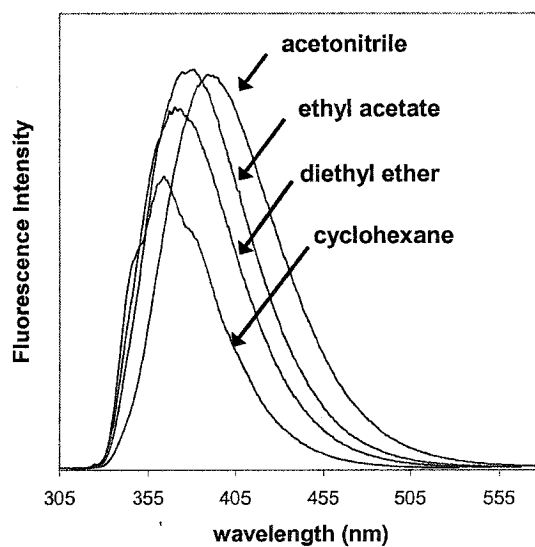


Figure 5.4 Fluorescence spectra of *trans*-114 (3'-methyl) in a series of four solvents.

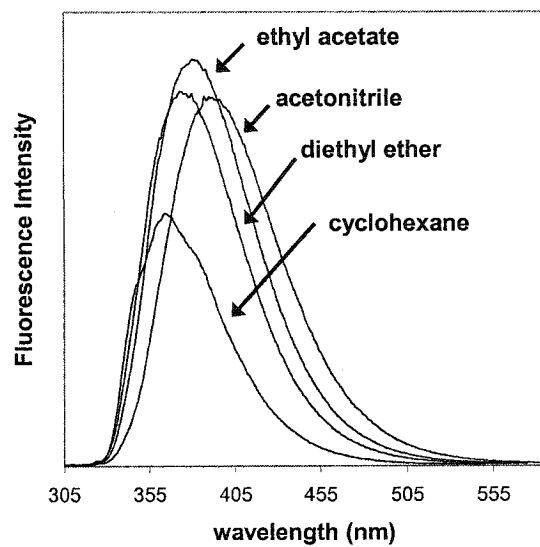


Figure 5.5 Fluorescence spectra of *trans*-115 (4'-fluoro) in a series of four solvents.

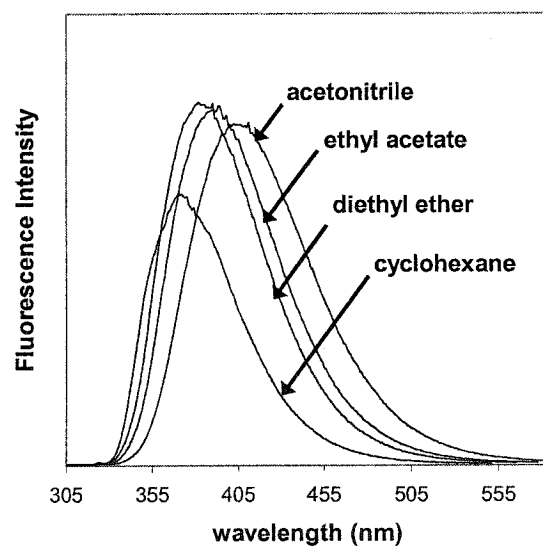


Figure 5.6 Fluorescence spectra of *trans*-116 (3'-fluoro) in a series of four solvents.



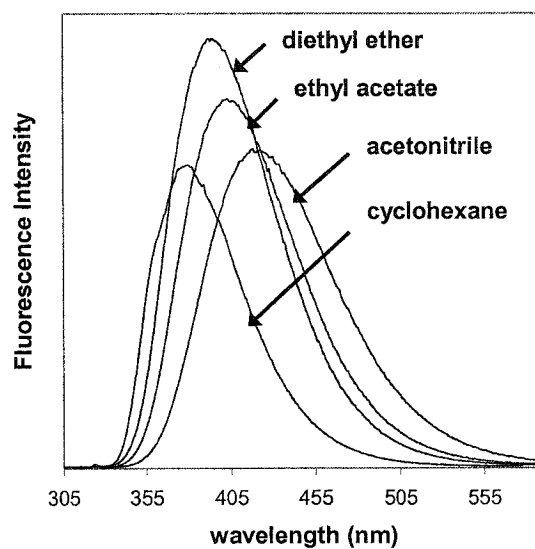


Figure 5.7 Fluorescence spectra of *trans*-117 (4'-trifluoromethyl) in a series of four solvents.

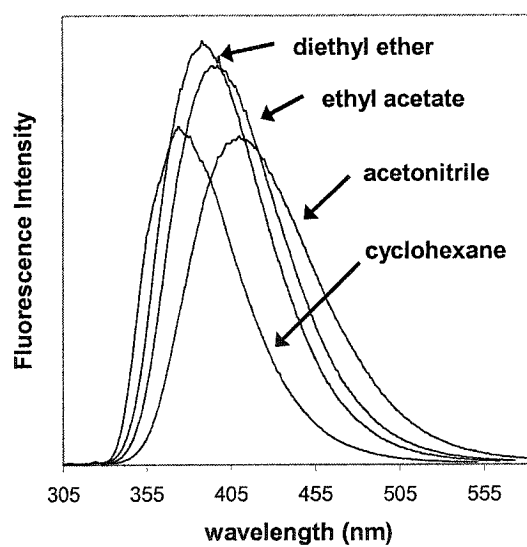


Figure 5.8 Fluorescence spectra of *trans*-118 (3'-trifluoromethyl) in a series of four solvents.

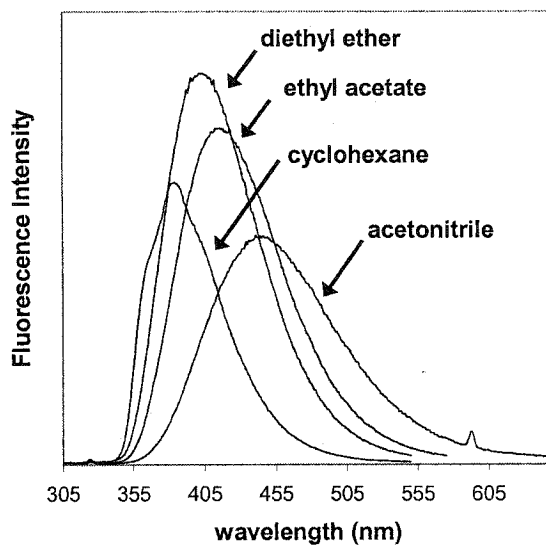


Figure 5.9 Fluorescence spectra of *trans*-118 (4'-cyano) in a series of four solvents.

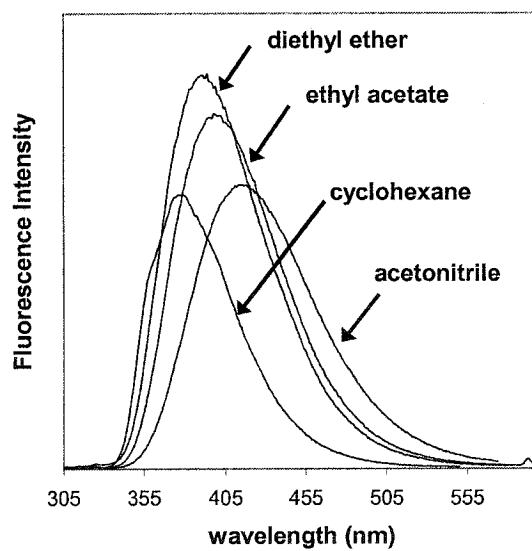


Figure 5.10 Fluorescence spectra of *trans*-118 (3'-cyano) in a series of four solvents.

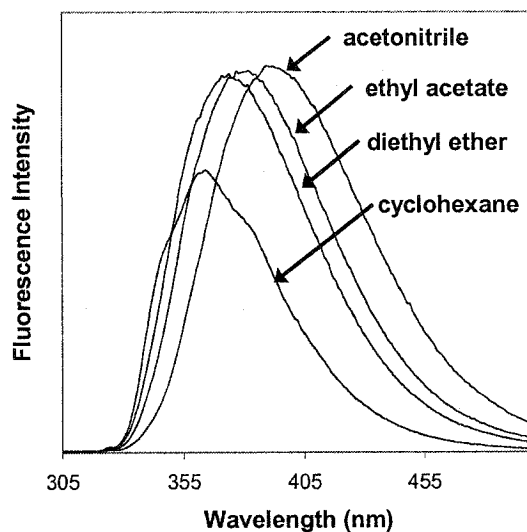


Figure 5.11 Fluorescence spectra of *trans*-73 (*trans*-3,5-dimethoxystilbene) in a series of four solvents.

The ten new substrates clearly display solvatochromic shifts in their fluorescence maxima, regardless of the intensity of the emission. The spectra are also significantly broadened in the more polar solvents. Although many substrates exhibit a steady rise in fluorescence intensity as the solvent polarity is increased, others reach a maximum fluorescence at a medium polarity solvent (diethyl ether or ethyl acetate) and then become *less* fluorescence in solvents of even higher polarity. An important note in this regard is that the fluorescence quantum yields (*vide infra*) have been calculated using the *area* under the fluorescence curves, as opposed to the *intensity* of fluorescence at a specific wavelength. Tables 5.3 and 5.4 display the solvent-induced Stokes' shifts using wavenumber units (*i.e.*,  $\nu_{\text{max}}(\text{ex}) - \nu_{\text{max}}(\text{fluor})$ ) for the para and meta substrates respectively. Plots of the Stokes' shifts versus the solvent parameter  $\Delta f$  are provided in Figures 5.12 and 5.13 (the numerical values of  $\Delta f$  are given in the two tables). As a point of reference, *trans*-3,5-dimethoxystilbene (*trans*-73) has been included in both data sets.

Solvent	$\Delta f$	<i>trans</i> -111 (4'-OCH <sub>3</sub> )	<i>trans</i> -113 (4'-CH <sub>3</sub> )	<i>trans</i> -73 (H)	<i>trans</i> -115 (4'-F)	<i>trans</i> -117 (4'-CF <sub>3</sub> )	<i>trans</i> -119 (4'-CN)
cyclohexane	0.101	3837	4349	4476	4375	5361	4633
dibutyl ether	0.194	3888	4223	5170	4792	5872	4895
diethyl ether	0.256	3669	4450	5211	5345	6265	5767
ethyl acetate	0.292	4078	4922	5771	5735	7033	6333
2-propanol	0.366	4055	5109	5976	5704	6954	6921
acetonitrile	0.394	4126	5873	6513	6513	7823	7719

Table 5.3 Stokes' shifts (in wavenumbers, cm<sup>-1</sup>) for the fluorescence of the *para*-substituted derivatives of *trans*-73 in a series of six solvents.

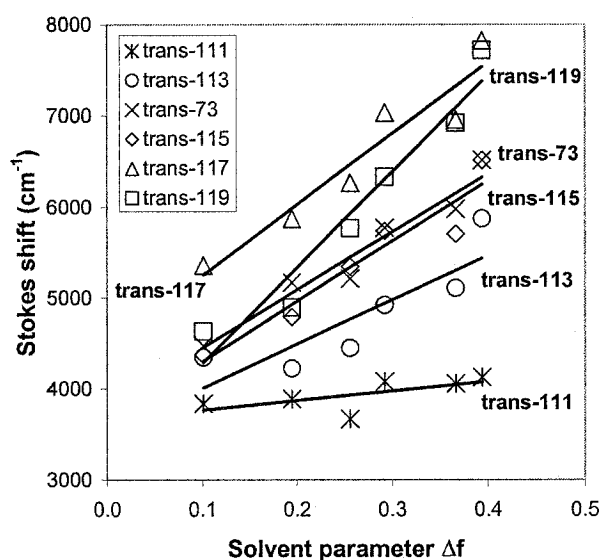


Figure 5.12 Plot of the Stokes' shift (in wavenumbers) versus the solvent parameter  $\Delta f$  for the *para*-substituted derivatives of *trans*-73 in a series of six solvents.

Solvent	$\Delta f$	<i>trans</i> -112 (3'-OCH <sub>3</sub> )	<i>trans</i> -114 (3'-CH <sub>3</sub> )	<i>trans</i> -73 (H)	<i>trans</i> -116 (3'-F)	<i>trans</i> -118 (3'-CF <sub>3</sub> )	<i>trans</i> -120 (3'-CN)
cyclohexane	0.101	3974	4375	4476	4965	5008	5424
dibutyl ether	0.194	3905	4599	5170	5499	5702	6109
diethyl ether	0.256	4026	4922	5211	5669	6074	6568
ethyl acetate	0.292	4420	5702	5771	6504	6658	6949
2-propanol	0.366	5170	5669	5976	6430	6696	7318
acetonitrile	0.394	6005	6242	6513	7176	7559	7794

Table 5.4 Stokes' shifts (in wavenumbers, cm<sup>-1</sup>) for the fluorescence of the *meta*-substituted derivatives of *trans*-73 in a series of six solvents.

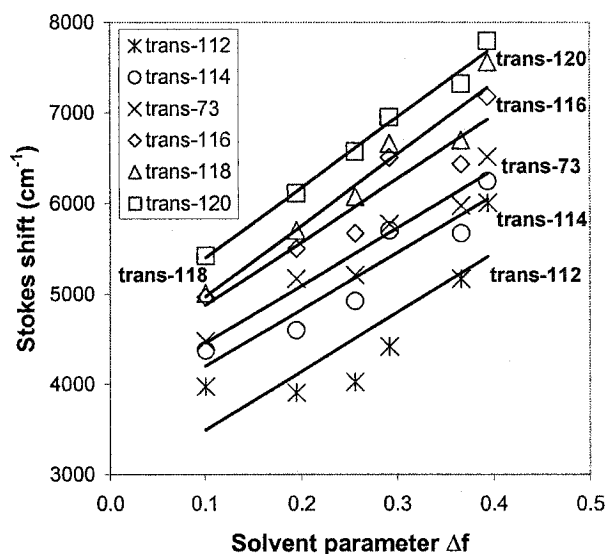


Figure 5.13 Plot of the Stokes' shift (in wavenumbers) *versus* the solvent parameter  $\Delta f$  for the *meta*-substituted derivatives of *trans*-73 in a series of six solvents.

The trends in Figures 5.12 and 5.13 indicate that solvent polarity does determine the fluorescence maxima of these substrates, and that the solvent parameter  $\Delta f$  is able to accurately represent this relationship. Values for the slopes, intercepts, and correlation coefficients of the solvatochromic plots are provided in Tables 5.5 and 5.6. Curiously, the *para* substrates have very different solvatochromic slopes ( $m_{\text{para}} = 1000 - 10500 \text{ cm}^{-1}$ ), whereas the slopes of the *meta* substrates are all quite similar ( $m_{\text{meta}} = 6300 - 7300 \text{ cm}^{-1}$ ). In comparison to the original set of five methoxy substituted stilbenes (*vide supra*, Table 4.10), the Stokes' shifts of nine of the eleven substrates in the current data set are well correlated with  $\Delta f$  ( $r^2 \geq 0.90$ ). Further inspection of the data reveals that the methoxy- and methyl-substituted substrates are not as well correlated with  $\Delta f$ , probably because these substrates also give quite shallow slopes. In contrast, the trifluoromethyl- and cyano-substituted compounds display the highest correlations and the steepest slopes. At the time of this writing, the calculations of the ground state dipole moments ( $\mu_g$ ) for the

new substrates have not been completed. Because these values are required for determination of the excited state dipole moments ( $\mu_e$ ), the latter values are not provided in Tables 5.5 and 5.6. The one exception to this statement, however, is the 4'-cyano derivative *trans*-**119**, which displays the largest solvatochromic slope of the eleven substrates. For *trans*-**119**, the ground state dipole moment was calculated as  $\mu_g = 6.6$  D; using a solvent cavity radius of  $a = 5 \times 10^{-10}$  m in Equation 4.7 provides a value of  $\mu_e = 19.8$  D for the excited state dipole moment.

Compound	slope cm <sup>-1</sup>	intercept cm <sup>-1</sup>	r <sup>2</sup>
<i>trans</i> - <b>111</b>	1000	3700	0.42
<i>trans</i> - <b>113</b>	4900	3500	0.74
<i>trans</i> - <b>73</b>	6400	3800	0.94
<i>trans</i> - <b>115</b>	6600	3600	0.91
<i>trans</i> - <b>117</b>	7800	4500	0.91
<i>trans</i> - <b>119</b>	10500	3200	0.94

Table 5.5 Data for the solvatochromic plots (Figure 5.12) of the *para*-substituted derivatives of *trans*-3,5-dimethoxystilbene.

Compound	slope cm <sup>-1</sup>	intercept cm <sup>-1</sup>	r <sup>2</sup>
<i>trans</i> - <b>112</b>	6600	2800	0.73
<i>trans</i> - <b>114</b>	6300	3800	0.89
<i>trans</i> - <b>73</b>	6400	3800	0.94
<i>trans</i> - <b>116</b>	7000	4200	0.90
<i>trans</i> - <b>118</b>	7900	4200	0.93
<i>trans</i> - <b>120</b>	7800	4600	0.99

Table 5.6 Data for the solvatochromic plots (Figure 5.13) of the *meta*-substituted derivatives of *trans*-3,5-dimethoxystilbene.

As was indicated earlier, the quantum yields of fluorescence for *trans*-111-120 are also solvent-dependent. Tables 5.7 and 5.8 provide values for the quantum yields of fluorescence of the *para* and *meta* substrates, respectively. The data in these tables are plotted versus the solvent parameter  $\Delta f$  in Figures 5.14 and 5.15.

Solvent	$\Delta f$	<i>trans</i> -111 (4'-OCH <sub>3</sub> )	<i>trans</i> -113 (4'-CH <sub>3</sub> )	<i>trans</i> -73 (H)	<i>trans</i> -115 (4'-F)	<i>trans</i> -117 (4'-CF <sub>3</sub> )	<i>trans</i> -119 (4'-CN)
cyclohexane	0.101	0.027	0.082	0.18	0.18	0.19	0.11
dibutyl ether	0.194	0.024	0.097	0.26	0.21	0.25	0.17
diethyl ether	0.256	0.014	0.084	0.27	0.22	0.26	0.19
ethyl acetate	0.292	0.014	0.106	0.29	0.25	0.26	0.19
2-propanol	0.366	0.014	0.090	0.27	0.22	0.27	0.15
acetonitrile	0.394	0.007	0.077	0.32	0.25	0.26	0.16

Table 5.7 Fluorescence quantum yields for the *para*-substituted derivatives of *trans*-3,5-dimethoxystilbene in a series of six solvents.

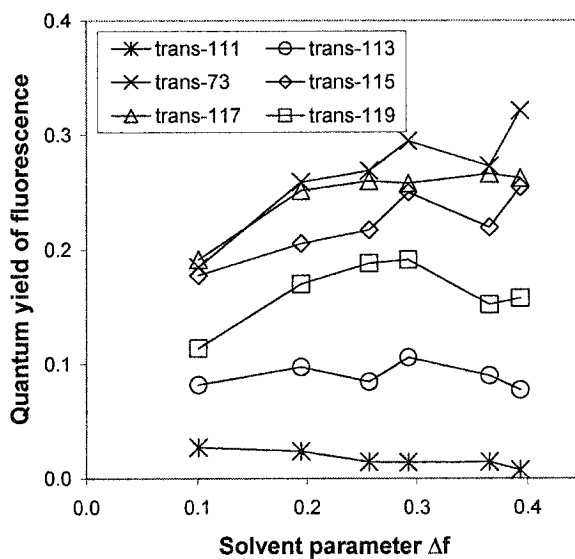


Figure 5.14 Plot of fluorescence quantum yield  $\phi_f$  versus solvent parameter  $\Delta f$  for the *para*-substituted derivatives of *trans*-73 in a series of six solvents.

Solvent	$\Delta f$	<i>trans</i> -112 (3'-OCH <sub>3</sub> )	<i>trans</i> -114 (3'-CH <sub>3</sub> )	<i>trans</i> -73 (H)	<i>trans</i> -116 (3'-F)	<i>trans</i> -118 (3'-CF <sub>3</sub> )	<i>trans</i> -120 (3'-CN)
cyclohexane	0.101	0.20	0.15	0.18	0.22	0.27	0.26
dibutyl ether	0.194	0.24	0.20	0.26	0.27	0.31	0.31
diethyl ether	0.256	0.24	0.20	0.27	0.31	0.36	0.28
ethyl acetate	0.292	0.27	0.24	0.29	0.32	0.38	0.27
2-propanol	0.366	0.25	0.22	0.27	0.30	0.35	0.32
acetonitrile	0.394	0.29	0.26	0.32	0.34	0.34	0.30

Table 5.8 Fluorescence quantum yields for the *meta*-substituted derivatives of *trans*-3,5-dimethoxystilbene in a series of six solvents.

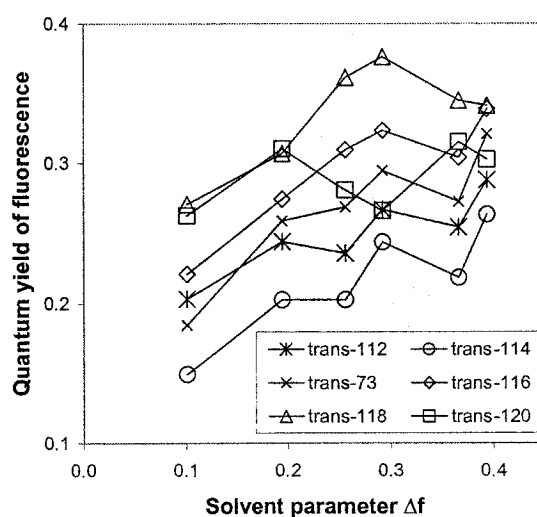


Figure 5.15 Plot of fluorescence quantum yield  $\phi_f$  versus solvent parameter  $\Delta f$  for the *meta*-substituted derivatives of *trans*-73 in a series of six solvents.

The plots of  $\phi_f$  versus  $\Delta f$  in Figures 5.14 and 5.15 are not linear, but there are still some interesting trends in the data. For the para substrates, an increase in polarity induces a slight decrease in  $\phi_f$  for those derivatives with electron donating substituents (*i.e.*, 4'-methoxy *trans*-111 and 4'-methyl *trans*-113). The original compound *trans*-73 displays virtually the same trend in  $\phi_f$  as the 4'-fluoro substrate *trans*-115; both substrates become progressively more fluorescent through the entire solvent series (cyclohexane  $\rightarrow$  acetonitrile). The fluorescence intensity of the 4'-trifluoromethyl substrate *trans*-117 is



essentially constant for most of the solvents used ( $\phi_f \approx 0.26$ ). The 4'-cyano derivative *trans*-119 reaches a maximum value of  $\phi_f = 0.19$  in diethyl ether and ethyl acetate; in solvents of higher or lower polarity the substrate is less fluorescent. The behaviour of the meta derivatives is more uniform: *trans*-73, *trans*-112, *trans*-114, and *trans*-116 all display a steady increase in  $\phi_f$  with increasing solvent polarity. The 3'-trifluoromethyl compound *trans*-118 behaves in a similar fashion as *trans*-119 (4'-cyano), with a maximum emission intensity ( $\phi_f = 0.38$ ) in medium-polarity ethyl acetate. Finally, the results for the 3'-cyano substrate are somewhat anomalous, with substantial variations in  $\phi_f$  across the entire solvent series.

The solvent dependence of the singlet lifetimes of the ten new substrates was also investigated. The lifetime of the 4'-methoxy substrate *trans*-111 was too short to be measured in any of the six solvents. The fluorescence decay data of the other nine substrates *trans*-112-120 were fit reasonably well to a monoexponential decay model. However, as was the case for *trans*-3,5-dimethoxystilbene (*vide supra*, Section 4.2.3), the use of a biexponential decay model gave closer fits to the data and decreased the systematic error in the residual plots. The biexponential model provides both short and long components, although in some cases the value of the short component was below the reliable limit of 0.5 ns for the single photon counting instrument. The short (para substrates Table 5.9, meta substrates Table 5.10) and long (para Table 5.11, meta Table 5.12) components of the lifetimes are provided below, and plots of the lifetimes *versus* the solvent parameter  $\Delta f$  are displayed in Figures 5.16 – 5.19. Also included in the data tables are the average percent contributions from a given component to the overall decay

model; these values changed only slightly from solvent to solvent, and so an average value is adequate for the current discussion.

Solvent	$\Delta f$	<i>trans</i> -111 (4'-OCH <sub>3</sub> )	<i>trans</i> -113 (4'-CH <sub>3</sub> )	<i>trans</i> -73 (H)	<i>trans</i> -115 (4'-F)	<i>trans</i> -117 (4'-CF <sub>3</sub> )	<i>trans</i> -119 (4'-CN)
cyclohexane	0.101	-	0.5	0.9	0.6	1.9	1.3
dibutyl ether	0.194	-	1.2	1.6	1.7	2.7	2.5
diethyl ether	0.256	-	-	1.7	0.3	4.4	3.1
ethyl acetate	0.292	-	0.5	2.1	1.5	4.9	3.7
2-propanol	0.366	-	-	2.0	1.8	4.8	3.1
acetonitrile	0.394	-	0.7	3.9	3.7	5.5	4.4
Average % Contribution		-	85	50	53	45	70

Table 5.9 Short component of biexponential singlet lifetimes for the *para*-substituted derivatives of *trans*-73 in a series of six solvents (all values in nanoseconds).

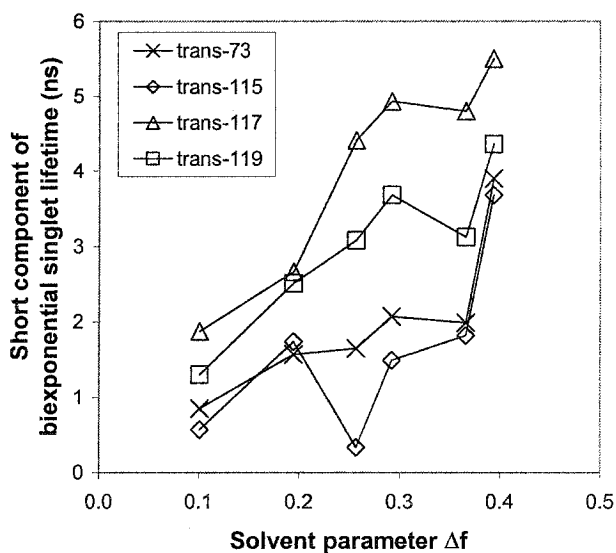


Figure 5.16 Plot of the short component of biexponential singlet lifetimes versus the solvent parameter  $\Delta f$  for the *para*-substituted derivatives of *trans*-73 in a series of six solvents.

Solvent	$\Delta f$	<i>trans</i> -112 (3'-OCH <sub>3</sub> )	<i>trans</i> -114 (3'-CH <sub>3</sub> )	<i>trans</i> -73 (H)	<i>trans</i> -116 (3'-F)	<i>trans</i> -118 (3'-CF <sub>3</sub> )	<i>trans</i> -120 (3'-CN)
cyclohexane	0.101	-	0.3	0.9	1.2	2.0	2.7
dibutyl ether	0.194	0.6	0.8	1.6	3.1	3.4	4.0
diethyl ether	0.256	-	1.6	1.7	3.5	6.1	4.5
ethyl acetate	0.292	-	2.5	2.1	3.7	5.4	5.4
2-propanol	0.366	1.2	1.6	2.0	4.4	4.8	4.4
acetonitrile	0.394	1.9	2.6	3.9	6.4	7.3	4.8
Average % Contribution		53	54	50	33	35	46

Table 5.10 *Short component of biexponential singlet lifetimes for the meta-substituted derivatives of trans-73 in a series of six solvents (all values in nanoseconds).*

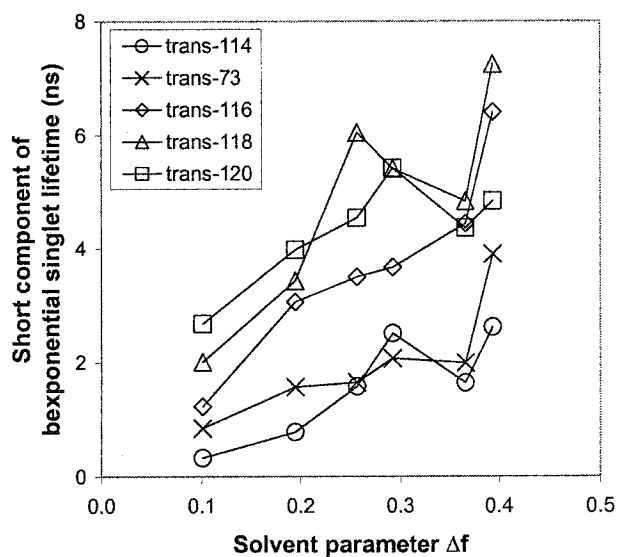


Figure 5.17 Plot of the *short* component of biexponential singlet lifetimes *versus* the solvent parameter  $\Delta f$  for the *meta*-substituted derivatives of *trans*-73 in a series of six solvents.

Solvent	$\Delta f$	<i>trans</i> -111 (4'-OCH <sub>3</sub> )	<i>trans</i> -113 (4'-CH <sub>3</sub> )	<i>trans</i> -73 (H)	<i>trans</i> -115 (4'-F)	<i>trans</i> -117 (4'-CF <sub>3</sub> )	<i>trans</i> -119 (4'-CN)
cyclohexane	0.101	-	1.2	4.0	3.7	8.4	6.3
dibutyl ether	0.194	-	3.0	7.6	6.8	12.9	13.0
diethyl ether	0.256	-	2.8	9.6	8.8	17.3	13.9
ethyl acetate	0.292	-	4.2	12.9	11.6	20.2	17.3
2-propanol	0.366	-	5.3	13.8	12.4	21.7	18.6
acetonitrile	0.394	-	7.0	18.5	16.8	22.7	20.6
Average % Contribution		-	15	50	47	55	30

Table 5.11 *Long component of biexponential singlet lifetimes for the para-substituted derivatives of trans-73 in a series of six solvents (all values in nanoseconds).*

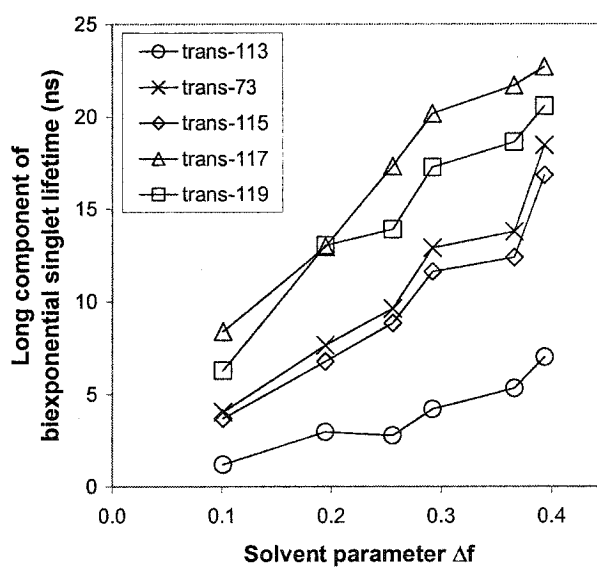


Figure 5.18 Plot of the *long* component of biexponential singlet lifetimes versus the solvent parameter  $\Delta f$  for the *para*-substituted derivatives of *trans*-73 in a series of six solvents.

Solvent	$\Delta f$	<i>trans</i> -112 (3'-OCH <sub>3</sub> )	<i>trans</i> -114 (3'-CH <sub>3</sub> )	<i>trans</i> -73 (H)	<i>trans</i> -116 (3'-F)	<i>trans</i> -118 (3'-CF <sub>3</sub> )	<i>trans</i> -120 (3'-CN)
cyclohexane	0.101	2.3	2.6	4.0	7.3	9.2	9.3
dibutyl ether	0.194	4.5	5.2	7.6	12.2	14.1	14.0
diethyl ether	0.256	6.4	7.4	9.6	15.1	18.9	17.1
ethyl acetate	0.292	8.3	10.5	12.9	18.0	21.8	20.6
2-propanol	0.366	11.0	11.5	13.8	19.5	21.4	20.6
acetonitrile	0.394	16.0	15.6	18.5	24.2	24.2	18.0
Average % Contribution		47	46	50	67	65	53

Table 5.12 Long component of biexponential singlet lifetimes for the *meta*-substituted derivatives of *trans*-73 in a series of six solvents (all values in nanoseconds).

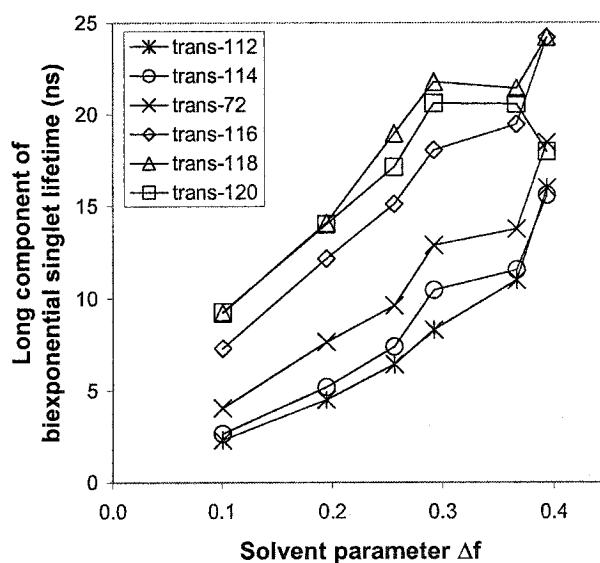


Figure 5.19 Plot of the long component of biexponential singlet lifetimes versus the solvent parameter  $\Delta f$  for the *meta*-substituted derivatives of *trans*-73 in a series of six solvents.

The singlet lifetime results obtained for the nine substituted derivatives of *trans*-3,5-dimethoxystilbene (*trans*-73) are generally the same as for the original substrate itself. Both components of the biexponential fluorescence decay have longer lifetimes in more polar solvents. This trend is more easily observed in the plots for the long components of the para (Figure 5.18) and meta (Figure 5.19) derivatives. The increased scatter in the plots of the short components is due in part to the truncated vertical axis (relative to the long component plots). Another important trend in the data is the longer lifetimes for substrates possessing electron withdrawing substituents – the longest lifetimes in all four data sets are due to the trifluoromethyl derivatives (*trans*-117 or *trans*-118). In contrast, those substrates possessing electron donating substituents have much shorter lifetimes.

The effect of solvent polarity on the quantum yields of fluorescence of *trans*-111-120 was also determined, using the same techniques (300 nm steady state irradiation), solvents (cyclohexane, acetonitrile) and standard (*trans*-stilbene in cyclohexane) as for the investigations in Chapter 4. As indicated in Table 5.13, these results also display some interesting trends. First, the majority of substrates display quantum yields of *trans*-cis isomerization that are lower than that of *trans*-stilbene in cyclohexane ( $\phi_{tc} = 0.40$ )<sup>108</sup> or acetonitrile ( $\phi_{tc} = 0.45$ )<sup>92</sup> – the quantum yield of *trans*-111 in acetonitrile ( $\phi_{tc} = 0.60$ ) is the only value that is significantly larger. The changes in  $\phi_{tc}$  that occur upon increasing the solvent polarity are also quite interesting. As indicated by the arrows in Table 5.13, the substrates can be divided into three categories: 1) those with electron donating substituents (either para or meta), for which  $\phi_{tc}$  is *larger* in a more polar solvent; 2) substrates with electron withdrawing substituents in the para position, for which  $\phi_{tc}$  is

*smaller* in a more polar solvent; 3) substrates with electron withdrawing substituents in the meta position, for which  $\phi_{tc}$  is essentially the *same* in both solvents (note that the unsubstituted compound *trans*-73 is included in the final group).

Substrate	Substituent	$\phi_{tc}^a$ (cyclohexane)	$\phi_{tc}^a$ (acetonitrile)	Change <sup>b</sup> (cyc. → acn.)
<i>trans</i> -111	4'-OCH <sub>3</sub>	0.43	0.60	↑
<i>trans</i> -112	3'-OCH <sub>3</sub>	0.23	0.29	↑
<i>trans</i> -113	4'-CH <sub>3</sub>	0.34	0.44	↑
<i>trans</i> -114	3'-CH <sub>3</sub>	0.21	0.29	↑
<i>trans</i> -73	H	0.29	0.28	—
<i>trans</i> -115	4'-F	0.29	0.23	↓
<i>trans</i> -116	3'-F	0.18	0.18	—
<i>trans</i> -117	4'-CF <sub>3</sub>	0.30	0.24	↓
<i>trans</i> -118	3'-CF <sub>3</sub>	0.21	0.22	—
<i>trans</i> -119	4'-CN	0.42	0.39	↓
<i>trans</i> -120	3'-CN	0.29	0.29	—

a) Determined by steady state irradiation at 300 nm relative to *trans*-stilbene in cyclohexane,  $\phi_{tc} = 0.40$  (Reference 108).

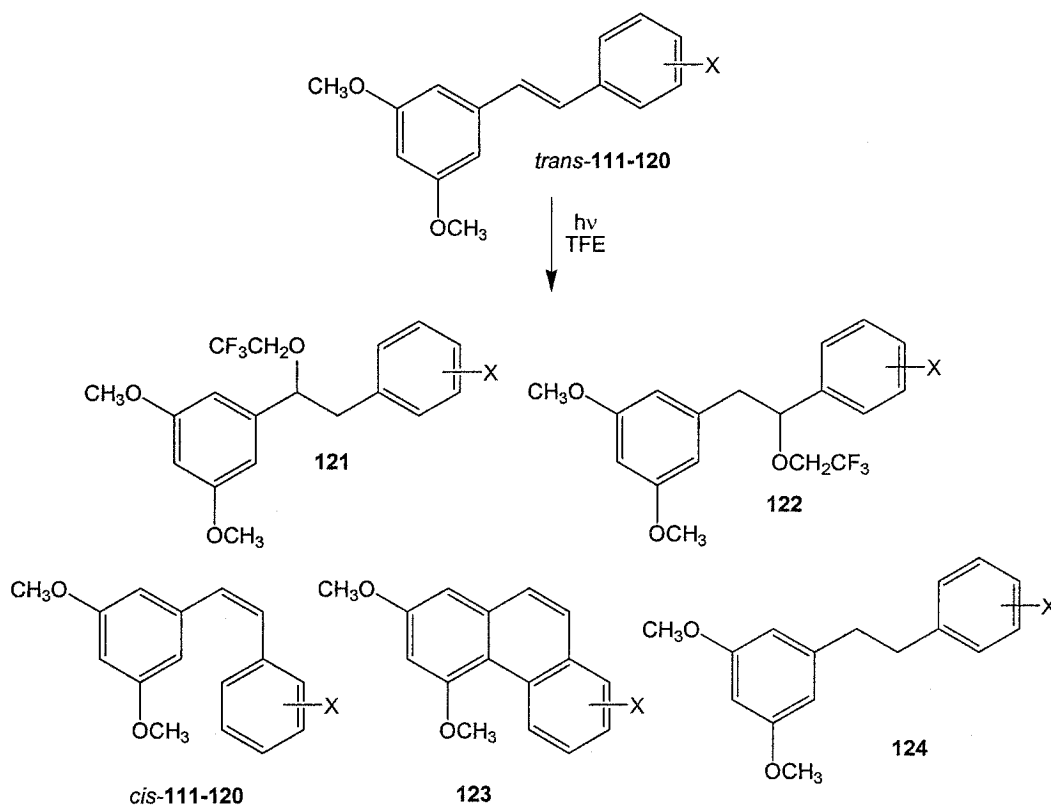
b) The effect of increasing solvent polarity on  $\phi_{tc}$ : increase ↑, no change —, or decrease ↓.

Table 5.13 Quantum yields of isomerization for *trans*-73 and the substituted derivatives *trans*-111-120 in cyclohexane and acetonitrile.

#### 5.2.4 Irradiations of *trans*-111-120 in TFE

The products formed by 300 nm irradiation of *trans*-111-120 in TFE (Scheme 5.5) are essentially the same as those produced by irradiation of the original set of methoxy-substituted *trans*-stilbenes (*vide supra*, Section 3.2.4). Following the initial trans-cis isomerization process, the TFE adducts 121 and 122 are the major products from all ten

irradiations. In addition, small amounts of the phenanthrene product **123** and the reduced product **124** were detected in the reaction mixture. As in previous chapters, these products were assigned on the basis of their GC-MS fragmentation patterns. Many of the reactions are close to completion after ten minutes of irradiation, although *trans*-**111** (4'-methoxy) and *trans*-**120** (3'-cyano) require 30 minutes to reach completion, and *trans*-**119** (4'-cyano) reacts even more slowly (50% conversion after 50 minutes). The yield *versus* time plots are shown in Figures 5.20 (methoxy substituted), 5.21 (methyl), 5.22 (fluoro), 5.23 (trifluoromethyl), and 5.24 (cyano), and the percent conversions and product yields are provided in Table 5.14.



Scheme 5.5 Products detected following 300 nm irradiation of *trans*-**111-120** in TFE.



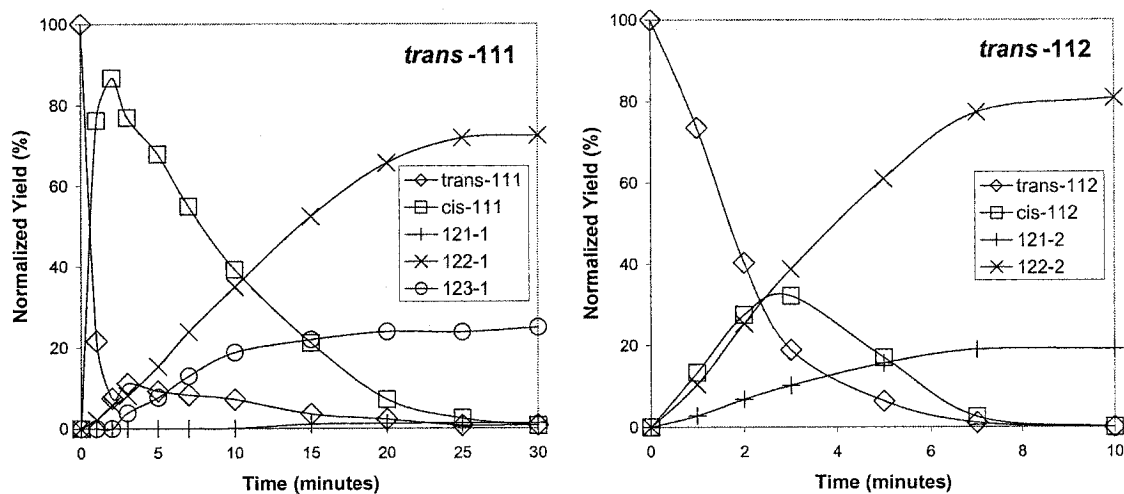


Figure 5.20 Yield versus time plots for the irradiation of *trans*-111 (4'-methoxy, 30 minutes) and *trans*-112 (3'-methoxy, 10 minutes) in TFE (300 nm).

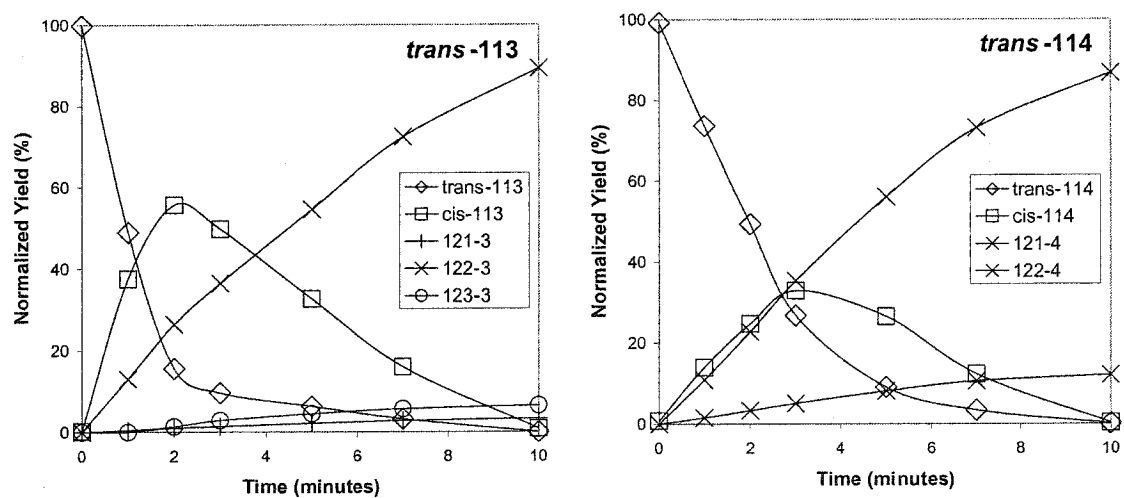


Figure 5.21 Yield versus time plots for the irradiation of *trans*-113 (4'-methyl) and *trans*-114 (3'-methyl) in TFE (300 nm, 10 minutes each).

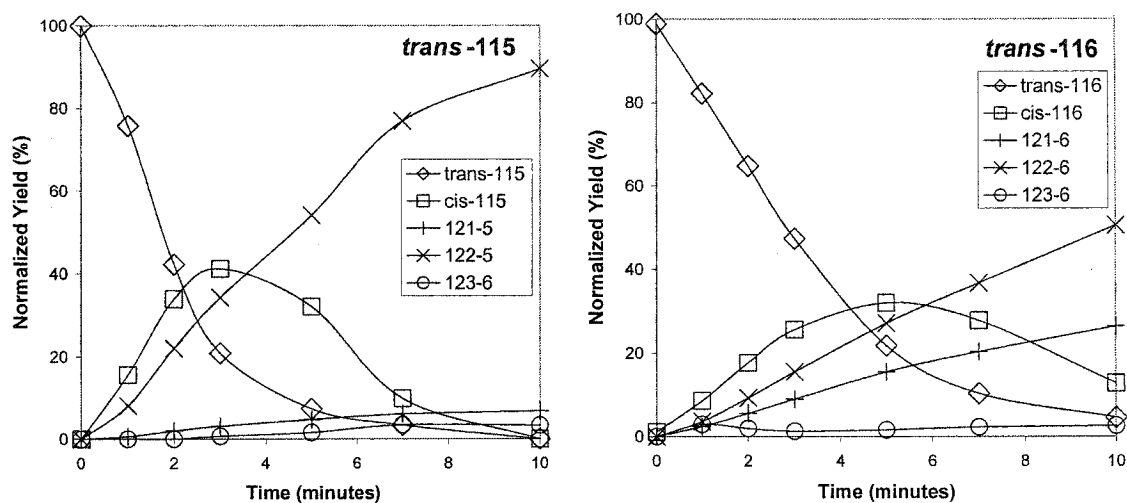


Figure 5.22 Yield versus time plots for the irradiation of *trans*-115 (4'-fluoro) and *trans*-116 (3'-fluoro) in TFE (300 nm, 10 minutes each).

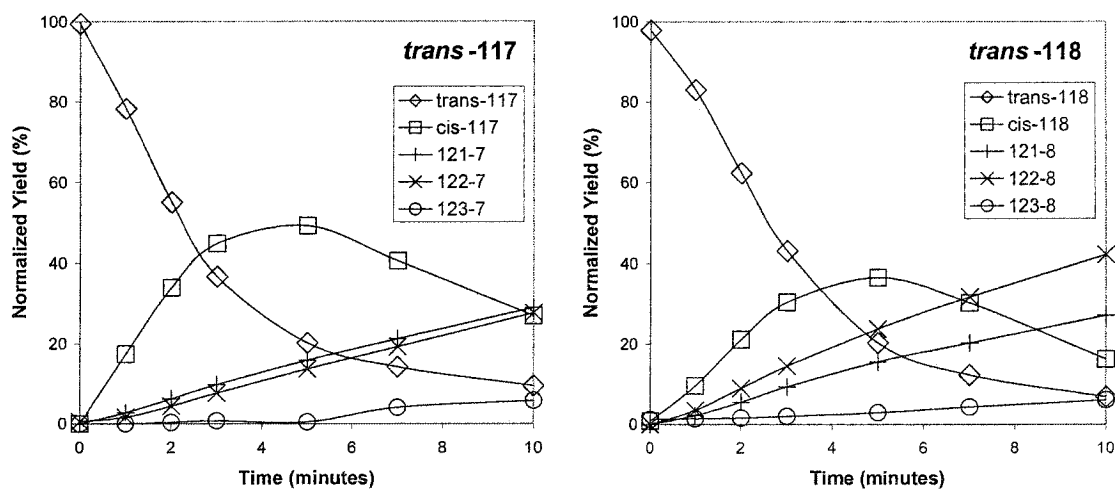


Figure 5.23 Yield versus time plots for the irradiation of *trans*-117 (4'-trifluoromethyl) and *trans*-118 (3'-trifluoromethyl) in TFE (300 nm, 10 minutes each).

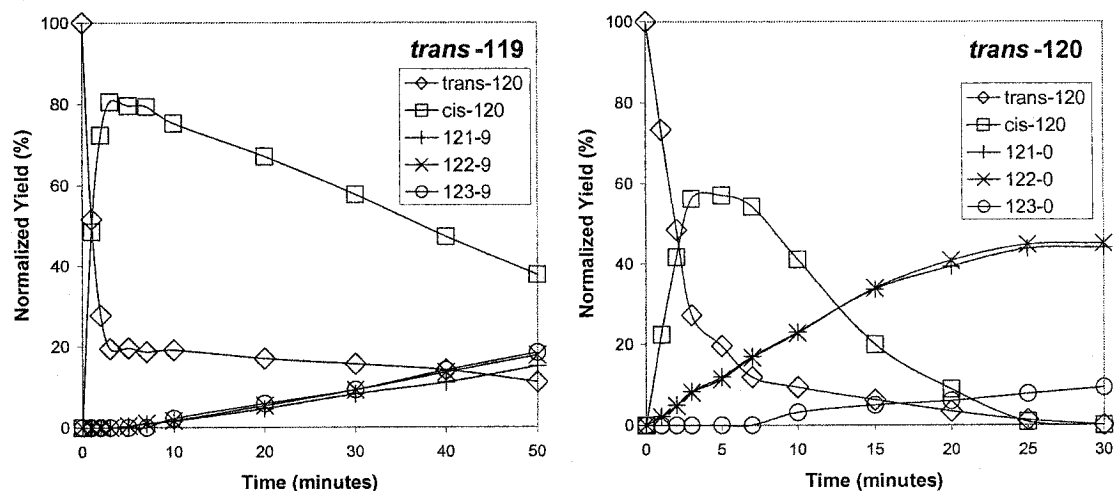


Figure 5.24 Yield *versus* time plots for the irradiation of *trans*-119 (4'-cyano, 50 minutes) and *trans*-120 (3'-cyano, 30 minutes) in TFE (300 nm).

Substrate	Substituent	% Conv. ( <i>cis</i> + <i>trans</i> )	121	122	123	124
<i>trans</i> -111	4'-OCH <sub>3</sub>	42	0	65	35	0
<i>trans</i> -112	3'-OCH <sub>3</sub>	100	19	81	0	0
<i>trans</i> -113	4'-CH <sub>3</sub>	99	3	90	7	0
<i>trans</i> -114	3'-CH <sub>3</sub>	99	12	87	0	1
<i>trans</i> -73	H	100	14	82	2	1
<i>trans</i> -115	4'-F	100	7	90	3	0
<i>trans</i> -116	3'-F	83	32	61	3	4
<i>trans</i> -117	4'-CF <sub>3</sub>	64	46	43	9	2
<i>trans</i> -118	3'-CF <sub>3</sub>	77	35	55	8	2
<i>trans</i> -119	4'-CN	22	29	30	41	0
<i>trans</i> -120	3'-CN	50	46	46	6	1

Table 5.14 Percent conversions and product yields following ten minute irradiation of *trans*-73 and *trans*-111-120 in TFE (300 nm).

Several of the substrates display very high reactivity in TFE; *trans*-112, *trans*-113, *trans*-114, *trans*-73, and *trans*-115 are all completely converted to product within ten minutes of irradiation. Unfortunately, these substrates react so quickly that comparisons of reactivity within this set of five compounds are actually quite difficult. Given that most of the reactive substrates possess electron donating substituents, the very low reactivity of *trans*-111 (4'-methoxy) is somewhat anomalous. For the remaining five substrates (*trans*-116-120), the presence of more powerful electron withdrawing substituents decreases the rate of the TFE addition reaction. Furthermore, the ratio of 122:121 decreases from 30:1 for *trans*-113 (4'-methyl) to 1:1 for *trans*-119 (4'-cyano). Clearly the aryl substituents are capable of controlling the rate of solvent addition, as well as the regiochemistry in the final product mixture.

### 5.3 Discussion of Results

#### 5.3.1 Photophysical Properties of the Substituted Derivatives of *trans*-3,5-Dimethoxystilbene

The majority of the substituted derivatives of *trans*-3,5-dimethoxystilbene (*trans*-73) display properties that are remarkably similar to the original substrate. Compared to *trans*-stilbene itself, these substrates display longer-wavelength fluorescence maxima, much higher quantum yields of fluorescence, reduced quantum yields of trans-cis isomerization, and much longer singlet lifetimes. Although all of these properties have already been well-established for a variety of meta aminostilbenes,<sup>98,100</sup> several important characteristics of the *trans*-3,5-dimethoxystilbene chromophore make this "meta methoxy effect" a completely novel phenomenon.

In Chapters 3 and 4, the unique photophysical properties of *trans*-73 were explained on the basis of the meta effect. This theory was originally described by Lewis and co-workers in order to rationalize the small quantum yield of isomerization, large quantum yield of fluorescence, and long singlet lifetime displayed by *trans*-3-aminostilbene (*trans*-63).<sup>98</sup> Indeed, this effect (an increase in the barrier for excited state C=C bond torsion) does explain very similar photophysical properties of *trans*-63 and *trans*-73. In addition to the apparent connection between  $\phi_{tc}$ ,  $\phi_f$ , and  $\tau_s$ , both substrates have quite high excited state dipole moments ( $\mu_e = 13.2$  D for *trans*-73, 11.9 D for *trans*-63). However, the two compounds display different changes in their photophysical properties as solvent polarity is increased. For *trans*-63, the quantum yield of isomerization increases ( $\phi_{tc} = 0.09$  in cyclohexane, 0.24 in acetonitrile), the quantum yield of fluorescence decreases ( $\phi_f = 0.78$  in cyclohexane, 0.40 in acetonitrile), and the singlet lifetime becomes longer ( $\tau_s = 7.5$  ns in cyclohexane, 11.7 ns in acetonitrile).<sup>98</sup> The monoexponential singlet lifetime of *trans*-73 also becomes longer as the polarity of the solution is increased ( $\tau_s = 3.7$  ns in cyclohexane, 16.9 ns in acetonitrile), but the fluorescence quantum yield *increases* ( $\phi_f = 0.17$  in cyclohexane, 0.32 in acetonitrile) and the quantum yield of isomerization remains constant ( $\phi_{tc} = 0.29$ ). The observation of higher  $\phi_f$  values in more polar solvents is an indication that the excited state of *trans*-73 displays significant charge transfer character. Thus, *trans*-3,5-dimethoxystilbene appears to possess the properties of *both* meta amino stilbenes *and* traditional donor-acceptor stilbenes.

The investigations that have been performed for the substituted derivatives of *trans*-73 (*trans*-111-120) reinforce the ideas presented above. In most cases the

photophysical properties of these new substrates are similar to those of *trans*-73, and many differences from the parent chromophore can be explained on the basis of the electron donating or electron withdrawing nature of the substituent. The 4'-methoxy substrate *trans*-111 is the exception for this generalization. Most of the properties displayed by *trans*-111 are more similar to those of *trans*-stilbene itself than to the other substrates in the current study. In particular, the fluorescence quantum yield of this substrate is quite low, and decreases even further as the solvent polarity is increased ( $\phi_f = 0.03$  in cyclohexane, 0.007 in acetonitrile). These values are very similar to those of *trans*-4-methoxystilbene (*trans*-71) from the investigations in Chapters 3 and 4 ( $\phi_f = 0.02$  in cyclohexane, 0.006 in acetonitrile). Indeed, these two substrates also display very similar isomerization properties, and neither compound was amenable to singlet lifetime measurements. These results indicate that a 4-methoxy substituent determines the photochemistry of the stilbene chromophore, even when conjugated to the 3,5-dimethoxyphenyl system. The photophysical properties of *trans*-4-methoxy-4'-cyanostilbene ( $\phi_f = 0.008$ ,  $\tau_s = 0.020$  ns), reported in the literature by Likhtenshtein and co-workers,<sup>147</sup> indicate that conjugation to a strong electron donor does not significantly alter the behaviour of the 4-methoxystilbene chromophore.

Aside from the behaviour of *trans*-111, some very clear trends are observed in the data for the substituted derivatives of *trans*-3,5-dimethoxystilbene. The solvent-induced Stokes' shifts indicate that the emitting states of most of the substrates *trans*-112-120 are highly polarized, and are likely to display a high degree of charge transfer character. The increase in solvatochromic slope for substrates bearing electron withdrawing substituents in the para position supports the early hypothesis that the 3,5-dimethoxyphenyl ring acts

as an electron donor in the excited state. In other words, decreasing the electron density in the central C=C bond accentuates the excited state charge transfer process. The very similar solvatochromic slopes of the meta substituted derivatives are consistent with the expectation that meta substituents are less able to alter the electron density in the alkene bond. Although the excited state dipole moments of most derivatives have not yet been calculated, the value obtained for the 4'-cyano substrate *trans*-**119** ( $\mu_e = 19.8$  D) provides excellent support that charge transfer states are formed following excitation. Indeed, this value is greater than that of *trans*-**73** itself ( $\mu_e = 13.2$  D), and is actually quite close to the literature value for the extensively studied donor acceptor stilbene **109** ( $\mu_e = 21$  D).<sup>143</sup>

The fluorescence quantum yield measurements are more difficult to interpret. Although the fluorescence intensity of *trans*-**73** increases steadily across the entire series of solvents, several of the para substrates reach a maximum fluorescence intensity in medium polarity solvents, and  $\phi_f$  then decreases as the polarity is raised further (Figure 5.14). The 4'-cyano derivative *trans*-**119** provides the best example of this effect. Another interesting observation is that, for any given solvent, the typical values of  $\phi_f$  increase through the series of electron donating substituents (4'-methoxy < 4'-methyl < unsubstituted) and then *decrease* through the series of electron withdrawing substituents (unsubstituted > 4'-fluoro  $\approx$  4'-trifluoromethyl > 4'-cyano). The reasons behind these trends are not immediately clear. However, Gruen and Görner have reported that the quantum yield of fluorescence of the donor-acceptor stilbene *trans*-4-N,N-dimethylamino-4'-nitrostilbene (the nitro analogue of **109**) increases from  $\phi_f = 0.33$  in cyclohexane to  $\phi_f = 0.55$  in diethyl ether, and then falls to  $\phi_f = 0.002$  in acetonitrile.<sup>146</sup> The researchers proposed that, in polar solvents, radiationless decay of highly polarized

ICT states becomes a more important deactivation pathway. A similar effect could account for some of the trends observed in Figure 5.14. In general, the meta-substituted derivatives of *trans*-**73** become more highly fluorescent in more polar solvents (Figure 5.15), and do not display the same behaviour as the para substrates.

The observation that most of the substituted derivatives of *trans*-3,5-dimethoxystilbene display biexponential singlet lifetimes is of great interest. This type of behaviour has not been observed for any of the meta amino derivatives investigated by Lewis and co-workers. That both components of the lifetimes become longer in solvents of higher polarity indicates that the two emitting states are themselves polar. Furthermore, both components of the singlet lifetimes are generally longer for substrates bearing electron withdrawing substituents. The only two singlet states that are postulated in the energy co-ordinate diagram for donor-acceptor stilbene photochemistry (Scheme 5.2) are the Frank-Condon state  $t_{S_1}^{FC}$  and the charge transfer state  $t_{S_1}^{CT}$ . Thus, tentative assignments for the short and long components of the singlet lifetimes are  $t_{S_1}^{FC}$  and  $t_{S_1}^{CT}$ , respectively.

The detection of both  $t_{S_1}^{FC}$  and  $t_{S_1}^{CT}$  using fluorescence spectroscopy at nanosecond resolution is a very surprising observation. As such, great care must be taken to ensure that one of the two components is not due to some other chemical species in the same sample. Based on the studies by Lewis and co-workers for *cis*- and *trans*-3-aminostilbene,<sup>99,98</sup> the *cis* isomers of *trans*-**112-120** are unlikely to be responsible for either of the fluorescent signals. Future investigations will be required to ascertain that the substrates do not contain some emissive impurity. However, this possibility seems very unlikely, given the steps taken to purify each compound and the absence of any other species by GC or NMR. For the time being, the best explanation for the observations is



that  $t_{S_1}^{FC}$  and  $t_{S_1}^{CT}$  are responsible for the biexponential lifetimes of *trans*-**73** and *trans*-**112-120**. Provided that these assignments are correct, the question arises; Why are these two species so long-lived for the case of the 3,5-dimethoxystilbene system? The best explanation is that the lifetime of  $t_{S_1}^{FC}$  is prolonged by the meta methoxy effect, while  $t_{S_1}^{CT}$  is a highly stabilized charge transfer state that may involve twisting about C-O or C-C single bonds. Without further investigations, assessment of these proposals is impossible.

Finally, the solvent dependence of the isomerization quantum yields deserves some discussion. For those substrates bearing electron donating substituents,  $\phi_{tc}$  is slightly larger in acetonitrile than in cyclohexane; this may indicate that the barrier for excited state bond torsion is polarizable for these substrates. Note that this set of compounds includes the 4'-methoxy substrate *trans*-**111**, for which this explanation seems very likely. In contrast, those substrates with electron withdrawing substituents in the para position have lower values of  $\phi_{tc}$  in more polar solvents. Formation of ICT states should be quite favourable for these substrates. Zachariasse and co-workers have determined that, for donor-acceptor stilbenes such as **109**, the stabilization of  $t_{S_1}^{CT}$  by polar solvents leads to an *increase* in the barrier for excited state bond rotation (process  $t_{S_1}^{CT} \rightarrow p_{S_1}$  in Scheme 5.2). Measurements for **109** indicate that the torsional barrier is raised from 3.3 kcal/mol in heptane to 5.4 kcal/mol in acetonitrile.<sup>143</sup> This behaviour, which is opposite to the decrease in the barrier for *trans*-stilbene, accounts for the observed decrease in the quantum yield of isomerization for **109** ( $\phi_{tc} = 0.45$  in cyclohexane, 0.40 in acetonitrile).<sup>101</sup> A similar effect appears to be present for *trans*-**115** (4'-fluoro), *trans*-**117** (4'-trifluoromethyl), and *trans*-**119** (4'-cyano). In contrast,

substrates possessing electron donors in the meta position (and also *trans*-73 itself) have essentially the same quantum yields of isomerization in either solvent. Apparently for these substrates the two affects of higher polarity solvents (stabilization of  $t_{S1}^{CT}$  and polarization of the  $t_{S1}^{CT} \rightarrow p_{S1}$  barrier) perfectly offset one another.

### 5.3.2 Photoprotonation of the Substituted Derivatives of *trans*-3,5-Dimethoxystilbene

The claim that the photophysical properties of *trans*-111-120 are similar to those of the parent *trans*-3,5-dimethoxystilbene *trans*-73 is further supported by the photochemistry of these substrates in TFE. Most of the ten derivatives undergo rapid addition of TFE during the steady state irradiations. That the 4'-methoxy substrate *trans*-111 is the least reactive compound studied is likely due to its high quantum yield of isomerization in polar solvents ( $\phi_{tc} = 0.60$  in acetonitrile). Like the 4-methoxystilbenes investigated in Chapters 3 and 4 (*trans*-71 and *trans*-74), deactivation of the *trans*-111 excited state by rapid trans-cis isomerization decreases the rate of the solvent addition reaction.

The trends in reactivity displayed by the other ten substrates provide further insight into the photoprotonation mechanism that was proposed in Chapter 4. The observation that substrates with electron donating substituents undergo TFE addition more rapidly than those compounds bearing electron withdrawing substituents might appear to contradict the earlier mechanistic arguments. In particular, the order of reactivity displayed by the original set of five methoxy-substituted *trans*-stilbenes was determined in large part by their singlet lifetimes – longer lifetimes were believed to increase the likelihood of the bimolecular photoprotonation step. Since the discussion in

Section 5.3.1 has established that substrates bearing electron donating substituents possess long-lived charge transfer states, these substrates might also be expected to be the most reactive towards photoprotonation reactions.

The line of reasoning just offered neglects the important fact that the critical step in the solvent addition reactions is, in essence, an acid-base reaction. Although the presence of electron withdrawing substituents does enhance the formation ICT states, the *location* of electron density in the ICT state itself is likely to be critical factor for the reactivity of a given substrate. Strong electron withdrawing substituents, while promoting ICT, probably also increase electron density on the aryl ring rather than at the central alkene bond. Since the latter position is the site of photoprotonation that leads to formation of solvent adducts **121** and **122**, efficient formation of a highly polarized ICT state does not completely ensure rapid product formation.

Another important aspect of the reactions described in Section 5.2.4 is that virtually all of the substrates have quite long singlet lifetimes and low quantum yields of isomerization. In particular, the substrate-to-substrate variation in  $\tau_s$  is not nearly as great for *trans*-**112-120** as it was for the methoxy-substituted *trans*-stilbenes studied in Chapters 3 and 4. For the latter substrates, the enormous variation in  $\tau_s$  (over two orders of magnitude) determined the order of reactivity in the solvent addition reactions; for the new substituted derivatives, where the values of  $\tau_s$  are all quite similar, the *location* of electron density in the excited state also becomes important. The situation is similar to that of the methoxy-substituted styrenes and *trans*-1-arylpropenes, for which trans-cis isomerization is not the major pathway for deactivation of the excited state (*vide supra*, Section 4.3.3).

The final point of discussion for the TFE addition reactions is the regiochemistry in the products. An initial hypothesis for these experiments was that the relative yields of **121** and **122** might somehow correlate with the biexponential lifetime results, *i.e.*, that trapping of either  $t_{S_1}^{FC}$  or  $t_{S_1}^{CT}$  might provide unique products. The data do not appear to support this notion; the relative contributions from the short ( $t_{S_1}^{FC}$ ) and long ( $t_{S_1}^{CT}$ ) components of the fluorescence decay are generally quite similar ( $\approx 50:50$ ) for most substrates, but the ratios of **121** and **122** are more variable.

A more thorough inspection of the data clearly indicates that the yields of the two solvent adducts are mechanistically related. Figures 5.25 and 5.26 provide Hammett plots for the formation of **121** and **122**, respectively. For this analysis, Equations 5.1 and 5.2 were employed. The yields in these equations are those of **121** and **122** (the TFE adducts formed by reaction of the substituted derivatives *trans*-**111**-**120**, Scheme 5.5) and **75b-3** and **76b-3** (the *same* two TFE adducts for the *unsubstituted* compound *trans*-**73**, Scheme 3.5). The important difference between these equations and the original Hammett treatment (Equation 1.4) is the use of product yields instead of reaction rates. The expectation that the photoprotonation reactions are irreversible means that the treatment should be valid. The values of  $\sigma^+$  in Table 1.1 were used for the data analysis. Unfortunately, the results for the 4'-methoxy substrate *trans*-**111** and the two cyano substrates *trans*-**119** and *trans*-**120** did not fit the trends observed in the Hammett plots – none of the products from these three compounds are included in Figures 5.25 and 5.26.

$$\log \left( \frac{\% \text{ Yield of } \mathbf{121}}{\% \text{ Yield of } \mathbf{75b-3}} \right) = \rho^+ \sigma^+ \quad (5.1)$$

$$\log \left( \frac{\% \text{ Yield of } \mathbf{122}}{\% \text{ Yield of } \mathbf{76b-3}} \right) = \rho^+ \sigma^+ \quad (5.2)$$

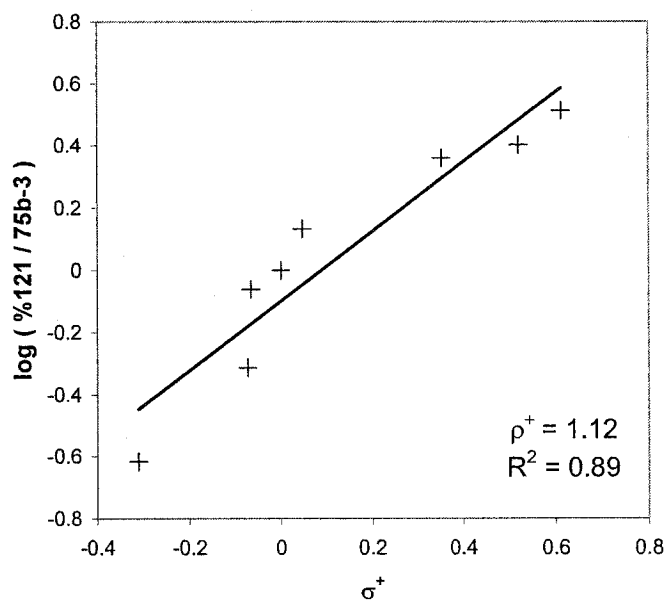


Figure 5.25 Plot of the yield of TFE adduct **121** (data in Table 5.14) *versus*  $\sigma^+$  (values in Table 1.1) using a modified Hammett treatment (Equation 5.1).

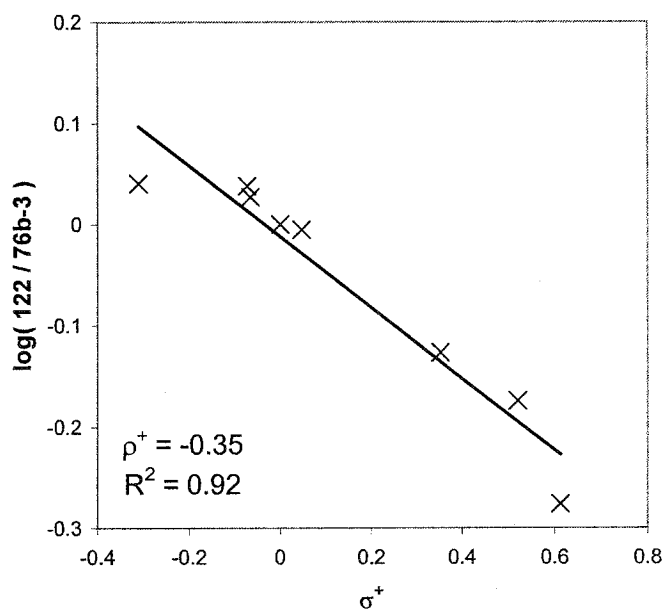


Figure 5.26 Plot of the yield of TFE adduct **122** (data in Table 5.14) *versus*  $\sigma^+$  (values in Table 1.1) using a modified Hammett treatment (Equation 5.2).

The good linear correlations from these results ( $r^2 = 0.89$  for **121**, 0.92 for **122**) indicate that the relationships in Equations 5.1 and 5.2 are valid. Furthermore, the magnitude and sign of the  $\rho^+$  values corroborate the mechanistic details that were outlined in Chapter 4. The formation of **122** proceeds by way of a short-lived carbocation intermediate with positive charge on the carbon adjacent to the substituted ring, as indicated by the small, negative value of  $\rho^+ = -0.35$  (i.e., favoured for electron donating substituents). In contrast, the positive value of  $\rho^+ = 1.12$  for the formation of **121** is somewhat surprising, given that the reaction should also involve a carbocation intermediate. However, the cation that leads to **121** will be remote from the substituted ring, and so the influence of these substituents on the transition state leading to the carbocation will actually be quite small. Instead, the substituents assist in the formation of **121** by favouring the polarized excited state that leads to formation of the cation intermediate. Although products **121** and **122** are produced by identical mechanistic pathways (protonation of excited states to yield carbocation intermediates), the ability of the substituents to assist in product formation depends entirely on the charge requirement at the benzylic site next to the substituted ring. That the magnitude of  $\rho^+$  is larger for **121** than for **122** may support the idea that protonation is the rate-limiting step in the reaction mechanism.

## Chapter 6                      Conclusions and Future Work

### 6.1      Summary and Conclusions

Although the initial goal of this research – the direct observation of carbocation rearrangements by laser flash techniques – was not realized, the work has provided much information regarding the formation of carbocations *via* photochemical reactions. The investigations of the bichromophoric ester **44** (Chapter 2) emphasized the importance of orbital overlap for carbocation rearrangement reactions. The results indicate that **44** does yield carbocation intermediates upon photofragmentation, but that the subsequent reactions of the cation do not involve the expected 1,2-hydride shift. Instead, the cation undergoes either nucleophilic attack or deprotonation by alcohol solvents. The absence of rearrangement chemistry is attributed to conformational restriction of the intermediate cation, which in turn prevents the prerequisite orbital overlap.

Despite the difficulties encountered with the rearrangement studies, a by-product of the ester photolysis reaction displayed some interesting photochemistry of its own. In particular, the photochemical addition of TFE to the methoxy-substituted stilbene derivative **52** was found to be a reasonably efficient reaction. The experiments described in Chapter 3 demonstrate that this photoaddition reaction is general for methoxy-substituted stilbenes, and that the rate of the reaction is enhanced by meta methoxy substituents. In addition to the differences in photochemical reactivity, the substrates also have very different photophysical properties. Of particular interest is *trans*-3,5-dimethoxystilbene (*trans*-**73**), which has a highly fluorescent, long-lived singlet state in comparison to typical stilbene derivatives. Furthermore, the fluorescence of this substrate

is quenched in mixtures of acetonitrile and TFE in a trend that parallels the yield of solvent adduct from steady state irradiations.

The mechanism of the TFE photoaddition reaction was investigated more completely in Chapter 4. The order of reactivity for the photochemical addition of TFE to several methoxystyrenes and *trans*-1-arylpropenes is quite different than the order of reactivity for the corresponding methoxystilbenes, indicating that the stilbene reactions are controlled by different excited state properties. The main difference is concluded to be the rate of *trans*-*cis* isomerization, which is a much more rapid process for the stilbene derivatives. The solvatochromic behaviour of the stilbenes revealed that their excited states are highly polarized in comparison to their ground states. This effect is particularly strong for the 3,5-dimethoxy substrate, which was also found to display biexponential fluorescence decay. In addition, both the fluorescence quantum yield and singlet lifetime of the 3,5-dimethoxy substrate are increased in more polar solvents. The other four stilbene derivatives (unsubstituted, 4-methoxy, 3-methoxy, and 3,4-dimethoxy) are all less fluorescent in polar solvents. Furthermore, the quantum yields of isomerization for these four substrates are higher in acetonitrile than in cyclohexane – a model involving polarization of the barrier for excited state bond torsion may explain this behaviour.

Preliminary LFP investigations of the methoxy stilbenes in HFIP solution produced transient species, which are assigned as carbocation intermediates resulting from photoprotonation substrates. Following irradiation of the substrates in deuterated TFE (TFE-OD),  $^1\text{H}$  NMR and GC-MS experiments indicated that deuterium and the trifluoroethoxy nucleophile are bound to different carbons in the photoproducts. The ratios of *syn* addition to *anti* addition (determined by  $^1\text{H}$  NMR) are consistent with the



proposed photoprotonation mechanism, and also with the expected stability of the carbocation intermediates.

The goal of the work described in Chapter 5 was to explore the unique photophysical and photochemical properties of the *trans*-3,5-dimethoxystilbene chromophore. To this end, a series of substituted derivatives of this substrate were synthesized with methoxy, methyl, fluoro, trifluoromethyl, and cyano substituents in the 3' and 4' positions. The photophysical properties displayed by most of these substrates are very similar to those of the parent chromophore: high fluorescence quantum yields, reduced trans-cis isomerization quantum yields, and long-lived singlet states that decay with biexponential kinetics. Furthermore, the solvatochromic slopes obtained for these compounds indicate that electron withdrawing substituents enhance the formation of highly polarized, internal charge transfer excited states. These substrates are also quite reactive in TFE; the yields of the two addition products are well correlated with the  $\sigma^+$  scale, further supporting the presence of carbocations in the reaction mechanism.

## 6.2 Future Work

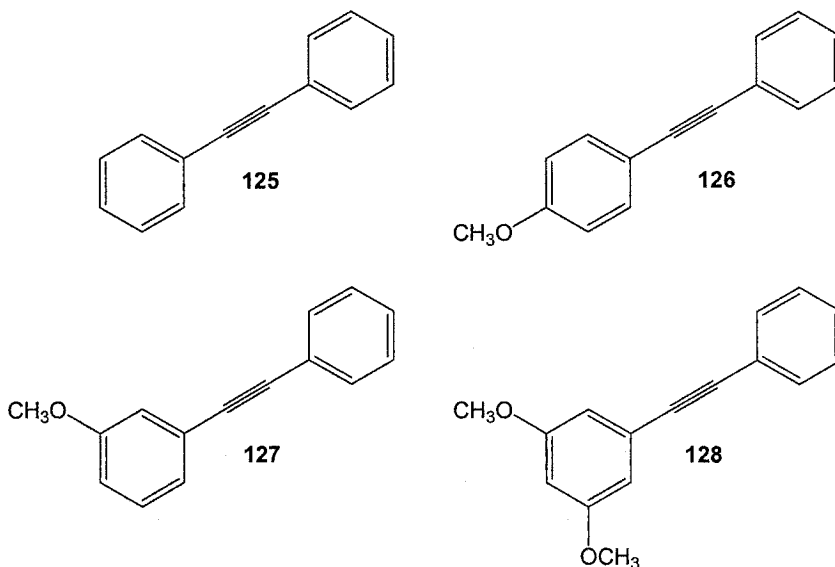
There are three different categories of experiments that fit under the heading of "future work." The first category corresponds to those experiments which definitely need to be performed in order to complete the current investigations. For example, the LFP studies discussed in Chapter 4 need to be revisited. Although the transient signals from the methoxy-substituted stilbene derivatives are more difficult to detect than those of the original styrene substrates, perhaps careful experiments with purified solvents will provide values of  $k_{\text{HFIP}}$  that are closer to the literature values.<sup>47</sup> In addition, further

experiments should allow determination of rate constants for the quenching of the transients by nucleophiles.

Another aspect of the current investigations that should be addressed in the near future is the calculation of dipole moments for the ground and excited states of *trans*-111-120. The solvatochromic slopes indicate that these substrates should possess very large values of  $\mu_e$ , which may provide some insight into the other photophysical properties. The biexponential lifetimes displayed by these substrates definitely need to be pursued in greater detail. As indicated in Section 5.3.2, an unusual observation such as this needs to be fully validated in order to be sure that the excited state manifolds of the substrates are responsible for *both* emitting species.

The second division of future work encompasses some new experiments that may provide additional information regarding the systems described in the current report. For example, the quenching of methoxystilbene fluorescence in aqueous systems may allow direct comparisons between the photoprotonation behaviour of the methoxystilbenes and the extensively studied styrenes. Another area of potential investigation is the temperature dependence of the photophysical properties of the methoxy-substituted stilbene derivatives. The determination of the heights of the barriers for excited state bond torsion is important for a complete discussion of these substrates and their photochemistry. Lewis and co-workers have had great success with the aminostilbenes in this regard, and a true comparison of the meta methoxy effect and the meta amino effect is certainly of interest. Recent results from the Pincock group have employed similar methods to investigate the temperature dependence of photochemical reactions,<sup>148</sup> so an investigation of the stilbene derivatives is a viable prospect.

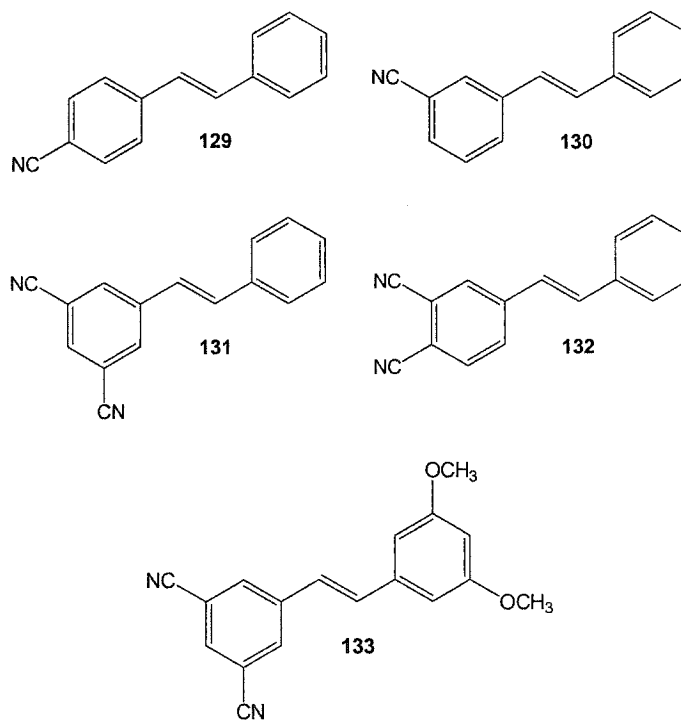
Finally, there are several new projects that may be investigated in relation to the current work. One project already in progress is the photophysical properties of methoxy-substituted diphenylacetylene derivatives, **125-128**.<sup>149</sup> The photohydration reactions of many phenyl acetylenes have been extensively studied, and so extension to the diphenylacetylene system is a logical progression for the current studies.



The charge transfer excited states displayed by *trans*-3,5-dimethoxystilbene and its substituted derivatives *trans*-**111-120** present ample opportunity for new investigations. The role that TICT states may play in the unusual photophysical properties of these substrates needs to be further evaluated. Detection of these structural changes is often accomplished by comparing the properties of the original substrate with those of a bridged derivative for which rotation about single bonds is impossible (**107** and **108** are examples, Section 5.1.1). The synthesis of substrates that restrict the motion of the *trans*-3,5-dimethoxystilbene chromophore may be investigated in the future.

A final potential research project is much more speculative in nature, but should not be difficult to attempt. The meta effect in stilbene photochemistry is thus far

restricted to electron donating substituents. However, the study of substrates with electron *withdrawing* substituents may yield interesting results. The cyano-substituted derivatives **129-132** should be easily prepared by Wittig chemistry, and would make for an interesting comparison with the methoxy derivatives from the current report. Another substrate that may display very interesting photophysical properties is the meta donor-acceptor stilbene **133**, where an excited state electron *donor* (3,5-dimethoxyphenyl) is coupled to an excited state electron *acceptor*. Clearly, there are many interesting projects that may be pursued in the future.



## Chapter 7 Experimental Details

### 7.1 General Methods and Techniques

#### 7.1.1 Introduction

This chapter provides details regarding the experiments described in Chapters 2-5. Following a description of the techniques that were employed throughout the current studies (Section 7.1.2), Sections 2-5 will give explanations of methods and results particular to the corresponding chapter (for example, Section 7.2 describes the methods/results from Chapter 2, and so forth).

#### 7.1.2 Experimental Methods

$^1\text{H}$  and  $^{13}\text{C}$  NMR spectra were recorded in deuterated chloroform on a Bruker AC 250F instrument (Chapter 2) or a Bruker AVANCE 500 MHz instrument (Chapters 3-5). Chemical shifts ( $\delta$ ) are reported as parts per million (ppm) relative to tetramethylsilane internal standard. The coupling constants of the ABX systems observed in several compounds were analyzed by matching the line positions with those of simulated spectra. Gas chromatography was performed on a Perkin-Elmer Autosystem XL instrument (controlled by a computer with TurboMass and TurboChrom software) with one Turbomass detector and one flame ionization detector (both columns: Supelco 30 m / 0.25 mm MDN-5S 5% phenyl methylsiloxane, film thickness 0.50  $\mu\text{m}$ ). For GC-MS, the injection volume was 1  $\mu\text{L}$ ; mass spectral characterization data are reported in units of mass over charge ( $m/z$ ) with intensities relative to the base peak (in brackets) for those signals greater than 10% relative to the base peak. For GC-FID, an injection volume of 2.5  $\mu\text{L}$  was used. High resolution mass spectra (HRMS) were obtained using a

Consolidated Electrodynamics Corporation 21-110B sector instrument with 70 eV ionization. Ultraviolet spectra were recorded on a Varian – Cary Bio 100 spectrometer using a path length of 1 cm and baseline correction for the solvent. Fluorescence spectra were recorded with a PTI Model L201M fluorescence spectrometer with dual model 101 monochromators, a 75 W Xenon lamp, and a model 814 photomultiplier detector. All fluorescence spectra were corrected for the response of the instrument. Singlet lifetimes were determined by monitoring fluorescence decay with a PRA system 3000, which was equipped with a hydrogen filled model 510 PRA arc lamp operating at 30 000 Hz. The pulse width at half height was approximately 1.8 ns (a separate lamp profile was recorded following each measurement). All fluorescence data (steady-state and time-resolved) were obtained using a path length of 1 cm and samples that were degassed by three freeze-pump-thaw cycles. LFP was performed using either a Continuum Nd:Yag NY-61 laser (266 nm, 15 mJ/pulse, 8 ns pulse width) for the experiments in Chapter 2, or a Lambda-Physik XeCl excimer laser (308 nm, 75 mJ/pulse, 8 ns pulse width) for the experiments in Chapter 4. Analysis and plotting of most data was performed using the Microsoft Excel 2003 software package, but the singlet lifetimes were determined using the MatLab 6.5 software package.

### **7.1.3 Common Laboratory Reagents**

For preparative reactions, methanol, water, ethyl acetate and hexanes were all distilled prior to use. Dichloromethane, benzene, dimethylsulfoxide (DMSO), diethyl ether, and pentane were all reagent grade solvents that were used without further purification. Tetrahydrofuran (THF) was distilled from sodium/ benzophenone. For photochemical studies, acetonitrile, 2-propanol, methanol, ethyl acetate, hexanes, and cyclohexane were all spectrophotometric or HPLC grade solvents, while dibutyl ether and diethyl ether were anhydrous reagent grade. All starting materials required for synthetic

reactions were supplied by Aldrich Chemicals, with the following exceptions: 3,5-dimethoxyaniline, 3,5-dimethoxybenzaldehyde, 4-fluorobenzaldehyde, 3-fluorobenzaldehyde, 3-trifluorobenzaldehyde, and triphenylphosphine (Avocado Chemicals), trans-stilbene and sodium sulphate (BDH). Thin layer chromatography was performed using plates from Eastman-Kodak. Preparative chromatography was performed using 60-250 mesh silica gel from Silicycle.

## 7.2 Procedures for Chapter 2 Experiments

### 7.2.1 Synthetic Procedures

3,5-Dimethoxybromobenzene (**48**). This compound was prepared from the diazonium ion made from 3,5-dimethoxyaniline using the procedure described<sup>74</sup> for the synthesis of *o*-bromochlorobenzene, yield 33%: mp 64-65 °C, lit.<sup>75</sup> 64-66 °C; <sup>1</sup>H NMR  $\delta$ : 6.66 (d, 2H, *J* = 2.4 Hz), 6.37 (t, 3H, *J* = 2.4 Hz), 3.76 (s, 6H); <sup>13</sup>C NMR  $\delta$ : 161.2, 123.0, 109.8, 99.8, 55.5; GC-MS *m/z*: 218 (82.6), 216 (100.0), 108 (69.7), 79 (41.6), 77 (56.2), 63 (48.9).

2-(4-Methoxyphenyl)ethanal (**49**). This compound was prepared from 4-methoxybenzaldehyde by glycidic ester condensation as described by Macchia and co-workers,<sup>76</sup> yield of 74% over three steps: <sup>1</sup>H NMR  $\delta$ : 9.66 (d, 1H, *J* = 2.4 Hz), 7.09 (d, 2H, *J* = 8.5 Hz), 6.88 (d, 2H, *J* = 8.5 Hz), 3.75 (s, 3H), 3.57 (d, 2H, *J* = 2.4 Hz); <sup>13</sup>C NMR  $\delta$ : 199.8, 159.0, 130.8, 123.9, 144.4, 55.2, 49.6; GC-MS *m/z*: 121 (100), 91 (20.5), 78 (23.9), 77 (31.2), 51 (12.2).

1-(3,5-Dimethoxyphenyl)-2-(4-methoxyphenyl)ethan-1-ol (**47**). For this reaction, all glassware was dried in an oven and purged with nitrogen gas prior to use. Liquid transfers were performed using a cannula needle under positive pressure. A solution of

3,5-dimethoxybromobenzene **48** (4.00 g, 18.4 mmol) in THF (20 mL) was prepared, and then transferred to a dropping funnel atop a three-necked 100-mL round-bottomed flask containing magnesium turnings (2.68 g, 110 mmol) in THF (5 mL). Approximately 10% of the aryl halide solution was run into the flask, along with a small crystal of iodine. After 15 minutes stirring, the yellow colour of the iodine disappeared, and the mixture began to reflux. The remaining solution in the dropping funnel was added to the magnesium over 15 minutes, and the mixture was refluxed for 30 minutes after the addition was complete. After cooling to room temperature, the resulting orange solution was transferred under nitrogen to a clean three-necked flask.

A solution of 2-(4-methoxyphenyl)ethanal **49** (2.76 g, 18.4 mmol, distilled under vacuum prior to use) in THF (20 mL) was prepared. The solution was then added dropwise to the solution containing the Grignard reagent, and the resulting mixture was refluxed for 30 minutes after the addition was complete. After cooling to room temperature, the yellow solution was poured into a separatory funnel containing saturated ammonium chloride solution (100 mL) and dichloromethane (50 mL). The layers were separated, and the aqueous portion was extracted with dichloromethane (2 x 50 mL). The combined organic extracts were washed with distilled water and saturated sodium chloride solution (2 x 75 mL each). After drying over anhydrous magnesium sulfate and filtering, the solvent was removed under reduced pressure to give 5.10 g of the product alcohol (96%). Further reactions were performed using the crude material, although characterization was performed using a sample recrystallized from ethyl acetate/hexanes; mp: 97-99 °C;  $^1\text{H}$  NMR  $\delta$ : 7.09 (d, 2H,  $J = 8.6$  Hz), 6.83 (d, 2H,  $J = 8.6$  Hz), 6.49 (d, 2H,  $J = 2.4$  Hz), 6.36 (t, 1H,  $J = 2.4$  Hz), 4.76 (m, 1H,  $J_1 = 8.5$ ,  $J_2 = 4.9$  Hz,  $J_3 = 2.4$  Hz), 3.77 (s, 9H), 2.95 (m, 1H,  $J_1 = 13.7$  Hz,  $J_2 = 4.9$  Hz), 2.89 (m, 1H,  $J_1 = 13.7$  Hz,  $J_2 = 8.5$  Hz), 2.07 (d, 1H,  $J = 2.4$  Hz);  $^{13}\text{C}$  NMR  $\delta$ : 160.8, 158.4, 146.5, 130.5, 130.0, 113.9, 103.8, 99.6, 75.4, 55.4, 55.3, 45.1; GC-MS  $m/z$ : 271 (5.6), 270 (35.8), 167 (13.1), 139 (35.8), 122 (100.0), 121 (49.9), 77 (16.0); HRMS: 288.1361 (calculated),  $288.1357 \pm 0.0008$  (found).



1-(3,5-Dimethoxyphenyl)-2-(4-methoxyphenyl)ethyl ethanoate (**44**). This compound was prepared using the method of Steglich and Neises.<sup>77</sup> A solution of N,N-dimethyl-4-aminopyridine (63 mg, 0.52 mmol) and acetic acid (312 mg, 5.2 mmol) in dichloromethane (25 mL) was prepared, and then added to a solution of 1-(3,5-dimethoxyphenyl)-2-(4-methoxyphenyl)ethan-1-ol **47** (1.5 g, 5.2 mmol) in dichloromethane (30 mL). After the resulting solution was cooled in an ice bath, 1,3-dicyclohexylcarbodiimide (1.17 g, 5.67 mmol) was added in one portion. The resulting mixture was stirred at 0 °C for five minutes, and then allowed to stir at room temperature for three hours. The urea precipitate was filtered off, the solvent was removed under reduced pressure, and the residue was taken up in dichloromethane (50 mL) and filtered again. The clear solution was then washed with 0.5 M hydrochloric acid and distilled water (2 x 25 mL each). The organic material was then dried with anhydrous magnesium sulfate, filtered, and the solvent removed under reduced pressure to give a clear oil. The oil was adsorbed onto silica for column chromatography. Using 5% ethyl acetate/hexanes as the eluant provided 1.5 g of a solid product, which was recrystallized from the same solvent mixture to give 1.2 g of colourless crystals (70%); mp: 68-69 °C; <sup>1</sup>H NMR  $\delta$ : 7.03 (d, 2H, J = 8.6 Hz), 6.78 (d, 2H, J = 8.6 Hz), 6.40 (d, 2H, J = 2.4 Hz), 6.37 (t, 1H, J = 2.4 Hz), 5.81 (m, 1H, J<sub>1</sub> = 7.9 Hz, J<sub>2</sub> = 6.1 Hz), 3.77 (s, 3H), 3.75 (s, 6H), 3.08 (m, 1H, J<sub>1</sub> = 14.0 Hz, J<sub>2</sub> = 7.9 Hz), 2.97 (m, 1H, J<sub>1</sub> = 14.0 Hz, J<sub>2</sub> = 6.1 Hz), 2.02 (s, 3H); <sup>13</sup>C NMR  $\delta$ : 170.1, 160.7, 158.3, 142.6, 130.5, 129.1, 113.6, 104.6, 99.7, 76.7, 55.3, 55.2, 42.1, 21.2; GC-MS *m/z*: 270 (41.5), 167 (49.1), 139 (20.3), 121 (100), 77 (14.9); HRMS: 330.1467 (calculated), 330.1461  $\pm$  0.0008 (found).

1-(3,5-Dimethoxyphenyl)-2-(4-methoxyphenyl)-1-methoxyethane (**50a**). A 60% sodium hydride/oil suspension (0.08 g of suspension, 0.002 mmol NaH) was washed with hexane to remove the oil. After decanting the washes, the residue was taken up in DMSO (2 mL) and added to a solution of 1-(3,5-dimethoxyphenyl)-2-(4-methoxyphenyl)ethan-1-ol **47**

(0.288 g, 1.00 mmol) in DMSO (5 mL). The mixture was stirred at room temperature for 30 minutes, and then a solution of methyl iodide (0.284 g, 2.00 mmol) in 5 mL DMSO (5 mL) was added dropwise. After stirring the solution for 3.5 hours, distilled water (12 mL) was added slowly to quench the reaction. The organic layer was drawn off, and the aqueous portion was extracted with dichloromethane (3 x 10 mL). The combined organic material was washed with distilled water (3 x 25 mL), dried with anhydrous magnesium sulfate, and filtered. Removal of the solvent under reduced pressure gave 0.25 g of material, which was adsorbed onto silica for column chromatography. Elution using 2.5% ethyl acetate/hexanes gave the pure ether (0.098 g, 32%). Characterization was performed on a sample that was further purified by bulb-to-bulb distillation;  $^1\text{H}$  NMR  $\delta$ : 7.03 (d, 2H,  $J = 6.7$  Hz), 6.78 (d, 2H,  $J = 6.7$  Hz), 6.38 (m, 3H), 4.21 (dd, 1H,  $J_1 = 5.5$  Hz,  $J_2 = 7.6$  Hz), 3.77 (s, 3H), 3.75 (s, 6H), 3.20 (s, 3H), 3.01 (dd, 1H,  $J_1 = 7.6$  Hz,  $J_2 = 13.7$  Hz), 2.82 (dd, 1H,  $J_1 = 5.5$  Hz,  $J_2 = 13.7$  Hz);  $^{13}\text{C}$  NMR  $\delta$ : 160.8, 158.0, 144.4, 130.4, 113.5, 104.6, 99.6, 85.4, 56.9, 55.3, 55.2, 43.8; GC-MS  $m/z$ : 303 (0.8), 302 (4.4), 271 (1.5), 270 (6.3), 182 (10.4), 181 (100.0), 121 (12.1); HRMS: 302.1518 (calculated), 302.1522  $\pm$  0.0008 (found).

1-(3,5-Dimethoxyphenyl)-2-(4-methoxyphenyl)-1-(trifluoroethoxy)ethane (**50b**). This compound was prepared using the method of Falck.<sup>79</sup> To a solution of 1-(3,5-dimethoxyphenyl)-2-(4-methoxyphenyl)ethan-1-ol **47** (0.300 g, 1.04 mmol) in benzene (20 mL) was added 1,1'-(azodicarbonyl)dipiperidine (0.525 g, 2.08 mmol). The flask was purged with nitrogen for ten minutes, and tri(*n*-butyl)phosphine (0.421 g, 2.08 mmol) was added. After stirring the reaction mixture for another 15 minutes, 2,2,2-trifluoroethanol (1.04 g, 10.4 mmol) was added. The mixture was stirred at room temperature for one hour, and the solvent was then removed under reduced pressure. The residue was taken up in dichloromethane, filtered, and the liquid then adsorbed onto silica gel for column chromatography. Elution with 5% ethyl acetate/hexanes gave the desired

product (0.154 g, 40% yield).  $^1\text{H}$  NMR  $\delta$ : 7.03 (2H, d,  $J$  = 8.6 Hz), 6.78 (d, 2H,  $J$  = 8.6 Hz), 6.38 (s, 3H), 4.43 (dd, 1H,  $J_1$  = 5.5 Hz,  $J_2$  = 7.3 Hz), 3.77 (s, 3H), 3.75, (s, 6H), 3.64 (m, 2H), 3.09 (dd, 1H,  $J_1$  = 14.0 Hz,  $J_2$  = 7.3 Hz), 2.86 (dd, 1H,  $J_1$  = 14.0 Hz,  $J_2$  = 5.5 Hz);  $^{13}\text{C}$  NMR  $\delta$ : 161.0, 158.2, 142.6, 130.5, 129.7, 124.0 (q,  $J$  = 278.6 Hz), 113.5, 104.6, 100.1, 84.9, 66.0 (q,  $J$  = 34.3 Hz), 55.3, 55.2, 43.5; GC-MS ( $m/z$ ): 371 (1.5), 370 (7.9), 270 (6.8), 250 (11.6), 249 (100.0), 166 (22.1), 121 (81.1); HRMS: 370.1392 (calculated)  $370.1392 \pm 0.0008$  (found).

2-(3,5-Dimethoxyphenyl)ethanal (**58**). The sodium salt of 3-(3,5-dimethoxyphenyl)-glycidic acid was prepared in two steps (62% yield) using same procedures as described for the synthesis of 2-(4-methoxyphenyl)ethanal **49**.<sup>76</sup> Decarboxylation of the sodium salt was accomplished using the method of Bullimore and co-workers,<sup>150</sup> giving the desired aldehyde in 20% yield (12% over three steps);  $^1\text{H}$  NMR  $\delta$ : 9.69 (t, 1H,  $J$  = 2.4 Hz), 6.40 (t, 1H,  $J$  = 1.8 Hz), 6.35 (d, 2H,  $J$  = 1.8 Hz), 3.77 (s, 6H), 3.58 (d, 2H,  $J$  = 2.4 Hz);  $^{13}\text{C}$  NMR  $\delta$ : 199.2, 161.3, 134.0, 107.6, 99.3, 55.3, 50.7.

1-(4-Methoxyphenyl)-2-(3,5-dimethoxyphenyl)ethan-1-ol (**59**). A solution of 4-bromoanisole (1.04 g, 5.55 mmol) in THF (10 mL) was prepared under nitrogen, and then transferred to a dropping funnel atop a three-necked 100 mL round-bottomed flask containing magnesium turnings (0.81 g, 33.3 mmol). Approximately 10% of the aryl halide solution was added to the magnesium along with an iodine crystal, and the reaction began within ten minutes. The remaining aryl halide solution was added over five minutes, and the resulting mixture was heated to reflux for 30 minutes after the addition was complete. After cooling to room temperature, the resulting orange solution was transferred under nitrogen to a clean three-necked flask.

A solution of 2-(3,5-dimethoxyphenyl)ethanal **58** (1.00 g, 5.55 mmol) in THF (10 mL) was added dropwise to the Grignard reagent, and the resulting mixture was refluxed

gently for 30 minutes. The mixture was then cooled, and added to a separatory funnel containing saturated ammonium chloride (50 mL) and dichloromethane (25 mL). The layers were separated, and the aqueous portion was extracted with dichloromethane (2 x 50 mL). The combined organic extracts were washed with water and saturated sodium chloride (2 x 25 mL each), and then dried with anhydrous magnesium sulfate. Removal of solvent under reduced pressure gave a crude oil, which was purified by column chromatography (10% ethyl acetate/hexanes eluant) to give the desired product (1.00 g, 63% yield).  $^1\text{H}$  NMR  $\delta$ : 7.26 (d, 2H,  $J = 8.5$  Hz), 6.87 (d, 2H,  $J = 8.5$  Hz), 6.33 (s, 3H), 4.81 (dd, 1H,  $J_1 = 8.5$  Hz,  $J_2 = 4.9$  Hz), 3.78 (s, 3H), 3.73 (s, 6H), 2.92 (m, 2H,  $J_1 = 8.5$  Hz,  $J_2 = 4.9$  Hz,  $J_3 = 13.7$  Hz), 2.12 (s, 1H);  $^{13}\text{C}$  NMR  $\delta$ : 160.7, 159.0, 140.6, 136.1, 127.2, 113.7, 107.4, 98.6, 74.7, 55.3, 55.2, 46.3.

2-(3,5-Dimethoxyphenyl)-1-(4-methoxyphenyl)-1-methoxyethane (**51a**). A 60% sodium hydride/oil suspension (0.083 g of suspension, 2.08 mmol NaH) was washed with hexane to remove the oil. After decanting the washes, the residue was taken up in DMSO (5 mL) and added to a solution of 2-(3,5-dimethoxyphenyl)-1-(4-methoxyphenyl)ethan-1-ol **59** (0.300 g, 1.00 mmol) in DMSO (10 mL). The mixture was stirred at room temperature for 30 minutes, and then a solution of methyl iodide (0.295 g, 2.08 mmol) in DMSO (5 mL) was added dropwise. After stirring the solution for five hours, distilled water (15 mL) was added slowly to quench the reaction. The organic layer was drawn off, and the aqueous portion was extracted with dichloromethane (3 x 20 mL). The combined organic material was washed with distilled water and saturated sodium chloride solution (2 x 20 mL each), dried with anhydrous magnesium sulfate, and filtered. Removal of the solvent under reduced pressure gave 0.34 g of material, which was adsorbed onto silica for column chromatography. Elution using 5% ethyl acetate/hexanes gave the pure ether (0.24 g, 32%). Characterization was performed on a sample that was further purified by bulb-to-bulb distillation.  $^1\text{H}$  NMR  $\delta$ : 7.15 (d, 2H,  $J = 8.5$  Hz), 6.87 (d, 2H,  $J = 8.5$  Hz),

6.29 (t, 1H,  $J = 1.8$  Hz), 6.26 (d, 2H,  $J = 1.8$  Hz), 4.27 (dd, 1H,  $J_1 = 6.2$  Hz,  $J_2 = 7.4$  Hz), 3.80 (s, 3H), 3.71 (s, 6H), 3.17 (s, 3H), 3.06 (dd, 1H,  $J_1 = 13.4$  Hz,  $J_2 = 7.4$  Hz), 2.80 (dd, 1H,  $J_1 = 13.4$  Hz,  $J_2 = 6.2$  Hz);  $^{13}\text{C}$  NMR  $\delta$ : 160.4, 159.1, 140.9, 133.6, 128.0, 113.7, 107.4, 98.3, 84.4, 56.5, 55.2 (two signals), 45.0; GC-MS ( $m/z$ ): 302 (not observed), 286 (9.3), 270 (6.7), 165 (11.5), 151 (29.8), 122 (9.2), 121 (100.0); HRMS: 302.1518 (calculated),  $302.1526 \pm 0.0008$  (found).

2-(3,5-Dimethoxyphenyl)-1-(4-methoxyphenyl)-1-(trifluoroethoxy)ethane (**51b**). This compound was prepared using the method of Falck and co-workers.<sup>79</sup> To a solution of 2-(3,5-dimethoxyphenyl)-1-(4-methoxyphenyl)ethan-1-ol **59** (0.300 g, 1.04 mmol) in benzene (20 mL) was added 1,1'-(azodicarbonyl)dipiperidine (0.525 g, 2.08 mmol). The flask was purged with nitrogen for ten minutes, and tri(*n*-butyl)phosphine (0.421 g, 2.08 mmol) was added. After stirring the reaction mixture for another 15 minutes, 2,2,2-trifluoroethanol (1.04 g, 10.4 mmol) was added. The mixture was stirred at room temperature for one hour, and the solvent was then removed under reduced pressure. The residue was taken up in dichloromethane, filtered, and the liquid then adsorbed onto silica gel for column chromatography. Elution with 5% ethyl acetate/hexanes gave the desired product (0.210 g, 55% yield).  $^1\text{H}$  NMR  $\delta$ : 7.16 (d, 2H,  $J = 9.2$  Hz), 6.30 (d, 2H,  $J = 9.2$  Hz), 6.31 (t, 1H,  $J = 1.8$  Hz), 6.29 (d, 2H,  $J = 1.8$  Hz), 4.50 (dd, 1H,  $J_1 = 5.5$  Hz,  $J_2 = 7.3$  Hz), 3.80 (s, 3H), 3.72 (s, 6H), 3.62 (m, 2H), 3.14 (dd, 1H,  $J_1 = 14.0$  Hz,  $J_2 = 7.3$  Hz), 2.83 (dd, 1H,  $J_1 = 14.0$  Hz,  $J_2 = 5.5$  Hz);  $^{13}\text{C}$  NMR  $\delta$ : 160.5, 159.6, 140.1, 132.0, 128.1, 124.0 (q,  $J = 278.6$  Hz), 114.0, 107.4, 98.8, 84.1, 65.8 (q,  $J = 34.3$  Hz), 55.3, 55.2, 44.8; GC-MS ( $m/z$ ): 370 (1.1), 271 (5.8), 270 (27.6), 220 (10.6), 219 (100.0), 135 (27.3); HRMS: 370.1392 (calculated),  $370.1389 \pm 0.0008$  (found).

*trans*-3,4',5-Trimethoxystilbene (**52**). A solution of 1-(3,5-dimethoxyphenyl)-2-(4-methoxyphenyl)ethan-1-ol **47** (4.00 g, 13.9 mmol) in benzene (600 mL) was prepared in a

three-necked round-bottomed flask. A portion of *p*-toluenesulfonic acid (0.29 g, 1.5 mmol) was added, and the solution was heated to reflux with stirring. Water was removed from the mixture by way of a Dean-Stark trap. After six hours, analysis by GC-MS indicated that 97% of the starting material had reacted, and the reaction mixture was allowed to cool to room temperature. The solution was then washed with distilled water, and saturated sodium chloride solution (2 x 200 mL each). A portion of benzene (100 mL) was used to re-extract the aqueous washes. The combined organic material was then dried with anhydrous magnesium sulfate, filtered, and the solvent was removed under reduced pressure to give an orange oil. Isolation of the desired product was achieved using column chromatography with 20% ethyl acetate/hexanes eluant. Recrystallization of the resulting product from pentane gave white crystals (1.27 g, 34% yield); mp: 55-57 °C, lit.<sup>151</sup> 53-54 °C; <sup>1</sup>H NMR  $\delta$ : 7.43 (d, 2H, *J* = 8.6 Hz), 7.05 (d, 1H, *J* = 16.5 Hz), 6.91 (d, 1H, *J* = 16.5 Hz), 6.90 (d, 2H, *J* = 8.6 Hz), 6.65 (d, 2H, *J* = 2.4 Hz), 6.38 (t, 1H, *J* = 2.4 Hz), 3.83 (s, 9H) ; <sup>13</sup>C NMR  $\delta$ : 161.0, 159.4, 139.7, 129.9, 128.7, 127.8, 126.6, 114.1, 104.3, 99.6, 55.4, 55.3; GC-MS *m/z*: 271 (17.6), 270 (100.0), 269 (15.5), 239 (19.7), 224 (13.0), 196 (12.7), 195 (12.33), 165 (10.3), 153 (12.4), 152 (17.6), 141 (10.5); HRMS: 270.1256 (calculated), 270.1263  $\pm$  0.0008 (found).

*cis*-3,4',5-Trimethoxystilbene (**53**). A solution of *trans*-3,4',5-trimethoxystilbene **52** (0.40 g, 1.5 mmol) in acetonitrile (340 mL) was prepared in a large photolysis reaction vessel, and purged with nitrogen for 30 minutes. A 450 W, medium-pressure Hanovia mercury lamp with a Pyrex filter (300 nm cut-off) was employed to irradiate the solution for 30 minutes. Analysis by GC-FID indicated that by this time the mixture had achieved a photostationary state consisting of a 2:1 ratio of the *cis* and *trans* isomers. The solvent was removed under reduced pressure, and the residue was prepared for column chromatography. Separation of the isomers was achieved using 2.5% ethyl acetate/hexanes eluant, and the pure *cis* isomer was isolated as a clear oil (0.15 g, 38%

yield);  $^1\text{H}$  NMR  $\delta$ : 7.19 (d, 2H,  $J = 8.5$  Hz), 6.78 (d, 2H,  $J = 8.5$  Hz), 6.52 (d, 1H,  $J = 12.2$  Hz), 6.44 (d, 1H,  $J = 12.2$  Hz), 6.43 (d, 2H,  $J = 2.4$  Hz), 6.32 (t, 1H,  $J = 2.4$  Hz), 3.78 (s, 3H), 3.67 (s, 6H);  $^{13}\text{C}$  NMR  $\delta$ : 160.6, 158.7, 139.5, 130.3, 130.2, 129.6, 128.7, 113.5, 106.6, 99.7, 55.2; GC-MS  $m/z$ : 271 (16.44), 270 (100.0), 269 (17.5), 239 (22.5), 224 (14.5), 165 (10.6), 153 (12.7), 152 (18.6), 141 (10.6), 127 (11.2), 115 (14.6); HRMS: 270.1256 (calculated),  $270.1254 \pm 0.0008$  (found).

2,4,6-Trimethoxyphenanthrene (**54**). A solution of *trans*-3,4',5-trimethoxystilbene **52** (0.30 mg, 1.1 mmol) in methanol (340 mL) was prepared in a large photolysis reaction vessel. In order to promote the formation of the desired product, no nitrogen was used. A 450 W, medium-pressure Hanovia mercury lamp with a Pyrex filter (280 nm cut-off) was employed to irradiate the solution for seven hours. The solvent was removed under reduced pressure, and the residue was adsorbed onto silica and placed at the top of a dry-flash column (2 cm diameter, 7.5 cm length). Elution with 2.5% ethyl acetate/hexanes gave 0.10 g of a white solid. Recrystallization from methanol gave the desired product as clear crystals (0.076 g, 25% yield); mp: 111-113 °C;  $^1\text{H}$  NMR  $\delta$ : 9.08 (d, 1H,  $J = 2.8$  Hz), 7.76 (d, 1H,  $J = 8.8$  Hz), 7.65 (d, 1H,  $J = 8.6$ ), 7.49 (d, 1H,  $J = 8.8$  Hz), 7.17 (dd, 1H,  $J_1 = 2.8$  Hz,  $J_2 = 8.6$  Hz), 6.88 (d, 1H,  $J = 2.7$  Hz), 6.74 (d, 1H,  $J = 2.7$  Hz), 4.10 (s, 3H), 3.99 (s, 3H), 3.95 (s, 3H);  $^{13}\text{C}$  NMR  $\delta$ : 161.9, 160.0, 158.2, 158.1, 136.0, 131.6, 129.4, 128.1, 124.5, 115.4, 114.7, 109.6, 101.3, 99.0, 55.8, 55.4, 55.3; GC-MS  $m/z$ : 269 (18.1), 268 (100.0), 225 (16.4), 210 (22.7), 152 (15.6), 139 (18.2); HRMS: 268.1099 (calculated)  $268.1112 \pm 0.0008$  (found).

1-(3,5-Dimethoxyphenyl)-2-(4-methoxyphenyl)ethane (**55**). A solution of 1-(3,5-dimethoxyphenyl)-2-(4-methoxyphenyl)-1-methoxyethane **50a** (0.0523 g, 0.173 mmol) in methanol (50 mL) was prepared and poured into a quartz reaction vessel. After purging with nitrogen gas for 30 minutes, the stirred solution was irradiated for five hours at 25

°C. The solvent was removed under reduced pressure, and the residue was purified by column chromatography (2.5% ethyl acetate hexanes eluant) to give the desired product (0.020 g, 42% yield).  $^1\text{H}$  NMR  $\delta$ : 7.10 (d, 2H,  $J = 8.5$  Hz), 6.83 (d, 2H,  $J = 8.5$  Hz), 6.33 (s, 3H), 3.79 (s, 3H), 3.77 (s, 6H), 2.84 (s, 2H);  $^{13}\text{C}$  NMR  $\delta$ : 160.7, 157.87, 144.3, 133.8, 129.4, 113.8, 106.5, 97.9, 55.3, 55.2, 38.5, 36.8; GC-MS  $m/z$ : 273 (2.1), 272 (11.4), 151 (2.0), 122 (9.1), 121 (100.0).

2-(3,5-Dimethoxyphenyl)-1-(4-methoxyphenyl)propane (**56**). This photoproduct was not synthesized or isolated; thus, the identification rests solely on the GC-MS spectrum  $m/z$ : 287 (2.3), 286 (12.0), 165 (15.0), 122 (10.2), 121 (100.0). The molecular ion of  $m/z$  286 and the major fragment ions of  $m/z$  165 and  $m/z$  122 (the two benzylic carbocations that may be formed by cleavage of the molecular ion) strongly support the assignment.

### 7.2.2 Photolysis Procedures

In all four photolysis reactions, a similar procedure was used. The solid starting material (**44**: 100 mg, 0.30 mmol; **52**: 50 mg, 0.20 mmol) was placed in a 100-mL volumetric flask, and the flask was filled to the mark with the solvent of interest. After the substrate was fully dissolved, the solution was poured into a quartz reaction vessel and purged with nitrogen for 30 minutes. The solution was thermostated at 25 °C with an immersion circulating water tube, and mixed with a magnetic stirrer. In the reactions involving **52**, an equimolar amount of acetic acid (11  $\mu\text{L}$ , 0.20 mmol) was added to the solution, and the solution was stirred overnight to check for the presence of ground-state reactions (none were found). The photolyses were performed using a Rayonet reactor with 10 low-pressure mercury lamps (254 nm emission). While the reaction was in progress, 1 mL samples were taken for GC-FID analysis. Following the completion of



the irradiation experiment, the solvent was removed under reduced pressure, and the residue was taken up in dichloromethane for GC-MS analysis.

The purified photoproducts (from the syntheses procedures described in Section 7.2.1) were used to obtain calibrations for the GC-FID response of each compound as a function of concentration. The equations derived from the calibration experiments are provided in Equations 7.1-8, where 'A' represents the peak area observed for the substrate of interest. All substrates were best fit to a linear relationship over the range of concentrations required, with the exception of the ester **44** which required a second-order treatment. Sufficient quantities of the radical-derived products **55** and **56** could not be isolated for preparation of calibration curves and so both of those compounds were approximated using the equation for the methanol adduct **50a** (Equation 7.2).

$$A = (1.2612 \times 10^{10})[\mathbf{44}]^2 + (5.3362 \times 10^8)[\mathbf{44}] + 71611 \quad (7.1)$$

$$A = (4.6709 \times 10^8)[\mathbf{50a}] - 1057 \quad (7.2)$$

$$A = (4.1941 \times 10^8)[\mathbf{50b}] - 312 \quad (7.3)$$

$$A = (3.6204 \times 10^8)[\mathbf{51a}] - 281 \quad (7.4)$$

$$A = (3.3744 \times 10^8)[\mathbf{51b}] - 408 \quad (7.5)$$

$$A = (6.3876 \times 10^8)[\mathbf{52}] - 38969 \quad (7.6)$$

$$A = (5.4156 \times 10^8)[\mathbf{53}] - 12267 \quad (7.7)$$

$$A = (6.0755 \times 10^8)[\mathbf{54}] - 11661 \quad (7.8)$$

An example of the procedure used to process the raw chromatogram data is shown in Scheme 7.1. The data used for the example is that of the irradiation of the methoxy-substituted *trans*-stilbene derivative **52** in TFE (yield versus time plot shown in Figure 2.5-B). The peak areas from each sample are tabulated for all the compounds observed over the course of the irradiation (Step 1). The equations listed above are then used to convert the chromatogram data to concentrations of each (\*\*Continued on page 247\*\*)

## 1) Raw data: peak areas from chromatograms

Time (hours)	50b	51b	52	53	54	Total area
0	0	0	1130779	0	0	1130779
0.5	11715	147719	515361	278240	38952	991987
1	24871	318090	217798	219683	70391	850833
1.5	31504	411199	126503	137977	79442	786625
2	31801	474120	75362	85380	83504	750167
3	26791	547469	40711	37754	93401	746126
4	20139	577523	25508	16044	87280	726494

## 2) Use calibrations to convert peak areas to concentrations

Time (hours)	50b	51b	52	53	54	Total area
0	0.00E+00	0.00E+00	1.83E-03	0.00E+00	0.00E+00	1.83E-03
0.5	2.87E-05	4.39E-04	8.68E-04	5.36E-04	8.33E-05	1.96E-03
1	6.00E-05	9.44E-04	4.02E-04	4.28E-04	1.35E-04	1.97E-03
1.5	7.59E-05	1.22E-03	2.59E-04	2.77E-04	1.50E-04	1.98E-03
2	7.66E-05	1.41E-03	1.79E-04	1.80E-04	1.57E-04	2.00E-03
3	6.46E-05	1.62E-03	1.25E-04	9.24E-05	1.73E-04	2.08E-03
4	4.88E-05	1.71E-03	1.01E-04	5.23E-05	1.63E-04	2.08E-03

3) Convert concentrations into percentages of initial concentration of **52** (starting material)

Time (hours)	50b	51b	52	53	54	Total area
0	0.00	0.00	100.00	0.00	0.00	100.00
0.5	1.57	23.97	47.39	29.29	4.55	106.77
1	3.28	51.54	21.95	23.39	7.37	107.53
1.5	4.14	66.61	14.15	15.15	8.19	108.23
2	4.18	76.79	9.77	9.85	8.55	109.15
3	3.53	88.66	6.81	5.04	9.44	113.49
4	2.66	93.52	5.51	2.85	8.89	113.45

## 4) Normalized yields to 100% for each sample

Time (hours)	50b	51b	52	53	54	Total area
0	0.00	0.00	100.00	0.00	0.00	100.00
0.5	1.47	22.45	44.39	27.44	4.26	100.00
1	3.05	47.93	20.41	21.75	6.86	100.00
1.5	3.83	61.54	13.07	14.00	7.57	100.00
2	3.83	70.36	8.96	9.02	7.84	100.00
3	3.11	78.12	6.00	4.44	8.32	100.00
4	2.35	82.44	4.86	2.52	7.84	100.00

Scheme 7.1 The method used to process the raw chromatogram data for Chapter 2 photolysis experiments using the irradiation of **52** in TFE as an example.

(\*\*\*Continued from page 245\*\*\*) component in the reaction mixture (Step 2). Next, the concentrations are converted to percentages based on the initial concentration of the starting material (Step 3). Finally, the data are normalized so that the total area for each sample equals 100% (Step 4). Without the calibration adjustments of the data, the mass balance for the reaction would be only 64% of the original response. Although there is certainly some error in the calibrations (as indicated by the final mass balance for the data after calibration, 113%), the results obtained by this method are likely to be more reliable than they would be otherwise.

## 7.3 Procedures for Chapter 3 Experiments

### 7.3.1 Synthetic Procedures

The same procedure was used for the syntheses of the eight methoxy-substituted stilbene derivatives. Benzyltriphenylphosphonium bromide was produced by addition of triphenylphosphine (15.3 g, 0.058 mol) to a solution of benzyl bromide (10.0 g, 0.058 mol) in benzene (50 mL). The resulting mixture was stirred overnight at room temperature, and the precipitate (20.0 g, 80% yield) was isolated by suction filtration and washed with diethyl ether. The isolated bromide salt (10.0 g, 0.023 mol) was reacted with one equivalent of sodium ethoxide, followed by an equimolar amount of the appropriate aldehyde. The reaction mixture was heated to 80 °C while stirring overnight, and the cooled reaction mixture was extracted with methylene chloride. Typical yields were on the order of 40% for each pair of isomers. The *trans*- and *cis*-stilbenes were separated by column chromatography using a mixture of ethyl acetate and hexanes as the eluant. The yields and characterization of the substrates are given below.

*trans*-4-Methoxystilbene (*trans*-71). Isolated yield: 14%.  $^1\text{H}$  NMR  $\delta$ : 7.48 (d, 2H,  $J = 7.5$  Hz), 7.44 (d, 2H,  $J = 8.4$  Hz), 7.34 (m, 2H), 7.25 (m, 1H), 7.06 (d, 1H,  $J = 16.3$  Hz), 6.97 (d, 1H,  $J = 16.3$  Hz), 6.90 (d, 2H,  $J = 8.4$  Hz), 3.83 (s, 3H).  $^{13}\text{C}$  NMR  $\delta$ : 159.3, 137.7, 130.2, 128.7, 127.7, 127.2, 126.7, 126.3, 114.2, 55.3; GC-MS  $m/z$ : 63 (11.8), 76 (11.6), 82 (13.6), 83 (10.4), 89 (21.7), 105 (10.3), 152 (27.1), 165 (39.6), 166 (13.2), 167 (34.6), 179 (16.5), 195 (23.1), 209 (17.7), 210 (100.0), 211 (14.8); HRMS: 210.1045 (calculated),  $210.1054 \pm 0.0008$  (found); purity by GC-FID: 98%.

*cis*-4-Methoxystilbene (*cis*-71). Isolated yield: 19%.  $^1\text{H}$  NMR  $\delta$ : 7.25 (d, 2H,  $J = 8.3$  Hz), 7.22 (m, 3H), 7.17 (d, 2H,  $J = 7.5$  Hz), 6.74 (d, 2H,  $J = 8.3$  Hz), 6.52 (d, 1H,  $J = 12.6$  Hz), 6.49 (d, 1H,  $J = 12.6$  Hz), 3.75 (s, 3H).  $^{13}\text{C}$  NMR  $\delta$ : 158.8, 137.7, 130.2, 129.8, 129.7, 128.9, 128.3, 127.0, 113.7, 55.2; GC-MS  $m/z$ : 63 (10.4), 76 (10.2), 82 (12.3), 89 (20.8), 152 (28.2), 165 (40.8), 166 (13.7), 167 (35.8), 195 (23.1), 209 (19.1), 210 (100.0), 211 (14.9); HRMS: 210.1045 (calculated),  $210.1036 \pm 0.0008$  (found); purity by GC-FID: 95%.

*trans*-3-Methoxystilbene (*trans*-72). Isolated yield: 15%.  $^1\text{H}$  NMR  $\delta$ : 7.50 (d, 2H,  $J = 7.0$  Hz), 7.34 (m, 2H), 7.25 (m, 2H), 7.08 (m, 4H), 6.81 (d, 1H,  $J = 7.9$  Hz), 3.82 (s, 3H).  $^{13}\text{C}$  NMR  $\delta$ : 160.0, 138.9, 137.3, 129.7, 129.1, 128.7, 128.6, 127.7, 126.6, 119.3, 113.4, 111.8, 55.3; GC-MS  $m/z$ : 50 (13.0), 51 (36.0), 62 (10.5), 63 (44.4), 64 (11.6), 65 (21.3), 70 (15.4), 74 (10.9), 75 (18.1), 76 (47.2), 77 (31.1), 78 (14.0), 82 (39.1), 83 (29.5), 88 (20.3), 89 (52.5), 102 (15.6), 105 (20.9), 115 (24.3), 128 (11.4), 139 (15.4), 151 (12.6), 152 (58.4), 165 (100.0), 166 (31.3), 167 (48.1), 176 (16.5), 177 (28.6), 178 (62.2), 179

(66.8), 180 (10.1), 194 (33.2), 209 (27.3), 210 (76.8), 211 (10.3); HRMS: 210.1045 (calculated),  $210.1046 \pm 0.0008$  (found); purity by GC-FID: 97%.

*cis*-3-Methoxystilbene (*cis*-72). Isolated yield: 18%.  $^1\text{H}$  NMR  $\delta$ : 7.27 (d, 2H,  $J = 7.2$  Hz), 7.21 (m, 2H), 7.17 (d, 1H,  $J = 7.0$  Hz), 7.12 (m, 1H), 6.83 (d, 1H,  $J = 7.5$  Hz), 6.78 (s, 1H), 6.73 (d, 1H,  $J = 8.2$  Hz), 6.59 (d, 1H,  $J = 12.2$  Hz), 6.55 (d, 1H,  $J = 12.2$  Hz), 3.61 (s, 3H).  $^{13}\text{C}$  NMR  $\delta$ : 159.4, 138.6, 137.3, 130.6, 130.2, 129.3, 129.0, 128.3, 127.2, 121.6, 113.8, 113.4, 55.0; GC-MS  $m/z$ : 89 (12.6), 152 (22.0), 165 (44.8), 166 (14.9), 167 (22.6), 176 (10.2), 177 (18.7), 178 (37.9), 179 (42.9), 194 (30.4), 195 (20.9), 209 (35.2), 210 (100.0), 211 (15.3); HRMS: 210.1045 (calculated),  $210.1030 \pm 0.0008$  (found); purity by GC-FID: 99%.

*trans*-3,5-Dimethoxystilbene (*trans*-73). Isolated yield: 12%.  $^1\text{H}$  NMR  $\delta$ : 7.50 (d, 2H,  $J = 7.6$  Hz), 7.35 (m, 2H), 7.26 (m, 1H), 7.08 (d, 1H,  $J = 16.3$  Hz), 7.03 (d, 1H,  $J = 16.3$  Hz), 6.67 (s, 2H), 6.40 (s, 1H), 3.82 (s, 6H).  $^{13}\text{C}$  NMR  $\delta$ : 161.0, 139.4, 137.2, 129.2, 128.7, 127.8, 126.6, 104.6, 100.0, 55.4 (note: one peak less than expected, presumably due to coincidental overlap of two signals); GC-MS  $m/z$ : 51 (36.6), 32 (37.2), 69 (14.4), 75 (11.1), 76 (28.0), 77 (29.6), 82 (10.0), 89 (13.6), 102 (11.4), 115 (21.8), 128 (12.3), 152 (49.7), 153 (40.1), 154 (10.5), 165 (94.0), 166 (19.6), 178 (13.8), 194 (19.4), 208 (12.4), 209 (20.9), 239 (41.5), 240 (100.0); HRMS: 240.1150 (calculated),  $240.1142 \pm 0.0008$  (found); purity by GC-FID: 99%.

*cis*-3,5-Dimethoxystilbene (*cis*-**73**). Isolated yield: 15%.  $^1\text{H}$  NMR  $\delta$ : 7.23 (m, 5H), 6.60 (d, 1H, 12.2 Hz), 6.52 (d, 1H, 12.2 Hz), 6.39 (s, 2H), 6.31 (s, 1H), 3.62 (s, 6H).  $^{13}\text{C}$  NMR  $\delta$ : 160.6, 139.1, 137.3, 130.7, 130.3, 129.0, 128.2, 127.2, 106.8, 100.0, 55.2; GC-MS  $m/z$ : 152 (24.0), 153 (17.8), 165 (47.0), 166 (11.8), 178 (11.0), 194 (17.4), 208 (13.8), 209 (21.2), 224 (13.5), 225 (13.9), 239 (45.8), 240 (100.0), 241 (15.6); HRMS: 240.1150 (calculated),  $240.1142 \pm 0.0008$  (found); purity by GC-FID: 95%.

*trans*-3,4-Dimethoxystilbene (*trans*-**74**). Isolated yield: 14%.  $^1\text{H}$  NMR  $\delta$ : 7.49 (d, 2H,  $J = 7.5$  Hz), 7.35 (m, 2H), 7.24 (m, 1H), 7.06 (m, 3H), 6.98 (d, 1H,  $J = 16.3$  Hz), 6.86 (d, 1H, 8.1 Hz), 3.94 (s, 3H), 3.90 (s, 3H).  $^{13}\text{C}$  NMR  $\delta$ : 149.2, 149.0, 137.6, 130.5, 128.7, 128.5, 127.3, 126.9, 126.3, 119.9, 111.3, 108.8, 56.0, 55.9; GC-MS  $m/z$ : 76 (21.4), 77 (11.6), 82 (12.6), 89 (10.1), 91 (26.1), 119 (10.9), 152 (27.3), 153 (22.5), 154 (12.2), 165 (56.2), 166 (14.1), 178 (16.2), 179 (10.0), 225 (38.2), 240 (100.0), 241 (16.2); HRMS: 240.1150 (calculated),  $240.1149 \pm 0.0008$  (found); purity by GC-FID: 98%.

*cis*-3,4-Dimethoxystilbene (*cis*-**74**). Isolated yield: 13%.  $^1\text{H}$  NMR  $\delta$ : 7.29 (d, 2H,  $J = 7.4$  Hz), 7.25 (m, 2H), 7.18 (m, 1H), 6.81 (d, 1H,  $J = 8.2$  Hz), 6.75 (m, 2H), 6.53 (m, 2H), 3.85 (s, 3H), 3.58 (s, 3H).  $^{13}\text{C}$  NMR  $\delta$ : 148.3, 148.2, 137.7, 130.0, 129.9, 128.9, 128.3, 127.0, 121.9, 111.8, 110.8, 55.8, 55.4; GC-MS  $m/z$ : 76 (12.9), 91 (16.0), 152 (19.5), 153 (15.6), 165 (37.2), 178 (11.1), 225 (35.5), 240 (100.0), 241 (16.4); HRMS: 240.1150 (calculated),  $240.1163 \pm 0.0008$  (found); purity by GC-FID: 98%.

### 7.3.2 Photophysical Characterization Procedures

As outlined in Section 7.1.2, the fluorescence spectra for all five *trans*-stilbenes (*trans*-60 and *trans*-71-74) were obtained using solutions for which the absorbance was 0.25 at 295 nm, the excitation wavelength. All solutions were degassed with three freeze-pump-thaw cycles prior to recording spectra, although this procedure was found to be unnecessary for the study of *trans*-60 and *trans*-71. The values of  $\lambda_{0,0}$  listed in Table 3.2 were taken as the point of overlap for the normalized fluorescence and excitation spectra. The excitation spectra were obtained by monitoring the intensity of fluorescence at  $\lambda_{\max}$  (fluor) for a given substrate as a function of the excitation wavelength. Fluorescence quantum yield measurements were obtained by employing Equation 3.2 as described in Section 3.2.2.

Quantum yields of isomerization were obtained by irradiating nitrogen-purged solutions of the *trans* isomers ( $1.6 \times 10^{-3}$  M in the solvent of interest) with one 300 nm lamp in a Rayonet reactor. The yields of the photochemically-formed *cis* isomers were obtained over time by analyzing aliquots of the reaction mixture by GC-FID. At low conversions of the *trans* isomers, the rates of *cis* isomer formation were linear in time, and the slope of the plot was assumed to be proportional to the quantum yield of isomerization for a given substrate. The  $\phi_{tc}$  values were then calculated by employing Equation 3.3 as described in Section 3.2.2.

Unfortunately, initial experiments using this method gave unrealistically high values of  $\phi_{tc}$  for some of the substrates. For example, the values of  $\phi_{tc}$  for *trans*-4-methoxystilbene (*trans*-71) in cyclohexane was reported as 0.40 by Güsten and Klasinc,<sup>108</sup> but the method described above gave a value of 0.62. The source of this error

was discovered in a separate experiment. Solutions containing equal concentrations of both isomers of a given substrate were prepared and analyzed by GC-FID. Contrary to expectation, the *cis* isomers of all four methoxy-substituted stilbenes gave *higher* FID responses than their *trans* counterparts. Furthermore, the magnitude of this difference was not the same for all substrates. The ratio of the *cis* and *trans* responses for the five substrates are given in Table 7.1 – these values were used as correction factors for the original photoisomerization data. Comparison of the slopes for the yield versus time plots of the corrected data provided values of  $\phi_{tc}$  that are in excellent agreement with the literature results, as indicated in Section 3.3.1.

Compound	cis/trans
<b>60</b>	0.964
<b>71</b>	1.344
<b>72</b>	1.181
<b>73</b>	1.082
<b>74</b>	1.210

Table 7.1 Ratios of *cis:trans* FID response for stilbene substrates.

### 7.3.3 Irradiation Procedures

A  $1 \times 10^{-3}$  M solution (50 mL) of the substrate of interest was thermostated at 25 °C in a quartz reaction vessel and purged with nitrogen for 30 minutes. Irradiations were performed in a Rayonet reactor with 10 low-pressure mercury lamps (300 nm emission). Aliquots taken during the reaction were analysed by GC-FID to determine product yields. The large number of products precluded the use of the calibration techniques described in Section 7.2.2. The simplified procedure employed for the analysis of the Chapter 3 irradiation results is shown in Scheme 7.2 using the irradiation of *trans*-**73** in TFE as an example (yield *versus* time plot in Figure 3.8).



## 1) Raw data: peak areas from chromatograms

Time (min)	<i>trans</i> -73	<i>cis</i> -73	75b-3	76b-3	77	78	Total
0	888921	3350	0	0	0	0	892271
1	654028	135413	28362	141928	0	0	959731
2	340309	239397	60052	301647	0	2671	944076
4	78631	197450	115146	587450	15631	6140	1000448
7	0	6779	153504	829695	28393	10167	1028538
10	0	0	144820	863077	25774	12729	1046400

2) Convert peak areas into percentages of initial concentration of *trans*-73 (starting material)

Time (min)	<i>trans</i> -73	<i>cis</i> -73	75b-3	76b-3	77	78	Total
0	100.00	0.38	0.00	0.00	0.00	0.00	100.38
1	73.58	15.23	3.19	15.97	0.00	0.00	107.97
2	38.28	26.93	6.76	33.93	0.00	0.30	106.20
4	8.85	22.21	12.95	66.09	1.76	0.69	112.55
7	0.00	0.76	17.27	93.34	3.19	1.14	115.71
10	0.00	0.00	16.29	97.09	2.90	1.43	117.72

## 3) Normalize yields to 100% for each sample

Time (min)	<i>trans</i> -73	<i>cis</i> -73	75b-3	76b-3	77	78	Total
0	99.62	0.38	0.00	0.00	0.00	0.00	100.00
1	68.15	14.11	2.96	14.79	0.00	0.00	100.00
2	36.05	25.36	6.36	31.95	0.00	0.28	100.00
4	7.86	19.74	11.51	58.72	1.56	0.61	100.00
7	0.00	0.66	14.92	80.67	2.76	0.99	100.00
10	0.00	0.00	13.84	82.48	2.46	1.22	100.00

Scheme 7.2 The method used to process the raw chromatogram data for Chapter 3 irradiation experiments using the irradiation of *trans*-52 in TFE as an example.

The peak areas from each sample are tabulated for all the compounds observed over the course of the irradiation (Step 1). The peak areas are then converted to percentages based on the initial peak area of the starting material (Step 2). Finally, the data are normalized so that the total area for each sample equals 100% (Step 3). That the yields obtained prior to normalization indicate a mass balance of 118% (compared to the

original value) indicates that the FID response of one of the products has been underestimated. Similar deviations were observed for the other substrates, but the absence of rigorous response calibrations does not appear to lead to serious problems in the analysis.

As was discussed in Section 3.2.3, identification of many photoproducts was achieved by analysis of the GC-MS spectra. These data are listed below for the products identified in Chapter 3 experiments.

Products detected following irradiation of *trans*-60 or *cis*-60:

1,2-Diphenyl-1-methoxyethane (**75a-0**). GC-MS *m/z*: 310 (not observed), 122 (10.3), 121 (100), 91 (18.4), 77 (24.0).

1-(2,2,2-trifluoroethoxy)-1,2-Diphenylethane (**75b-0**). GC-MS *m/z*: 212 (not observed), 189 (100.0), 109 (14.9), 105 (16.3), 91 (20.4), 79 (14.9), 77 (21.6).

Phenanthrene (**77-0**). GC-MS *m/z*: 179 (15.0), 178 (100.0), 176 (20.1), 152 (13.3), 89 (14.1), 88 (10.8), 76 (15.0).

1,2-Diphenylethane (**78-0**). GC-MS *m/z*: 183 (3.7), 182 (24.9), 91 (100), 65 (11.4).

Products detected following irradiation of *trans*-71 or *cis*-71:

1-(4-Methoxyphenyl)-1-methoxy-2-phenylethane (**75a-1**). GC-MS *m/z*: 242 (not observed), 210 (34.4), 167 (21.1), 165 (29.5), 152 (29.2), 151 (100.0), 135 (13.1).

1-(2,2,2-Trifluoroethoxy)-1-(4-methoxyphenyl)-2-phenylethane (**75b-1**). GC-MS  $m/z$ : 310 (not observed), 219 (86.2), 211 (17.1), 210 (100.0), 209 (18.5), 195 (22.3), 179 (15.3), 167 (29.5), 166 (11.7), 165 (35.2), 152 (22.9), 121 (13.9), 136 (10.2), 135 (20.7).

3-Methoxyphenanthrene (**77-1**). GC-MS  $m/z$ : 63 (12.1), 76 (10.4), 115 (10.9), 152 (41.2), 165 (61.9), 166 (19.6), 167 (47.3), 178 (10.7), 179 (18.4), 195 (23.8), 209 (18.2), 210 (100.0), 211 (14.2).

1-(4-Methoxyphenyl)-2-phenylethane (**78-1**). GC-MS  $m/z$ : 212 (not observed), 135 (100.0), 107 (10.4), 103 (30.8), 91 (16.6), 79 (41.9), 77 (18.3).

Products detected following irradiation of *trans*-**72** or *cis*-**72**:

1-(3-Methoxyphenyl)-1-methoxy-2-phenylethane (**75a-2**). GC-MS  $m/z$ : 242 (not observed), 152 (13.3), 151 (100.0), 135 (10.4), 108 (10.5), 91 (16.1), 77 (10.9).

1-(2,2,2-Trifluoroethoxy)-1-(3-methoxyphenyl)-2-phenylethane (**75b-2**). GC-MS  $m/z$ : 310 (not observed), 219 (100.0), 136 (24.3), 135 (24.2), 91 (13.3), 77 (11.3).

2-(3-Methoxyphenyl)-1-methoxy-1-phenylethane (**76a-2**): GC-MS  $m/z$ : 242 (not observed), 121 (100.0), 91 (26.6), 78 (15.3), 77 (48.3).

1-(2,2,2-Trifluoroethoxy)-2-(3-methoxyphenyl)-1-phenylethane (**76b-2**). GC-MS  $m/z$ : 310 (not observed), 210 (11.6), 189 (100.0), 77 (10.0).

2-Methoxyphenanthrene and/or 4-Methoxyphenanthrene (**77-2**). GC-MS *m/z*: 209 (12.3), 208 (80.9), 193 (18.9), 166 (13.4), 165 (100.0), 164 (16.8), 163 (17.8),

Products detected following irradiation of *trans*-**73** or *cis*-**73**:

1-(3,5-Dimethoxyphenyl)-1-methoxy-2-phenylethane (**75a-3**). GC-MS *m/z*: 272 (not observed), 181 (100.0), 166 (12.9), 165 (13.0), 138 (11.2), 91 (20.4), 77 (12.9).

1-(2,2,2-Trifluoroethoxy)-1-(3,5-dimethoxyphenyl)-2-phenylethane (**75b-3**). GC-MS *m/z*: 340 (not observed), 249 (100.0), 166 (24.7), 165 (13.2), 91 (16.2).

2-(3,5-Dimethoxyphenyl)-1-methoxy-1-phenylethane (**76a-3**). GC-MS *m/z*: 272 (2.0), 121 (100.0), 91 (18.0), 77 (26.0).

1-(2,2,2-Trifluoroethoxy)-2-(3,5-dimethoxyphenyl)-1-phenylethane (**76b-3**). GC-MS *m/z*: 340 (7.0), 240 (11.4), 189 (100.0), 77 (11.6).

2,4-Dimethoxyphenanthrene (**77-3**). GC-MS *m/z*: 239 (16.1), 238 (100.0), 223 (32.0), 195 (29.8), 180 (29.2), 165 (11.2), 163 (12.6), 152 (49.7), 151 (13.1).

1-(3,5-Dimethoxyphenyl)-2-phenylethane (**78-3**). GC-MS *m/z*: 243 (4.9), 242 (33.9), 152 (11.6), 151 (100.0), 91 (48.9), 78 (14.7), 77 (18.2), 65 (18.2).

Products detected following irradiation of *trans*-74 or *cis*-74:

1-(3,4-Dimethoxyphenyl)-1-methoxy-2-phenylethane (**75a-4**). GC-MS *m/z*: 272 (not observed), 240 (25.8), 182 (10.8), 181 (100.0), 166 (28.7), 165 (46.4), 153 (16.8), 152 (23.2), 151 (10.4), 91 (38.7), 77 (33.5), 76 (25.8), 65 (22.1), 63 (19.9).

1-(2,2,2-Trifluoroethoxy)-1-(3,4-dimethoxyphenyl)-2-phenylethane (**75b-4**). GC-MS *m/z*: 340 (not observed), 249 (100.0), 241 (14.4), 240 (86.0), 225 (38.5), 179 (10.5), 178 (15.3), 167 (13.6), 166 (64.0), 165 (80.2), 154 (14.0), 153 (27.0), 152 (34.6), 151 (15.6), 119 (13.8), 91 (39.9), 77 (23.8), 76 (23.6), 65 (13.8), 63 (13.0).

2-(3,4-Dimethoxyphenyl)-1-methoxy-1-phenylethane (**76a-4**). GC-MS *m/z*: 272 (not observed), 121 (100.0), 77 (16.3).

1-(2,2,2-Trifluoroethoxy)-2-(3,4-dimethoxyphenyl)-1-phenylethane (**76b-4**). GC-MS *m/z*: 340 (not observed), 240 (10.3), 189 (15.8), 152 (14.6), 151 (100).

2,3-Dimethoxyphenanthrene and/or 3,4-Dimethoxyphenanthrene (**77-4**). GC-MS *m/z*: 239 (8.9), 238 (97.1), 223 (13.2), 195 (24.0), 180 (13.4), 177 (40.4), 167 (33.4), 165 (42.0), 163 (10.5), 152 (100.0), 151 (24.2), 150 (10.7), 76 (12.7).

1-(3,4-Dimethoxyphenyl)-2-phenylethane (**78-4**). GC-MS *m/z*: 242 (not observed), 151 (100.0), 91 (92.6), 78 (13.8), 65 (61.7), 51 (23.2).

### 7.3.4 Analysis of Fluorescence Quenching Results

Given the curvature of the Stern-Volmer plots (Figure 3.11) for the fluorescence of *trans*-**73** in TFE and TFE-OD, the usual analysis of these results (slope =  $k_q\tau_s$ ) was not possible. However, over *small sections* of the plot ( $\Delta(\%TFE) = 20\%$ ) the slope can be estimated, thereby allowing the calculation of approximate rate constants for bimolecular quenching ( $k_{TFE}$ ). The following calculations employ the data in Table 3.6, as well as the densities of TFE (1.373 g/mL) and TFE-OD (1.387 g/mL), the molecular weights of TFE (100.04 g/mol) and TFE-OD (101.05), and the singlet lifetime of *trans*-**73** ( $\tau_s = 16.9$  ns).

- 1) From 0% TFE to 20% TFE the change in ( $\phi_f^0/\phi_f$ ) is 0.04.

A 20% solution of TFE contains 274.6 g per 1 L solution, or 2.747 mol/L.

From 0% TFE to 20% TFE, the slope is:  $m = (0.04)/(2.747 \text{ M})$ .

Using the usual Stern-Volmer treatment,  $k_{TFE} = m/\tau_s = 8.7 \times 10^6 \text{ s}^{-1}\text{M}^{-1}$ .

- 2) From 80% TFE to 100% TFE the change in ( $\phi_f^0/\phi_f$ ) is 6.46.

The change in %TFE is still 20%, or 2.747 M.

From 80% TFE to 100% TFE, the slope is:  $m = (6.46)/(2.747 \text{ M})$ .

Using the usual Stern-Volmer treatment,  $k_{TFE} = m/\tau_s = 1.4 \times 10^8 \text{ s}^{-1}\text{M}^{-1}$ .

- 3) From 80% TFE-OD to 100% TFE-OD the change in ( $\phi_f^0/\phi_f$ ) is 2.33.

A 20% solution of TFE-OD contains 277.4 g per 1 L solution, or 2.803 mol/L.

From 0% TFE-OD to 20% TFE-OD, the slope is:  $m = (2.33)/(2.803 \text{ M})$ .

Using the usual Stern-Volmer treatment,  $k_{TFE-OD} = m/\tau_s = 4.9 \times 10^7 \text{ s}^{-1}\text{M}^{-1}$ .

The quenching ratio is therefore  $k_{TFE}/k_{TFE-OD} = 2.9 \approx 3$ .

## 7.4 Procedures for Chapter 4 Experiments

### 7.4.1 Synthetic Procedures

3,5-Dimethoxystyrene (**93**). To an oven-dried flask was added magnesium (0.29 g, 12 mmol) followed by dropwise addition of a solution of methyl iodide (0.94 g, 6.6 mmol) in diethyl ether (12 mL). The resulting mixture began to reflux on its own after light heating. After the reaction had ceased, a solution of 3,5-dimethoxybenzaldehyde (1.0 g, 6.0 mmol) in diethyl ether (12 mL). Following a vigorous reaction and cooling of the mixture to room temperature, a portion of ammonium chloride was added to quench the reaction. The mixture was extracted with diethyl ether (2 x 20 mL) and dried with sodium sulphate. Removal of the solvent under reduced pressure and column chromatography provided the desired intermediate, 1-(3,5-dimethoxyphenyl)ethanol (1.0 g, 91% yield). This compound was taken up in benzene (100 mL), *p*-toluenesulfonic acid was added (0.1 g, 0.6 mmol), and the solution was heated to reflux for four hours (Dean-Stark trap). After cooling to room temperature, the organic material was washed with saturated sodium bicarbonate and saturated sodium chloride (2 x 25 mL each) and dried with sodium sulphate. After removal of solvent, the residue was purified by column chromatography, giving white crystals of the desired product (0.30 g, 36%).  $^1\text{H}$  NMR  $\delta$ : 6.62 (dd 1H,  $J_1 = 18$  Hz,  $J_2 = 11$  Hz), 6.55 (d, 2H,  $J = 2$  Hz), 6.37 (t, 1H,  $J = 2$  Hz), 5.71 (d, 1H,  $J = 18$  Hz), 5.22 (d, 1H,  $J = 11$  Hz), 3.76 (s, 6H);  $^{13}\text{C}$  NMR  $\delta$ : 161.1, 139.8, 137.1, 114.5, 104.5, 100.2, 55.4; GC-MS  $m/z$ : 165 (13.3), 164 (100.0), 135 (76.4), 134 (19.6), 121 (27.4), 120 (10.2), 106 (17.2), 105 (48.9), 104 (32.6), 103 (34.9), 92 (10.3), 91 (90.9), 90 (19.3), 89 (41.3), 79 (25.2), 78 (81.8), 77 (62.8); HRMS: 164.0837 (calculated), 164.0840  $\pm$  0.0008 (found).

The same procedure was used for the syntheses of the four *trans*-1-arylpropenes *trans*-96-99. To an oven dried flask under nitrogen was added magnesium (0.24 g, 10 mmol), followed by dropwise addition of ethyl iodide (1.2 g, 8.0 mmol) in diethyl ether (10 mL). Light heat was used to initiate and maintain reflux over 30 minutes. To the cooled mixture was added the appropriate methoxy-substituted aldehyde (7.3 mmol) in diethyl ether (15 mL), giving a vigorous reaction. Substantial preceptitation often occurred at this point in the synthesis, and fast stirring was required to ensure complete mixing of the reagents. The mixture was quenched by the addition of saturated ammonium chloride solution, and then poured into diethyl ether and water (25 mL each). After separating the layers, the aqueous portion was extracted with diethyl ether (2 x 25 mL). The combined organics were washed with saturated sodium chloride solution (2 x 25 mL) and dried with sodium sulphate. Removal of solvent provided the desired 1-arylpropanols as intermediates. The crude material was taken up in benzene (100 mL), *p*-toluenesulfonic acid was added (0.13 g, 0.7 mmol), and the mixture was heated to reflux for 1.5 hours (Dean-Stark trap). The cooled solution was washed with saturated sodium bicarbonate and saturated sodium chloride solutions (2 x 25 mL each) and then dried with sodium sulphate. Removal of solvent followed by column chromatography provided the desired *trans*-1-arylalkenes *trans*-96-99 in 20-50% yield.

*trans*-(4-Methoxyphenyl)propene (*trans*-96).  $^1\text{H}$  NMR  $\delta$ : 7.24 (d, 2H,  $J = 7.5$  Hz), 8.82 (d, 2H,  $J = 7.5$  Hz), 6.33 (d, 1H,  $J = 16$  Hz), 6.09 (dq, 1H,  $J_1 = 16$  Hz,  $J_2 = 7$  Hz), 3.77 (s, 3H), 1.87 (d, 3H);  $^{13}\text{C}$  NMR  $\delta$ : 158.8, 131.0, 130.6, 127.1, 123.6, 114.1, 55.4, 18.0. GC-MS  $m/z$ : 149 (11.0), 148 (100.0), 147 (63.2), 133 (27.1), 121 (21.5), 117 (37.6), 115



(25.0), 105 (34.0), 103 (26.8), 91 (26.5), 79 (26.6), 78 (18.7), 77 (45.7), 63 (17.2); HRMS: 148.0888 (calculated),  $148.0886 \pm 0.0008$  (found); purity by GC-FID: 94%.

*trans*-(3-Methoxyphenyl)propene (*trans*-97).  $^1\text{H}$  NMR  $\delta$ : 7.32 (t, 1H,  $J = 8$  Hz), 7.05 (d, 1H,  $J = 7.5$  Hz), 7.00 (s, 1H), 6.87 (d, 1H,  $J = 8$  Hz), 6.49 (d, 1H,  $J = 16$  Hz), 6.36 (dq,  $J_1 = 16$  Hz,  $J_2 = 10$  Hz), 3.91 (s, 3H), 2.01 (d, 3H,  $J = 10$  Hz);  $^{13}\text{C}$  NMR  $\delta$ : 160.1, 139.7, 131.2, 129.7, 126.2, 118.8, 111.5, 55.3, 18.6; GC-MS  $m/z$ : 149 (30.3), 148 (100.0), 147 (85.0), 133 (61.5), 132 (12.8), 131 (13.6), 121 (29.1), 119 (14.8), 118 (20.5), 117 (88.9), 116 (48.9), 115 (78.7), 105 (73.4), 104 (16.3), 103 (56.5), 102 (15.8), 91 (72.9), 89 (21.8), 79 (54.7), 78 (42.7), 77 (73.9); HRMS: 148.0888 (calculated),  $148.0889 \pm 0.0008$  (found); purity by GC-FID: 96%.

*trans*-(3,5-Dimethoxyphenyl)propene (*trans*-98).  $^1\text{H}$  NMR  $\delta$ : 6.57 (d, 2H,  $J = 2$  Hz), 6.41 (t, 1H,  $J = 2$  Hz), 6.40 (d, 1H,  $J = 16$  Hz), 6.31 (dq, 1H,  $J_1 = 15.5$  Hz,  $J_2 = 6.5$  Hz), 3.85 (s, 6H), 1.95 (d, 3H,  $J = 6.5$  Hz);  $^{13}\text{C}$  NMR  $\delta$ : 161.1, 140.2, 131.2, 126.4, 104.2, 99.3, 55.3, 18.6; GC-MS  $m/z$ : 179 (43.4), 178 (100.0), 177 (84.1), 164 (10.1), 163 (74.0), 162 (13.3), 151 (21.7), 149 (34.6), 147 (90.5), 146 (25.7), 135 (51.8), 133 (21.6), 132 (22.9), 131 (33.8), 122 (10.0), 121 (69.9), 120 (18.3), 119 (31.8), 117 (55.3), 115 (54.3), 107 (19.8), 105 (56.9), 104 (32.8), 103 (80.9); HRMS: 178.0994 (calculated),  $178.0997 \pm 0.0008$  (found); purity by GC-FID: 97%.

*trans*-(3,4-Dimethoxyphenyl)propene (*trans*-99).  $^1\text{H}$  NMR  $\delta$ : 6.94 (d, 1H,  $J = 2$  Hz), 6.89 (dd, 1H,  $J_1 = 2$  Hz,  $J_2 = 8$  Hz), 6.83 (d, 1H,  $J = 8$  Hz), 6.38 (dd, 1H,  $J_1 = 1.5$  Hz,  $J_2 = 15.5$

Hz), 6.15 (dq, 1H,  $J_1 = 15.5$  Hz,  $J_2 = 6.5$  Hz), 3.93 (s, 3H), 3.90 (s, 3H), 1.91 (dd,  $J_1 = 6.5$  Hz,  $J_2 = 1.5$  Hz);  $^{13}\text{C}$  NMR  $\delta$ : 149.2, 148.4, 131.3, 130.8, 123.9, 118.8, 111.4, 108.7, 56.06, 56.03, 18.5; GC-MS  $m/z$ : 179 (37.5), 178 (100.0), 164 (16.4), 163 (78.6), 147 (51.1), 146 (12.0), 135 (41.2), 131 (19.7), 120 (16.0), 119 (16.7), 117 (26.3), 115 (57.4), 107 (78.7), 105 (41.4), 104 (20.7), 103 (69.4), 92 (25.1), 91 (74.9), 89 (27.3); HRMS: 178.0994 (calculated),  $178.0993 \pm 0.0008$  (found); purity by GC-FID: 95%.

#### 7.4.2 Irradiation Procedures

Irradiations were carried out using the same experimental methods and data analysis techniques that were described in Section 7.3.3. The GC-MS characterizations of the photoproducts are listed below.

Products detected following irradiation of **91**:

1-(2,2,2-Trifluoromethyl)-1-(4-methoxyphenyl)ethane (**100-1**). GC-MS  $m/z$ : 235 (2.2), 234 (19.4), 219 (87.1), 136 (26.2), 135 (100.0), 120 (10.9), 119 (55.5), 105 (20.4), 103 (16.5), 92 (14.7), 91 (74.0), 79 (11.8), 77 (25.9), 65 (35.7), 63 (20.1).

Products detected following irradiation of **92**:

1-(2,2,2-Trifluoromethyl)-1-(3-methoxyphenyl)ethane (**100-2**). GC-MS  $m/z$ : 235 (4.5), 234 (41.4), 220 (10.1), 219 (100.0), 136 (61.1), 135 (86.4), 134 (23.7), 121 (14.5), 107 (10.5), 105 (25.5), 103 (22.3), 92 (14.5), 91 (37.7), 83 (10.5), 79 (12.4), 78 (13.1), 77 (26.9).

Products detected following irradiation of **93**:

1-(2,2,2-Trifluoromethyl)-1-(3,5-dimethoxyphenyl)ethane (**100-3**). GC-MS *m/z*: 265 (4.0), 264 (33.9), 249 (35.2), 167 (15.0), 166 (100.0), 165 (59.9), 164 (22.0), 151 (20.2), 137 (13.6), 135 (27.6), 122 (10.5), 121 (15.6), 109 (11.0), 107 (11.5), 103 (12.6).

Products detected following irradiation of **94**:

1-(2,2,2-Trifluoromethyl)-1-(3,4-dimethoxyphenyl)ethane (**100-4**). GC-MS *m/z*: 264 (7.6), 249 (21.4), 166 (36.2), 165 (100.0), 164 (66.6), 150 (18.8), 149 (38.9), 121 (42.6), 120 (10.4), 119 (16.9), 107 (13.8), 105 (16.9), 103 (50.9), 95 (12.6), 93 (18.4), 92 (12.2), 91 (90.0), 77 (97.2).

Products detected following irradiation of *trans*-**96**:

*cis*-1-(4-Methoxyphenyl)propene (*cis*-**96**). GC-MS *m/z*: 152 (16.9), 148 (78.1), 147 (48.3), 133 (25.9), 122 (10.8), 121 (95.8), 117 (41.8), 115 (32.1), 105 (54.8), 103 (40.9), 89 (22.7), 79 (47.2), 78 (56.8), 77 (100.0), 76 (10.7), 74 (10.6), 65 (30.8), 64 (12.8).

1-(2,2,2-Trifluoromethyl)-1-(4-methoxyphenyl)propane (**101-6**). GC-MS *m/z*: 249 (2.4), 248 (20.3), 220 (25.9), 219 (100.0), 149 (30.3), 148 (18.8), 147 (11.9), 136 (62.0), 135 (80.8), 121 (52.8), 117 (10.1), 115 (11.8), 107 (12.1), 105 (12.5), 103 (11.0), 91 (40.0), 78 (25.8), 77 (57.1), 65 (33.4).

Products detected following irradiation of *trans*-97:

*cis*-1-(3-Methoxyphenyl)propene (*cis*-97). GC-MS *m/z*: 149 (6.8), 148 (74.8), 147 (28.3), 136 (73.3), 135 (78.2), 133 (18.5), 122 (21.5), 121 (28.4), 117 (57.6), 116 (17.1), 115 (37.6), 107 (38.7), 105 (40.9), 103 (26.2), 91 (52.1), 78 (43.6), 77 (100.0), 63 (55.0).

1-(2,2,2-Trifluoromethyl)-1-(3-methoxyphenyl)propane (**101-7**). GC-MS *m/z*: 248 (11.3), 220 (10.5), 219 (100.0), 136 (27.5), 135 (22.2), 77 (11.3).

Products detected following irradiation of *trans*-98:

*cis*-1-(3,5-Dimethoxyphenyl)propene (*cis*-98). GC-MS *m/z*: 179 (12.3), 178 (100.0), 177 (34.5), 163 (19.1), 147 (43.5), 121 (15.7), 115 (10.2), 103 (26.2), 91 (30.0), 77 (16.2).

1-(2,2,2-Trifluoromethyl)-1-(3,5-dimethoxyphenyl)propane (**101-8**). GC-MS *m/z*: 279 (6.3), 278 (47.7), 250 (21.6), 249 (100.0), 180 (41.8), 179 (19.7), 167 (21.4), 166 (77.2), 165 (60.4), 152 (14.3), 151 (16.7), 139 (15.2), 138 (11.2), 137 (14.4), 135 (20.6), 121 (13.2), 109 (13.3), 107 (10.2), 103 (10.2), 95 (10.2).

Products detected following irradiation of *trans*-99:

*cis*-1-(3,4-Dimethoxyphenyl)propene (*cis*-99). GC-MS *m/z*: 179 (15.1), 178 (100.0), 163 (49.6), 147 (14.2), 135 (11.5), 115 (15.4), 107 (44.9), 105 (10.1), 103 (28.7), 91 (37.3), 79 (14.6), 77 (16.6), 65 (11.5).

1-(2,2,2-Trifluoromethyl)-1-(3,4-dimethoxyphenyl)propane (**101-9**). GC-MS  $m/z$ : 279 (4.4), 278 (32.6), 250 (18.5), 249 (100.0), 179 (25.9), 178 (34.3), 166 (74.0), 165 (38.4), 163 (16.8), 151 (30.5), 107 (23.1), 103 (15.3), 95 (13.4), 91 (27.9), 79 (16.0), 77 (27.1), 65 (16.7), 63 (10.8).

1-(2,2,2-Trifluoromethyl)-2-(3,4-dimethoxyphenyl)propane (**102-9**). GC-MS  $m/z$ : 279 (2.5), 278 (18.3), 152 (10.9), 151 (100.0).

### 7.4.3 Calculation of Excited State Dipole Moments

The Stokes' shifts are provided in Table 7.2 in wavenumber units ( $\text{cm}^{-1}$ ), rather than the nanometer units given in Table 4.9.

Solvent	<i>trans</i> - <b>60</b>	<i>trans</i> - <b>71</b>	<i>trans</i> - <b>72</b>	<i>trans</i> - <b>73</b>	<i>trans</i> - <b>74</b>
cyclohexane	3814	3583	3713	4476	3513
dibutyl ether	3709	3905	3613	5170	3821
diethyl ether	3814	3830	3836	5211	3678
ethyl acetate	3709	3637	3613	5771	4217
2-propanol	3627	3755	3735	5976	4031
acetonitrile	3896	4318	3790	6513	4514

Table 7.2 Stokes' shifts (in wavenumbers) for the fluorescence of *trans*-**60** and *trans*-**71-74** in a series of six solvents.

Plots of these values versus the solvent parameter  $\Delta f$  provided the solvatochromic slopes shown in Table 4.10. Setting this slope ( $m$ ) equal to  $(\mu_e(\mu_e - \mu_g))/2\pi\epsilon_0\hbar c a^3$  and rearranging Equation 4.7 gives a quadratic equation with  $\mu_e$  as the variable, Equation 7.9. This equation is solved using the quadratic formula with the physical constants in the List

of Symbols and Abbreviations. Two important conversion factors that are required for this calculation are  $1 \text{ J} = 1.1 \times 10^{-10} \text{ C}^2 \text{ m}^{-1}$  and  $1 \text{ D} = 3.33 \times 10^{-30} \text{ Cm}$ .

$$\mu_e^2 - \mu_g \mu_e - 2\pi\epsilon_0 \hbar c a^3 m = 0 \quad (7.9)$$

#### 7.4.4 LFP Procedures

Solutions used for LFP studies had an absorbance of 0.4 at the incident wavelength of the laser (308 nm). Surprisingly, the absorbance spectra of all substrates were slightly blue shifted (5-10 nm) in TFE compared to acetonitrile solution. Although this change did not have a large effect on the laser experiments, the fluorescence quenching studies (Section 4.3.5) required the use of more concentrated TFE solutions in order to keep the same absorbance (0.25) for the quantum yield determinations. The difference in concentration is not expected to alter the results significantly.

LFP solutions were prepared by adding a small volume ( $\approx 5 \text{ }\mu\text{L}$ ) of acetonitrile stock solution to a 0.7 cm cuvette with 2mL of the fluorinated solvent. This method required good mixing (shaking) of the samples prior to irradiation in order to ensure homogenous solutions. Further mixing of the sample was performed before every laser flash, but even with this technique the high reactivity of the substrates towards trans-cis isomerization restricted every sample to less than three flashes each. The kinetic traces taken from these experiments were analysed using the KaleidaGraph software package.

#### 7.4.5 $^1\text{H}$ NMR Calculations

As indicated in the text, the peak integrations in Table 4.24 were obtained with  $H_X = 1$  as the reference value. For the determination of the relative importance of each mechanism, the percentage of potential carbene product is calculated first, according to Equation 7.10. In effect, this calculation assumes that the total of  $H_A$  and  $H_B$  should be equal to the integral of  $H_X$  *if no carbene insertion occurs*. In that event that  $(H_A + H_B) > H_X$ , it is because the area of the reference ( $H_X$ ) has been overestimated, and some amount of carbene insertion has occurred. With the percentage of carbene insertion available, the relative amounts of anti and syn addition can be calculated using Equations 7.11 and 7.12, respectively.

$$\% \text{ Carbene Insertion} = \left[ 1 - \left( \frac{H_X}{H_A + H_B} \right) \right] \times 100\% \quad (7.10)$$

$$\% \text{ Anti Addition} = \left( 100\% - \% \text{ Carbene Insertion} \right) \times \left( \frac{H_B}{H_A + H_B} \right) \quad (7.11)$$

$$\% \text{ Syn Addition} = \left( 100\% - \% \text{ Carbene Insertion} \right) \times \left( \frac{H_A}{H_A + H_B} \right) \quad (7.12)$$

Two important points should be made with regards to this analysis. First, the method used for determining the percentage of carbene insertion is somewhat tenuous, given the assumptions in the calculations. Indeed,  $(H_A + H_B)$  is slightly greater than  $H_X$  for most of the *non*-deuterated mixtures in Table 4.24. Although no correction for this effect has been employed, the observation emphasizes the fact that the relative amount of

carbene insertion must be very small. The GC-MS results also indicate that very little deuterium is incorporated on the same carbon as the nucleophile. A second point is that, even if the amounts of carbene insertion are greater than the values in Table 4.24 (which is very unlikely), the information regarding the *relative* importance of the syn and anti addition pathways should still be reliable. Therefore, the mechanistic details that have been obtained from those values (Section 4.3.3) should also be correct.

## 7.5 Procedures for Chapter 5 Experiments

### 7.5.1 Synthetic Procedures

*trans*-3,3',5-Trimethoxystilbene (*trans*-112). The synthesis of this substrate involved a multi-step sequence, as indicated in Scheme 5.4 (*vide supra*). The first step followed the procedure of Mandal and Mahajan.<sup>152</sup> A mixture of 3,5-dimethoxybenzyl alcohol (5.0 g, 30 mmol) and sodium bromide (5.6 g, 45 mmol) was added to acetonitrile (75 mL) in an oven-dried flask under nitrogen atmosphere. To the solution was added boron trifluoro etherate (5.6 mL, 30 mmol), and the resulting solution was heated to reflux for three hours. After cooling, the mixture was poured into a mixture of dichloromethane (75 mL) and saturated sodium bicarbonate (25 mL), after separating the two layers (organic on top), the aqueous portion was extracted with dichloromethane (2 x 25 mL). The combined organic material (now on bottom) was washed with 10% sodium meta bisulfite ( $\text{Na}_2\text{S}_2\text{O}_3$ ) and saturated sodium chloride solution (2 x 25 mL each). After drying with sodium sulphate, the solvent was removed under reduced pressure to give a yellow oil that solidified upon standing, and gave a positive result from the NaI/acetone test. Recrystallization from hexanes provided the desired intermediate, 3,5-dimethoxybenzyl bromide (2.5 g, 37%). The isolated bromide (6.7 g, 29 mmol, the combined material



from two syntheses) was dissolved in benzene (25 mL). A solution of triphenylphosphene (7.6 g, 29 mmol) in benzene (20 mL) was added, and the mixture was left to stir at room temperature overnight. A white precipitate was isolated (11.0 g, 77%) by suction filtration and washed with ether. The intermediate triphenylphosphonium salt was reacted with 3-methoxybenzaldehyde using the procedure described for **71-74** in Section 6.3.1, giving the pure stilbene *trans*-**112** after column chromatography (0.3 g, 11%).  $^1\text{H}$  NMR  $\delta$ : 7.34 (t, 1H,  $J = 8$  Hz), 7.18 (d, 1H,  $J = 8$  Hz), 7.13 (d, 1H,  $J = 16.5$  Hz), 7.11 (s, 1H), 7.10 (d, 1H,  $J = 16.5$  Hz), 6.89 (d, 1H,  $J = 8$  Hz), 6.74 (d, 2H,  $J = 2$  Hz), 6.48 (t, 1H,  $J = 2$  Hz), 3.91 (s, 3H), 3.89 (s, 6H);  $^{13}\text{C}$  NMR  $\delta$ : 161.2, 160.1, 139.5, 138.8, 129.8, 129.3, 129.2, 119.5, 113.6, 112.0, 104.8, 100.3, 55.5, 55.4; GC-MS  $m/z$ : 271 (10.3), 270 (100.0), 255 (16.8), 239 (37.8), 224 (17.5), 195 (22.4), 181 (10.9), 165 (19.2), 153 (15.6), 152 (26.0), 141 (11.7), 139 (10.1), 115 (20.8); HRMS: 270.1256 (calculated), 270.1252  $\pm$  0.0008 (found); purity by GC-FID: 99%.

The syntheses of the substituted derivatives *trans*-**113-120** were accomplished using the same procedure described in Section 7.3.1 for stilbene derivatives **71-74**. The appropriately-substituted benzyl bromide was reacted with triphenylphosphene to give the requisite Wittig salt, and reaction with 3,5-dimethoxybenzaldehyde provided mixtures of *cis* and *trans* isomers. The desired *trans* isomer was isolated by column chromatography, in yields of 10-20%, and in purities greater than 98% for all substrates.

*trans*-3,5-Dimethoxy-4'-methylstilbene (*trans*-**113**).  $^1\text{H}$  NMR  $\delta$ : 7.46 (d, 2H,  $J = 8$  Hz), 7.23 (d, 2H,  $J = 8$  Hz), 7.11 (d, 1H,  $J = 16.5$  Hz), 7.06 (d, 1H,  $J = 16.5$  Hz), 6.72 (d, 2H,  $J$

= 2.5 Hz), 6.45 (t, 1H,  $J = 2.5$  Hz), 3.89 (s, 6H), 2.42 (s, 3H);  $^{13}\text{C}$  NMR  $\delta$ : 161.2, 139.8, 137.8, 134.5, 129.6, 129.3, 127.9, 126.7, 104.7, 100.0, 55.5, 21.4; GC-MS  $m/z$ : 255 (16.2), 254 (100.0), 253 (21.3), 239 (43.2), 224 (14.8), 223 (16.2), 208 (26.8), 179 (23.1), 178 (19.6), 165 (29.8), 153 (14.2), 152 (26.2), 126 (15.3), 115 (14.6), 89 (15.9), 76 (12.1); HRMS: 254.1307 (calculated),  $254.1306 \pm 0.0008$  (found).

*trans*-3,5-Dimethoxy-3'-methylstilbene (*trans*-114).  $^1\text{H}$  NMR  $\delta$ : 7.40 (s, 1H), 7.38 (d, 1H,  $J = 8$  Hz), 7.32 (t, 1H,  $J = 7.5$  Hz), 7.16 (d, 1H,  $J = 7.5$  Hz), 7.13 (d, 1H,  $J = 16$  Hz), 7.10 (d, 1H,  $J = 16$  Hz), 6.74 (d, 1H,  $J = 2$  Hz), 6.47 (t, 1H,  $J = 2$  Hz), 3.90 (s, 6H), 2.45 (s, 3H);  $^{13}\text{C}$  NMR: 161.2, 139.7, 138.4, 137.3, 129.5, 128.8, 127.5, 124.0, 104.8, 100.1, 55.5, 21.6 (note: one peak less than expected, presumably due to coincidental overlap of two signals); GC-MS  $m/z$ : 255 (17.2), 254 (100.0), 253 (28.7), 239 (35.7), 224 (12.9), 223 (18.5), 222 (10.7), 208 (24.1), 179 (24.1), 178 (20.0), 165 (28.6), 153 (15.4), 152 (23.4), 126 (13.4), 115 (15.2); HRMS: 254.1307 (calculated),  $254.1308 \pm 0.0008$  (found).

*trans*-4'-Fluoro-3,5-dimethoxystilbene (*trans*-115).  $^1\text{H}$  NMR  $\delta$ : 7.52 (m, 2H), 7.10 (m, 2H), 7.09 (d, 1H,  $J = 16$  Hz), 6.99 (d, 1H,  $J = 16$  Hz), 6.72 (d, 2H,  $J = 2$  Hz), 6.46 (t, 1H,  $J = 2$  Hz), 3.89 (s, 6H);  $^{13}\text{C}$  NMR  $\delta$ : 162.6 (d,  $J = 247.4$ ), 161.2, 139.4, 133.5, 128.6 (d,  $J = 2.4$  Hz), 128.24 (d,  $J = 7.9$  Hz), 128.16 (d,  $J = 0.8$  Hz), 115.8 (d,  $J = 20.9$  Hz), 104.7, 100.2, 55.5; GC-MS  $m/z$ : 259 (15.7), 258 (100.0), 257 (35.1), 242 (11.3), 227 (16.8), 212 (16.5), 183 (38.7), 171 (15.7); HRMS: 258.1056 (calculated),  $258.1052 \pm 0.0008$  (found).

*trans*-3'-Fluoro-3,5-dimethoxystilbene (*trans*-116).  $^1\text{H}$  NMR  $\delta$ : 7.36 (m, 1H), 7.31 (d, 1H,  $J = 7.5$  Hz), 7.26 (m, 1H), 7.09 (s, 2H), 7.01 (m, 1H), 3.89 (s, 6H);  $^{13}\text{C}$  NMR  $\delta$ : 163.4 (d,  $J = 245.3$  Hz), 161.2, 139.7 (d,  $J = 7.8$  Hz), 139.0, 130.3, 130.23, 130.18, 128.2 (d,  $J = 2.8$  Hz), 122.7 (d,  $J = 2.8$  Hz), 114.7 (d,  $J = 21.5$ ), 113.0 (d,  $J = 21.9$  Hz), 104.9, 100.5, 55.6; GC-MS  $m/z$ : 259 (15.7), 258 (100.0), 257 (38.8), 227 (19.8), 226 (12.0), 212 (16.9), 183 (41.2), 170 (15.7); HRMS: 258.1056 (calculated), 258.1054  $\pm$  0.0008 (found).

*trans*-4'-Trifluoromethyl-3,5-dimethoxystilbene (*trans*-117).  $^1\text{H}$  NMR  $\delta$ : 7.66 (d, 2H,  $J = 8.5$  Hz), 7.63 (d, 2H,  $J = 8.5$  Hz), 7.16 (d, 1H,  $J = 16.5$  Hz), 7.14 (d, 1H,  $J = 16.5$  Hz), 6.75 (d, 2H,  $J = 2$  Hz), 6.50 (t, 2H,  $J = 2$  Hz), 3.89 (s, 6H);  $^{13}\text{C}$  NMR  $\delta$ : 161.3, 140.8 (q,  $J = 1.4$  Hz), 138.8, 129.5 (q,  $J = 33.4$  Hz), 127.8, 126.9, 126.8, 125.8 (q,  $J = 3.9$  Hz), 124.4 (q,  $J = 271.9$  Hz), 105.1, 100.7, 55.5; GC-MS  $m/z$ : 309 (16.4), 308 (100.0), 307 (38.1), 292 (12.1), 277 (18.1), 262 (14.5), 239 (15.1), 233 (25.3), 183 (12.4), 178 (12.9), 165 (38.0), 151 (18.9), 152 (29.0); HRMS: 308.1024 (calculated), 308.1024  $\pm$  0.0008 (found).

*trans*-3'-Trifluoromethyl-3,5-dimethoxystilbene (*trans*-118).  $^1\text{H}$  NMR  $\delta$ : 7.80 (s, 1H), 7.71 (d, 1H,  $J = 8$  Hz), 7.56 (d, 1H,  $J = 8$  Hz), 7.52 (t, 1H,  $J = 8$  Hz), 7.15 (s, 2H), 6.74 (d, 2H,  $J = 2$  Hz), 6.50 (t, 1H,  $J = 2$  Hz), 3.89 (s, 6H);  $^{13}\text{C}$  NMR  $\delta$ : 161.2, 138.9, 138.1, 131.1 (q,  $J = 32.2$  Hz), 130.7, 129.8 (q,  $J = 1.3$  Hz), 129.3, 127.8, 124.33 (q,  $J = 272.5$  Hz), 124.29 (q,  $J = 3.8$  Hz), 123.3 (q,  $J = 3.9$  Hz), 103.0, 100.7, 55.5; GC-MS  $m/z$ : 309 (17.5), 308 (100.0), 307 (29.9), 277 (15.0), 262 (11.5), 233 (16.9), 165 (25.7), 153 (12.6), 152 (17.0), 69 (17.2); HRMS: 308.1024 (calculated), 308.1021  $\pm$  0.0008 (found).

*trans*-4'-Cyano-3,5-dimethoxystilbene (*trans*-**119**).  $^1\text{H}$  NMR  $\delta$ : 7.66 (d, 2H,  $J = 8$  Hz), 7.6 (d, 2H,  $J = 8$  Hz), 7.17 (d, 1H,  $J = 16.5$  Hz), 7.09 (d, 1H,  $J = 16.5$  Hz), 6.71 (d, 2H,  $J = 2$  Hz), 6.48 (t, 2H,  $J = 2$  Hz), 3.87 (s, 6H);  $^{13}\text{C}$  NMR  $\delta$ : 161.1, 141.7, 138.3, 132.5, 132.4, 127.3, 127.0, 119.0, 110.7, 105.1, 100.9, 55.5; GC-MS  $m/z$ : 266 (17.2), 265 (100.0), 264 (49.8), 249 (11.4), 234 (16.4), 219 (14.4), 191 (10.5), 190 (32.2), 178 (12.6), 151 (10.8); HRMS: 265.1103 (calculated),  $265.1105 \pm 0.0008$  (found).

*trans*-3'-Cyano-3,5-dimethoxystilbene (*trans*-**120**).  $^1\text{H}$  NMR  $\delta$ : 7.80 (s, 1H), 7.74 (d, 1H,  $J = 8$  Hz), 7.56 (d, 1H,  $J = 7.5$  Hz), 7.49 (t, 1H,  $J = 7.5$  Hz), 7.11 (d, 1H,  $J = 16.5$  Hz), 7.07 (d, 1H,  $J = 16.5$  Hz), 6.71 (d, 2H,  $J = 2$  Hz), 6.49 (t, 1H,  $J = 2$  Hz), 3.88 (s, 6H);  $^{13}\text{C}$  NMR  $\delta$ : 161.3, 138.6, 138.5, 131.5, 130.9, 130.7, 130.1, 129.6, 126.8, 118.9, 113.1, 105.1, 100.8, 55.6; GC-MS  $m/z$ : 266 (21.0), 265 (100.0), 264 (54.4), 249 (15.4), 234 (26.4), 219 (21.1), 204 (12.2), 191 (15.8), 190 (41.3), 178 (18.1), 177 (13.1), 165 (11.6), 151 (15.1), 125 (11.5); HRMS: 265.1103 (calculated),  $265.1102 \pm 0.0008$  (found).

### 7.5.2 Irradiation Procedures

Irradiations were carried out using the same experimental methods and data analysis techniques that were described in Section 7.3.3. The GC-MS characterizations of the photoproducts are listed below.

Products detected following the irradiation of *trans*-**112**:

*cis*-3,3',5-Trimethoxystilbene (*cis*-**112**). GC-MS  $m/z$ : 271 (11.1), 270 (100.0), 255 (14.8), 239 (37.4), 224 (17.9), 195 (20.5), 165 (17.7), 152 (24.4), 115 (19.2).

1-(2,2,2-Trifluoroethoxy)-1-(3,5-dimethoxyphenyl)-2-(3-methoxyphenyl)ethane  
**(121-2)**. GC-MS *m/z*: 371 (1.8), 370 (9.4), 220 (22.4), 219 (100.0), 136 (41.7),  
 135 (49.9), 107 (10.7), 91 (12.1), 78 (13.1), 77 (20.3), 65 (13.1).

1-(2,2,2-Trifluoroethoxy)-2-(3,5-dimethoxyphenyl)-1-(3-methoxyphenyl)ethane  
**(122-2)**. GC-MS *m/z*: 370 (5.4), 250 (12.0), 249 (100.0), 166 (26.0), 165 (10.8).

Products detected following the irradiation of *trans*-113:

*cis*-3,5-Dimethoxy-4'-methylstilbene (*cis*-113). GC-MS *m/z*: 255 (17.9), 254  
 (100.0), 253 (23.5), 239 (46.8), 238 (11.9), 224 (17.0), 223 (17.7), 222 (11.9), 209  
 (10.4), 208 (31.3), 179 (27.9), 178 (23.9), 166 (10.1), 165 (34.0), 153 (18.2), 152  
 (31.5), 126 (15.6), 115 (19.0),

1-(2,2,2-Trifluoroethoxy)-1-(3,5-dimethoxyphenyl)-2-(4-methylphenyl)ethane  
**(121-3)**. GC-MS *m/z*: 354 (4.7), 254 (28.5), 203 (100.0), 119 (20.6), 91 (13.7).

1-(2,2,2-Trifluoroethoxy)-2-(3,5-dimethoxyphenyl)-1-(4-methylphenyl)ethane  
**(122-3)**. GC-MS *m/z*: 354 (not observed), 249 (100.0), 167 (16.4), 166 (10.8).

Products detected following the irradiation of *trans*-114:

*cis*-3,5-Dimethoxy-3'-methylstilbene (*cis*-114). GC-MS *m/z*: 255 (17.5), 254  
 (100.0), 253 (29.4), 239 (38.2), 238 (11.2), 224 (14.6), 223 (20.1), 222 (12.5), 208  
 (29.4), 181 (10.9), 179 (29.4), 178 (25.2), 166 (11.4), 165 (35.4), 153 (19.4), 152  
 (31.8), 126 (16.2), 115 (20.3).

1-(2,2,2-Trifluoroethoxy)-1-(3,5-dimethoxyphenyl)-2-(3-methylphenyl)ethane

(121-4). GC-MS *m/z*: 354 (6.9), 254 (17.3), 203 (100.0), 119 (19.0), 91 (15.4).

1-(2,2,2-Trifluoroethoxy)-2-(3,5-dimethoxyphenyl)-1-(3-methylphenyl)ethane

(122-4). GC-MS *m/z*: 354 (2.9), 254 (10.6), 249 (100.0), 166 (30.1), 165 (15.3).

Products detected following the irradiation of *trans*-115:

*cis*-4'-Fluoro-3,5-dimethoxystilbene (*cis*-115). GC-MS *m/z*: 259 (16.5), 258 (100.0), 257 (37.0), 252 (12.4), 227 (16.5), 226 (10.8), 212 (16.1), 183 (34.5), 171 (13.5), 170 (13.7).

1-(2,2,2-Trifluoroethoxy)-1-(3,5-dimethoxyphenyl)-2-(4-fluorophenyl)ethane

(121-5). GC-MS *m/z*: 358 (6.1), 207 (100.0), 123 (11.1).

1-(2,2,2-Trifluoroethoxy)-2-(3,5-dimethoxyphenyl)-1-(4-fluorophenyl)ethane

(122-5). GC-MS *m/z*: 358 (not observed), 249 (100.0), 166 (40.2), 165 (11.8), 109 (16.0).

Products detected following irradiation of *trans*-116:

*cis*-3'-Fluoro-3,5-dimethoxystilbene (*cis*-116). GC-MS *m/z*: 258 (100.0), 257 (38.8), 252 (11.2), 227 (19.5), 226 (12.8), 212 (17.5), 196 (10.2), 184 (11.5), 183 (42.2), 171 (15.8), 170 (17.2), 165 (10.4), 133 (11.8), 121 (10.5).

1-(2,2,2-Trifluoroethoxy)-1-(3,5-dimethoxyphenyl)-2-(3-fluorophenyl)ethane

(121-6). GC-MS *m/z*: 358 (12.5), 207 (100.0), 151 (21.4), 127 (12.9).

1-(2,2,2-Trifluoroethoxy)-2-(3,5-dimethoxyphenyl)-1-(3-fluorophenyl)ethane  
(**122-6**). GC-MS *m/z*: 358 (3.1), 250 (11.0), 249 (100.0), 166 (42.4), 165 (13.8),  
109 (13.3).

Products detected following irradiation of *trans*-**117**:

*cis*-4'-Trifluoromethyl-3,5-dimethoxystilbene (*cis*-**117**). GC-MS *m/z*: 309 (15.9),  
308 (100.0), 307 (40.1), 292 (12.8), 277 (17.3), 276 (12.3), 262 (13.4), 239 (15.3),  
233 (19.7), 165 (20.0), 152 (14.6).

1-(2,2,2-Trifluoroethoxy)-1-(3,5-dimethoxyphenyl)-2-(4-trifluoromethyl-  
phenyl)ethane (**121-7**). GC-MS *m/z*: 408 (7.7), 257 (96.0), 177 (18.1), 152 (11.0),  
151 (100.0), 127 (14.0), 91 (12.1), 83 (12.1), 83 (16.1), 77 (12.7).

1-(2,2,2-Trifluoroethoxy)-2-(3,5-dimethoxyphenyl)-1-(4-trifluoromethyl-  
phenyl)ethane (**122-7**). GC-MS *m/z*: 408 (1.7), 250 (10.6), 249 (100.0), 166  
(33.0), 165 (13.2).

Products detected following irradiation of *trans*-**118**:

*cis*-3'-Trifluoromethyl-3,5-dimethoxystilbene (*cis*-**118**). GC-MS *m/z*: 309 (16.8),  
308 (100.0), 307 (30.5), 277 (16.1), 262 (13.1), 239 (11.0), 233 (20.8), 183 (10.4),  
178 (12.1), 166 (10.3), 165 (33.3), 153 (16.9), 152 (23.9).

1-(2,2,2-Trifluoroethoxy)-1-(3,5-dimethoxyphenyl)-2-(3-trifluoromethyl-phenyl)ethane (**121-8**). GC-MS *m/z*: 408 (6.7), 257 (100.0), 177 (23.2), 166 (10.4), 151 (77.5), 127 (10.6), 91 (21.8), 83 (25.3), 77 (13.8).

1-(2,2,2-Trifluoroethoxy)-2-(3,5-dimethoxyphenyl)-1-(3-trifluoromethyl-phenyl)ethane (**122-8**). GC-MS *m/z*: 408 (3.2), 250 (12.6), 249 (100.0), 166 (23.1).

Products detected following irradiation of *trans*-**119**:

*cis*-4'-Cyano-3,5-dimethoxystilbene (*cis*-**119**). GC-MS *m/z*: 266 (17.2), 265 (100.0), 264 (49.8), 249 (11.4), 234 (16.4), 219 (14.4), 191 (10.5), 190 (32.2), 178 (12.6), 151 (10.8).

1-(2,2,2-Trifluoroethoxy)-1-(3,5-dimethoxyphenyl)-2-(4-cyanophenyl)ethane (**121-9**). GC-MS *m/z*: 366 (2.5), 265 (16.8), 214 (50.0), 152 (13.4), 151 (100.0), 134 (30.4), 130 (17.7), 116 (11.4), 104 (22.6), 91 (34.3), 89 (10.1), 83 (30.0), 79 (13.8), 78 (33.9), 77 (43.4), 76 (13.1), 69 (11.4), 65 (29.9), 63 (16.9), 51 (23.6).

1-(2,2,2-Trifluoroethoxy)-2-(3,5-dimethoxyphenyl)-1-(4-cyanophenyl)ethane (**122-9**). GC-MS *m/z*: 365 (11.4), 214 (50.2), 152 (13.2), 151 (100.0), 134 (30.7), 130 (17.8), 116 (14.7), 108 (10.0), 104 (24.5), 102 (25.4), 91 (36.6), 89 (12.6), 83 (34.1), 79 (16.1), 78 (40.6), 77 (50.3), 76 (15.5), 65 (36.8), 64 (10.7), 63 (20.5).



6-Cyano-2,4-dimethoxyphenanthrene (**123-9**). GC-MS *m/z*: 264 (15.1), 263 (100.0), 248 (24.7), 220 (42.1), 205 (31.4), 190 (17.0), 188 (17.3), 178 (11.4), 177 (86.8), 151 (10.8), 150 (19.0).

Products detected following irradiation of *trans*-**120**:

*cis*-3'-Cyano-3,5-dimethoxystilbene (*cis*-**120**). GC-MS *m/z*: 266 (21.0), 265 (100.0), 264 (54.4), 249 (15.4), 234 (26.4), 219 (21.1), 204 (12.2), 191 (15.8), 190 (41.3), 178 (18.1), 177 (13.1), 165 (11.6), 152 (11.2), 151 (15.1), 140 (10.1), 125 (11.5).

1-(2,2,2-Trifluoroethoxy)-2-(3,5-dimethoxyphenyl)-1-(3-cyanophenyl)ethane (**121-0**). GC-MS *m/z*: 366 (3.2), 365 (16.7), 214 (46.7), 152 (11.1), 151 (100.0), 134 (13.7), 91 (11.6), 83 (12.1), 78 (10.1), 77 (15.1).

1-(2,2,2-Trifluoroethoxy)-1-(3,5-dimethoxyphenyl)-2-(3-cyanophenyl)ethane (**122-0**). GC-MS *m/z*: 365 (5.74), 265 (12.1), 250 (12.2), 249 (100.0), 166 (26.4), 165 (11.8).

## References

1. Gold, V. *Pure & Appl. Chem.* **1983**, *55*, 1281-1371.
2. Olah, G.A. *J. Org. Chem.* **2001**, *18*, 5943-5957.
3. Traynham, J.G. *J. Chem. Ed.* **1989**, *66*, 451-452.
4. Baeyer, A.; Villiger, V. *Chem. Ber.* **1902**, *35*, 1189-1201.
5. Gomberg, M. *Chem. Ber.* **1902**, *35*, 2397-2408.
6. (a) Gomberg, M.; Cone, L.H. *Ann. Chem.* **1909**, *370*, 142-208. (b) Hofmann, K.A.; Kirmreuther, H. *Chem. Ber.* **1909**, *42*, 4856-4865.
7. Meerwein, H.; van Emster, K. *Chem. Ber.* **1922**, *55*, 2500-2522.
8. Ward, A.M. *J. Chem. Soc.* **1927**, 445-458.
9. Ingold, C.K.; Rothstein, E. *J. Chem. Soc.* **1928**, 1217-1221.
10. Ingold, C.K. *Structure and Mechanism in Organic Chemistry*, Cornell University Press: Ithaca, New York, 1953; pp 306-418, and references therein.
11. Whitmore, F.C. *J. Am. Chem. Soc.* **1932**, *54*, 3274-3283.
12. (a) Whitmore, F.C.; Johnston, F. *J. Am. Chem. Soc.* **1933**, *55*, 5020-5022. (b) Ecke, G.G.; Cook, N.C.; Whitmore, F.C. *J. Am. Chem. Soc.* **1950**, *72*, 1511-1513.
13. Pocker, Y.; Stevens, K.D. *J. Am. Chem. Soc.* **1969**, *91*, 4205-4210.
14. Ege, S. *Organic Chemistry: Structure and Reactivity* (3<sup>rd</sup> ed); D.C. Heath and Co.: Lexington, 1994.
15. Carey, F.A.; Sundberg, R.J. *Advanced Organic Chemistry* (4<sup>th</sup> ed); Kluwer Academic/Plenum: New York, 2000; Chapter 5.
16. Lowry, T.H.; Richardson, K.S. *Mechanism and Theory in Organic Chemistry* (3<sup>rd</sup> ed.); Harper and Row: New York, 1987; Chapters 4 and 5.

17. Carroll, F.A. *Perspectives on Structure and Mechanism in Organic Chemistry*; Brooks/Cole: Pacific Grove, 1998; Chapters 5 – 9.
18. McClelland, R.A. in *Reactive Intermediate Chemistry*, Moss, R.A.; Platz, M.S.; Jones, M. editors; John Wiley and Sons: Hoboken, 2004; Chapter 1.
19. Bethell, D.; Gold, V. *Carbonium Ions: An Introduction*; Academic Press: London, 1967.
20. *Carbonium Ions*, Olah, G.A.; Schleyer, P.V.R. editors; John Wiley and Sons: New York, 1968; Volumes I-V.
21. Vogel, P. *Carbocation Chemistry*; Elsevier: Amsterdam, 1985.
22. Hammett, L.P.; Deyrup, A.J. *J. Am. Chem. Soc.* **1932**, *54*, 2721-2739.
23. Deno, N.C.; Jaruzelski, J.J.; Schriesheim, A. *J. Am. Chem. Soc.* **1955**, *77*, 3044-3051.
24. (a) Okamoto, Y.; Brown, H.C. *J. Org. Chem.* **1957**, *22*, 485-494. (b) Brown, H.C.; Okamoto, Y. *J. Am. Chem. Soc.* **1948**, *80*, 4979-4987.
25. Hammett, L.P. *Physical Organic Chemistry: Reaction Rates, Equilibria, and Mechanisms* (2<sup>nd</sup> ed.); McGraw-Hill: New York, 1970; Chapter 11, and references therein.
26. Stock, L.M.; Brown, H.C. *Adv. Phys. Org. Chem.* **1963**, *1*, 35-154.
27. Hammond, G.S. *J. Am. Chem. Soc.* **1955**, *77*, 334-338.
28. Reference 19, page 90.
29. Schubert, W.M.; Keefe, J.R. *J. Am. Chem. Soc.* **1972**, *94*, 559-566.
30. Yates, K.; McDonald, R.S.; Shapiro, S.A. *J. Org. Chem.* **1973**, *38*, 2460-2463.
31. Noyce, D.S.; Hartter, D.R.; Miles, F.B. *J. Am. Chem. Soc.* **1968**, *90*, 3794-3796.

32. Harrison, A.G.; Kaberle, P.; Lossing, F.P. *J. Am. Chem. Soc.* **1961**, *83*, 777-780.
33. Sim, B.A.; Milne, P.H.; Griller, D.; Wayner, D.D.M. *J. Am. Chem. Soc.* **1990**, *112*, 6635-6638.
34. Houle, F.A.; Beauchamp, J.L. *J. Am. Chem. Soc.* **1979**, *101*, 4067-4074.
35. Aue, D.H.; Bowers, M.T. in *Gas Phase Ion Chemistry*, Bowers, M.T. editor; Academic Press, New York, 1979.
36. Karaman, R.; Huang, J.-T.L.; Fry, J.L. *J. Org. Chem.* **1991**, *56*, 188-195.
37. Cheng, J.P.; Handoo, K.L.; Parker, V.D. *J. Am. Chem. Soc.* **1993**, *115*, 2655-2660.
38. Olah, G.A.; Prakash, G.K.S.; Sommer, J. *Superacids*; John Wiley and Sons: New York, 1985.
39. Olah, G.A. *J. Org. Chem.* **2001**, *66*, 5943-5957.
40. Olah, G.A.; Baker, E.B.; Evans, J.C.; Tolgyesi, W.S.; McIntyre, J.S.; Bastien, I.J. *J. Am. Chem. Soc.* **1964**, *86*, 1360-1373.
41. Olah, G.A.; Donovan, D.J. *J. Am. Chem. Soc.* **1977**, *99*, 5026-5039.
42. Arnett, E.M.; Hofelich, T.C. *J. Am. Chem. Soc.* **1983**, *105*, 2889-2895.
43. Saunders, M.; Kates, M.R. *J. Am. Chem. Soc.* **1978**, *100*, 7082-7083.
44. Raber, D.J.; Harris, J.M.; Hall, R.E.; Schleyer, P.V.R. *J. Am. Chem. Soc.* **1971**, *93*, 4821-4828.
45. Ta-Shma, R.; Rappoport, Z. *J. Am. Chem. Soc.* **1983**, *105*, 6082-6095.
46. (a) Richard, J.P.; Jencks, W.P. *J. Am. Chem. Soc.* **1982**, *104*, 4689-4691. (b) Richard, J.P.; Jencks, W.P. *J. Am. Chem. Soc.* **1982**, *104*, 4691-4695.
47. Cozens, F.L.; Kanagasabapathy, V.M.; McClelland, R.M.; Steenken, S. *Can. J. Chem.* **1999**, *77*, 2069-2082.

48. McClelland, R.A.; Chan, C.; Cozens, F.; Modro, A.; Steenken, S. *Angew. Chem. Int. Ed. Engl.* **1991**, *30*, 1337-1339.
49. Pezacki, J.P.; Shukla, D.; Lusztyk, J.; Warkentin, J. *J. Am. Chem. Soc.* **1999**, *121*, 6589-6598.
50. Reference 17, Chapter 11.
51. Turro, N.J. *Modern Molecular Photochemistry*; Benjamin/Cummings Publishing Company: Menlo Park, 1978.
52. Lifschitz, J. *Chem. Ber.* **1919**, *52*, 1919-1926.
53. Harris, L.; Kaminsky, J.; Simard, R.G. *J. Am. Chem. Soc.* **1935**, *57*, 1151-1154.
54. Holmes, E.O. *J. Phys. Chem.* **1957**, *61*, 434-441.
55. Zimmerman, H.E.; Sandel, V.R. *J. Am. Chem. Soc.* **1963**, *85*, 915-921.
56. (a) Zimmerman, H.E. *J. Am. Chem. Soc.* **1995**, *117*, 8988-8991. (b) Zimmerman, H.E. *J. Phys. Chem.* **1998**, *102*, 5616-5621.
57. (a) DeCosta, D.P.; Pincock, J.A. *J. Am. Chem. Soc.* **1989**, *111*, 8948-8950. (b) DeCosta, D.P.; Pincock, J.A. *J. Am. Chem. Soc.* **1993**, *115*, 2180-2190.
58. Hilborn, J.W.; MacKnight, E.; Pincock, J.A.; Wedge, P.J. *J. Am. Chem. Soc.* **1994**, *116*, 3337-3346.
59. Hilborn, J.W.; Pincock, J.A. *J. Am. Chem. Soc.* **1991**, *113*, 2683-2686.
60. Milne, P.H.; Wayner, D.D.M.; DeCosta, D.P.; Pincock, J.A. *Can. J. Chem.* **1992**, *70*, 121-127.
61. Marcus, R.A. *Angew. Chem.* **1993**, *32*, 1111-1122.
62. Pincock, J.A. *Acc Chem. Res.* **1997**, *30*, 43-49.
63. Pincock, J.A.; Wedge, P.J. *J. Org. Chem.* **1994**, *59*, 5587-5595.

64. Goshima, T.; Itoh, Y.; Shirai, H.; Kojima, M. *J. Photochem. Photobiol. A: Chem.* **2001**, *141*, 139-145.
65. (a) Cozens, F.L.; Pincock, A.L.; Pincock, J.A.; Smith, R. *J. Org. Chem.* **1998**, *63*, 434-435. (b) DeCosta, D.P.; Howell, N.; Pincock, A.L.; Pincock, J.A.; Rifai, S. *J. Org. Chem.* **2000**, *65*, 4698-4705.
66. Beugelmans, R.; Marcheville, H.C. *Chem. Comm.* **1969**, 241-242.
67. (a) Cristol, S.J.; Mayo, G.O.; Lee, G.A. *J. Am. Chem. Soc.* **1968**, *90*, 4191-4192. (b) Cristol, S.J.; Schloemer, G.C. *J. Am. Chem. Soc.* **1972**, *94*, 5916-5917.
68. Lin, C.-I.; Singh, P.; Ullman, E.F. *J. Am. Chem. Soc.* **1976**, *98*, 6711-6713.
69. Hoang, M.; Gadosy, T.; Ghazi, H.; Hou, D.-F.; Hopkinson, A.C.; Johnston, L.J.; Lee-Ruff, E. *J. Org. Chem.* **1998**, *63*, 7168-7171.
70. Mladenova, G.; Chen, L.; Rodriguez, C.F.; Siu, K.W.M.; Johnston, L.J.; Hopkinson, A.C.; Lee-Ruff, E. *J. Org. Chem.* **2001**, *66*, 1109-1114.
71. Wan, P.; Krogh, E. *J. Am. Chem. Soc.* **1989**, *111*, 4887-4895.
72. Fujio, M.; Goto, M.; Susuki, T.; Akasaka, I.; Mishima, M.; Tsuno, Y. *Bull. Chem. Soc. Jpn.* **1990**, *63*, 1146-1153.
73. Roberts, J.C.; Pincock, J.A. *Can. J. Chem.* **2003**, *81*, 709-722.
74. Vogel, A. *Vogel's Textbook of Organic Chemistry*. Longman Scientific and Technical: London, 1989; p. 935.
75. Detty, M.R.; Murray, B.J. *J. Am. Chem. Soc.* **1983**, *105*, 883-890.
76. Crotti, P.; Ferreti, M.; Macchia, F.; Stoppioni, A. *J. Org. Chem.* **1986**, *51*, 2759-2766.
77. Steglich, W.; Neises, B. *Angew. Chem. Int. Ed. Engl.* **1978**, *17*, 522-524.

78. Noller, K.; Dosteyn, f.; Meier, H. *Chem. Ber.* **1988**, *121*, 1609-1615.
79. Falck, J.R.; Yu, J.; Cho, H.S. *Tetrahedron Lett.* **1994**, *35*, 5997-6000.
80. Noyce, D.S.; Hartter, D.R.; Pollack, R.M. *J. Am. Chem. Soc.* **1968**, *90*, 3791-3794.
81. Woning, J.; Oudenampsen, A.; Laarhoven, W.H. *J. Chem. Soc. Perkin Trans. II* **1989**, 2147-2154.
82. Saltiel, J.; Charlton, J.L. in *Rearrangements in Ground and Excited States*; de Mayo, P., ed.; Academic Press: New York, 1980; Vol.3, pp 25-89.
83. Waldeck, D.H. *Chem. Rev.* **1991**, *91*, 415-436.
84. Hohlneicher, G.; Müller, M.; Demmer, M.; Lex, J.; Penn, J.H.; Gan, L.-X.; Loesel, P.D. *J. Am. Chem. Soc.* **1988**, *110*, 4483-4501.
85. Santoro, A.V.; Barrett, E.J.; Hoyer, H.H. *J. Am. Chem. Soc.* **1967**, *89*, 4545-4546.
86. Saltiel, J.; Waller, A.S.; Sears, D.F.; Garrett, C.Z. *J. Phys. Chem.* **1993**, *97*, 2516-2522.
87. Saltiel, J.S.; Zafirou, O.C.; Megarity, E.D. *J. Am. Chem. Soc.* **1968**, *90*, 4759-4760.
88. Gegiou, D.S.; Muszkat, K.A.; Fischer, E. *J. Am. Chem. Soc.* **1968**, *90*, 12-18.
89. Gegiou, D.S.; Muszkat, K.A.; Fischer, E. *J. Am. Chem. Soc.* **1968**, *90*, 3907-3918.
90. a) Dyck, R.H.; McClure, D.S. *J. Chem. Phys.* **1962**, *36*, 2326-2345. b) Saltiel, J.S.; Charleton, J.L. *J. Phys. Chem.* **1977**, *81*, 1940-1944.
91. Sivakumar, N.; Hoburg, E.A.; Waldeck, D.H. *J. Chem. Phys.* **1989**, *90*, 2305-2316.
92. Muzzucato, U. *Pure & Appl. Chem.* **1982**, *54*, 1704-1721.
93. Saltiel, J.; Waller, A.S.; Sears, D.F. *J. Am. Chem. Soc.* **1993**, *115*, 2453-2465.

94. a) Abrash, S.; Repinec, S.; Hochstrasser, R.M. *J. Chem. Phys.* **1990**, *93*, 1041-1053. b) Todd, D.C.; Jean, J.M.; Rosenthal, S.J.; Ruggiero, A.J.; Yang, D.; Fleming, G.R. *J. Chem. Phys.* **1990**, *93*, 8658-8668.
95. Kim, S.K.; Courtney, S.H.; Fleming, G.R. *Chem. Phys. Lett.* **1989**, *159*, 543-548.
96. (a) Mallory, F.B.; Mallory, C.W. in *Organic Reactions*; Dauben, W.G. ed.; John Wiley and Sons: New York, 1984; Vol.30, pp 1-456. (b) Gilbert, A. in *CRC Handbook of Organic Photochemistry and Photobiology*; Horspool, W. and Lenci, F. eds; CRC Press, 2004, pp 33-1 – 33-11.
97. Lewis, F.D.; Yang, J.-S. *J. Am. Chem. Soc.* **1997**, *119*, 3834-3835.
98. Lewis, F.D.; Kalgutkar, R.S.; Yang, J.-S. *J. Am. Chem. Soc.* **1999**, *121*, 12045-12053.
99. Lewis, F.D.; Kalgutkar, R.S. *J. Phys. Chem. A* **2001**, *105*, 285-291.
100. Lewis, F.D.; Weigel, W.; Zuo, X. *J. Phys. Chem. A* **2001**, *105*, 4691-4696.
101. Lewis, F.D.; Weigel, W. *J. Phys. Chem. A* **2000**, *104*, 8146-8153.
102. Yang, J.-S.; Wang, C.-M.; Hwang, C.-Y.; Liao, K.-L.; Chiou, S.-Y. *Photochem. Photobiol Sci.* **2003**, *2*, 1225-1231.
103. Yang, J.-S.; Lin, Y.-D.; Lin, Y.-H.; Liao, F.-L. *J. Org. Chem.* **2004**, *69*, 3517-3525.
104. Yang, J.-S.; Liao, K.-L.; Wang, C.-M.; Hwang, C.-Y. *J. Am. Chem. Soc.* **2004**, *126*, 12325-12335.
105. Sakuragi, M.; Sakuragi, H.; Hasegawa, M. *Bull. Chem. Soc. Jpn.* **1977**, *50*, 1562-1566.
106. Lewis, F.D.; Crompton, E.M. *J. Am. Chem. Soc.* **2003**, *125*, 4044-4045.



107. Murohoshi, T.; Kaneda, K.; Ikegami, M.; Arai, T. *Photochem. Photobiol. Sci.* **2003**, *2*, 1247-1249.
108. Güsten, H.; Kasinc, L. *Tetrahedron Lett.* **1968**, *26*, 3097-3101.
109. Roberts, J.C.; Pincock, J.A. *J. Org. Chem.* **2004**, *69*, 4279-4282.
110. Hara, M.; Tojo, S.; Majima, T. *J. Photochem. Photobiol. A: Chem.* **2004**, *162*, 121-128.
111. Ho, J.-H.; Ho, T.-I.; Liu, R.S.H. *Org. Lett.* **2001**, *3*, 409-411.
112. Reference 17, Chapter 6.
113. a) Kropp, P.J. *Org. Photochem.* **1979**, *4*, 1-32. b) Kropp, P.J. in *CRC Handbook of Photochemistry and Photobiology*; Horspool, W. and Lenci, F. eds; CRC Press 2004, pp 9-1 – 9-11.
114. Kropp, P.J.; Reardon, E.J.; Gaibel, Z.L.F.; Williard, K.F.; Hattaway, J.H. *J. Am. Chem. Soc.* **1973**, *95*, 7058-7067.
115. Kropp, P.J.; Tise, F.P. *J. Am. Chem. Soc.* **1981**, *103*, 7293-7298.
116. Bonneau, R.; Jousset-Dubien, J.; Salem, L.; Yarwood, A.J. *J. Am. Chem. Soc.* **1976**, *98*, 4329-4330.
117. Marshall, J.A. *Acc. Chem. Res.* **1969**, *2*, 33-40.
118. Kropp, P.J. *J. Am. Chem. Soc.* **1973**, *95*, 4611-4619.
119. Hixson, S.S. *Tetrahedron Lett.* **1973**, 277-280.
120. Miyamoto, N.; Kawanisi, M.; Nozaki, H. *Tetrahedron Lett.* **1971**, 2565-2566.
121. Leigh, W.J.; Postigo, J.A. *Can. J. Chem.* **1995**, *73*, 191-203.
122. Woolridge, T.; Roberts, T.D. *Tetrahedron Lett.* **1973**, *41*, 4007-4008.

123. Roberts, T.D.; Ardemagni, L, Schechter, H.; *J. Am. Chem. Soc.* **1969**, *91*, 6185-6186.
124. Wan, P.; Yates, K. *Rev. Chem. Intermed.* **1984**, *5*, 157-181, and references therein.
125. Wan, P.; Davis, M.J.; Teo, M.A. *J. Org. Chem.* **1989**, *54*, 1354-1359.
126. McEwen, J.; Yates, K. *J. Phys. Org. Chem.* **1991**, *4*, 193-206.
127. Wan, P.; Turro, N.J. *J. Photochem.* **1985**, *28*, 93-102.
128. Boyd, M.K.; Lai, H.Y.; Yates, K. *J. Am. Chem. Soc.* **1991**, *113*, 7294-7300.
129. McClelland, R.A.; Kanagasabapathy, V.M.; Steenken, S. *J. Am. Chem. Soc.* **1988**, *110*, 6913-6914.
130. McClelland, R.A.; Cozens, F.; Steenken, S. *Tetrahedron Lett.* **1990**, 2821-2824.
131. Anderson, S.W.; Yates, K. *Can. J. Chem.* **1988**, *66*, 2412-2421.
132. a) Steenken, S.; McClelland, R.A. *J. Am. Chem. Soc.* **1990**, *112*, 9648-9649. b) Mathivanan, N.; Cozens, F.; McClelland, R.A.; Steenken, S. *J. Am. Chem. Soc.* **1992**, *114*, 2198-2203.
133. Lewis, F.D.; Bassani, D.M.; Caldwell, R.A.; Unett, D.J. *J. Am. Chem. Soc.* **1994**, *116*, 10477-10485.
134. Condirston, D.A.; Laposa, J.D. *Chem. Phys. Lett.* **1979**, *63*, 313-317.
135. Lewis, F.D.; Zuo, X. *J. Am. Chem. Soc.* **2003**, *125*, 8806-8813.
136. Kingsbury, C.A.; Thornton, W.B. *J. Org. Chem.* **1966**, *31*, 1000-1004.
137. de Silva, A.P.; Gunaratne, H.Q.N.; Gunnlaugsson, T.; Huxley, A.J.M.; McCoy, C.P.; Rademacher, J.T.; Rice, T.E. *Chem. Rev.* **1997**, *97*, 1515-1566.
138. Grabowski, Z.R.; Rotkiewicz, K.; Retting, W. *Chem. Rev.* **2003**, *103*, 3899-4031.
139. Rettig, W. *Angew. Chem. Int. Ed. Engl.* **1986**, *25*, 971-988.

140. Hicks, J.M.; Vandersall, M.T.; Sitzmann, E.V.; Eisenthal, K.B. *Chem. Phys. Lett.* **1987**, *135*, 413-420.
141. Görner, H.; Kuhn, H.J. *Advan. Photochem.* **1995**, *19*, 1-117.
142. Lapouyade, R.; Czeschka, K.; Majenz, W.; Retting, W.; Gilabert, E.; Rullière, C. *J. Phys. Chem.* **1992**, *96*, 9643-9650.
143. Il'ichev, Y.V.; Kuhnle, W.; Zachariasse, *Chem. Physics.* **1996**, *211*, 441-453.
144. Eilers-König, N.; Kuhnle, T.; Schwarzer, D.; Vöhringer, P.; Schroeder, J. *Chem. Phys. Lett.* **1996**, *253*, 69-76.
145. Kovalenko, S.A.; Schanz, R.; Senyushkina, T.A.; Erntsing, N.P. *Phys. Chem. Chem. Phys.* **2002**, *4*, 703-707.
146. Gruen, H.; Gorner, H. *J. Phys. Chem.* **1989**, *93*, 7144-7152.
147. Papper, V.; Pines, D.; Likhtenshtein, G.; Pines, E. *J. Photochem. Photobiol. A: Chem.* **1997**, *111*, 87-96.
148. González, C.M.; Pincock, J.A. *J. Am. Chem. Soc.* **2004**, *126*, 8870-8871.
149. González, C.M.; Pincock, J.A. unpublished results.
150. Bullimore, B.K.; McOmie, J.F.W.; Turner, A.B.; Galbraith, M.N.; Whalley, W.B. *J. Chem. Soc. C.* **1967**, 1289-1293.
151. Mannila, E.; Talvitie, A.; Kolehmainen, E. *Phytochemistry* **1993**, *33*, 813-816.
152. Mandal, A.K.; Mahajan, S.W. *Tetrahedron Lett.* **1985**, *26*, 3863-3866.